Nutrient Recovery from Source Separated Urine — Modelling and Experimental study

Thesis submitted by:

Leynard Natividad Marin

BEng. (Chemical Engineering) and MSc (Food Technology) *National University of Callao –(PERU)*

September 2019

This thesis is submitted for the degree of Doctor of Philosophy in the College of Science and Engineering at James Cook University

Acknowledgments

I would like to thank to my primary advisor *AProf. Phil Schneider* for his continuous support and suggestions in this work. His experience and encouragement were very valuable. I would also like to thank to my secondary supervisor *Dr. Madoc Sheehan* for his administrative assistance.

I would like to thank to *James Cook University* staff who indirectly contributed to this thesis during the first 3.5 years; electrical and mechanical staff, who collaborated in the building and operation of the reactor. Moreover, I would like to thank to *Murdoch University* technical and management staff, who collaborated with my research in the last stage.

I would like to thank the valuable support of my family. I thank to my father *Wilman Natividad* who challenged me to become PhD since I was a kid. I thank to my mother *Victoria Marin* for her love. I thank to my siblings: *Shirley* and *Jean Carlos* for their encouragement. I thank to all my teachers and lecturers who collaborated with my own professional development. I thank friends and people who helped me in very difficult times when I was trying to get the scholarship: *Eng. Ana Mercado del Pino* and *Dr. José Cáceres Paredes*. Finally, I thank to all candidate colleagues for cheering me up when I worked until very late hours in the office and laboratory.

Statement on the contribution of others

The directions of this work are contributed by *Dr. Philip A. Schneider*, and complementary suggestions in simulations and experimental data collection are attributed to fellow $PhD.$ *Candidate Max Burns*.

Financial support for my scholarship came from the *Peruvian Scholarship National Program* $(PRONABEC)$, a scholarship given by the Peruvian Government during the first 3 years; and the Commonwealth of Australia in the last 2 years.

Abstract

Phosphorus recovery from urine can make an important contribution towards global food security and environmental sustainability. Phosphorus can be recovered through formation of "struvite", a slow-release fertiliser, which forms by precipitation. Its precipitation was conducted by feeding magnesium and urine solutions to a continuous, well-mixed reactor. The resultant struvite particles were retained within the reactor, while the depleted nutrient solution exits. Most of previous research had arbitrary selected operational conditions. These studies did not consider any assessment of struvite productivity and neither thermodynamics. Struvite productivity comprises the quantity of struvite produced per volume of reactor. Thermodynamics simulations assisted to select a suitable conditions close to equilibrium. This work aimed to increase our process understanding through mathematical modelling, computer simulation and directed experimentation.

Model Development:

This thesis implemented a mathematical model comprising chemical thermodynamics, rate kinetics and mass balance relations. Thermodynamics includes chemical speciation where the activities of complexes are estimated from the total concentration of every element. Thermodynamic simulations can predict the saturation index at non-equilibrium conditions, and the quantity of struvite mass when the saturation index is set to zero at equilibrium. Kinetic models of the linear growth rate of struvite particles (G_L) as a function of the struvite saturation index and parameters ($G_L = k \cdot SI^n$) were evaluated. The mass balance considered eight elements present in urine composition (Mg, N, P, C, Na, K, S and Cl). This model considered a two-zone reactor with a mixing and reacting zone (bottom) and a settling zone (top). The model equations were solved in *Engineering Equation Solver* and *gPROMS* to design experimental struvite precipitation at laboratory and bench-scale.

Model Simulations:

The model was applied to batch, fed-batch and continuous struvite precipitation scenarios. Simulations predicted the struvite saturation index (SI_{MAP}) at non-equilibrium conditions, which drove the mass transfer, and the resultant struvite mass and element concentrations of P and Mg in solution.

The continuous reactor system consisted of a stirred vessel into which synthetic urine and $MgSO_4.7H_2O$ solutions were fed. Simulations assessed the effect of the Mg quantity added, seed quantity and hydraulic residence time within the liquid volume of the reactor. Simulations showed that Mg/P molar feed ratio greater unit does not increase the struvite production rate. Close to equilibrium continuous precipitation was achieved by increasing the seed mass and the hydraulic residence time. These simulations also showed that kinetic parameters are insensitive when conditions approach equilibrium. The rate coefficient $k = 1e-6\ m/h$, and the order $n = 1$ were suitable for process design.

Experimentation:

Struvite precipitation in batch experiments validated the nominated thermodynamics model by comparing the predicted P and Mg concentrations to the actual equilibrium solutions. Struvite mass was also accurately predicted. Elemental mass balances in P and Mg in each batch experiments also demonstrated very good consistency in the experimental results, leading to enhanced confidence in the results.

The dynamic model was validated against two separate continuous experiments, each operating more than 4 days. They were performed at the same hydraulic residence time (feed flow rate = 0.6 L/h), but varied the Mg/P feed molar ratio (0.34, 0.64 and 1.29). Model predictions of P and Mg concentration in the liquid phase well matched the laboratory measurements. Predicted struvite mass

was also within measurement uncertainty. The precipitated struvite was characterised by X-ray diffraction, elemental analysis of Mg and P, microscopy and particle size using electric sensing zone.

Table of Contents

Contents

List of Figures

List of Tables

1 Introduction and Background

Highlights:

- *Importance of nutrient recovery*
- *Research gaps in struvite precipitation process modelling and experimentation*
- *Research scope of this work*
- *Description of upcoming chapters*

1.1 Nutrient recovery importance

"We may be able to substitute nuclear power for coal, and plastics for wood, and yeast for meat, and friendliness for isolation – but for phosphorus there is neither substitute nor replacement".

Isaac Asimov

Phosphorus is a non-metallic element, fundamental for life, with no substitute in nature, absorbed by plants to promote cell growth. This element is obtained from phosphate rock, wherein 85 % of the world's reserves are limited to Morocco, China, The United States of America and Jordan (Ashley, Cordell, & Mavinic, 2011). While the cost of fertilizers is increasing, reserves are declining, with a possible production peak around 2030 — 2040 (Cordell, Drangert, & White, 2009) and an overall depletion between 100 and 250 years (Shu, Schneider, Jegatheesan, & Johnson, 2006). This element plays a key role in global food security. However, it is wasted during discharge to water bodies causing eutrophication (Ali and Schneider, 2008). Alum ($Al_2(SO_4)_3$) addition in wastewater treatment only "*removes*" P by forming less biodegradable sludge (Ashley et al., 2011; Shu et al., 2006). Therefore, P "*removal*" procedure should be changed to P "recovery".

Urine is a potentially valuable nutrient resource. The composition of domestic urine contains N and P. The addition of Mg to urine enables the precipitation of struvite ($MgNH_4PO_4.6H_2O$). However, this process still has unanswered questions, such as the quantity of Mg to be added, the struvite production rate, suitable flow rates, and the selection of monitoring variables during reactor operation. This work studied the precipitation of struvite ($MgNH_4PO_4.6H_2O$) by adding Mg to a synthetic urine matrix.

1.2 Modelling approach

Nutrient recovery understanding was developed by combining mathematical modelling and experimentation. Modelling is comprised by thermodynamics and kinetics, limited by assumptions, such as the set of equilibrium equations and the type of kinetics to employ.

Modelling has not been used appreciably in experimental design of continuous nutrient recovery systems. Even though, struvite recovery from urine source has been studied in different processes (Ronteltap, Maurer, & Gujer, 2007; Wilsenach, Schuurbiers, & van Loosdrecht, 2007), modelling was not applied to select, let alone, optimise operational conditions, such as feed flows, seed loading, and Mg addition rate to the reactor. Simulations can show process disturbance's effect in struvite production rate, saturation and mean particle size. Simulations were used to select operating conditions to refine and limit experimental efforts.

This work studied struvite precipitation in batch, fed-batch and continuous systems. While this research was strongly focused on continuous mode recovery reactors, batch and fed-batch experimentation was key to understand the thermodynamics and determine any chemical analytical interferences, before continuous process operations were undertaken. Experiments were performed with synthetic urine solutions to understand the speciation behaviour during struvite precipitation, to achieve better experimental control, repeatability and to avoid the organic chemistry effects.

Furthermore, deviations of predicted model with experimental data were assessed by considering uncertainty propagation in measurements, and adjusting model information.

1.3 Experimentation approach

This section provides an overview of experimental studies focused on struvite precipitation. Struvite precipitation studies using batch reactor were far more frequently encountered than continuous reactor investigations. Batch experiments were performed with 1-L beakers (Galbraith & Schneider, 2014; Ronteltap et al., 2007) or even at smaller scales (Le Corre, Valsami-Jones, Hobbs, & Parsons, 2007; Nelson, Mikkelsen, & Hesterberg, 2003) to determine experimental kinetic parameters and solubility characteristics in struvite. Small batch-scale experiments can provide an idea of kinetic mechanisms in struvite precipitation (Mehta & Batstone, 2013), however, at least a 4-L reactor is suitable for industrial scale-up (Mullin, 2001).

Measurements of pH were used as a monitoring and adjustable variable, without considering solution thermochemistry. A fed-batch pilot scale process has been operated using a simple and low concentrated nutrient, with pH as monitoring variable (Md. I. Ali & Schneider, 2006), however this approach could not be suitable with urine feed, since pH is highly buffered and gives no valid process information.

Experimental model validation in struvite precipitation can be assessed by comparing predicted and laboratory data. Most of analytical data were used to estimate parameters to fit simple (Nelson et al., 2003), and more complete (Galbraith, Schneider, & Flood, 2014) process kinetic models. Some studies have assessed the reliability of a model by only plotting measured and predicted data without including analytical uncertainty (Kazadi Mbamba, Tait, Flores-Alsina, & Batstone, 2015; Nelson et al., 2003). Other studies estimated the analytical uncertainty by considering sample preparation, dilution and glassware uncertainty (M. Burns, Natividad Marin, & Schneider, 2016). Propagation of uncertainty

in samples can provide a range where predicted data can be assessed. Some key cases of experimental errors and sources of uncertainties in struvite precipitation are cited as follows:

- Nutrient recovery studies using complex solutions such as urine (Ronteltap et al., 2007) did not assessed the possibility of analytical interferences in P and Mg analysis.
- Elemental mass balance of Mg and P before and after precipitation has not been developed in previous studies. This assessment improves reliability of distributed elemental composition in liquid and the solid phases. As a consequence, a more reliable Mg/P molar ratio can be measured in which unity indicates likely presence of struvite.
- Struvite purity has been excessively claimed by $X-ray$ diffraction in solid samples. This technique only provides an assessment of possible solid phases, but it cannot confirm that the overall solid is struvite. The analysis NH_3-N in the solid could suggest an approximate content of struvite in the solid phase because struvite is the only solid containing N.
- Insufficient information of sampling procedure during reactor operation. Continuous struvite precipitation modelling showed that the final quantity of struvite depends on the initial quantity of struvite (Schneider, Wallace, & Tickle, 2013). Therefore, extracting several samples from a small capacity reactor (Wilsenach et al., 2007) increases the gap between measured and predicted struvite mass. Implementing a mathematical model, considering the quantity of samples taken at different times, could adjust the real predicted struvite mass.
- Inappropriate selection of drying temperature (> 100 °C) for struvite samples has been previously reported (Harada et al., 2006). The presence of six molecules of water in struvite molecule structure can suggest that lower dehydration temperature is suitable to avoid molecular water loss because of excessive temperature. Other studies have been used dehydration temperatures between 40 °C to 50 °C (Md. I. Ali & Schneider, 2006), 30 °C (Ronteltap, Maurer, Hausherr, & Gujer, 2010), or even air drying (Suzuki et al., 2007), which relates lack of agreement between struvite dehydration procedure from different research works.

- Excessive reliance on laser diffraction, without considering presence of aggregates in struvite precipitation. Aggregates can be measured as bigger particles instead of several sticked nuclei. Sample sonication was applied to contrast mean particle size of aggregated (non-sonicated) and non-aggregated (sonicated) struvite crystals, showing significant differences (Burns, Natividad Marin, & Schneider, 2016). Coulter Counter could provide more reliable data since it counts particles passing a small aperture tube through impedance signal. However, Coulter Counter has not been previously tested in continuous and larger scale experiments, but only in batch experimentation (Galbraith et al., 2014).

Based on previous statements, struvite precipitation research tends to collect limited or poor quality experimental data from short and rushed experiments and then adds mathematical model complexity to compensate for this weakness. This work provides a clearer experimental approach, by assessing analytical methodologies and it applies simulations to deliver better *a priori* experimental conditions.

1.4 Thesis objectives

This study aimed to increase our understanding of continuous struvite precipitation at bench-scale by assessing the following:

i. Develop a dynamic model to predict nutrient recovery rate at arbitrary operating conditions.

ii. Sensitivity analysis of variables in a continuous process to select suitable operating conditions.

iii. Evaluation of kinetic parameters from experimental data.

iv. Validation of model against an independent process data.

In regards to objective (i), a dynamic model predicting nutrient recovery from wastewater source was previously assessed (Kazadi Mbamba, Batstone, Flores-Alsina, & Tait, 2015), however, it was developed in a batch reactor with a nutrient different than urine source. A dynamic model describing a continuous struvite precipitation reactor has been studied for the case of urine (Schneider et al.,

2013) with a power law kinetic model (M I Ali & Schneider, 2008). In previous model, the effect of surface area as a driving force for precipitation has been mentioned, but not clearly assessed through modelling and simulations using different operating conditions.

In regards to objective (ii), previous work had studied continuous struvite precipitation in a mixed suspension mixed product removal (Koralewska, Piotrowski, Wierzbowska, & Matynia, 2009). This thesis studied a reactor where the liquid phase is continuously leaving the reactor, while the solid phase was kept within the vessel.

In regards to objective (iii), kinetic parameters in struvite precipitation have been evaluated for batch systems, considering a power law model (Harrison, Johns, White, & Mehta, 2011) and population balance models (Galbraith et al., 2014). However, previous studies have not identified the magnitude of kinetic parameters suitable for a continuous bench-scale struvite reactor. This thesis intends to design experiments using kinetic parameters from literature review, but corroborate their magnitude after performing continuous experiments.

In regards to objective (iv), model and experimental data in continuous reactor with solid retention is a novel approach to develop nutrient recovery through struvite precipitation. Only one work attempted to understand continuous struvite precipitation from urine source through mathematical modelling (Schneider et al., 2013), however, experimental data to validate this model was not collected.

The achievement of the thesis objectives will make continuous reactor operation more consistent since the application of a reactor model provides the advantage of experimental design.

1.5 Research questions

Research questions of this work are related to modelling and experimentation.

The following questions were formulated for the modelling component:

a) *How does one model a struvite precipitation process?*

b) *What is the best way to operate the reactor?*

- *How much magnesium should be added to the urine?*
- *How much initial struvite seeds are necessary?*

The following questions were formulated for the experimental component:

- *Is the model suitable to describe reactor operation?*
- *Which process variables are suitable to validate the model?*

1.6 Thesis structure

This work connects modelling, simulation and experimentation continuously. A general description of every chapter is presented:

- *Chapter 2 combined thermodynamics, mass balance and kinetics to model nutrient recovery*
- *Chapter 3 simulated struvite precipitation and designed experiments for batch, fed-batch and continuous struvite precipitation*
- *Chapter 4 assessed experimental methods to obtain reliable experimental data*
- *Chapter 5 applied the dynamic model to assess continuous reactor operation*
- *Chapter 6 performed continuous experiments in a mixed-mode bench scale reactor and assessed dynamic model predictions*
- *Chapter 7 provided the conclusions and recommendation of this thesis*

2 Modelling of Batch, Fed-batch and Continuous Struvite Precipitation Reactors

---

Highlights:

- *Formulation of a general dynamic model to predict nutrient precipitation*
- *Consideration of the struvite production using a simplified population balance*
- *Discussion of the struvite production rate in terms of crystal growth rate*
- *Application of the dynamic model to batch, fed-batch and continuous operational modes*

2.1 Literature review

This section describes main features to implement within the process dynamic model, which includes thermodynamics, kinetics and the governing mass balance relations.

2.1.1 Thermodynamics

Thermodynamics is very well understood; but its application in wastewater is still in progress. Struvite precipitation was predicted by estimating its saturation index. This estimation was based on the ionic speciation of key ions: Mg^{2+}, NH_4^+ and PO_4^{3-}- in the liquid phase. Thermodynamics predicts struvite saturation index. A positive saturation index represents conditions above saturation, while negative is undersaturation. The estimation of SI_{MAP} requires chemical speciation and solving non-linear equations.

No consensus in the quantity of thermodynamic equations describing struvite precipitation can be found. Studies considered seven equilibrium equations in anaerobic supernatant (Ohlinger, Young, & Schroeder, 1998), urine solutions used carbonate chemistry with 14 equations (Harada et al., 2006), and other urine systems was described with 43 equations, but by adding carbonates, calcium, citrate and oxalate (Kai M Udert, Larsen, & Gujer, 2003).

It is logical to assume that larger quantity of equilibrium equations could provide better predictions especially in real waste water. However, increasing the quantity of equilibrium equations requires more input data and considering "zero" values for unknown concentrations (causing mathematical convergence problems). The equilibrium equations representing struvite precipitation from urine can be chosen based on prior similar research (Ronteltap et al., 2007; Kai M Udert et al., 2003); however, none of previous had developed a methodology to assess which are the most important equilibrium equations. Selection of key equilibrium equation could lead to a more parsimonious thermodynamic modelling description.

2.1.2 Kinetics

The struvite production can be expressed as a function of the mean particle size of every crystal and the number of particles. The particle size distribution has been modelled through population balance, which included kinetic mechanisms nucleation, growth and aggregation (Galbraith et al., 2014). Struvite crystals trend to aggregate, but this effect cannot be directly measured, but only inferred using microscopy (Galbraith, 2011) or sonication (M. W. Burns, 2017). Inclusion of the three mechanism would be suitable for process modelling, however, only one term (growth) could still be useful in system design with more focused on struvite precipitation than crystallisation.

Kinetic modelling can represent the overall struvite production rate as of the elemental concentration of limiting reagent in solution (Harrison et al., 2011; Nelson et al., 2003). A simplified population balance considering only the linear growth rate has been shown to be successful in the past to describe

fed-batch struvite precipitation (M I Ali & Schneider, 2008). This simplified version of the population balance model can be chosen instead of the complete one to assess experiments as a rapidly without immersing in mathematical complexity. The linear growth rate has been chosen in this thesis to predict mean particle size behaviour. This model was expressed as a power law equation including the saturation index and kinetic parameters. Saturation is assessed in this study as a key component of the precipitation driving force, while hydrodynamics and mixing speed are outside the scope of this work.

2.2 General process modelling

This section develops the model including the dynamic mass balance (§ 2.2.2), formulated for continuous struvite precipitation. The struvite production rate incorporated the kinetics (§ 2.2.6) into the dynamic mass balance. The thermodynamics was linked to the model through ionic speciation of every element and the struvite saturation index (SI_{MAP}) within the kinetic equation.

Struvite precipitation stoichiometry is represented by equation 2.1.

$$Mg^{2+} + NH_4^+ + PO_4^{3-} + 6H_2O \overset{K_{sp}}{\rightleftharpoons} MgNH_4PO_4.6H_2O_{(s)} \qquad 2.1$$

Equation 2.1 represents a reversible reaction of struvite precipitation. The reaction between Mg^{2+}, NH_4^+ and PO_4^{3-} ions with six molecules of water forms struvite in solid phase and this equilibrium is governed by the solubility product (K_{sp}). There is a 1:1 stoichiometric ratio between the constituent struvite ions.

2.2.1 Overall precipitation model

Figure 2.1 shows the overall modelling configuration of struvite precipitation. Mass balance, thermodynamics and kinetic components are coupled. Despite fluid dynamics was not included in the model, its effect is not neglected. and characteristics of the systems are reported in following sections.

The mass balance includes the elemental concentration distribution to its ionic species (*i.e.* P element to $P^{3}{}_{4}^{-}O$, HPO_4^{2-} , etc.). The thermodynamic component is key to determine the ionic distribution of the elements in the liquid phase through chemical equilibria. The kinetics connects the mass balance with the thermodynamics through the inclusion of the struvite production rate equation.

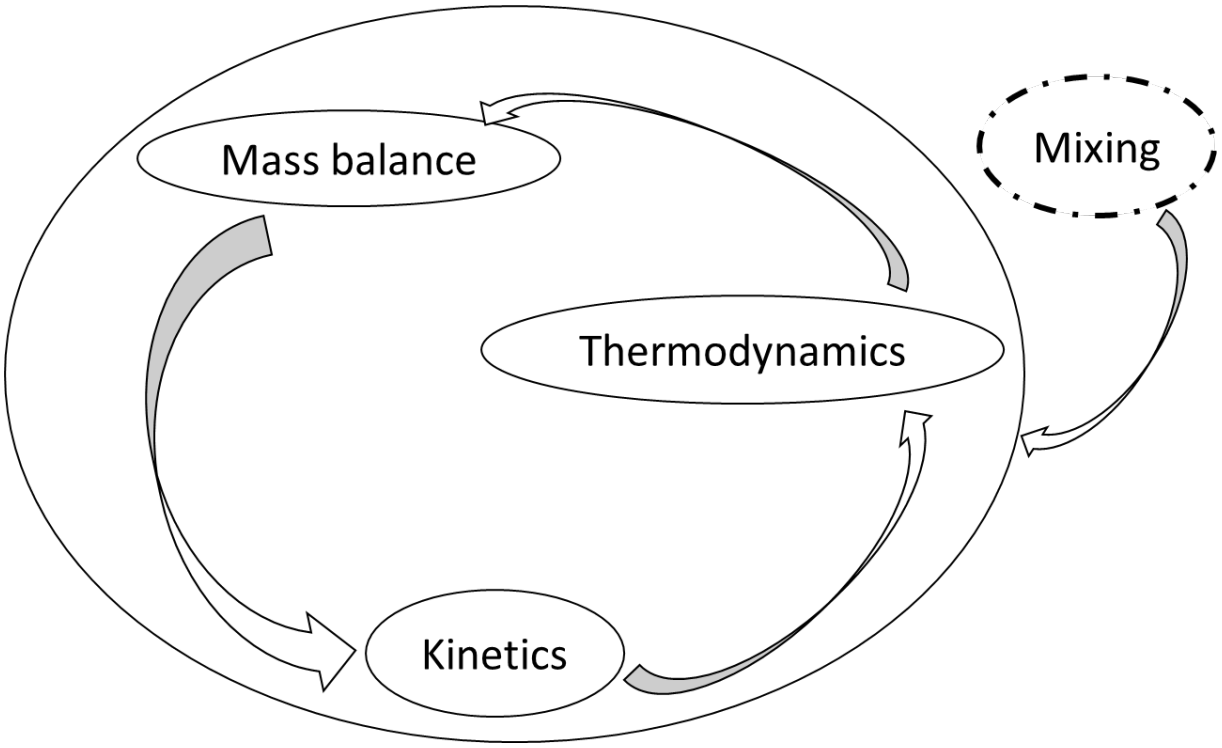

Figure 2.1 – Struvite precipitation modelling scheme, showing the interplay between mass conservation, thermodynamics and kinetics. Mixing also plays a role.

2.2.2 Dynamic mass balance

Figure 2.2 represents a continuous struvite precipitation process that retains the precipitating solid phase within the reactor. The recovery of P is achieved by mixing a Mg stream flow with a nutrient rich solution. The struvite seed will grow over time within the reactor. Growth of struvite crystals is a consequence of the struvite precipitation (equation 2.1). Since the precipitation implies mass transfer of the Mg, N and P from the liquid to the solid phase, the outflow stream leaves the reactor with lower nutrient concentration. Continuous mixing was applied to the reactor to keep particles suspended. Loss of particles in the outlet is considered negligible.

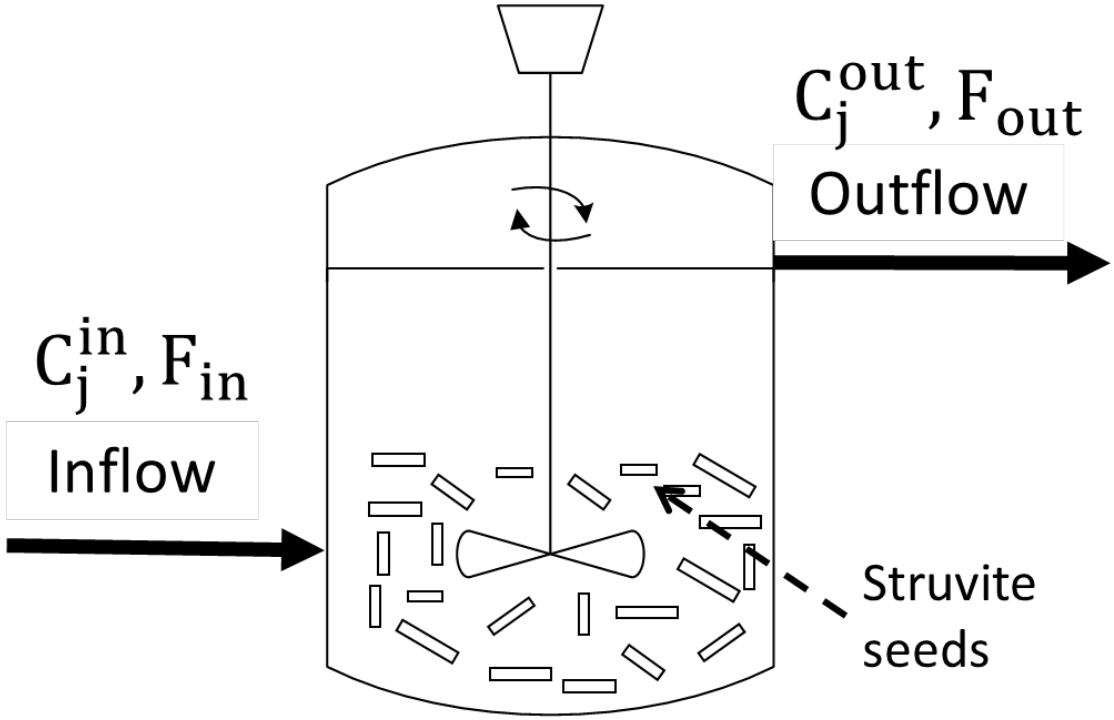

Figure 2.2 – Reactor with a nutrient rich inflow and nutrient depleted outflow, showing solid crystals retained in the reactor volume

In Figure 2.2, chemical elements are represented by the subscript "j". The total concentration of each of the elements (C_j) is expressed in in mol/L. In a continuous process the inflow and the outflow in L/h are the same to keep the liquid level constant. Equation 2.2 shows the dynamic elemental mass balance, predicting the elemental amount within the reactor over time.

$$\frac{d(n_j)}{dt} = \dot{n_{j,in}} - \dot{n_{j,out}} - \nu_{j,i} \cdot Rate_{solid} \qquad 2.2$$

The variable n_j is the molar amount of element j, expressed in moles, the $\dot{n_{j,in}}$ is the molar rate of element j entering to the reactor in mol/h, $\dot{n_{j,out}}$ is the molar rate of the element j leaving the reactor. The stoichiometric coefficient of the solid ($\nu_{j,i}$) is one according to reaction in equation 2.1, which for struvite is always equal to unity. The struvite production rate is *only* included when the elemental mass balances apply to N, P or Mg. The $Rate_{solid}$ term is the struvite production rate, expressed in mol/h.

Equation 2.2 is the main equation of the dynamic mass balance, however, it is written with variables which cannot measure directly. Therefore, this model was expressed as a function of the elemental concentration instead of molar flow rates.

$$\dot{n}_j = C_j \cdot F \tag{2.3}$$

Equation 2.3 expresses the molar rate ($\dot{n}_j$) as a function of the elemental concentration (C_j) in mol/L and flow rate (F) in L/h. Since the process is in continuous operation, the level of the liquid phase remains constant and therefore the inflow and the outflow have to have the same numerical value.

The molar amount in equation 2.2 can be expressed as a function of concentration and volume.

$$\frac{d(n_j)}{dt} = \frac{d(C_j \cdot V)}{dt} = \frac{d(C_j^{out} \cdot V)}{dt} = \frac{d(C_j^{out})}{dt} V + \frac{d(V)}{dt} C_j^{out} \tag{2.4}$$

Equation 2.4 contains four equivalent terms to introduce the concentration variable in equation 2.2. The quantity of moles (mol) was expressed in the second term of the equation as the multiplication of the concentration and the volume of liquid in the reactor. Since the model assumes a perfectly mixed reactor, the concentration of the element "j" is the same of the same element in the outlet stream. The fourth term of equation 2.4 expressed the derivative of the product between concentration of the element "j" in the outlet (mol/L) and the volume of the liquid phase. In the last term, dV/dt represents the change of liquid volume as the struvite precipitation progresses.. The change of liquid volume (L/h) is caused by the struvite solid production, which decreases the liquid volume as the solid volume increases in a fixed reactor volume. The last term of equation 2.4 is included as the first term in equation 2.2.

$$\frac{d(C_j^{out})}{dt} V + \frac{d(V)}{dt} C_j^{out} = C_j^{in} \cdot F_{in} - C_j^{out} \cdot F_{out} - \nu_{j,i} \cdot Rate_{solid} \tag{2.5}$$

Equation 2.5 showed the implemented equation to be solved during simulations. This equation is more practical for simulation purpose because it estimates the expected elemental concentration in the outlet stream.

2.2.3 Mass and quantity of particles

The struvite mass within the reactor can be correlated to the occupied volume and the struvite moles. Equation 2.6 defines the struvite mass m_{MAP} in (kg) as the product of the struvite density (ρ) in (kg/m^3) and the volume of struvite mass in (m^3).

$$m_{MAP} = \rho \cdot V_{MAP} \tag{2.6}$$

During the reactor operation, both m_{MAP} and V_{MAP} are increasing as the precipitation progresses. The mass of struvite (m_{MAP}) in kg can be correlated to the struvite moles N_{MAP} (mol) through the struvite molecular weight (MW_{MAP}) in kg/mol.

$$m_{MAP} = N_{MAP} \cdot MW_{MAP} \tag{2.7}$$

Equation 2.6 and 2.7 correlate the mass with the crystal particle size. This work modelled particles equivalent to spherical volume. The volume of struvite within the reactor (V_{MAP}) is also equivalent to the quantity of particles (Np) multiplied by the individual volume of particle (v).

$$V_{MAP} = Np \cdot v \tag{2.8}$$

Equation 2.8 defines the overall volume of struvite (m^3) as a function of the quantity and volume of every particle. The definition of the individual volume sphere is given in equation 2.9.

$$v = \frac{\pi}{6} \cdot \bar{L}^3 \tag{2.9}$$

Equation 2.9 correlates the sphere volume as a cubic function of the average volume equivalent sphere diameter ($\bar{L}$) in meters. The average volume equivalent sphere diameter will be cited as mean particle diameter in the following chapters.

$$v_0 = \frac{\pi}{6} \cdot \overline{L_0}^3 \qquad 2.10$$

Equation 2.10 shows the estimation of the initial particle volume within the initial mean particle size ($\overline{L_0}$). A key assumption is the constant quantity of particles during the process. Equation 2.11 indicates that the number of particles at any time (N_p) is the same as the initial quantity of particles (N_{p0}).

$$N_p = N_{p0} = \frac{V_{MAP_0}}{v_0} \qquad 2.11$$

Equation 2.11 describes the number of particles as the division between the initial struvite volume with the individual volume of one particle.

$$N_p = N_{p0} = \left(\frac{\pi}{6}\right)^{-1} \cdot \overline{L_0}^{-3} \cdot V_{MAP_0} \qquad 2.12$$

Equation 2.12 merges equation 2.10 and 2.11. This conversion expressed the number of particles as a function of the initial particle size and initial struvite volume.

$$N_p = N_{p0} = \left(\frac{\pi}{6}\right)^{-1} \cdot \overline{L_0}^{-3} \cdot \frac{m_{MAP_0}}{\rho} \qquad 2.13$$

Equation 2.13 combines equation 2.6 and 2.12 to estimate the initial volume of struvite as a function of the initial mass of struvite seed and the initial mean particle size. Equation 2.14 describes the quantity of particles as a function of the initial struvite moles (N_{MAP}) using equation 2.7.

$$N_p = N_{p0} = \left(\frac{\pi}{6}\right)^{-1} \cdot \overline{L_0}^{-3} \cdot \frac{N_{MAP_0} \cdot MW_{MAP}}{\rho} \qquad 2.14$$

Equation 2.13 and 2.14 estimate the quantity of particles in the process.

2.2.4 Struvite volume increase

Continuous struvite precipitation implies change in the struvite volume within the reactor. The increase of the struvite volume can be expressed as a differential equation.

$$\frac{dV_{MAP}}{dt} = N_p \cdot \frac{dv}{dt} \qquad 2.15$$

Equation 2.15 shows the derivative of equation 2.8. In this equation every term of the equation is express as m^3/h. The quantity of particles is the same ($N_p = N_{p0}$). The derivative of the individual particle volume can be estimated with the initial mean particle size from equation 2.9.

$$\frac{dV_{MAP}}{dt} = N_p \cdot 3 \cdot \frac{\pi}{6} \cdot \bar{L}^2 \cdot \frac{d\bar{L}}{dt} \qquad 2.16$$

Equation 2.16 shows the increasing rate of the overall struvite volume calculated with the quantity of particles, the square of the mean particles size and linear growth rate of the mean particle size (d_L/dt).

2.2.5 Struvite production rate

The struvite production rate is the increase of struvite moles over time. The mathematical expression is given in equation 2.5. This section aims to correlate the struvite model increase as a function of the increase in mean particle size of every particle.

$$Rate_{solid} = \frac{dN_{MAP}}{dt} \qquad 2.17$$

Equation 2.17 introduces the solid rate production already cited (equation 2.2 and 2.5). To determine the rate of change in the struvite moles over time, the equation 2.6 and 2.7 were employed.

$$N_{MAP} = \frac{m_{MAP}}{MW_{MAP}} = \frac{\rho}{MW_{MAP}} V_{MAP} \quad 2.18$$

Equation 2.18 expresses the struvite moles (N_{MAP}) as a function of the struvite volume in m^3. The next step was calculating the derivative of the equation 2.18.

$$\frac{dN_{MAP}}{dt} = \frac{\rho}{MW_{MAP}} \cdot \frac{dV_{MAP}}{dt} \quad 2.19$$

Equation 2.19 represents the rate of struvite mole increase as a function of the struvite volume increase within the reactor. The rate of volume increase has been calculated in previous section.

$$\frac{dN_{MAP}}{dt} = \frac{\rho}{MW_{MAP}} \cdot \left[N_p \cdot 3 \cdot \frac{\pi}{6} \cdot \bar{L}^2 \cdot \frac{d\bar{L}}{dt} \right] \quad 2.20$$

Equation 2.20 results from placing equation 2.16 into equation 2.19. This equation shows that the struvite mole production (mol/h) is directly proportional to the number of particles, the square of the mean particle size (related to interfacial surface area) and the linear growth rate of each individual particle.

$$\frac{dN_{MAP}}{dt} = \frac{\rho \cdot \pi}{2 \cdot MW_{MAP}} \cdot N_p \cdot \bar{L}^2 \cdot \frac{d\bar{L}}{dt} \quad 2.21$$

Equation 2.21 is the same equation 2.20 with reorganised variables. Since this equation has a square of the particle size, the total surface area (S) is introduced in equation 2.21.

$$S = N_p \cdot \pi \cdot \bar{L}^2 \quad 2.22$$

Equation 2.22 shows the overall surface area in m^2 calculation, which is based on the number of particles and the square of the mean particle size. A continuous reactor operation implies that the struvite will grow, and therefore the overall particle size.

$$\frac{dN_{MAP}}{dt} = \frac{\rho}{2 \cdot MW_{MAP}} \cdot S \cdot \frac{d\bar{L}}{dt} \quad 2.23$$

Equation 2.23 includes the surface area equation from equation 2.22 into equation 2.21.

The struvite production rate in mol/h can also be expressed as a function of the initial particle size. This equation was estimated by merging equation 2.13with equation 2.21.

$$\frac{dN_{MAP}}{dt} = \frac{\rho \cdot \pi}{2 \cdot MW_{MAP}} \cdot \left[\left(\frac{\pi}{6}\right)^{-1} \cdot \overline{L_0}^{-3} \cdot \frac{N_{MAP_0} \cdot MW_{MAP}}{\rho}\right] \cdot \bar{L}^2 \cdot \frac{d\bar{L}}{dt} \quad 2.24$$

Equation 2.24 suggests that the struvite production rate can be expressed as the change of the mean particle size multiplied by the square of the mean particle size. The initial mean particle size (L_0) and the initial struvite mass (N_{MAP_0}) are known initial condition variables.

$$\frac{dN_{MAP}}{dt} = 3 \cdot N_{MAP_0} \cdot \frac{\bar{L}^2}{\overline{L_0}^3} \cdot \frac{d\bar{L}}{dt} \quad 2.25$$

Equation 2.25 shows equation 2.24 after simplification of other constants such as molecular weight and the density.

$$\frac{dN_{MAP}}{dt} = \frac{3}{MW_{MAP}} \cdot m_{MAP_0} \cdot \frac{\bar{L}^2}{\overline{L_0}^3} \cdot \frac{d\bar{L}}{dt} \quad 2.26$$

The struvite production rate can be also calculated with the initial struvite mass using equation 2.7.

2.2.6 Inclusion of kinetic component

Kinetics were assumed to follow a power-law model. An overall growth rate (G) was considered to be a function of struvite saturation index (SI_{MAP}) in equation 2.27 (Md. I. Ali & Schneider, 2006).

$$G = \frac{d\bar{L}}{dt} = k \cdot SI_{MAP}^{n} \quad 2.27$$

Where k is the rate coefficient and n is the kinetic order. This model considered an equivalent sphere diameter for struvite crystals ($\bar{L}$), and negligible nucleation.

The linear growth rate expression (G) has already been shown in equation 2.16. Section 2.2.5 presented four key equations to determine the struvite production rate as a function of the linear growth rate (equation 2.21, 2.23, 2.25 and 2.26). Equation 2.27 was introduced in these equations.

$$\frac{dN_{MAP}}{dt} = \frac{\rho \cdot \pi}{2 \cdot MW_{MAP}} \cdot N_p \cdot \bar{L}^2 \cdot k \cdot SI_{MAP}^n \qquad 2.28$$

Equation 2.28 represents the struvite production rate as a function of the number of particles, the mean particle size and the saturation index. In this equation, the mean particle size also depends on the linear growth rate, while the quantity of particles can be estimated from the initial struvite mass and the initial mean particle size as stated in equation 2.13.

$$\frac{dN_{MAP}}{dt} = \frac{\rho}{2 \cdot MW_{MAP}} \cdot S \cdot k \cdot SI_{MAP}^n \qquad 2.29$$

Equation 2.29 includes the overall surface area (S) in m^2. This is the simplest version of the struvite production rate, and it clearly expresses the influence of the surface area and saturation in the overall struvite production rate. This equation shows that the surface area and the saturation index are inversely proportional for a constant struvite production rate. An increase in the surface area could lead a decrease in the saturation index, and therefore more proximity to equilibrium condition in continuous struvite precipitation.

$$\frac{dN_{MAP}}{dt} = 3 \cdot N_{MAP_0} \cdot \frac{\bar{L}^2}{\bar{L_0}^3} \cdot k \cdot SI_{MAP}^n \qquad 2.30$$

Equation 2.30 describes struvite production rate as a function of the initial struvite moles, the initial mean particle size, the mean particle size and the saturation index. In this equation the estimation of

the initial quantity of struvite moles can be accomplished by considering the initial struvite mass (seed).

$$\frac{dN_{MAP}}{dt} = \frac{3}{MW_{MAP}} \cdot m_{MAP_0} \cdot \frac{\overline{L}^2}{\overline{L_0}^3} \cdot k \cdot SI_{MAP}^n \quad 2.31$$

Equation 2.31 shows the most practical version of the struvite production rate, where struvite mass and the initial mean particle size are known information during struvite production.

2.2.7 Thermodynamic component

Struvite Saturation Index (SI_{MAP}) was estimated with equation 2.32

$$SI_{MAP} = log_{10}\left(\frac{IAP}{K_{sp}}\right) = log_{10}\left(\frac{a_{Mg^{2+}} \cdot a_{NH_4^+} \cdot a_{PO_4^{3-}}}{K_{sp}}\right) \quad 2.32$$

Where the numerator of previous logarithm relation represented the ion activity product (IAP) of the struvite ionic species (M. Burns et al., 2016; Galbraith & Schneider, 2014). The chemical activities of key ionic species ($a_{Mg^{2+}}$, $\cdot a_{NH_4^+}$, $\cdot a_{PO_4^{3-}}$) were estimated by chemical speciation using activity coefficients.

Debye-Hückel modified by Davies equation (equation 2.33) estimates the mean activity coefficients (Snoeyink & Jenkins, 1980) up to ionic strength (μ) of 0.2 M (Mullin, 2001) or 0.5 M (Ronteltap et al., 2007).

$$-log_{10}\gamma = AZ_i^2\left[\frac{\mu^{1/2}}{1 + a \cdot \mu^{1/2}} + b \cdot \mu\right] \quad 2.33$$

In equation 2.33, Z_i is the ionic valence ($\pm$1, $\pm$2 and $\pm$3),"a" is 1 and "b" is - 0.2 or - 0.3 at 25 °C depending on the year's (1938 or 1962) reference (Sohnel & Garside, 1992).

Bromley model predicts the activity coefficients at ionic strength (μ) up to 6 M (Sohnel & Garside, 1992); however, ionic contribution parameters such as HCO_3^-, $MgHCO_3^+$, $MgPO_4^-$, $NaHPO_4^-$, $MgOH^+$, $CaPO_4^-$ *and* $CaOH^+$, are not specified. The excessive ammonium compounds could limit its application in nutrient recovery (Bromley, 1974). Equation 2.34 can be applied up to 1.2 M ionic strength (Samson, Lemaire, Marchand, & Beaudoin, 1999) with the advantage of avoiding numerous interaction coefficients like models such as Pitzer or SIT (Fevotte, Gherras, & Moutte, 2013).

$$ln\,\gamma = -A' Z_i^2 \left[\frac{\mu^{1/2}}{1 + a' \cdot B' \cdot \mu^{1/2}}\right] + [-4.17 \times 10^{-15} \cdot \mu + 0.2] \cdot A' \cdot Z_i^2 \cdot \frac{\mu}{1000^{1/2}} \quad 2.34$$

Where $\mathrm{A'} = 1.172$, $\mathrm{B'} = 3.33 \times 10^9$, $\mathrm{a'} = 3.0 \times 10^{-10}$ m.

Equation 2.35 describes the charge balance (CB), which is key to predict pH solution.

$$CB = \sum C_i \cdot {Z_i}^2 \quad 2.35$$

Where C_i is the ionic concentration of the elements in mol/L, and Z_i is the charge of the ionic species (±1, ±2, and ±3).The model includes the definition of charge balance, which should be zero.

The "CB" model variable can be set to zero when compositional information of the liquid is known. In real systems when the liquid composition is partially known, the estimated CB is not zero. Therefore, CB cannot be set zero (even though by definition should be zero) in partially unknown composition solutions.

The thermodynamic description of nutrient recovery from domestic urine considered 8 elements in this research. Each element consisted in ionic complexes in dissolution (equation 2.36), and the ionic species concentration were estimated with the equilibrium constant shown in Appendix A.1.

$$C_{j,Total} = \sum C_i \quad 2.36$$

In previous equation, $C_{j,Total}$ is the total elemental concentration of each element in solution in mol/L, and C_i is the ionic concentration of the elements in mol/L.

2.2.8 Description of model solving and assumptions

The initial conditions for solving dynamic simulation were determined by considering a batch reactor model (Appendix B.2). Mass balance in the batch model does not consider the dynamic behaviour of elemental concentration or the struvite mass over time. This program is a tool to determine conditions when struvite is likely to precipitate. The batch model, including ionic chemical speciation and mass balance, was estimated with Engineering Equation Solver (EES). EES is a package which solves equations by blocks without considering a specific equation order. The batch model was solved in two stages:

i. Simulation at non-equilibrium by setting struvite mass to zero and calculating SI_{MAP}
ii. Simulation at equilibrium by setting SI_{MAP} to zero and calculating the struvite solid

To proceed with stage (ii), the selection of the concentration of the elements has to estimate a positive SI_{MAP} in stage (i). The elemental concentration when system achieves equilibrium (stage ii) becomes the initial condition for dynamic simulations. Some batch modelling assumptions and their implications are cited as following:

- Simulations at equilibrium considered that the system achieves a “pseudo” steady state where elemental concentration and struvite solid mass does not change significantly. An implication of this assumption is that predicted elemental concentration in the liquid phase are expected to be lower than measurements. However, this difference is expected to be small or negligible since measurements of equilibrium solution will be developed after several hours when most of the struvite has been precipitated.
- Simulations using batch model considered the only presence of struvite as precipitated solid, which implies the measured solid mass after precipitation could be larger than predicted if there

is presence of other solid phases. Even though, other solid phases could be present previous research using high N concentration solutions (urine) showed that the solid composition Is likely to be struvite (Gadekar & Pullammanappallil, 2009).

- The model also assumes a constant temperature of 25 °C, however, this variable can fluctuate in long time campaigns. Despite temperature variations in real experimentation, this thesis considered its effect negligible or small.
- This model assumes the summation of the ionic charge as zero (CB = 0) because the composition of the solution is fully known for synthetic solutions (unless simulations are developed with partially known composition of real urine).

The development of the dynamic model substitutes the elemental balance (section b.1 in Appendix B.2) by the differential equation (section 4.2 in Appendix B.3). The dynamic model considered the same assumptions from batch model. The initial condition for dynamic simulations considered an initial saturated solution at equilibrium ($SI_{MAP} = 0$). The initial quantity of struvite within the reactor was set to values larger than zero to avoid numerical instability during simulations.

2.3 Process modelling application

The same reactor can be operated in batch, fed-batch and continuous by changing the flow rates. In Figure 2.2, a batch process can be described by setting both the inflow and outflow to zero. In the same figure, eliminating the outflow. This section included assumptions related to continuous struvite production process related to the different zones in the reactor. Additional details about fed-batch operation and batch precipitation was also discussed based on the main dynamic equation.

2.3.1 Continuous reactor modelling

A tall reactor is suitable for continuous struvite precipitation when particles are intended to be kept inside the container. This reactor configuration has uncertainty in selecting the reacting volume because of the presence of two zones. These two zone are the bottom zone where the particles are

suspended and where the nutrient and Mg are feed, and top zone where negligible quantity of particles are present. The top zone is the settling zone.

Figure 2.3 on the left present the likely reactor configuration for continuous experiments. In this reactor there is bed zone with particles and a top where the depleted nutrient with lower concentration of Mg, P and N are leaving the reactor. In this configuration, the mixing speed was keeping the seed in suspension at the approximately the same height.

On the right configuration, it is presented the model approximation considered in following chapters. This reactor model considers two containers, where the bottom container is the one where the reaction occurs. Negligible intermixing between the bottom and top zone is considered at this stage. Therefore, the volume of the reactor considered (effective volume) was the volume of the suspended particles. Among additional assumption about the model application are the following:

- Mixing speed is enough to model the reactor as a continuous stirred tank reactor
- The solid is kept within the container all the time
- The solid is distributed uniformly within the reactor vessel
- Initially there is saturated solution within reactor

2.3.2 Fed-Batch reactor modelling

This reactor configuration is based on the continuous feeding of nutrient without continuous outflow.

- This scenario could be used to produce struvite seeds within the reactor
- The mass balance of this systems should consider the change in the volume over time
- A pilot fed-batch can be operated by continuous or discrete addition of nutrient
- Fed-batch precipitation of solid at laboratory-scale could consider the intermittent addition of nutrient to the reactor. This scenario could provide the advantage of monitored struvite precipitation

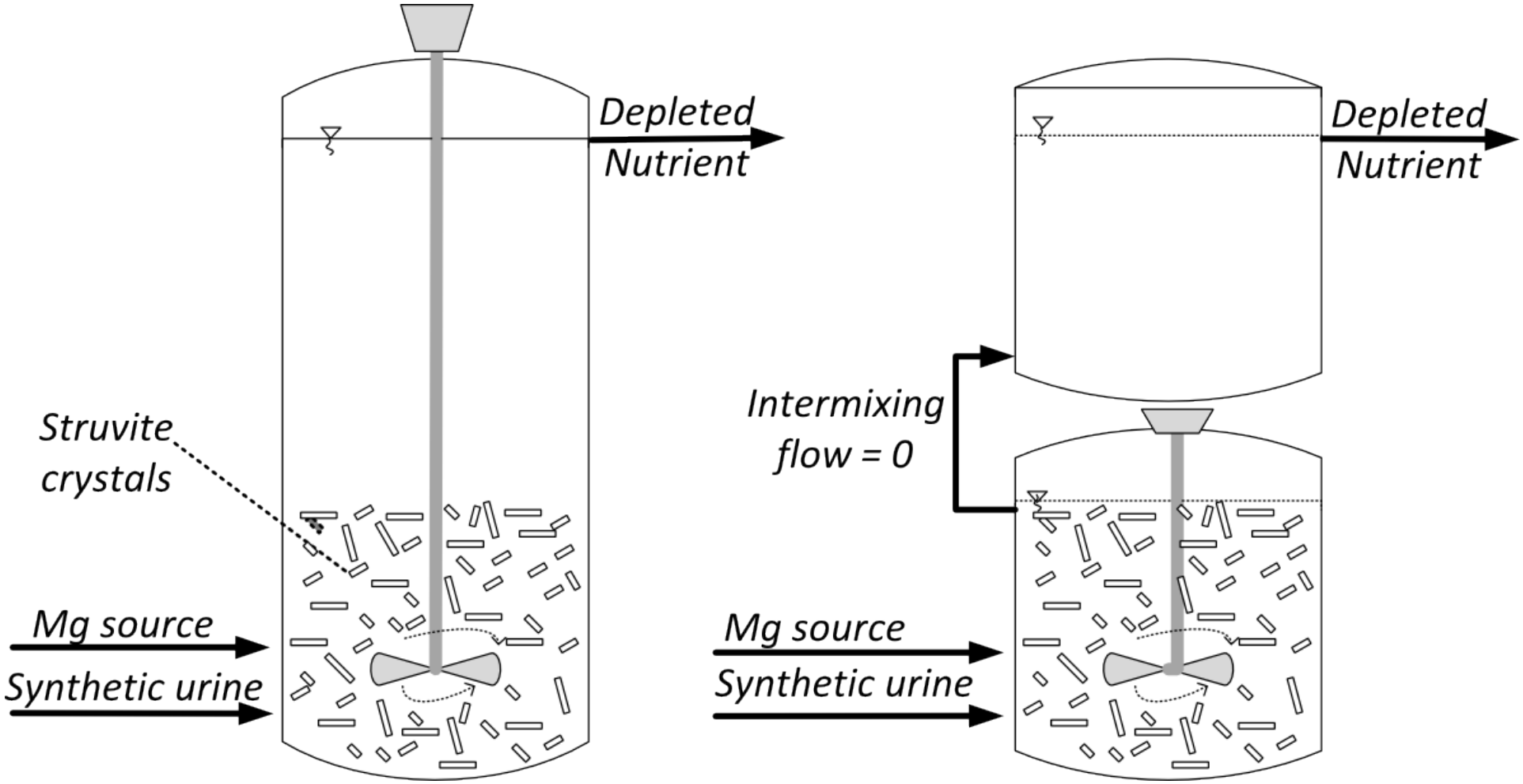

Figure 2.3 – Modelling of the continuous struvite precipitation in this thesis. On the left, typical reactor for continuous experiments. On the right, the assumed model configuration, where bottom vessel is the reaction zone and top vessel is the settling zone. The model considered no intermixng flow at this stage.

2.3.3 Batch reactor modelling

Batch precipitation happens when there is no inflow and neither outflow in Figure 2.2. This type of configuration is the most common in previous struvite precipitation. Its simplicity only requires the addition of the nutrient to precipitate struvite at laboratory-scale. The modelling of this system includes the elemental mass balance and the thermodynamics through chemical speciation.

Equation 2.37 shows the elemental mass balance of P. This balance describes the relationship between the total elemental concentration of this element in the liquid phase in mol/L, ionic elemental components distributed in equilibrium such as phosphates ions and the part of P transferred to the struvite solid after precipitation.

$$C_P = C_{PO_4^{3-}} + C_{H_2PO_4^-} + C_{HPO_4^{2-}} + \cdots + N_{MAP}/V \quad 2.37$$

Where C_P is the total elemental concentration of P in mol/L; $C_{PO_4^{3-}}$, $C_{H_2PO_4^-}$ and $C_{HPO_4^{2-}}$ are the ionic concentration in the liquid solution $[mol/L]$; N_{MAP} are the moles of struvite; and V is reactor volume $[L]$. Similar expressions were formulated for Mg and N, while the other elements are not considered in the N_{MAP}/V, since struvite only contains Mg, N and P.

2.4 Summary

- A dynamic mass balance can describe the composition of elements within a reactor over time
- Activity coefficients of ionic species were calculated with Debye-Hückel modified by Davies equation
- The overall struvite production rate can be described in terms of the linear growth rate
- Linear growth rate was defined as a power-law model considering struvite saturation index as a main variable
- Modelling of struvite batch precipitation did not require inclusion of kinetic component
- Reactors were modelled as perfectly stirred tank reactors

- Modelling of continuous nutrient recovery system considered a two zones reactor with a bottom reaction zone without intermixing flow rate

3 Simulation of Batch, Fed-batch and Continuous Struvite Precipitation

---

Highlights:

- *Thermodynamic model validation in batch struvite precipitation*
- *Thermodynamic assessment of nutrient recovery from synthetic ureolsysed urine*
- *Simulation of fed-batch process for struvite seed production*
- *Assessment of continuous nutrient recovery with dynamic simulations*

3.1 Literature review

This section reviews the determination of urine composition. Previous studies discussing methodologies to estimate chemical speciation and struvite saturation index are presented. A brief discussion of modelling gaps in struvite seed production in fed-batch systems and simulation of continuous experiments is offered.

3.1.1 Urine composition

Urine composition is diverse, because it depends on the nutrient profiles of a range of people. Human urine can be classified as non-ureolysed and ureolysed urine. In the first type ammonia is not released from the urea compound. The ureolysed urine comes from the decomposition of urea into NH_3 and CO_2. Ureolysed urine can be obtained by storing human urine for several weeks to stabilise it (Jönsson, Stenström, Svensson, & Sundin, 1997). The application of ureolysed urine in nutrient recovery is a good choice because of high NH_3 available, and a strongly buffered pH around 9 which could drive struvite precipitation when magnesium is added.

Urine is a good choice for nutrient recovery. Urine as nutrient source contains up to 90 % of N and 80 % of P excreted by humans. Urine source has been used in different studies to facilitate experimentation in laboratory because of absence of organic compounds which could add complexity in modelling assessment. Investigations in struvite precipitation were developed with real urine and synthetic solution sources. Real solutions such as urine (Ronteltap et al., 2007) , swine waste water (Nelson et al., 2003), digester supernatant (Ohlinger et al., 1998) and synthetic solutions containing N, P and Mg have been considered. The main characteristics of urine are high nitrogen concentration and high ionic strength between 0.33 M to 0.56 M (Ronteltap et al., 2007).

Artificial urine was formulated to imitate fresh urine in a close to neutral pH (Griffith, Musher, & Itin, 1976). These cases were formulated randomly, only based on elemental composition similarities. Formulation of synthetic solution considering fresh urine composition comprised urea, inorganic and organic components (Antonin, Santos, Garcia-Segura, & Brillas, 2015; Ipe & Ulett, 2016; Kabore, Ito, & Funamizu, 2016; B. Liu, Giannis, Zhang, Chang, & Wang, 2013; Tilley, Atwater, & Mavinic, 2008b; Wilsenach et al., 2007; Zhang et al., 2011). These formulations contained high urea, low ammonia and organic compounds (Griffith et al., 1976). According to Griffith (Griffith et al., 1976) these synthetic solutions required hydrolysis to release most of the ammonia needed for struvite precipitation (K. M. Udert, Larsen, & Gujer, 2006) which adds an extra step in nutrient recovery studies.

Ureolysed urine after storage, containing low urea and correspondingly high ammonia concentrations, is a more practical and realistic choice as nutrient source. Ureolysed urine contains Na, K, NH_4, Ca, Cl, PO_4, SO_4 and HCO_3^{-1} (Kirchmann & Petterson, 1995). Ureolysed urine composition have a reported a pH of around 9; while fresh artificial urine has neutral pH. Another advantage of ureolysed urine was its larger N concentration which increases the purity of struvite in the precipitated solid (Gadekar & Pullammanappallil, 2009). Artificial ureolysed urine did not consider urea in the formulation, but instead ammonia as inorganic compounds (Ronteltap et al., 2007; Schneider et al.,

2013). This formulation also contains ammonia solution ($NH_{3_{(l)}}$), but application of this compound cannot be applied to bench or full-scale experiments because of the reagent toxicity.

In Figure 3.1, complete ureolysis was assumed when 9 pH was reported (Grau, Rhoton, Brouckaert, & Buckley1, 2012). The effect of environment in urine composition is controversial, because it has been stated a negligible loss of $NH_{3_{(g)}}$ (K. M. Udert et al., 2006); while others suggested the opposite (Tilley, Atwater, & Mavinic, 2008a). This thesis included the elements in larger concentration without including calcium because it triggers precipitation in the nutrient source before magnesium addition.

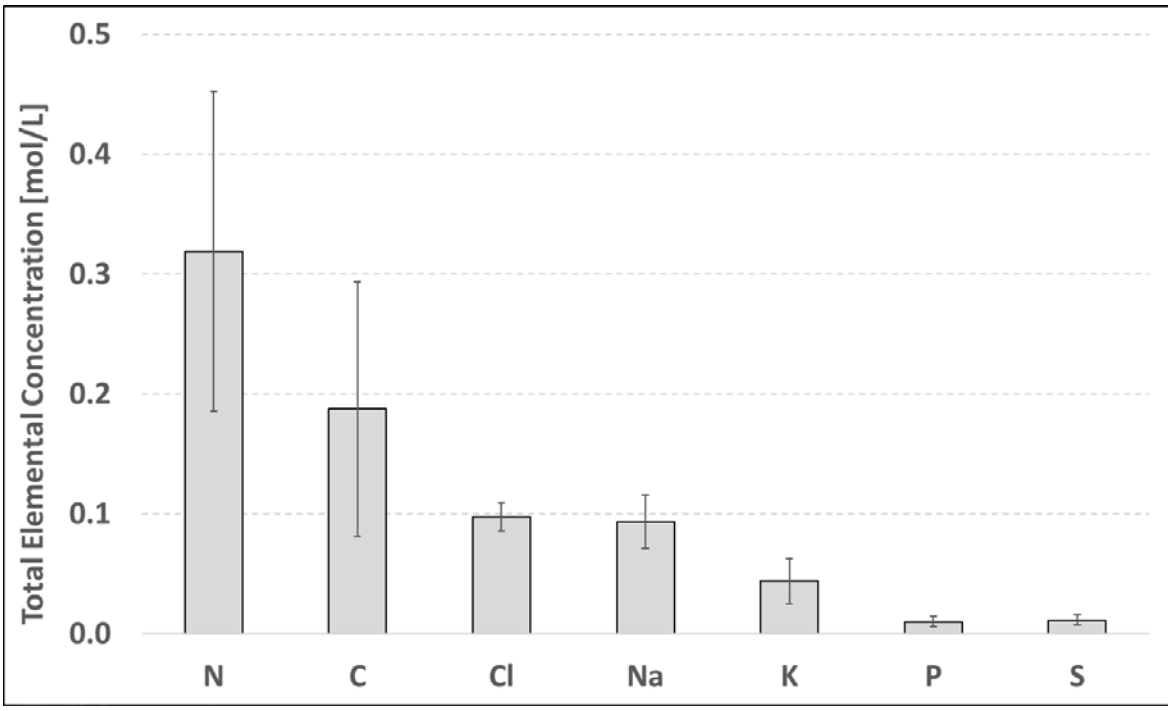

Figure 3.1 — Average composition of ureolysed urine across a range of studies (Barbosa, Peixoto, Meulman, Alves, & Pereira, 2016; Dai et al., 2014; Grau et al., 2012; Jönsson et al., 1997; B. Liu et al., 2013; Z. Liu et al., 2008; Ronteltap et al., 2010; Sakthivel, Tilley, & Udert, 2012; Triger, Pic, & Cabassud, 2012; K. M. Udert et al., 2006; K M Udert & Wächter, 2012). Error bars are presented as +/- 1 standard deviation.

3.1.2 Chemical speciation and saturation index

The selection of the thermodynamic equations and the chemical species for struvite precipitation using urine has not been fully assessed. Considering magnesium phosphate complex has been reported to have an effect in the estimation of solubility product in supernatant (Ohlinger et al., 1998), this indirectly suggests the importance of selecting the ionic species and the equilibria considering the composition of nutrient.

A model describing the struvite precipitation from different cited nutrient sources was implemented to determine the elemental concentration P, N and Mg at equilibrium (Gadekar & Pullammanappallil, 2009). Many other researchers use $PhreeqC$ to simulate solution thermodynamics (Battistoni, Paci, Fatone, & Pavan, 2005; Doyle & Parsons, 2002; Golubev, Pokrovsky, & Savenko, 2001; Harrison et al., 2011; Lee, Weon, Lee, & Koopman, 2003; B. Liu et al., 2013; Nelson et al., 2003; Türker & Celen, 2007) because this technique requires minimal programming. This software calculates with pre-existing equilibrium databases: "Amm", "$Pitzer$", "$MinteqV4$", "$Wateq4f$", "$PhreeqC$", "sit", "$minteq$", "$llnl$" and "ISO", but few studies reported the chosen database for simulations (Roncal-Herrero & Oelkers, 2011; Sakthivel et al., 2012). This situation highlights the strong possibility of inconsistent predictions, despite of using the same elemental input data. For instance,, struvite saturation index from swine waste water at pH = 8.4 (Nelson et al., 2003) was simulated using $PHREEQC$ with different software package database. Simulations showed the following predictions: 0.77 ($MinteqV4$), -27.97 ($Wateq4f$), -27.97 ($PhreeqC$), 1.04 (sit), 0.68 ($minteq$), -28.1 ($llnl$) and -27.97 (ISO). Previous results confirmed that selection of the thermodynamic database should be developed cautiously.

Thermodynamics studies in struvite precipitation from urine source require a deeper assessment in the equilibria to select. Liquid and solid equilibria to simulate struvite precipitation from urine source predicted the precipitation potential and assess the presence of other solid phases different than struvite.(Kai M Udert et al., 2003). Another similar study with urine source found the most relevant

ions and assess the struvite solubility (Ronteltap et al., 2007). This study applied $PHREEQC$ and $AQUASIM$ thermodynamics packages.

3.1.3 Struvite seed production

A common practice is the preparation of struvite seed crystals by mixing reagents without any previous modelling assessment. Previous studies prepared struvite seeds in a stirred 1-L glass reactor/beaker with low concentration of nutrient (0.01 M) (Mehta & Batstone, 2013). Seed preparation was also claimed to be prepared by dissolving previous synthetic crystals in supersaturation solution (Ariyanto, Sen, & Ang, 2014), however, it was not specified where the initial crystals come from.

Struvite batch precipitation could also be considered as a monitored struvite seed production. Some studies focused on kinetics with monitored pH (Nelson et al., 2003; Ohlinger et al., 1998; M S Rahaman, Ellis, & Mavinic, 2008). Struvite seed was also obtained as a sub-product of fines collection from continuous struvite operation (Shimamura, Hirasawa, Ishikawa, & Tanaka, 2006). An intentional continuous struvite seed production in a Poiseuille reactor was attempt, but with scaling difficulties in the long term implementation (M. Burns et al., 2016).

Struvite seed production in fed-batch processes is not a deeply studied topic through process modelling. A pilot fed-batch reactor was modelled using a dynamic model to predict mean particle size by including thermodynamics and kinetic modelling (M I Ali & Schneider, 2008); however, this research was focused on the operational conditions than model validation through pH or elemental composition in the liquid phase.

3.1.4 Simulations of continuous struvite precipitation

A dynamic model was implemented with mass balance, thermodynamics and kinetics to understand the behaviour of struvite precipitation in a continuous reactor using source separated urine (Schneider et al., 2013). This model explored the effect of dilutions and variations in the feed flow rates. Among

the main highlights of the simulations was the demonstration of the robustness behaviour of struvite precipitation despite variations in the model, and the initial insight that struvite saturation index prediction was mostly affected by the limiting component (Mg). Additionally, simulations showed that the addition of $NaOH$ was not needed and the advantage of seeding the reactor to keep low saturation index.

3.2 Thermodynamic evaluation

This section evaluated the dynamic model by predicting published data. The model calculated the quantity of salts to prepare the artificial urine. Simulations were performed to understand the effect of diluting the urine and the Mg addition in saturation index. Assessment of the selected thermodynamic equilibria was accomplished.

3.2.1 Struvite precipitation in a batch reactor

Thermodynamic model was validated with published data (Ronteltap et al., 2007) by comparing composition of equilibrium solution after precipitation. Elemental concentrations of P and Mg were predicted with the batch model at equilibrium because it was reported that minimum elemental concentration was achieved within first hours of struvite precipitation (Ronteltap et al., 2007). Simulations did not consider charge balance as zero because of incomplete composition of real urine, but instead pH was introduced as input data. The model included the conservation of the eight key elements in urine ($Mg,\ N,\ P,\ C,\ Cl,\ Na,\ K$ and S). Simulations were performed using 21 batch precipitations with real hydrolysed urine (Ronteltap et al., 2007). These simulations assumed that only struvite formed and equilibrium conditions (*i.e.* SI_{MAP} = 0) held after leaving the solution to reach a minimum concentration in the liquid phase.

Figure 3.2 shows reasonable agreement of predicted and measured P concentration at $Mg/P < 1$. Simulation were performed with *Debye-Hückel modified by Davies* and *Samson equations to determine activity coefficients*. In both cases, P and Mg concentration in the liquid phase were the

same. This thesis applied Davies model to keep consistency with previous research. Agreement between experimental and predicted data demonstrated that thermodynamic model used in this work was suitable to describe nutrient recovery from urine. Moreover, larger disagreement can be found at low Mg and P concentration in the estimations of the equilibrium solution. This information also suggested that the main solid phase in the precipitated product was struvite, because simulations were developed with this assumption.

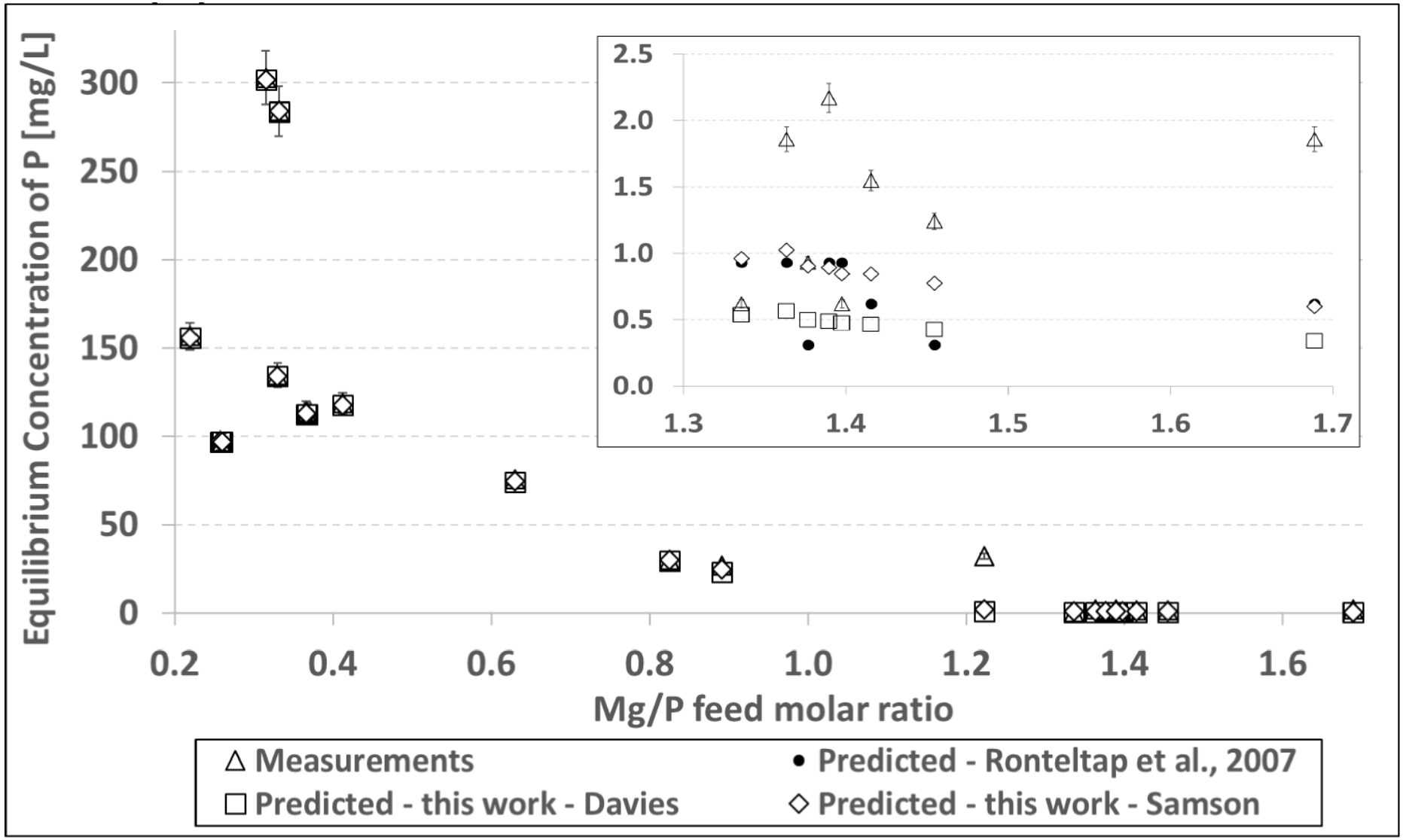

Figure 3.2 — Model validation at equilibrium using P concentrations. Error bars are +/- 1σ.

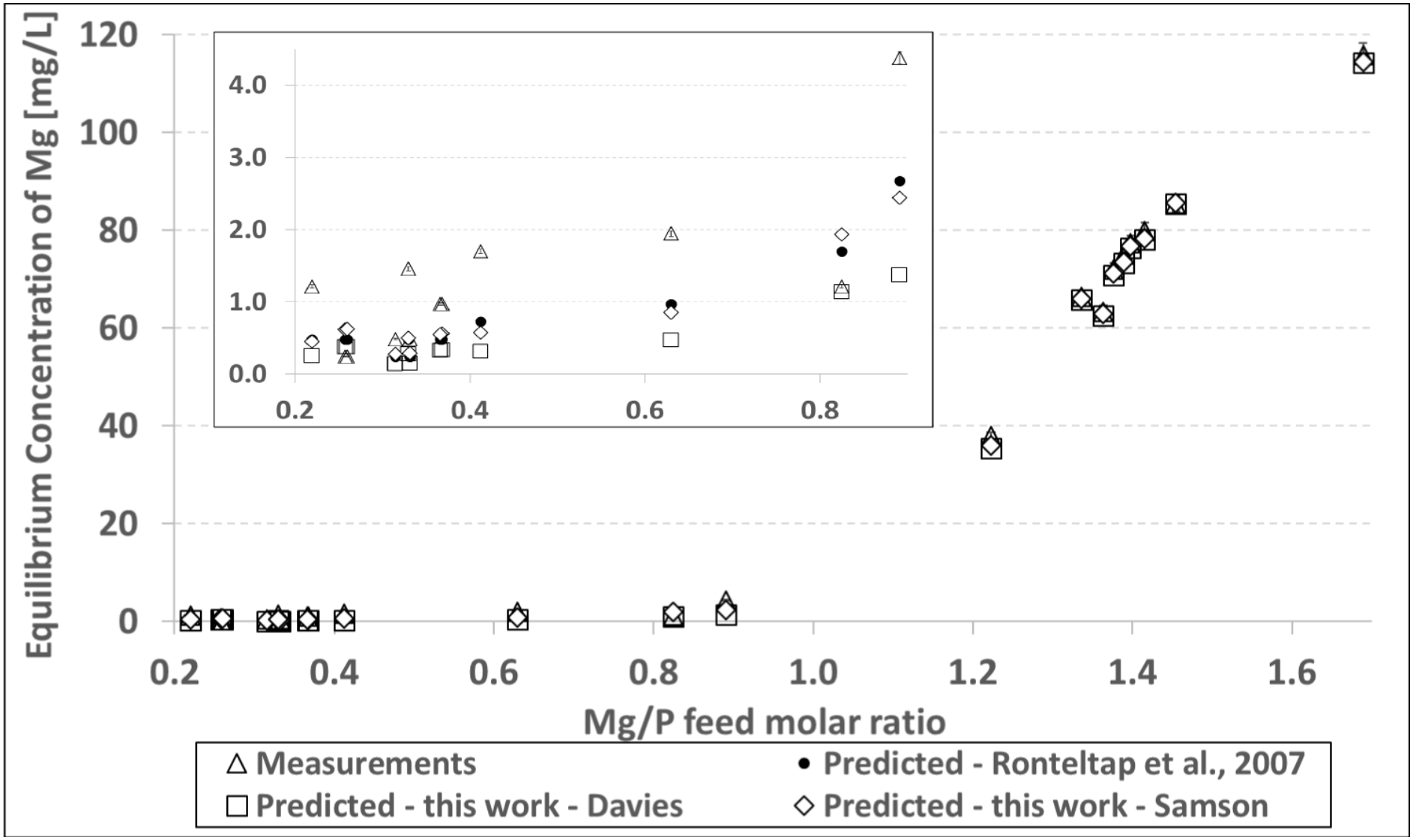

Figure 3.3 — Model validation at equilibrium using Mg concentrations. Error bars are +/- 1σ.

3.2.2 Calculation of salts to prepare synthetic ureolysed urine

Nutrient recovery studies have used both real and synthetic urine to develop an understanding of struvite precipitation. Real urine for nutrient recovery could be fresh (non-ureolysed) or stale (ureolysed). The main difference between both of them is that the later contained nitrogen as ammonia, which is more suitable for struvite precipitation. Previous research using synthetic urine solutions did not specify if the formulated artificial urine was intended to represent fresh or ureolysed urine. This thesis formulated an artificial urine intended to represent ureolysed urine by mixing chemical reagents containing key elements of N, C, Cl, Na, K, P and S. The chosen salts were NH_4Cl, NH_4HCO_3, $(NH_4)_2SO_4$, $NH_4H_2PO_4$. Bases such as $NaOH$ and KOH were included to adjust the pH.to 9. The total concentration of elements in SUU was considered from data in Figure 3.1.

The estimation of the quantity of salts to prepared SUU was developed in a batch model programmed in Engineering Equation Solver (EES). This program estimated the concentration of every salt by setting the elemental concentration of C, Na, S and P with the desired pH (9.0) and ionic strength (0.36 mol/L). The program calculates the concentration of the remaining elements and the quantity of every reagent. Table 3.1 summarised the composition of SUU applied in this research.

Table 3.1 — Recipe to prepare synthetic ureolysed urine

Chemical Salts	Concentration [mM]
NH_4HCO_3	90.80
KOH	50.46
NaOH	72.60
$(NH_4)_2SO_4$	7.40
NH_4Cl	201.53
$NH_4H_2PO_4$	17.80

The estimation of every reagent containing the elements to formulate SUU was required because a poorly designed recipe could cause excessive ionic strength due to chlorides or carbonates attached to N and C elements. In addition, excessive anions can also decrease the solution pH due to charge balance.

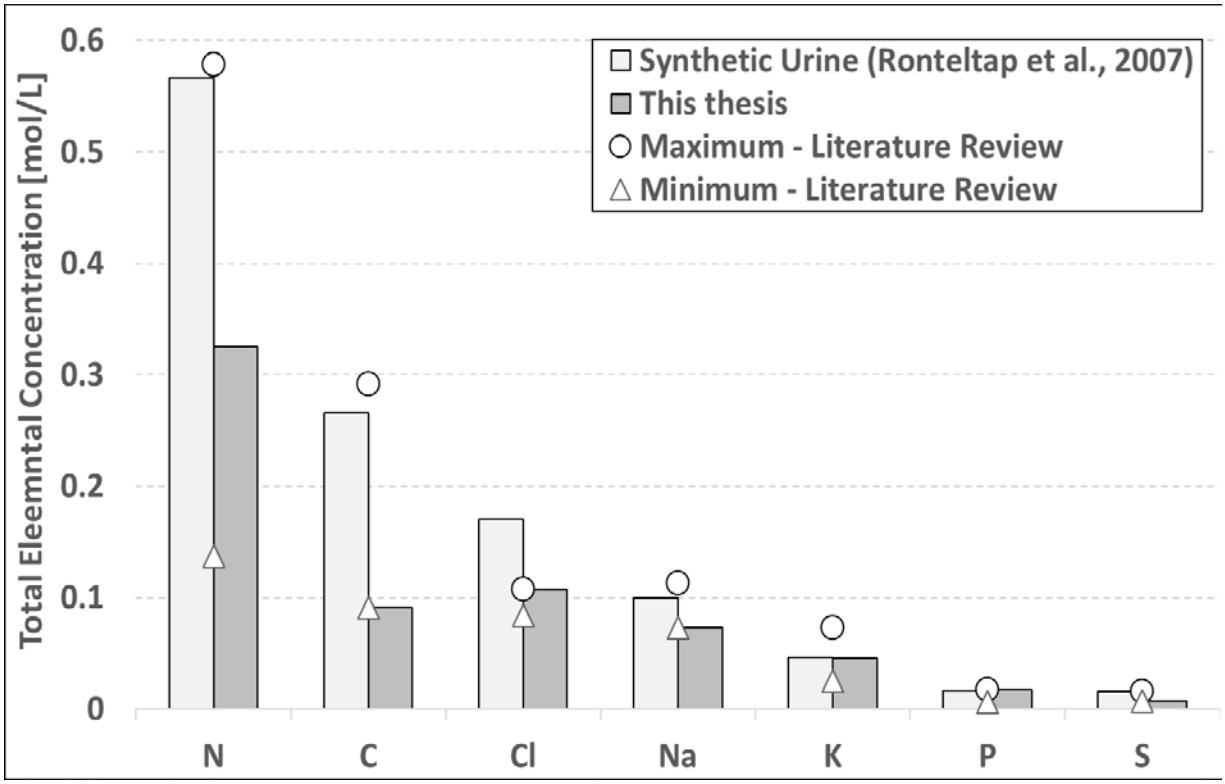

Figure 3.4 — Composition of urine matrix solution. Bar charts represent composition of urine in previous and this research. Marks represented the range of elemental concentration found from literature review discussed in Figure 3.1.

Figure 3.4 represented the elemental concentration of different cases focused on artificial urine composition. This thesis considers a synthetic ureolysed urine of lower concentration than previous similar work (Ronteltap et al., 2007), but it still is inside the elemental concentration range cited by the literature review.

3.2.3 Dilution effect in struvite saturation index

Simulations at non-equilibrium showed that certain small amounts of Mg added to SUU could achieve a saturated condition (*i.e.* $SI_{MAP} = 0$). Figure 3.5 demonstrates that dilution in urine decreased the saturation index. The dilution decreases the elemental concentration of Mg, N and P, and therefore decreases the ionic activities of Mg^{2+}, NH_4^+ and PO_4^{3-}, which are struvite's constituent ions. Simulations were performed to estimate the struvite saturation index, pH and ionic strength and results are show in Figure 3.5.

Figure 3.5 shows that the initial incremental addition of elemental Mg has a big impact on the increase in the SI_{MAP}, because of its limiting concentration. This plot also shows that magnesium addition did not change the pH by more than 0.05 pH over a range of Mg/P feed molar ratio between 0. to 1.4. This means that pH is not expected to change due to Mg addition in the synthetic ureolysed urine. Comparison of different dilution scenarios also indicated that undiluted urine required lower concentration of Mg concentration to achieve the same level of saturation compared to the diluted cases. Additionally, the ionic strength is highly affected by water addition based on this plot because of the change in overall elemental concentration.

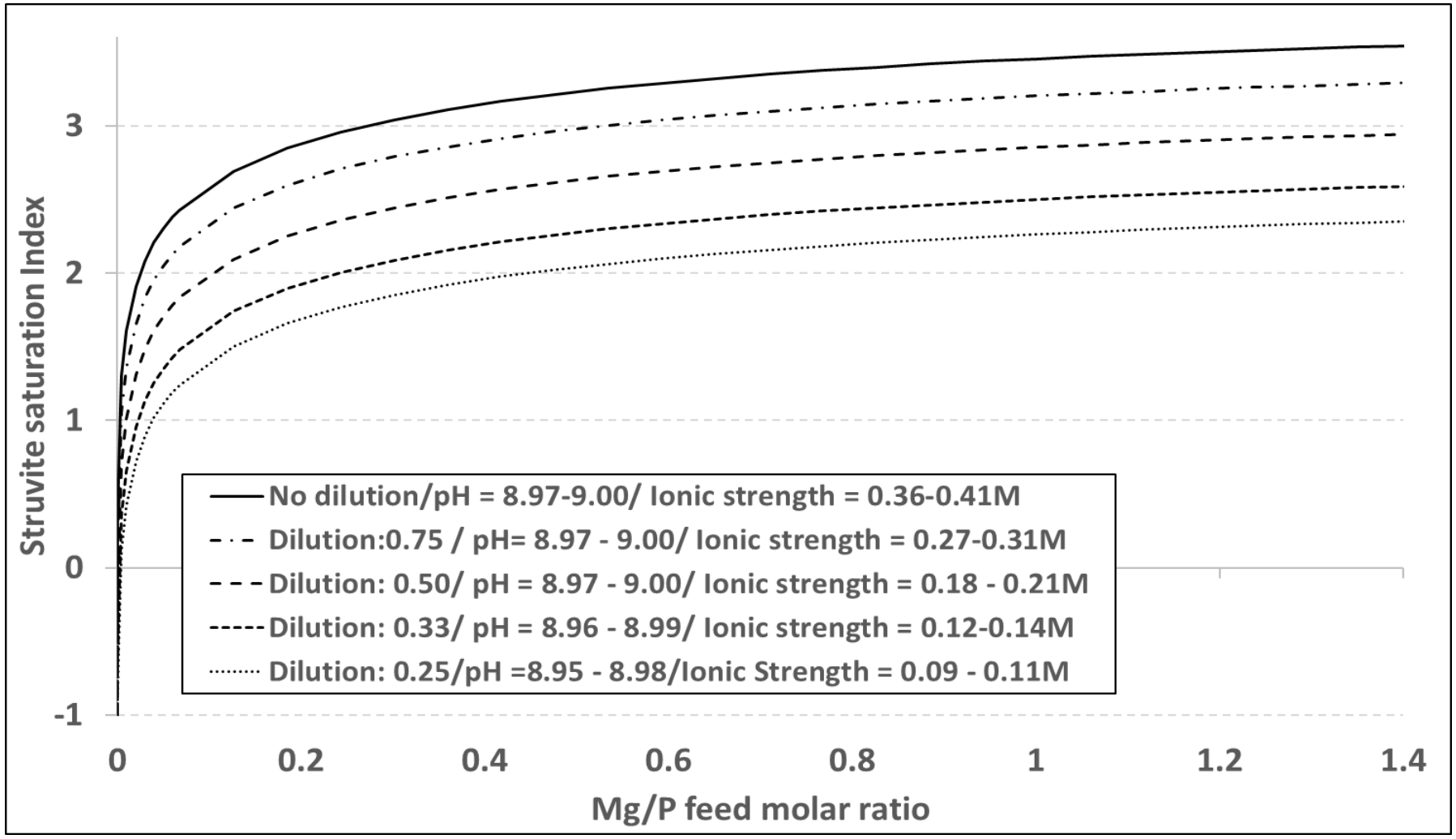

Figure 3.5 — Saturation index prediction from synthetic ureolysed urine at different dilutions. Legend indicate the calculated range of pH and ionic strength in each dilution case.

3.2.4 Selection of thermodynamic equilibria

The importance of considered ionic complexes in thermodynamic calculations depends on the system composition. For instance, the 27 equilibria equations stated in Appendix A.1 could be reduced to a smaller group if the effect of each of them in the calculation of SI_{MAP} is quantified. This section selected the key equilibrium required to describe sufficiently nutrient precipitation from ureolysed urine. To find the most sensitive equilibrium, a 5% uncertainty was set in each pK_{eq}, and then propagation of uncertainty was calculated to determine its effect in the struvite saturation index. Then the relative uncertainty in SI_{MAP} per each pK_{eq} was calculate to order the pK_{eq} from the one with largest to smaller effect in the SI calculation. Engineering Equation Solver has a feature of propagation of uncertainty analysis. Details about this topic are specified in the literature review of next chapter.

Figure 3.6 showed the summary of the uncertainty propagation simulation carried 27 times (number of equilibrium equations) in the synthetic ureolysed urine recipe chosen for this work, and the artificial urine composition cited by (Ronteltap et al., 2007). Simulations were developed at non-equilibrium (struvite mass = 0). This shows that 11 of the 27 equilibria could represent this system in terms of the SI_{MAP}. Equilibria containing the dissociation of HPO_4^-, NH_4^+, $MgPO_4^-$ and $H_2PO_4^-$ have the highest impact in SI_{MAP} but the other 7 equations were also considered to include all 8 key elements in SUU composition.

Despite this selection, it is key to consider that different equilibria could be chosen if the nutrient composition is different. In addition, key equilibria depends strongly on the system pH. However, since this thesis uses urine, the pH is highly buffered at $pH = \sim 9$. The closeness of these results also suggests that the model predictions are robust in the face of variations in feed quality/composition.

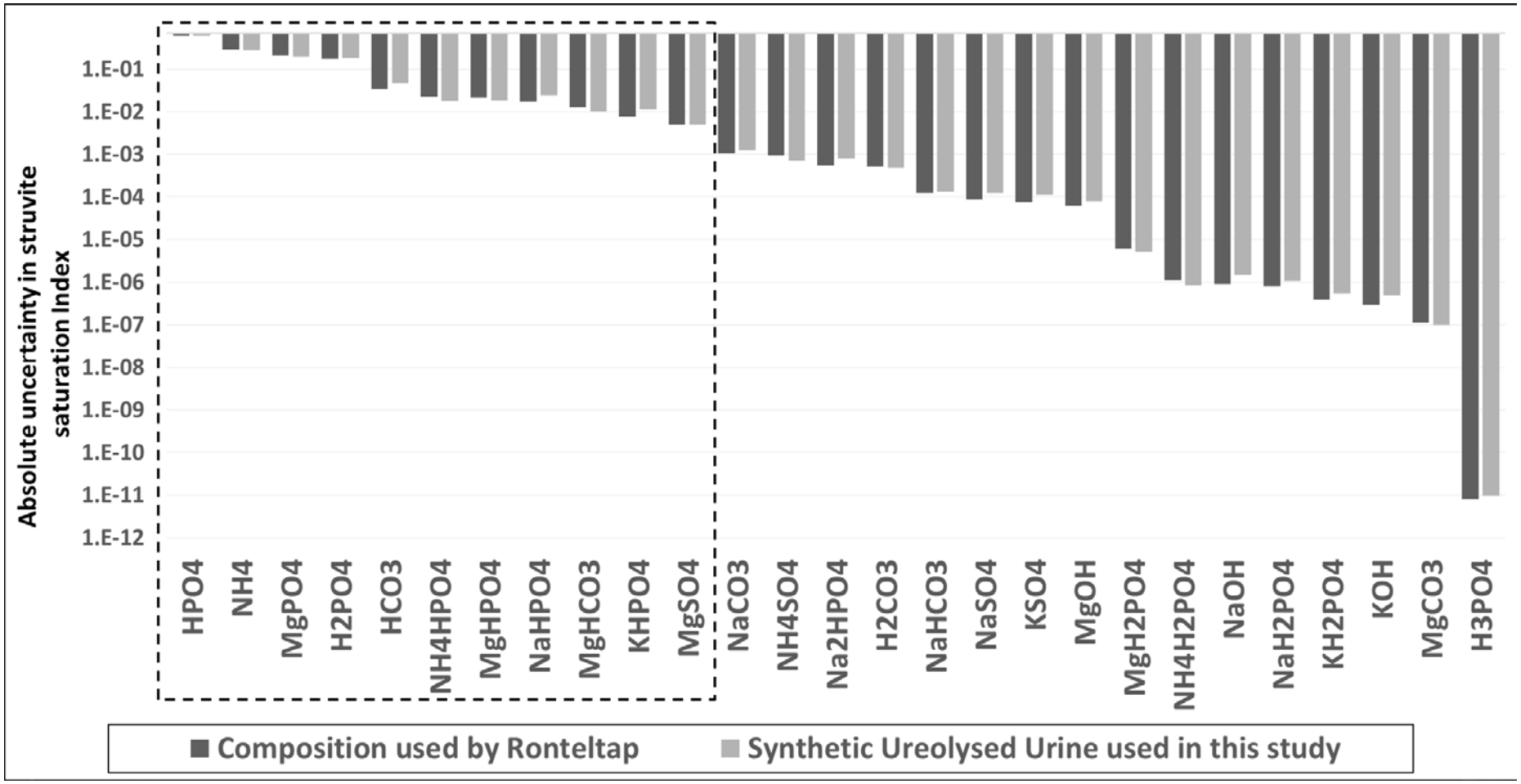

Figure 3.6 — Absolute uncertainty in struvite saturation index using 5% of relative uncertainty in pKeq. The dashed line box indicates the chosen equilibrium equations to include all the eight elements of urine composition.

.

3.2.5 Verification of thermodynamic model

Thermodynamics simulations (solutions) verified the solution consistency in three different software packages: EES, $PHREEQC$ and $gPROMS$. The chosen case was the synthetic urine composition cited by (Ronteltap et al., 2007). Simulations in EES and $gPROMS$ were developed with the employed equilibria (Appendix A.1 and A.2), and the chosen 11 equilibria from § 3.2.4. Simulations using $PHREEQC$ required the elaboration of custom database containing the same equilibrium equation used in EES and $gPROMS$ for consistency in predictions.

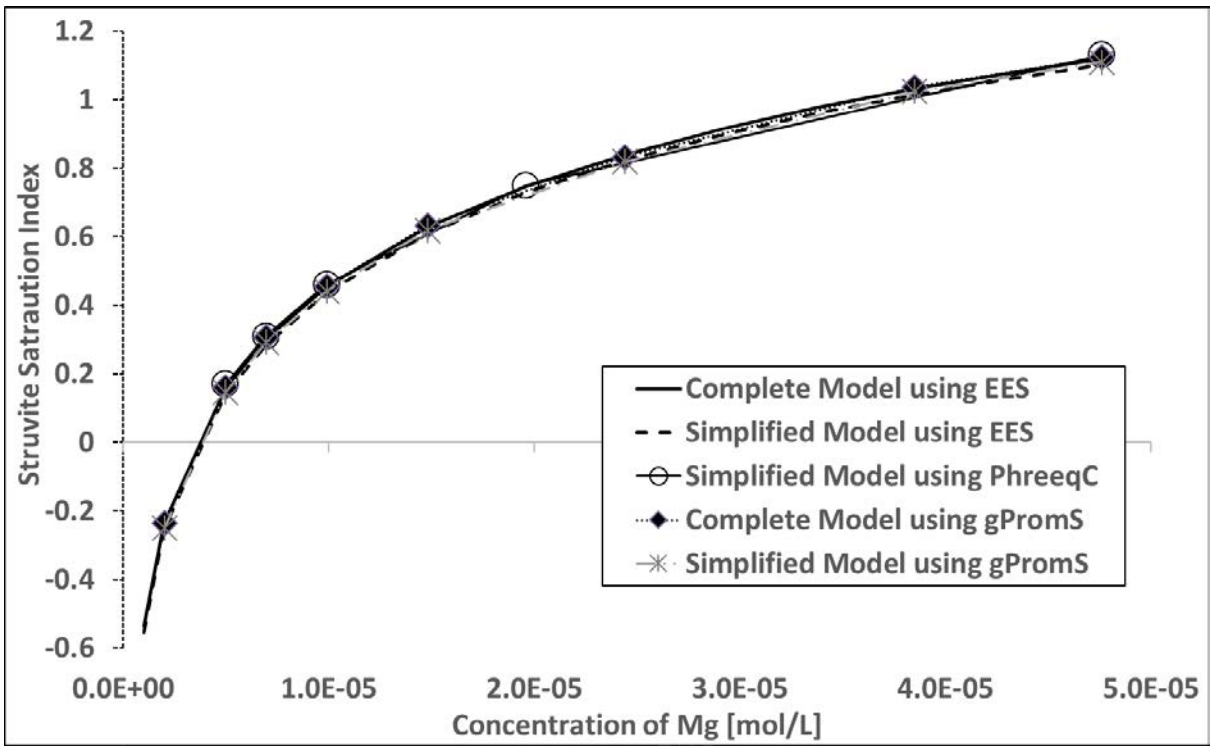

Figure 3.7 — Mathematical verification of the simplified thermodynamics with different solvers

Figure 3.7 showed that simulations accomplished the same SI_{MAP} using every solver at different Mg concentration in the artificial urine. The simplified and complete version of the thermodynamics also predicted the same SI_{MAP} to solve more complex modelling. The absolute different in the SI_{MAP} predicted by the complete and the simplified model is between 0.017 and 0.018 units.

3.3 Fed-batch process

Simulation of a fed-batch process to prepare struvite seed was discussed in this section. The model was presented in the same way it was programmed in in EES. The selection of the initial quantity of particles to run the simulation was also discussed. Fed-batch simulation profiles of key variables such as SI_{MAP}, elemental concentration in liquid phases and struvite mass are provided in the last part of this section. Even though it is possible to prepare seeds by mass nucleation and subsequent mass growth, an intermittent fed batch precipitation was chosen to assess modelling predictions and system behaviour.

3.3.1 Intermittent fed-batch process description

Simulations of a fed-batch system were developed in EES considering a 6-L volume reactor. This system considered an increasing volume during the intermittent addition of reagent with pipettes. Pulses of reagent were added at set time intervals because the purpose of this experiment was to observe the desaturation behaviour, where a maximum SI_{MAP} is achieved and it drops to a minimum at equilibrium. Addition of reagent at specific moments (pulses) causes numerical solving instability in a dynamic model solving. Therefore, the equation 3.1 was stated to describe the elemental mass balance of the liquid and solid phase at the start and at the end of the process.

$$C_{j,t}^{liquid} \cdot V_{liquid,t} = (C_{j,0}^{liquid} \cdot V_{liquid,0}) + (C_{j,added}^{liquid} \cdot V_{added}) - (n_{MAP,t} - n_{MAP,0}) \qquad 3.1$$

Where, $C_{j,t}^{liquid}$ is the concentration of an element in the liquid phase at certain time "t". Other variables in this expression are the liquid volume at time "t" ($V_{liquid,t}$), the starting concentration ($C_{j,0}^{liquid}$), the starting liquid volume ($V_{liquid,0}$), the concentration of the element added with volumetric pipette ($C_{j,added}^{liquid}$), the volume of reagent added at time "t" (V_{added}), the number of moles at time "t" ($n_{MAP,t}$), and the number of moles at the start ($n_{MAP,0}$).

The concentration of the saturated solution before and after addition of reagent was set to not exceed an ionic strength of 0.5 M to apply Debye-Hückel modified by Davies equation. Since excess of N in the initial saturated solution solution leads to a buffered system (pH = 9), the selection of N/P molar ratio in the initial saturated solution was based on a pH change of at least 0.1 units after Mg is added (the solution pH decreases when $MgCl_2.6H_2O_{(aq)}$ is added to the reactor, but when there is an excess of ammonia in the reactor the pH is buffered). Selection of N/P is important because the prediction of the pH over time was intended to be compared with on-line pH measurement in the experiment to indirectly visualise the likely behaviour of predicted SI_{MAP}.

Simulations were performed to decided initial saturated solution composition based on previous assumptions. Concentration of NH_4Cl was set to 0.40 M. Molar ratios of N/P around 8 to 20 were assessed, using $\mathrm{n_{NaOH}/n_P}$ = 10 and $\mathrm{n_{Mg}/n_P}$ = 2.5 as constants. A molar ratio (n_N/n_P) of 8 was suitable to observe a pH decreased from 6.18 to 6.00 at the start of the experiment. This pH decrease represented a desaturation, wherein the SI_{MAP} varied from 0.67 to 0, and it led to 3.57 g of struvite precipitation according to simulation. Addition of $MgCl_2.6H_2O$ decreases the pH, and it has to be carefully dosed to avoid a positive saturation index of newberyite, which would potentially lead to its formation. The stock solutions used during the process were 2 M $NaOH$, 1 M NH_4Cl and 1 M $MgCl_2.6H_2O$.

Table 3.2 provided further detail about the intermittent fed-batch process conditions and operation. In this table, the kinetic parameters were chosen arbitrarily considering similar range as previous modelling work in nutrient recovery (Schneider et al., 2013). The initial mean particle size was chosen as unity instead of zero (the reactor should start without any particle at the start) to avoid numerical solving instability. The addition interval of 6 hours depends on the chosen kinetic parameters, because faster desaturation can allow shorter time to achieve desaturation, and therefore, shorter time between reagent injection. The processing time was selected considering the maximum ionic strength limit of applicability for Debye-Hückel modified by Davies is applicable (0.5 M).

Table 3.2 — Fed-batch operation with intermittent feed addition

Variables	Magnitude
Initial nutrient volume within reactor [L]	5.075
Process time and addition interval [h]	105; 6
Initial nutrient composition [mol/L]	[P] = 0.0488; [N] =0.3941; [Mg] = 4.926e-3; [Na] = 0.0685; [Cl] = 0.4039
Initial mean particle size [µm]	1
Kinetic parameters:	k = 1e-5m/h, n=1.5
Addition of reagents with volumetric pipettes:	15 mL of 2M NaOH 25 mL of 1M NH4Cl 15 mL of 1M MgCl2.6H2O

3.3.2 Initial mass of struvite in the fed-batch model

Simulations required an initial quantity of struvite within the reactor at time zero, because without seed the model cannot affect an increase in struvite mass (by solving the $ODEs$). This quantity was selected by matching the profiles of saturation index and struvite mass over time.

.

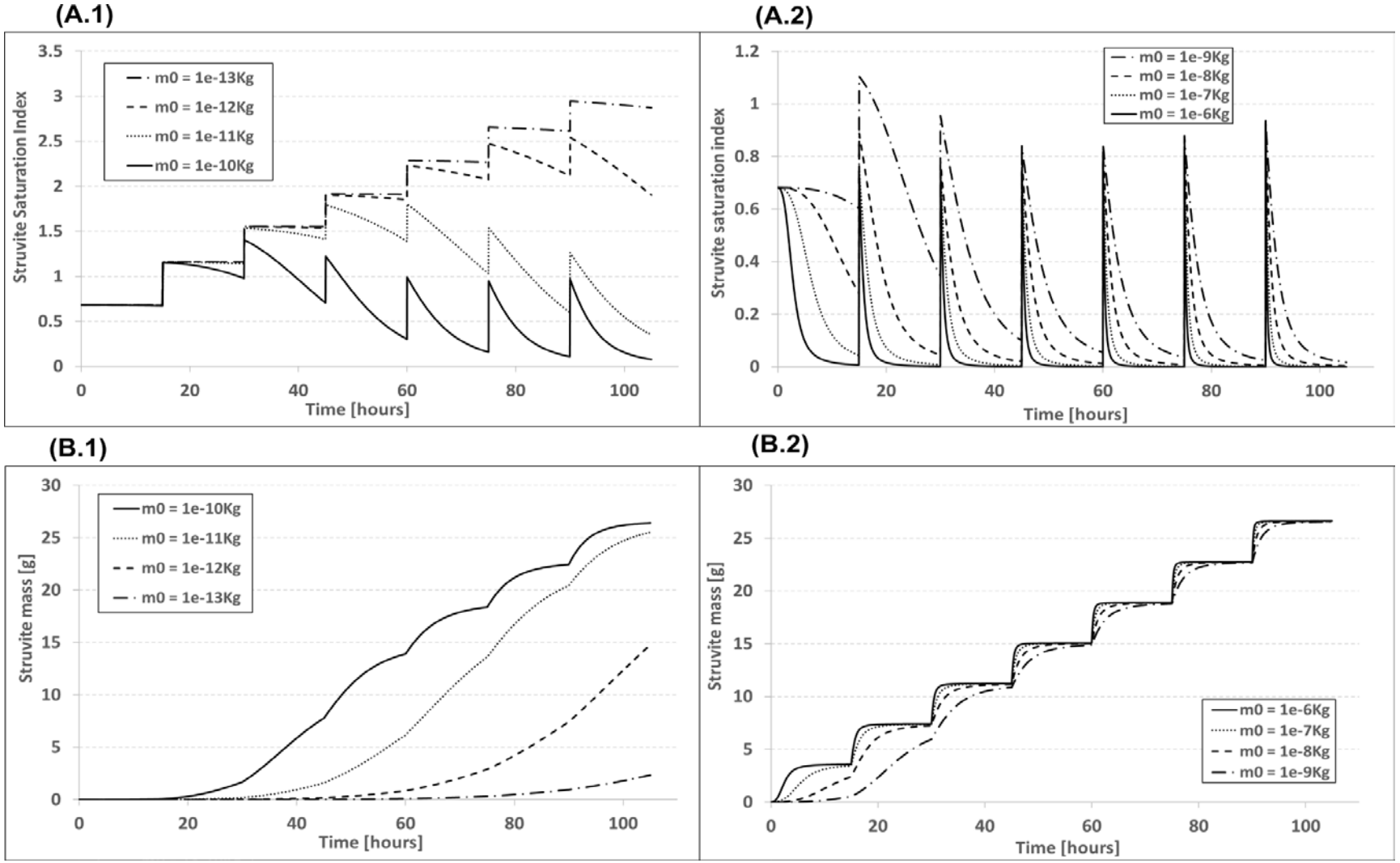

Figure 3.8 — Effect of initial struvite seed in the saturation index and mass profiles. Plots A.1 and A.2 predicted the struvite saturation index at using different quantity of initial quantity of seed. Plots B.1 and B.2 Shows predictions in the struvite mass at small quantity of seed.

The saturation index profiles were expected to achieve a maximum every time nutrient and base were added, with a following pH decay to equilibrium. Figure 3.8.A.1 and.A.2 show that small quantities of struvite triggered prediction of unwanted data points. In Figure 3.8.A.1, the saturation index "peaks" became more visible at larger quantity of seeds.

Figure 3.8.A.2 showed that quantity of struvite seed less than 1e-6 kg triggered a transient, but then the system relaxes to the saturation point (SI_{MAP} = 0). Predictions of struvite mass in Figure 3.8 B.1 showed small increments when struvite seeds where lower than 1e-11 kg. A consistent struvite mass profile can be observed when initial struvite seed was 1e-6 kg in Figure 3.8.B.2.

Assessment in Figure 3.8 highlighted the importance of selecting suitable initial condition to determine coherent and consistent process variable profiles.

3.3.3 Intermittent fed-batch simulations

Addition of nutrient and base to the initial saturated solution aimed to precipitate only struvite. Figure 3.9 showed that the saturation index of the solid phases other than struvite were negative. Negative saturation index in solid phases different than struvite indicates undersaturation of these solids during reactor operation.

A solid phase with negative saturation index is unlikely to precipitate. From Figure 3.9, it is clear that only Newberyite is the closest rival to struvite in solid precipitation, while the other solid phases matter even less. The presence of only one solid phase could facilitate validation of the system thermodynamics. Predicting saturation index of different solid phases could also suggest which solid phase is likely to be identified by experimental analysis, such as X-*ra*y diffraction.

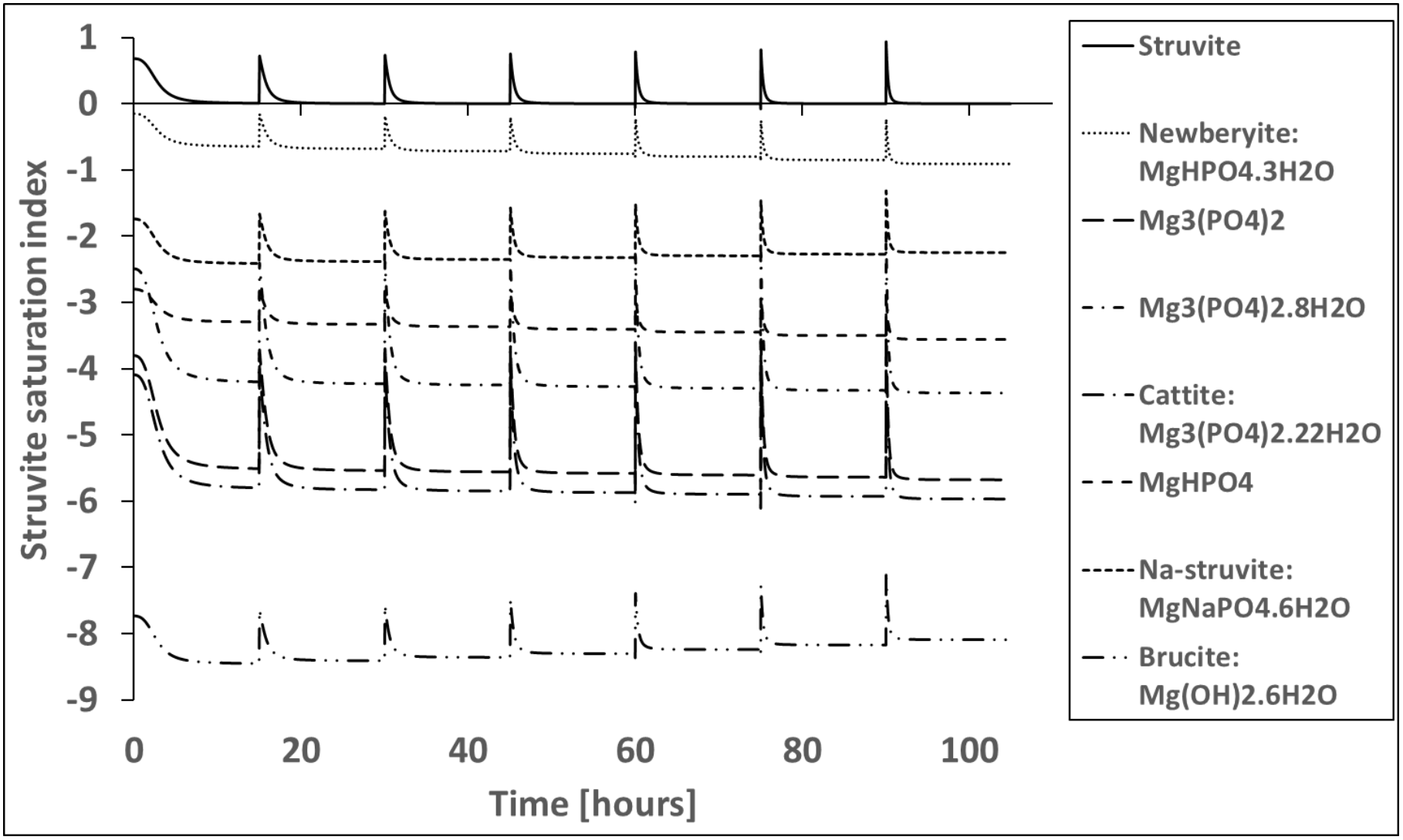

Figure 3.9 — Saturation index of different solid phase during struvite seed production

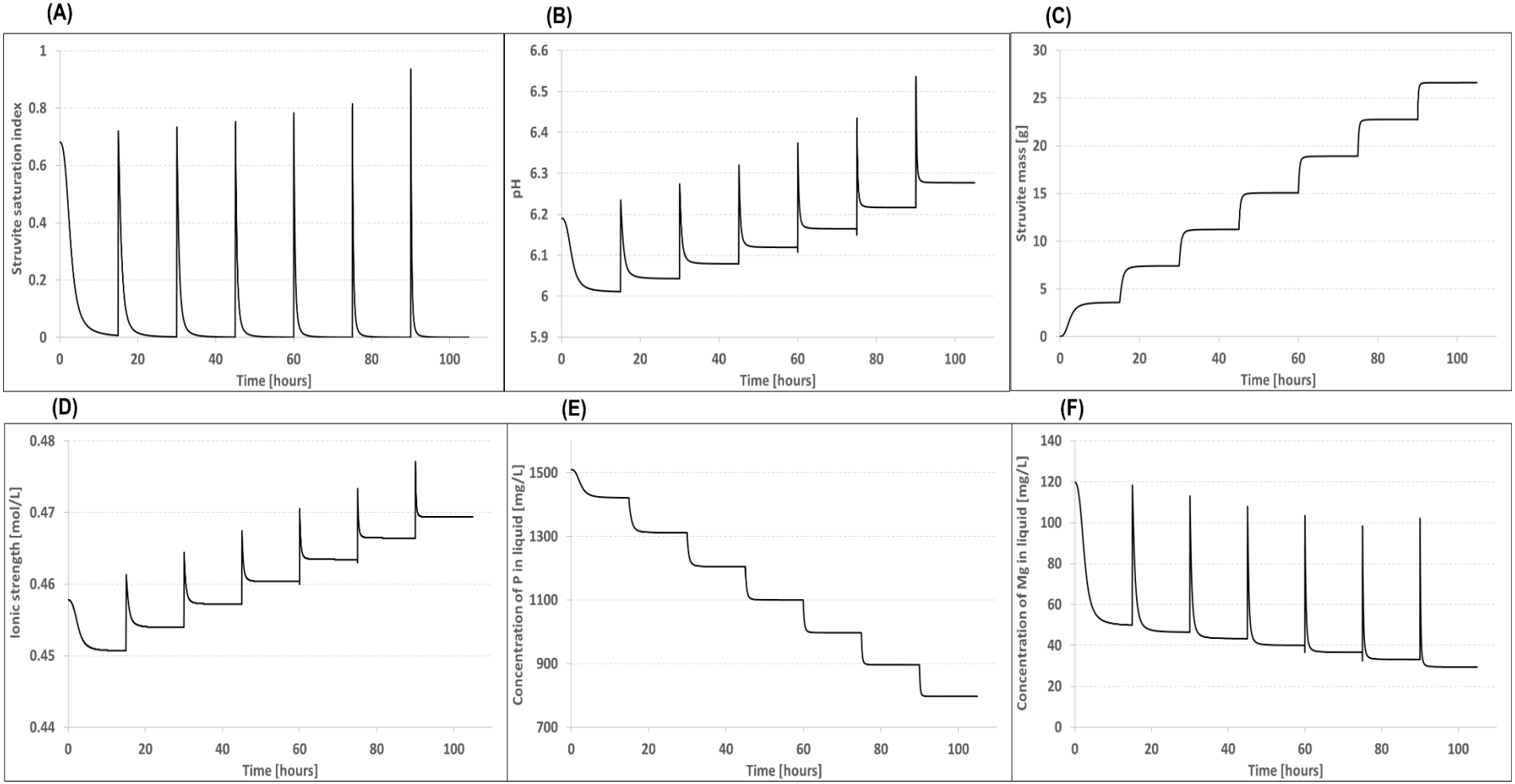

Figure 3.10 — Fed-batch process profiles of struvite saturation index (A), pH (B), struvite mass (C), ionic strength (D), elemental P concentration (E) and Elemental Mg concentration (F)

Figure 3.10 shows the key variable profiles, using an initial quantity of seeds of 1e-6 kg. Figure 3.10 also shows that the reagent addition ($nutrient$ and $NaOH$) affects in the saturation index (A), and it can be monitored through pH measurements (B). Simulations also shows every time the nutrient was added to the fed-batch reactor, all the variables provide a response. The profiles of saturation index, pH, ionic strength and elemental concentration of Mg are similar in shape. Similarities between these sub-plots indicate that the addition of Mg an important effect in the fed-batch process.

The profiles of P and an struvite mass within the reactor are showing opposite tendencies which is expected due to the P transfer from liquid phase to solid phase during struvite precipitation The behaviour shows that decrease in P concentration in the liquid phase is correlated with struvite mass precipitation. Moreover, the struvite mass increases gradually until saturation index achieves a minimum value. Experimental validation of previous designed process could consider continuous measurement of pH, which could act as a surrogate measure of the saturation index. Analysis of N in the liquid phase is irrelevant, because this element was found in excess.

Crystal morphological characteristics can be inferred from fed-batch operational data and process simulations. Concentration of elemental P in the initial saturated solution of around 0.05 M (Table 3.2) and solution pH between 6 to 7 units (Figure 3.10.B) suggested the possible presence of individual and aggregates struvite crystals (Abbona & Boistelle, 1985). Moreover, crystal habit was expected to be orthorhombic because of low saturation in most of the process (exception the intervals when reagent was injected). Intervals when the SI_{MAP} increased during the addition of Mg source with volumetric pipette could also originate presence of “star” shape crystals, which are common at large saturation solution.

3.4 Continuous process

Continuous struvite precipitation was simulated to understand the effect of diverse process variables. Process variables such as quantity were assessed at different hydraulic residence time. Mathematical equations to compare continuous processes were also discussed.

3.4.1 Input simulation parameters

Dynamic simulations of continuous struvite precipitation were developed considering an initial Mg/P feed molar ratio of 0.9 to achieve P concentration above limiting analytical detection threshold (Figure 3.2). Section 3.2.3 highlights that positive SI_{MAP} can be achieved at very low Mg/P feed molar ratio. The reactor was simulated by adding one stream of $MgSO_4.7H_2O$ and the other of nutrient stream. If the system is fed by Mg solution and synthetic ureolysed urine, a small deviation of Mg source flow rate could originate a significant change in the Mg/P feed molar ration fed to the reactor. To balance the uncertainty of Mg addition in a possible experiment, the model considered the feeding of the same flow rates of the Mg source solution and a concentrated synthetic ureolysed urine ($CSUU$). The $CSUU$ is a solution with double the concentration of the SUU.

Process configuration has already been presented in § 2.3.1. In this configuration the liquid phase enters and leaves the reactor continuously, while the struvite solid phase was kept within the reactor. This model considered negligible loss of solid phase in the outlet of the reactor. The effective volume of the rector was considered the same as the suspended particles (crystal bed). One overriding goal was to maintain the saturation index at values that would avoid excessive nucleation.

The initial saturated solution within the reactor was calculated by mixing the same volumes of the $CSUU$ and Mg source in each Mg/P feed molar ratio condition. This solution was estimated with a batch model by setting the saturation index to zero, then the elemental concentration in the liquid phase were used as an initial condition for simulations of continuous reactor operation. Table 3.3 shows input simulation data for the chosen base case scenario of Mg/P feed molar ratio = The initial

saturated solution was obtained by mixing equal volumes of $CSUU$ and Mg source in Mg/P feed molar ratio of 0.9.

Table 3.3 — Simulation parameter for continuous process modelling design

Variables	Magnitude
Volume of reactor[L]	6
Mg/P feed molar ratio	0.9
Simulation time [h]	100
Initial mean particle size [µm]	50
Initial saturated solution [mol/L]	P = 1.81e-3, N = 3.09e-1, Mg = 2.79e-5, K = 5.05e-2, S = 2.34e-2, C = 9.08e-2, Na = 7.26e-2, Cl = 2.02e-1
Kinetic parameters:	k = 1e-6 m/h, n = 1.5

3.4.2 Effect of hydraulic residence time

This assessment was developed by different scenarios using different hydraulic residence time during a reactor operation of 100 h. The dynamic model was simulated using different hydraulic residence time (HRT) to observe the profile of the saturation index at a given quantity of struvite seed (150 g).

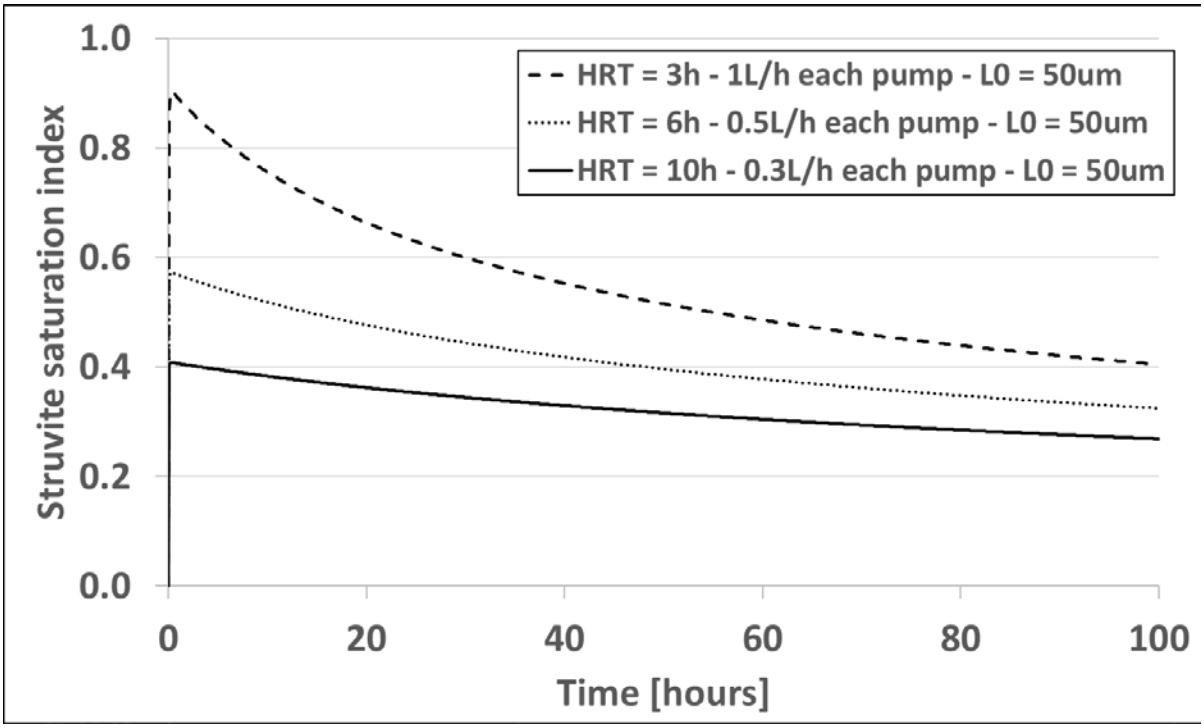

Figure 3.11 — Saturation index profile using 150 g of seed at Mg/P = 0.9

Figure 3.11 shows that an increase of the hydraulic residence time reduces the struvite saturation index. The profile of each case indicates that the maximum saturation index is calculated at the start of the process and this variable declines over time. Smaller HRT is linked to larger saturation index, therefore, continuous reactor operation should be developed at larger HRT to avoid nucleation. These SI_{MAP} profiles also indicate that the maximum saturation index is a better indicator to select operating conditions. The quantity of seed (150 g) was arbitrarily selected to indicate the presence of a maximum peak in SI_{MAP} trend, which also depends on the seed quantity (in following section).

3.4.3 Effect of quantity of seed

The presence of seed at the start of the process is important because it provides sufficient surface area to enhance struvite production rate. The presence surface are allows the mass transfer of the Mg^{2+}, NH_4^+ and PO_4^{3-} to the struvite solid phase. This section assesses what is the suitable quantity of struvite seed to run a continuous reactor experiment.

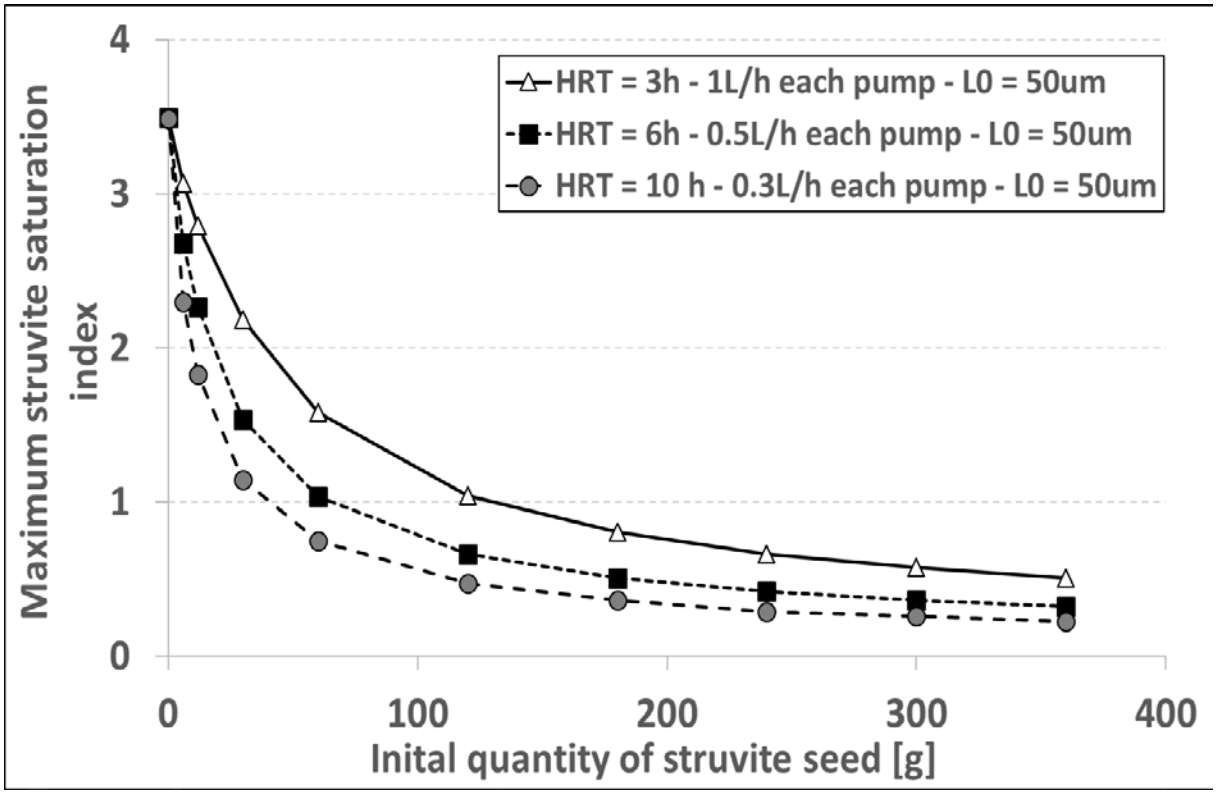

Figure 3.12 — Saturation index based on struvite crystals and hydraulic residence time at $\mathrm{Mg/P}$ = 0.9 showing the peak behaviour. Simulations considered an initial mean particle size of 50 μm

Figure 3.12 showed the maximum SI_{MAP} at different initial quantity of seed and HRT. This plot highlights that the maximum SI_{MAP} rapidly increases when the initial quantity of initial struvite seed is smaller than 150 g for different HRT cases. Therefore, considering struvite quantity of seeds larger than 150 g is a good choice for modelling and experimentation.

Aiming for $\mathrm{SI_{MAP}}$ values sufficiently low to minimise nucleation required the consideration of an additional degree of freedom, which can be lowering the Mg addition to the system (Mg/P < 0.9) at the beginning of the process or by increasing initial quantity of seeds. Reduction in the Mg addition by decreasing the concentration (or reducing the volumetric flow rate in real process) of the incoming solution could also decrease the struvite production rate.

3.4.4 Seed surface area

The initial particle size affects the available seed surface. Simulations in § 3.4.3 considered a nominal initial particle size of 50 μm (L_0) in every simulation. Smaller diameter seed crystals – for the same mass of seed crystal – will, according to the model chosen, provide a greater specific surface area (area/mass crystal). This, therefore, should lead to a greater struvite production rate for the same mass of seed, since the transfer of struvite constituent ions from solution to solid phase depends on the contact area between the two phases.

Figure 3.13 showed that a lower peak and subsequent saturation index was achieved at smaller initial particle size. Moreover, all sub- plots suggested that the initial particle size has a high impact on the predicted saturation index; and it should be considered in addition to the initial seed mass. Since real case scenarios are a mixture of crystals with different particle sizes, it is recommended the assumption of large quantity of seed with small sizes to keep the SI_{MAP} at lower values..

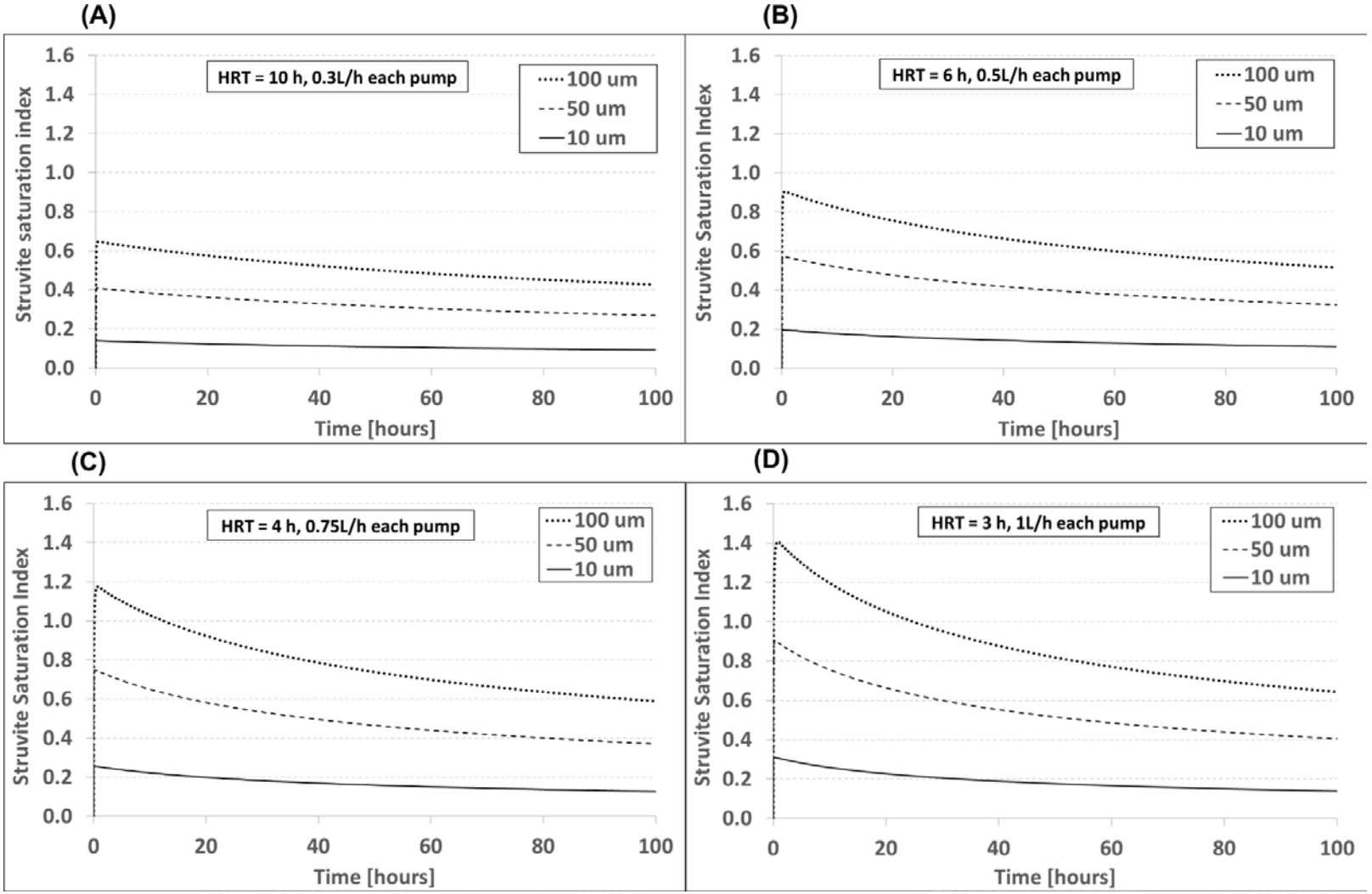

Figure 3.13 — Struvite Saturation Index using different initial particle size with 150 g of seeds at Mg/P = 0.9. Simulations were developed at HRT = 10 h (A), 6 h (B), 4 h (C) and 3 h (D)

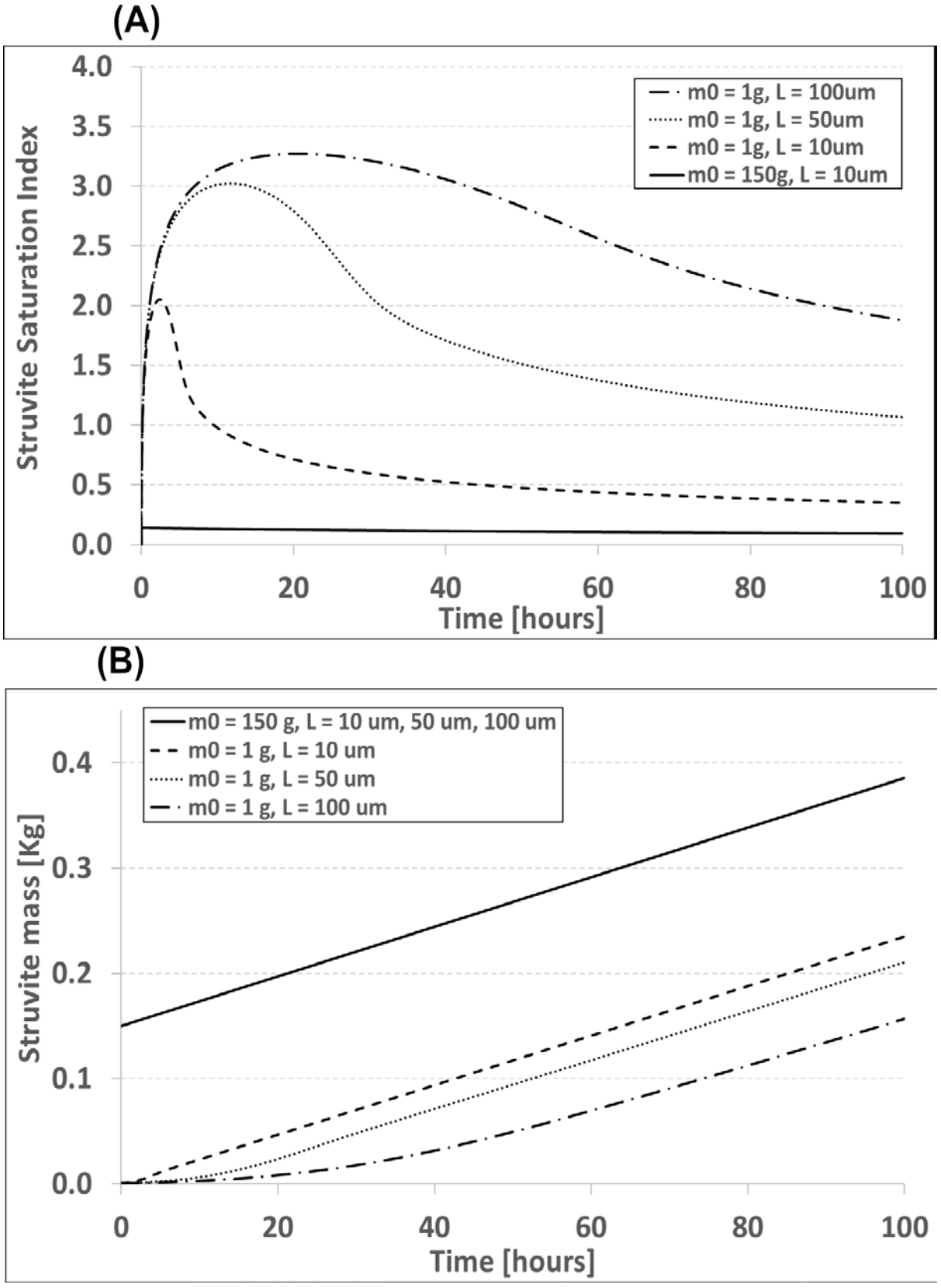

Figure 3.14 — Initial mean particle size effect in saturation index (A) and struvite mass (B). Every simulation was developed at Mg/P = 0.9

Figure 3.14 showed the importance of selecting the appropriate quantity of seed and its average size. Figure 3.14.A showed that oversaturation and excessive nucleation was likely to happen in system without available surface area (seeds). Figure 3.14.B also showed that larger saturation index could be related to slow struvite mass production (at 100 μm). The struvite production rate was independent of initial particle size when large quantity of seeds was applied. These findings mean that saturation index increases to compensate the lack of available surface area during continuous reactor operation as mentioned in previous work (Schneider et al., 2013).

3.4.5 Thermodynamic phosphorus recovery

The purpose of this section is identifying the type of equation more suitable to compare different process conditions. Different continuous reactor operation can be compared by the % of the overall P recovery (equation 3.2) and the % of thermodynamic P recovery (equation 3.3). Equation 3.2 was most commonly used in continuous struvite precipitation studies. This equation considers the difference of the concentration of P in the inlet and the outlet of the process divided by the inflow concentration of P.

$$\%Recovery_P = \frac{C_P^{in} \cdot F_{in} - C_P^{out} \cdot F_{out}}{C_P^{in} \cdot F_{in}} \times 100\% = \frac{C_P^{in} - C_P^{out}}{C_P^{in}} \times 100\% \quad 3.2$$

Where, C_P^{in} is the input concentration of element i in struvite (Mg, N or P) in the feed stream, C_P^{out} is the elemental concentration in the outlet stream of the reactor F_{in} and F_{out} are the total flow rates entering and leaving the reactor. In this work, they equal, since the system under study overflows at the outlet, thus they cancel.

$$\%Thermodynamic\ Rec._P = \frac{C_P^{in} \cdot F_{in} - C_P^{out} \cdot F_{out}}{C_P^{in} \cdot F_{in} - C_P^{eq} \cdot F_{out}} \times 100\% = \frac{C_P^{in} - C_P^{out}}{C_P^{in} - C_P^{eq}} \times 100\% \quad 3.3$$

Equation 3.3 was formulated in a similar simulation study (Schneider et al., 2013). Equation 3.2 is similar to 3.3 with the difference of the inclusion of the equilibrium concentration (C_P^{eq}) in the denominator.

Figure 3.15 shows simulation of continuous reactors considering different Mg/P feed molar ratio. The estimations of the % recovery and % thermodynamic recovery were developed after 100 h operation time in the continuous reactor.

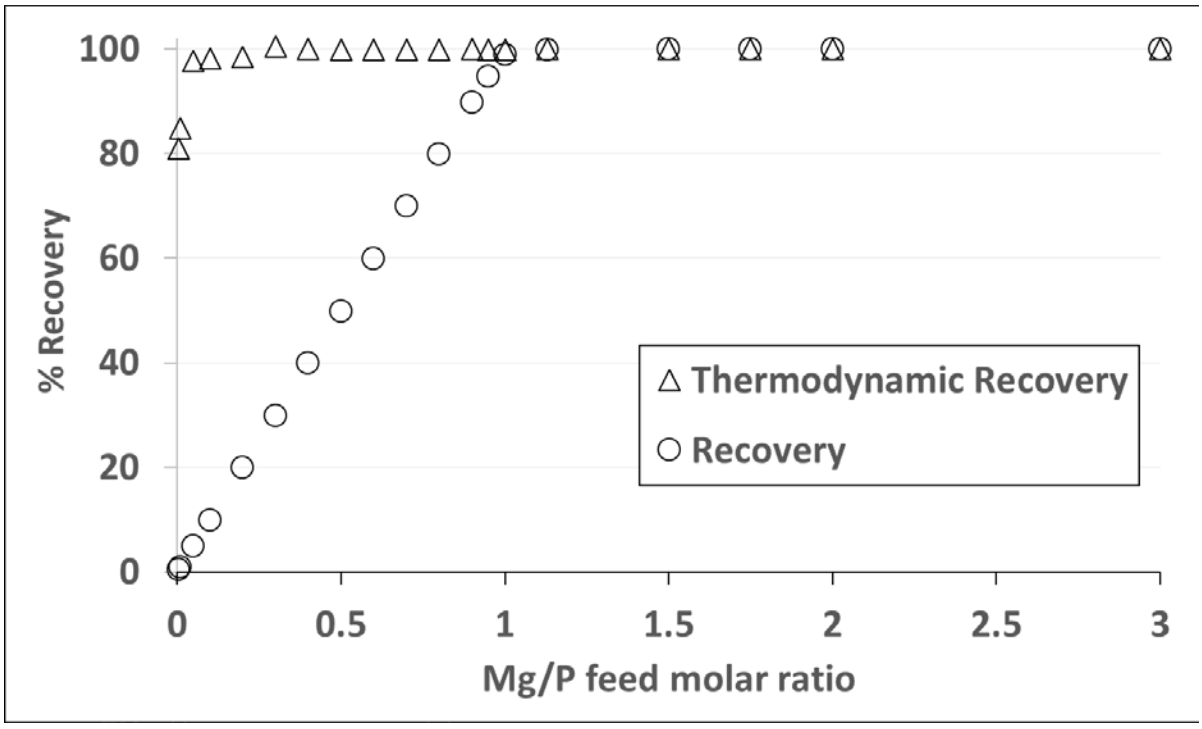

Figure 3.15 — Percentage of P recovery assessment at different Mg/P feed molar ratio

Profiles in Figure 3.15 indicate that % of recovery is a more suitable variable than the % thermodynamic recover, because the % recovery is directly related to the system productivity. The trend of %P recovery shows a "plateau" behaviours at Mg/P feed molar ratio larger than one. This could be explained by the thermodynamic characteristics of the system since the P concentration in the outlet of the reactor is estimated by mass balance and equilibria (ionic speciation). On the other hand, % thermodynamic recovery shows that the system is adequate thermodynamically for most of

the Mg/P feed molar ratio. This trend occurs due to the system driven by favourable thermodynamic condition, where the elemental P in the outlet is close to the one at equilibrium.

3.4.6 Specific struvite productivity

Another mathematical relationship was formulated to compare the effect of different Mg/P feed molar ratio in the struvite precipitation performance. The specific productivity rate (SPR) in Equation 3.4 defines the rate of struvite precipitation, the liquid volume and the struvite quantity within the reactor.

$$SPR = \frac{dN_{MAP}}{dt} \cdot \frac{1}{V_{liquid}} \cdot \frac{1}{N_{MAP}} \qquad 3.4$$

Where $\frac{dN_{MAP}}{dt}$ is the struvite mole production rate $[mol/h]$, V_{liquid} is the liquid volume in L (effective volume of 6-L in the reactor under study), and N_{MAP} is the struvite moles held within the reactor. The rationale for this variable is that in the mixed mode reactor (continuous liquid phase, batch solid phase) there is never a true steady state that takes hold.

Figure 3.16 showed that the SPR plateaus with Mg/P feed molar ratio greater than unity. Larger magnesium addition (Mg/P > 1) did not enhance the specific precipitation rate of struvite.

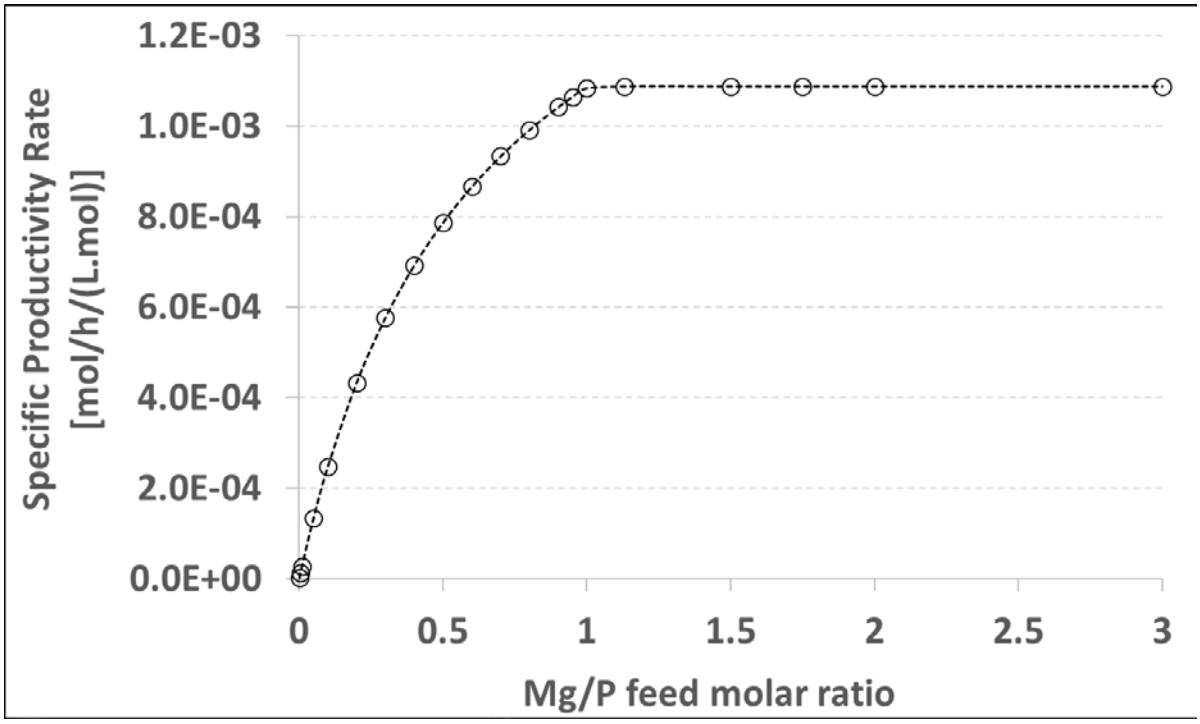

Figure 3.16 — Specific Productivity Rate after 100 h using different Mg/P feed molar ratios

Figure 3.16 shows a trend where there is a maximum specific productivity rate at Mg/P feed molar ratio larger than one. This profile can be explained by the low availability of PO_4^{3-} ions in the system due to pH buffering. This outcome is key to select the suitable quantity of Mg added to a continuous (or even batch) reactor. Despite of several studies applying arbitrary Mg/P feed molar ratios, this choice could be excessive since thermodynamic speciation is limiting the system by the presence of other ionic complexes different than PO_4^{3-}.

3.5 Summary

- Thermodynamics of struvite precipitation from urine source was validated with previous works.
- Composition of synthetic ureolysed urine was determined by literature review information and EES simulation to adjust the solution pH to 9, and ionic strength to 0.36 M.
- Larger dilution in synthetic urine decreased the saturation index, and it required larger Mg dosification.

- Propagation of uncertainty was applied to pK_{eq} parameters to determine key equilibrium equations describing nutrient recovery from synthetic ureolysed urine.
- Mathematical verification of model in EES was developed with $gPROMS$ and $PHREEQC$ software packages.
- The modelling of a fed-batch process using intermittent addition of magnesium required a simple balance of solution in liquid and solid phase, considering initial and final conditions.
- Fed-batch simulations were applied to produce struvite selectively by keeping as negative the saturation index values of other solid phases.
- Continuous struvite precipitation was designed with EES simulations to avoid over saturation.
- An additional expression called specific struvite productivity rate was stated to compare the struvite production rate at different magnesium addition.
- Simulations of batch experiments using Mg/P feed molar ratio could be applied in experimentation to corroborate maximum struvite precipitation in continuous operation.

4 Method Development - preliminary assessment of continuous struvite precipitation model

---

Highlights:

- *Presentation of analytical methodologies, and assessment of potential analytical interference*
- *Determination of struvite purity in precipitants based on N elemental composition*
- *Experimental description, and discussion of monitoring variables*
- *Tracer studies during continuous reactor operation, considering the two-zone mixing model*

4.1 Literature Review

This section describes some methodologies and methods found in literature review. Some experimental methodologies and mathematical formulations to discuss experimental data are reviewed.

4.1.1 Uncertainty propagation

Uncertainty propagation describes how the uncertainty in process input variables are propagated through to process output variables. This process could comprise laboratory analysis stages, such as sample dissolution, dilution and analysis itself (spectrophotometry, atomic absorption spectroscopy. etc.). For this purpose, the Engineering Equation Solver (EES) package, applies the $NIST$ method (Taylor & Kuyatt, 1994) implemented with numerical methods (Klein & Alvarado, 2002). The application of this technique is also referenced in previous similar studies focused on struvite precipitation process modelling (M. W. Burns, 2017; Galbraith, 2011).

$$u_c{}^2(y) = \sum_{i=1}^{N} \left(\frac{\partial f}{\partial x_i}\right)^2 u^2(x_i) + 2\sum_{i=1}^{N-1}\sum_{j=i+1}^{N} \frac{\partial f}{\partial x_i}\frac{\partial f}{\partial x_j} u(x_i, x_j) \quad 4.1$$

In equation 4.1, $\mathrm{u_c(y)}$ is the combined standard uncertainty of the measurement result, $\frac{\partial \mathrm{f}}{\partial \mathrm{x_i}}$ is the partial derivatives (sensitivity coefficients), $\mathrm{u(x_i)}$ is the standard uncertainty associated with the input variable and $\mathrm{u(x_i, x_j)}$ is the covariance considered as zero.

$$\%Unc_i = \frac{\left[\frac{\partial f}{\partial x_i} \cdot u(x_i)\right]^2}{u_c{}^2(y)} \times 100\% \quad 4.2$$

Equation 4.2, estimates the percentage of individual uncertainty $\%Unc_i$ related to one of the variables.

4.1.2 Tracer studies in precipitation reactors

Tracer studies in continuous struvite precipitation to identify mixing characteristics within reactors has not been widely investigated. The injection of 5% mass fraction of $NaCl$ into a Poiseuille reactor, which was monitored with conductivity measurements was performed to measure the residence time distribution (M. Burns et al., 2016). Fundamental of this technique can be found in chemical engineers books (Fogler, 1999), but it has not been applied yet to study mixing characteristics in struvite precipitation reactors.

4.1.3 Electric sensing zone in struvite studies

Particle size distribution in struvite precipitation studies has been widely performed with laser diffraction (M I Ali & Schneider, 2008; Ariyanto et al., 2014; M. Burns et al., 2016; Tarragó, Puig, Ruscalleda, Balaguer, & Colprim, 2016) compared to electric sensing zone (Galbraith et al., 2014). From previous studies, modelling and experimental data of struvite precipitation assessed the particle size distribution (Galbraith et al., 2014) or the mean particle size (M I Ali & Schneider, 2008), while the

others only reported experimental data without model prediction. Moreover, growth and aggregation modelling was discussed with electric sensing zone data using calcium oxalate monohydrate in batch systems (Bramley, Hounslow, & Ryall, 1997). This review showed that application of electric sensing zone combined modelling prediction has still need to be implemented.

A mathematical model without population balance could be compared to particle size distribution by converting a polydisperse to a monodisperse particle distribution The mean weight size could calculate a particle size (d_{mw}) of an assumed mono-disperse distribution that it is equivalent the same mass of the actual collection of particles (Jones, 2002). This mathematical expression is presented in equation 4.3, which formulates the mean weight diameter as a function of the quantity of particles (n_i) and the particle size (d_i).

$$d_{mw} = \sqrt[3]{\frac{\sum_i (n_i d_i^3)}{\sum_i n_i}} \qquad 4.3$$

4.2 Elemental analysis

This section discusses the development of the elemental analysis for P, Mg and N. Elemental analysis was performed to validate the model predictions with experimental data. A detailed assessment of possible elemental interferences is developed because of complex composition of the synthetic ureolysed urine (SUU). In the composition of SUU, Ca was not considered since it can precipitates other solid phases like hydroxyapatite The purpose of elemental analysis was to consolidate mass balance and validate model.

4.2.1 Phosphorus determination

Elemental concentration of P was measured by spectrophotometric analysis (Appendix C.3). Ionic interferences, such as Mg^{2+} , Na^{+}, K^{+}, NH_4^{+} , CO_3^{2-}, SO_4^{2-} , *and* Cl^{-} may affect the analysis (APHA, 1999). This section demonstrated that 1/5 dilution (volume sample/volume of final solution) was

suitable to avoid ionic interferences in the analysis. These interferences were assessed by comparing a "background standard" with KH_2PO_4.

Figure 4.1 showed that these "background standards" have the same absorbance than the KH_2PO_4 solutions. The "background standards" were prepared using a filtered equilibrium solution after precipitation, which means its P concentration will be depleted and well below the detection limit (*i.e.* $P < 0.2\ mg/L$) and a known quantity of $KH_2PO_4(s)$, and sufficient drops of 10.2 $M\ HCl$ to avoid solid formation. The equilibrium solution was prepared by mixing equal volumes of Mg source and concentrated synthetic ureolysed urine at a 1.20 Mg/P feed molar ratio, to ensure essentially 100% P reduction.

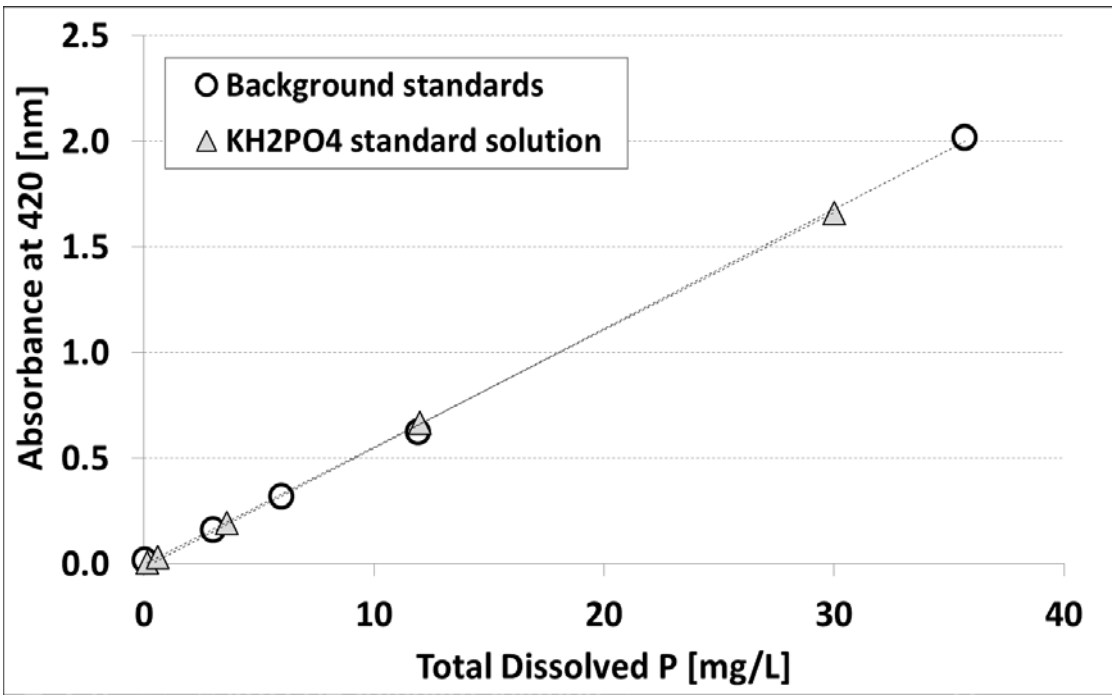

Figure 4.1 – Comparison of P standards prepared with deionised water and background solution.

Figure 4.2 presents the results at a 420 nm wavelength. The linear trends at 400 nm and 410 nm overlap at P concentrations lower than 6 mg/L; while, the linear trend at 420 nm was more consistent. This suggests that lower wavelengths may only be suitable for lower concentration samples. This work used the wavelength of 420 nm in the following sections.

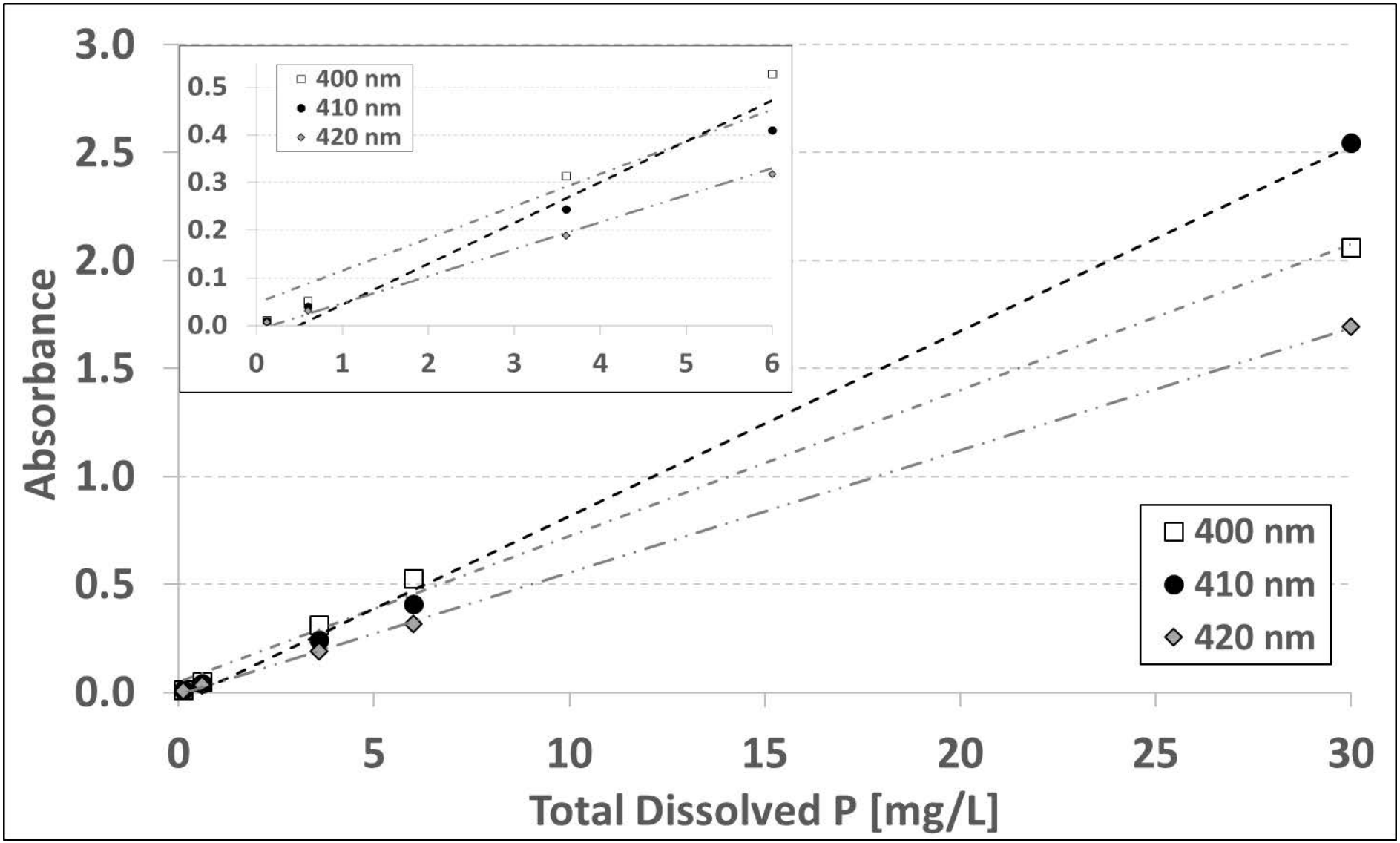

Figure 4.2 – Absorbance of P standards at different spectrophotometry wavelength. Sub-plot indicate the lower P concentration range from 0.2 to 6 mg/L.

4.2.2 Magnesium determination

Determination of elemental concentration of Mg was developed by Flame Atomic Absorption Spectroscopy ($FAAS$) (Appendix C.5). Previous work suggested the application of standards containing the same matrix composition to avoid analytical interferences (Moffett, 1995), so this issue was also explored in this work.

Figure 4.3 compares the absorbance of the "background standards", and $MgSO_4.7H_2O$ standard solution at 202.6 nm (A) and 285 nm (B). The "background standards" were prepared by mixing a low Mg concentration solution from a batch precipitation (0.56 Mg/P feed molar ratio to ensure very low background Mg in solution), $MgSO_4.7H_2O_{(s)}$, and sufficient drops of 10.2 $M\ HCl$ to maintain dissolution. This solution was diluted with the same "background solution" to prepare the standards, and a final water dilution (dilution factor = 1/5) was applied before $FASS$ analysis. Figure 4.3 shows that no absorbance inteference is present when samples are diluted 1/5 at both 202.6 nm and 285.2 nm.

4.2.3 Nitrogen determination

The determination of $NH_4 - N$ (ammonium as Nitrogen) was also done by spectrophotometry as detailed in Appendix C.4. This procedure consisted in mixing of the sample with colour forming reagents and 0.75 mL 1 $M\ NaOH$ at 25 °C. The maximum absorbance in preliminary tests was at 653 nm, which was employed for the rest of the method.

Trials determined that the suitable reaction times for full colour development were between 2 h to 3 h as can be seen in Figure 4.4. In this plot, absorbance increase is seen for a wide range of standard concentrations. Preliminary testing also considered warming the samples over hot plate at 38 °C, however, the decrease in the reaction time was not significant and the maximum absorbance in the samples was decreased.

The addition of $NaOH,$ was developed to increase the pH and ensure complete colour development, which is explored in Figure 4.5.

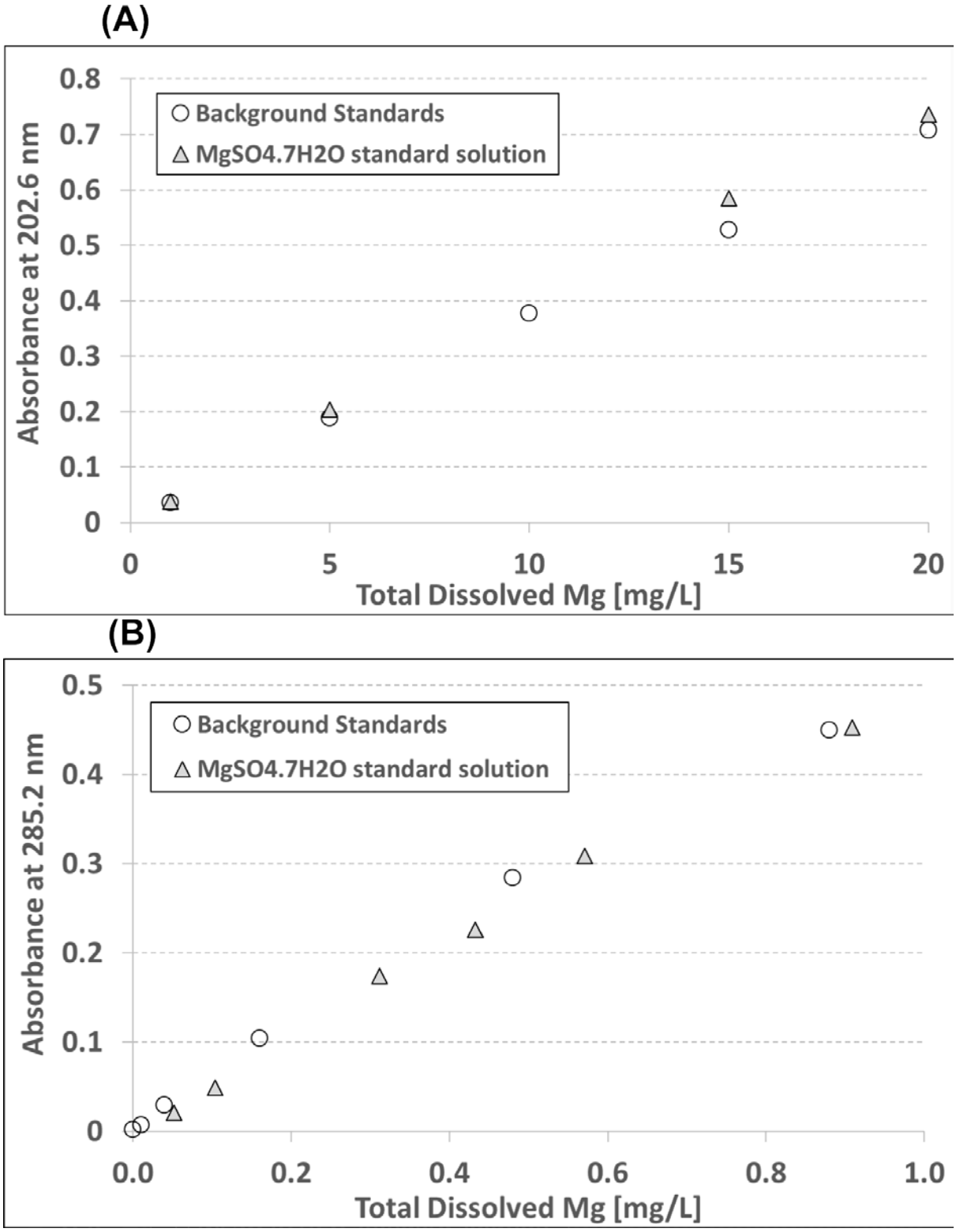

Figure 4.3 – Absorbance of $MgSO_4.7H_2O$ and background at 202.6 nm (A), and 285.2 nm (B).

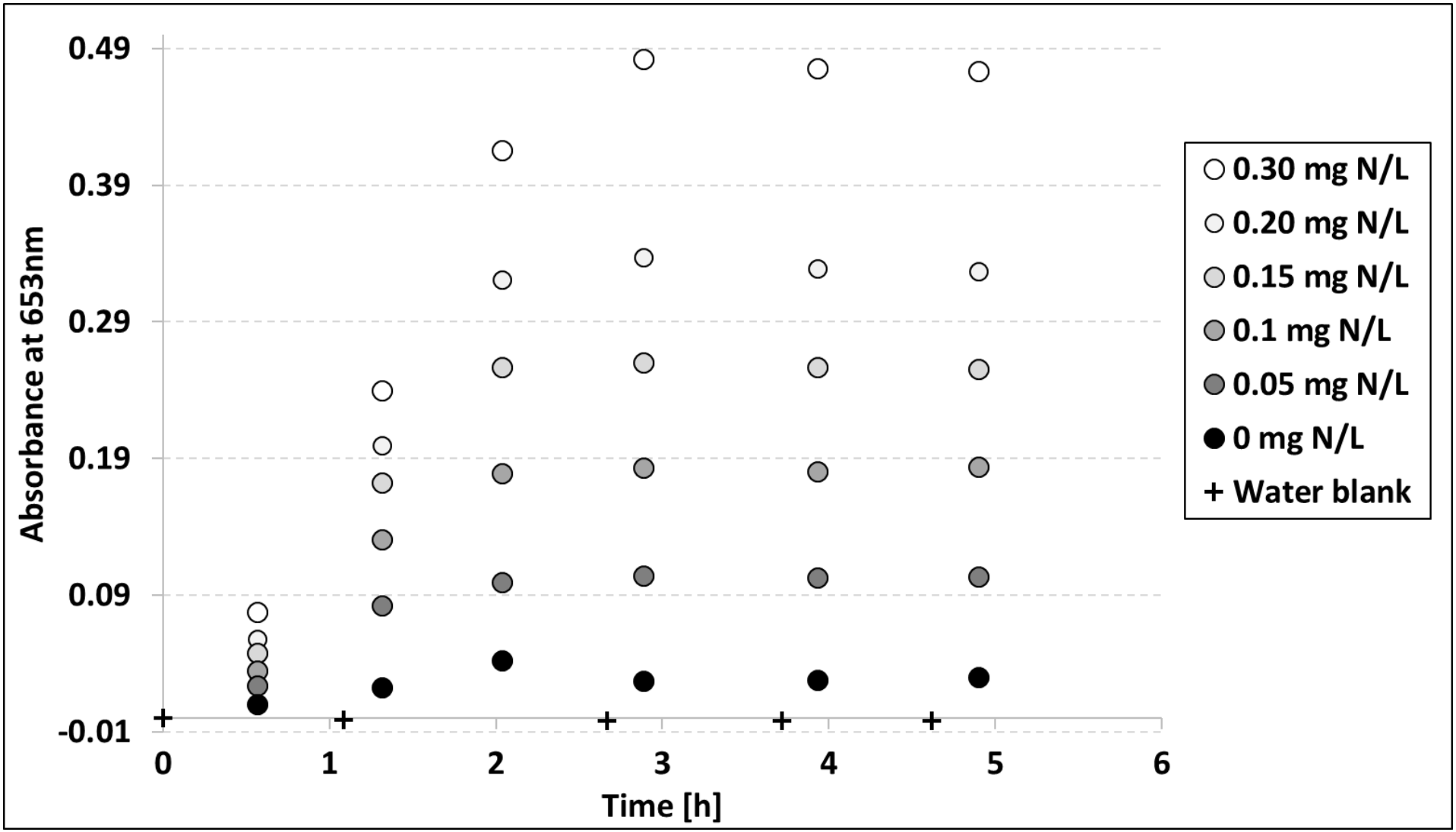

Figure 4.4 – Colour development for $NH_3 - N$ across a range of standard concentrations.

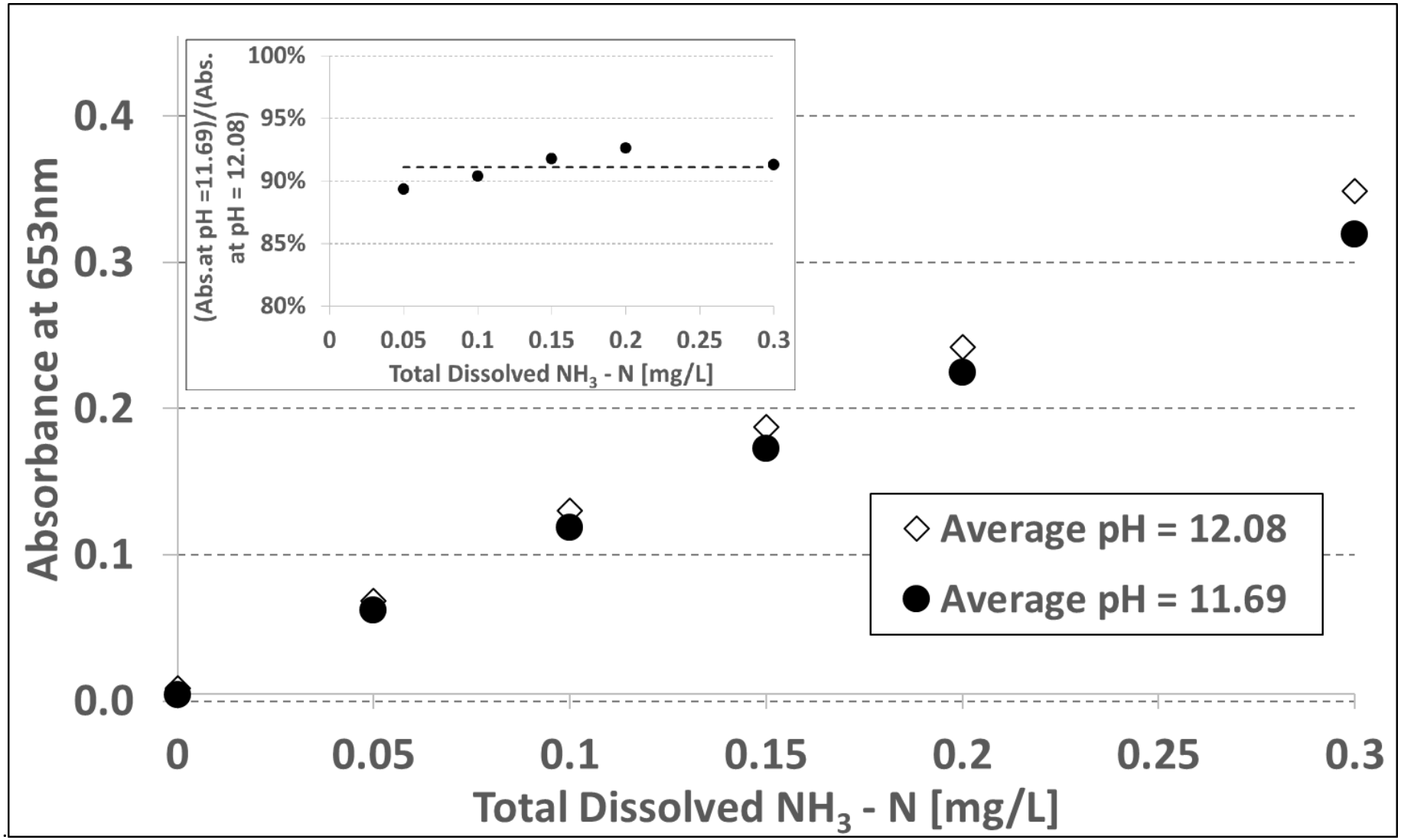

Figure 4.5 – Effect of pH in colour development for $NH_3 - N$ analysis.

Figure 4.5 shows differences in absorbance development before (pH = 11.69) and after $NaOH$ addition (pH = 12). The sub-plot highlighted an average absorbance around 91% of the full colour formation. This means that an increment of 0.30 pH units triggered an absorbance increment of around 10%. The variations in absorbance at different pH can be explained by the percentage of indophenol dissociated in the sample, previously estimated by the equilibrium dissociation equation (Verdouw, Van Echteld, & Dekkers, 1978) in equation 4.4.

$$pK_a = pH - log\frac{(indophenol\ dissociated)}{(indophenol)} \quad 4.4$$

In equation 4.3, pK_a for Salicylate method is 10.44 ± 0.23.

Figure 4.6 was a calculation of % indophenol dissociated at different pH with equation 4.3. This calculation shows that dissociation of indophenol can be greater than 97% at pH = 12. The subplot within Figure 4.6 indicates that there is less sensitivity of % of indophenol dissociation with respect to pH variability at higher pH. For instance, it is expected a variability of 15% at around pH = 11.70, compared to 10 % at pH = 12.0. While this variation could be decreased more at higher pH, this work considered a 12 pH based on the method developers (Verdouw et al., 1978).

Additional experiments were developed to assess possible elemental interferences and type of light exposure in the sample (Figure 4.7). Interference from Mg was considered negligible because the weight fraction in struvite (Mg/N = 1.74) was below the interference ratio (Verdouw et al., 1978). Interferences from P in the "Sodium Salicylate Method" (SSM) were assessed with different N/P molar ratio compounds: $(NH_4)_2SO_4$, $(NH_4)_2HPO_4$ and $NH_4H_2PO_4$. Figure 4.7 shows that P concentration does not interfere with $NH_3 - N$ analysis. The maximum absorbance was found at 653 nm wavelength, which is close to the value of 660nm cited by Verdouw et al (1978).

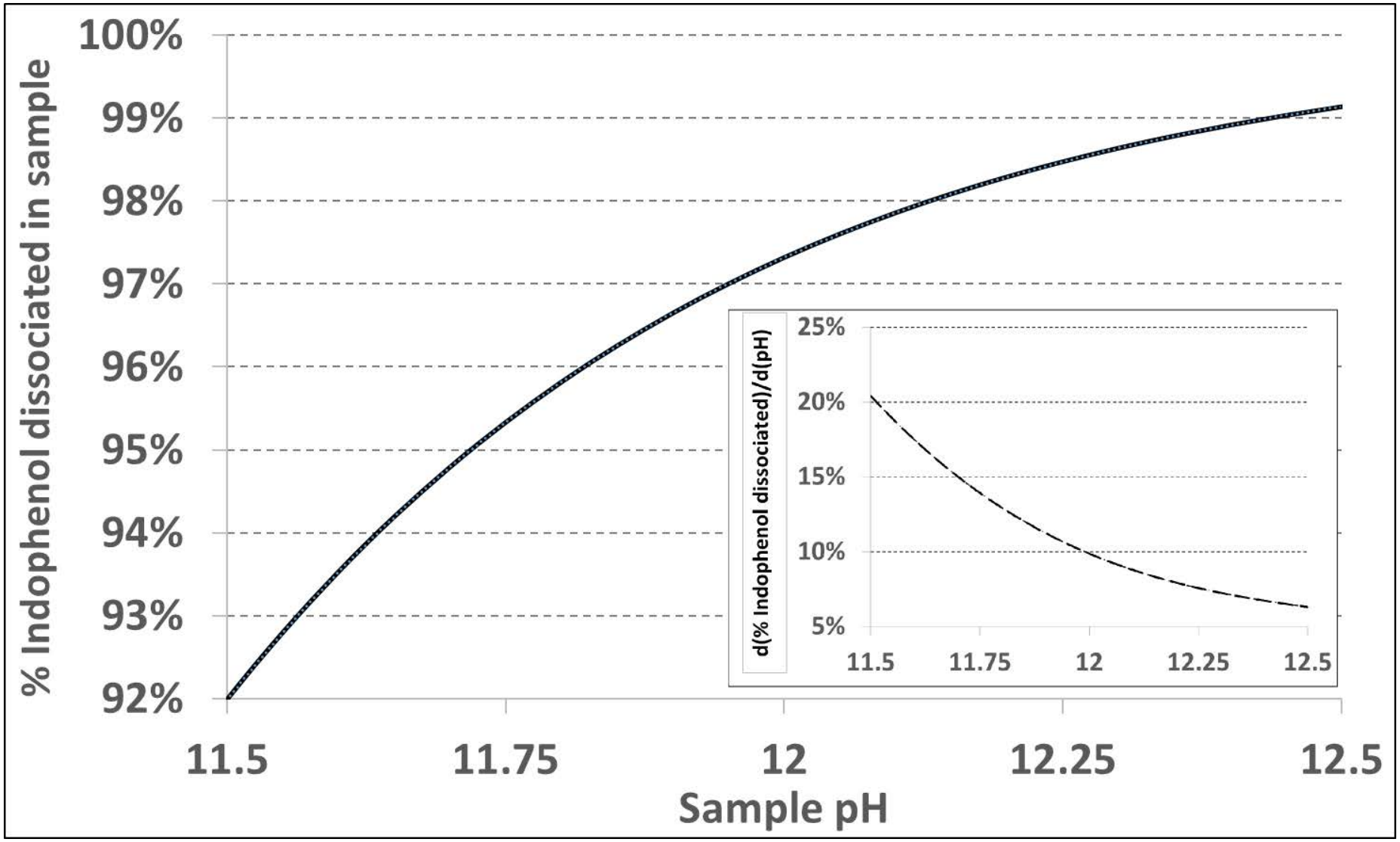

Figure 4.6 – Percentage of indophenol dissociated in sample according to different pH.

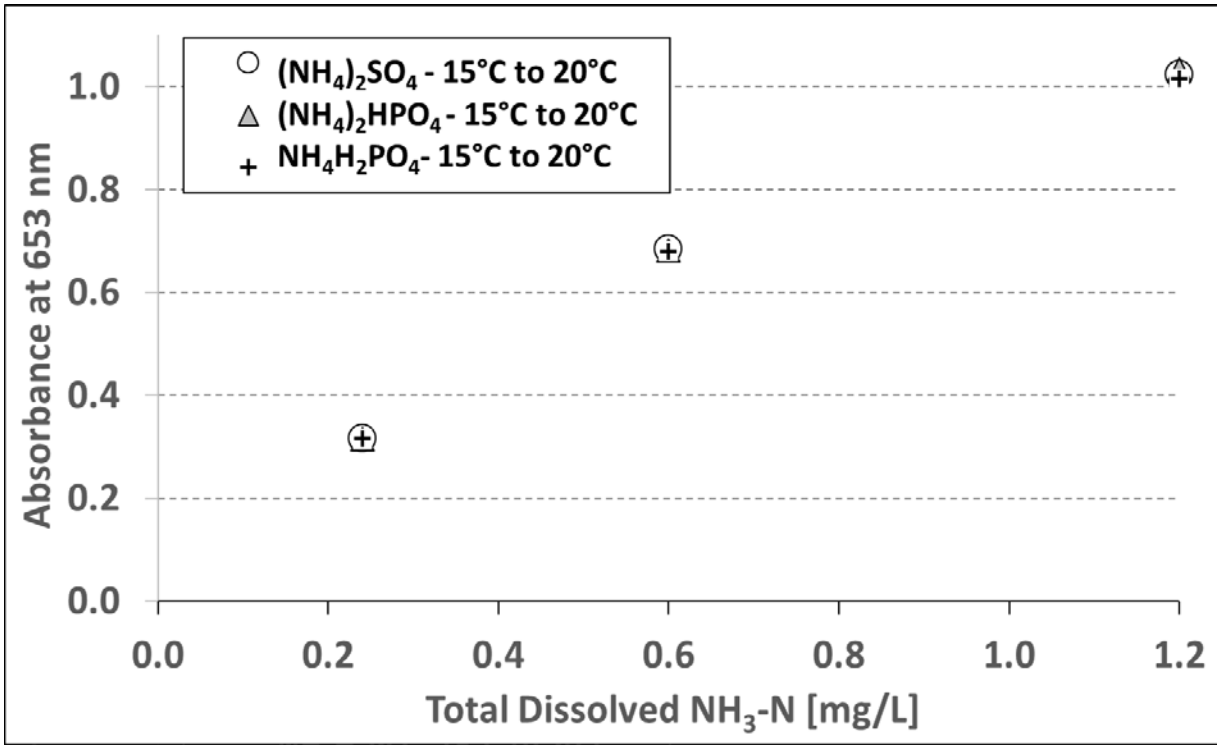

Figure 4.7 – Absorbance of samples using three different sources of $NH_3 - N$.

The impact of light application to the samples for colour development was also assessed, showing that UV-light (254 nm) has no effect in the colour development compared to laboratory light. This test was performed within 2 transparent plastic containers. Samples under UV-light developed a green colour compared to the blue from laboratory light. This could be explained by conversion of the p-Aminophenol (blue) to o-Aminophenol (green) (Bolleter, Bushman, & Tidwell, 1961).

Figure 4.8 shows that colour due to absorbance is more stable under laboratory than UV-light conditions for longer durations. Samples were therefore left under laboratory light for colour development in all analyses.

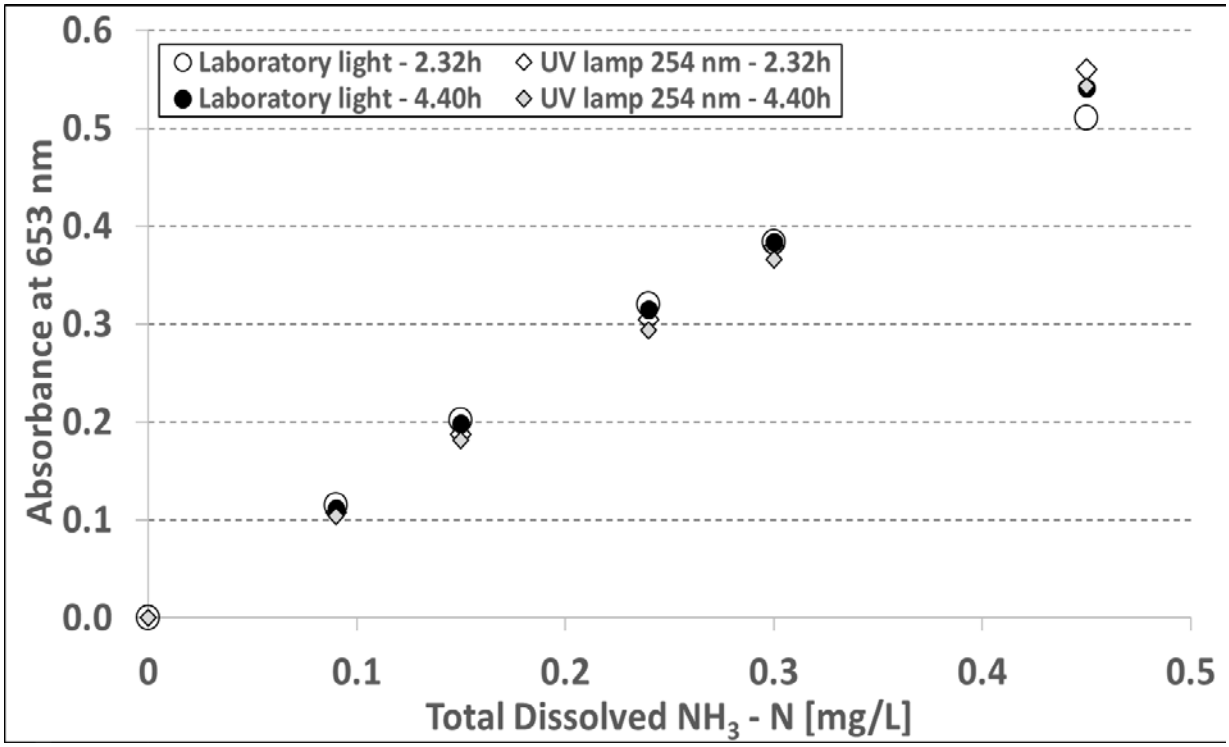

Figure 4.8 – Reaction time for $NH_3 - N$ analysis at 25 °C under laboratory light and UV-lamp.

4.3 Laboratory tests and model comparison

Laboratory-scale experiments were performed to applied the elemental analysis of N, P and Mg in struvite batch precipitation. Experimental data was combined with simulations to test model. Mass balance of Mg and P using the liquid and solid phase was estimated from experimental data to corroborate the reliability in the analytical measurements. The solid sample were dried in an oven at 40 °C between 12 to 24 hours. Sample were stored in desiccator to avoid moisture adsorption.

4.3.1 Propagation of uncertainty applied to solid phase analysis

The percentage of pure struvite was determined by quantification of % of N in the solid samples. The % N in the solid sample was determined by colorimetric determination of N in solid samples. The mass fraction of N in the solid sample *(*$\%\ w_N$*)* was estimated using the N concentration in the sample (C_N*),* the dissolution volume (V_s), and the solid mass (m_s) as stated in equation 4.5.

$$\%w_N = \frac{C_N \times V_s}{m_s} \times 100\% \qquad 4.5$$

Figure 4.9 shows the analysis of two samples from each of the experiments, and their repeat analysis: 2 from Expt. 1, and 3 for Expt. 2. This figure shows an atypical $\%\, N$ in the first repeat analysis from second experiment sample, which is much larger than the $\%\, N$ if all the solid sample were pure struvite (% N = 5.7 $\%\ w/w$). The third bar is this plot is related to a possible gross error in the analysis.

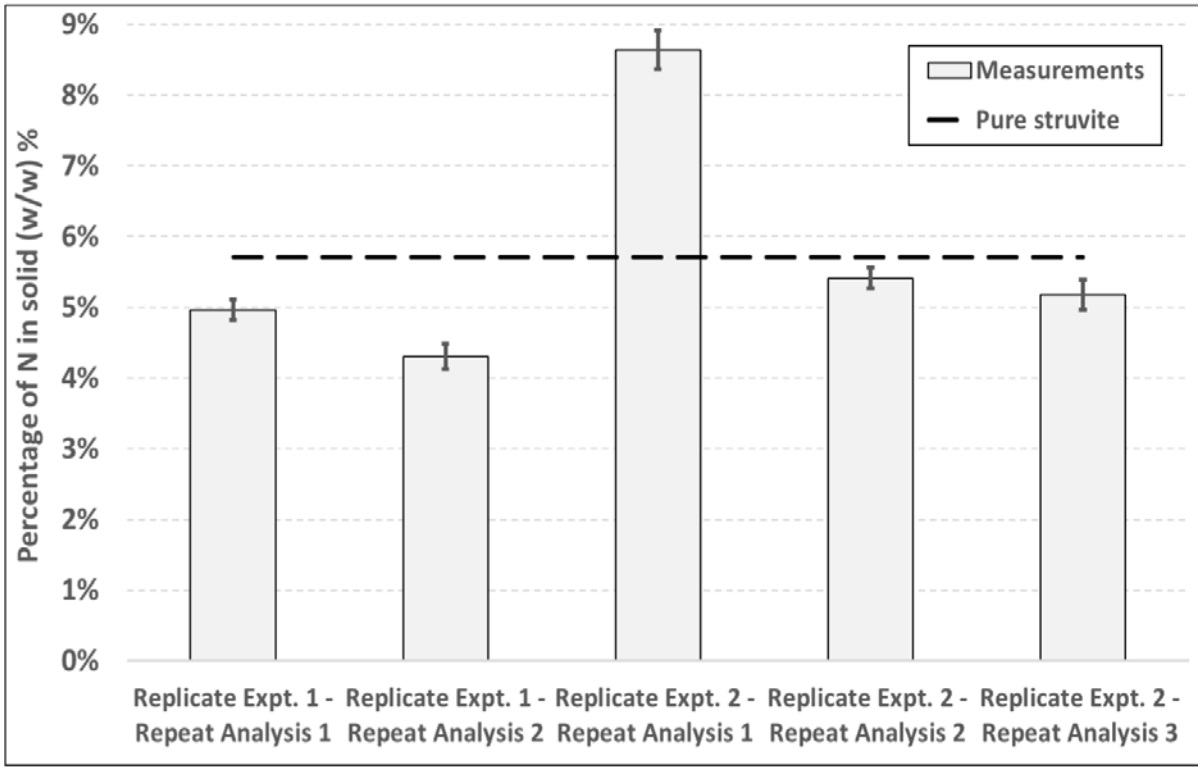

Figure 4.9 – Percentage of N in replicate and repeated analysis. Error bars are expressed as ±2σ of all measurements.

4.3.2 Concentrated synthetic ureolysed urine

Concentrated synthetic ureolysed urine ($CSUU$) was assessed in laboratory experiments to determine precipitation from unexpected positive cations which may have entered as impurities in the chemical salts used to synthesise these $CSUU$. An assessment of type of water was developed to avoid loss of phosphorus due to precipitation because of the presence of other cations in the water. Precipitation of P is possible when there is presence of other ions in the water, such as Mg^{2+}. Since experiments

are designed at bench-scale production, the application of tap water could be more feasible, however, precipitation of P due to tap water could significantly change the availability of this element before experiments. Indeed precipitated solids were found during preparation of $CSUU$, which decreases the concentration of the P from its nominal/intended level. Data in Figure 4.10 were obtained by using different types of water to compare with other potential interfering cations in the water. This data is the average of 2 replicates with $MilliQ$ water, 3 with deionised water, and 2 with tap water.

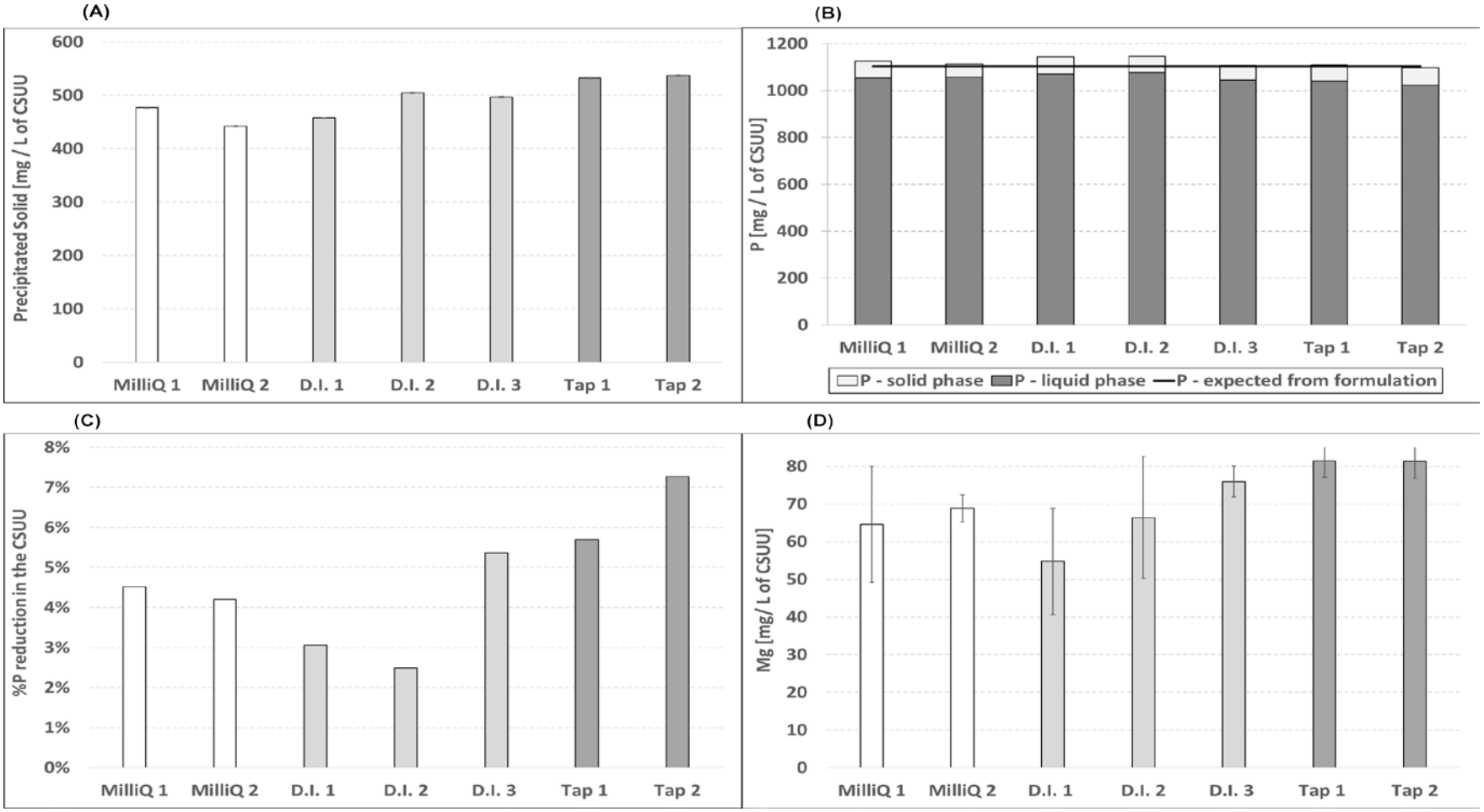

Figure 4.10 – Data from spontaneous precipitation in Concentrated Synthetic Ureolysed Urine ($CSUU$) with different types of water: $MilliQ$, deionised ($D.I$), and tap water. Error bars are +/- 2σ Subplot A is the mass of precipitated solid per volume of $CSUU$, (B) is P mass per L of $CSUU$, (C) is the % P reduction after precipitation in $CSUU$ and (D) is the quantity of Mg per volume of $CSUU$.

Figure 4.10.A shows the precipitated solid quantity per litre of concentrated of synthetic ureolysed urine, $CSUU$. These results show a similar quantity of solids in all cases, with a slight predominance in tap water. Tap water can contain other cations such as Ca, which could well trigger precipitation of additional solid phases, such as $CaCO_3$.

Figure 4.10.B shows the P elemental mass balance in liquid and solid phase after precipitation in $CSUU$. The concentration of P was measured in filtered equilibrium solution and in the dissolved recovered precipitated solid. The expected P from $CSUU$ formation is the initial quantity from $NH_4H_2PO_4$. In all these results, there is a strong agreement between the total initial P in $CSUU$ and the P in the resulting solid and equilibrium solution. These results indicate a high accuracy in the elemental determination of P, which gives great confidence in the results.

Figure 4.10.C shows the $\%\,P$ reduction in the filtered liquid from $CSUU$ after precipitation, by comparing with the initial expected concentration. The overall data showed that it is expected a % P reduction between 2 % to 7 %. The comparison of each of the data also demonstrated that P loss was greater with the use of tap water, while the average reduction of P in $MilliQ$ and deionised water are similar.

Figure 4.10.D shows that Mg was present as a possible contaminant from chemical reagents, because $CSUU$ formulation did not contain Mg salts. The Mg concentration in the filtered liquid sample solution was < 0.01 mg/L, while most of the Mg concentration came from analysis of the dissolved solid sample. Therefore, the overall data suggested that an initial P analysis of the liquid phase after spontaneous precipitation in $CSUU$ is key for later experiments. Deionised water was applied for batch and continuous precipitation experiments, due to the apparent larger reduction found in tap water, and the high cost in using $MilliQ$ water.

Figure 4.11 shows that most of the solid samples in $CSUU$ experiments is struvite, based on the N mass fraction. Experimental data show that there is an apparent larger content of pure struvite in $MilliQ$ compared to tap water experiments. In this analysis, an additional replicate analysis was

developed for each case, especially to corroborate the atypical point found in the first replicate analysis using deionised water. The duplicate analysis in this point showed that duplicate analysis could ensure reliability in samples with much lower expected % N (5.7 % for pure struvite).

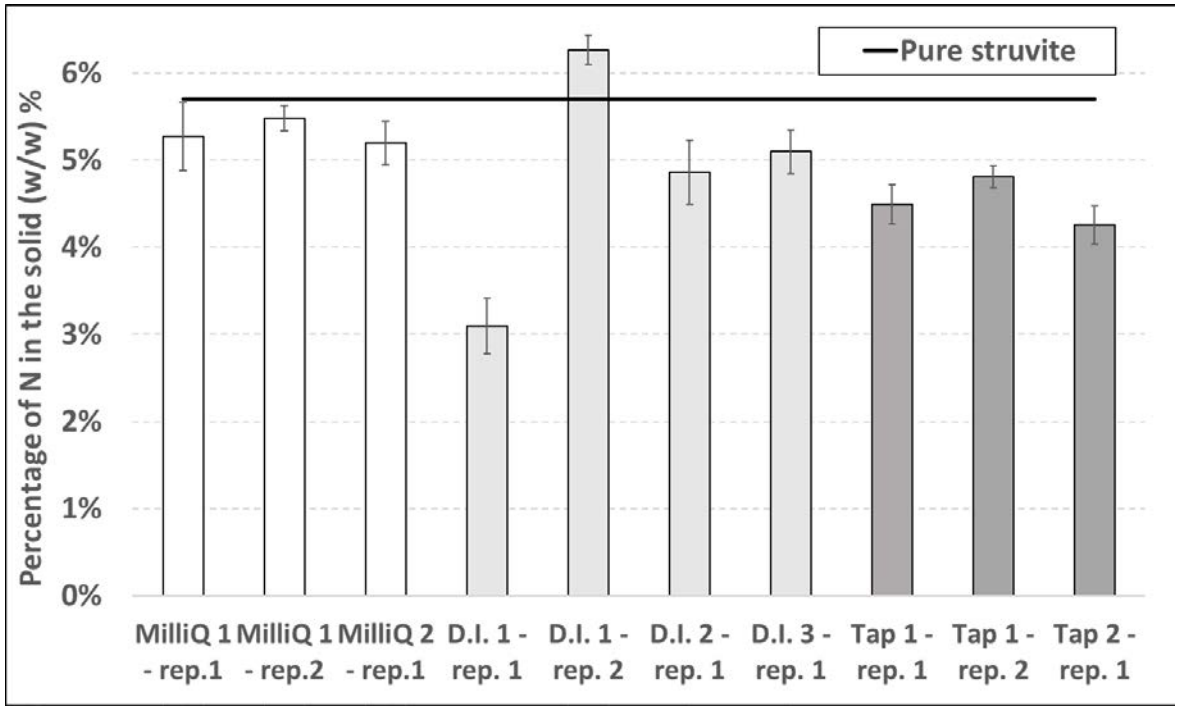

Figure 4.11 – Percentage of N in precipitated solid from $CSUU$ experiments. Error bars are +/- 2σ.

4.3.3 Validation in in batch experiments

Two duplicate set of experiments (batch 1 and 2) - with six batch precipitations each - were developed with different additions of Mg/P feed molar ratios. The precipitation process was obtained by mixing of 250 mL of filtered $CSUU$ with 250 mL of $MgSO_4.7H_2O_{(aq)}$ in 500-mL closed bottles. Equilibrium solutions were filtered after 24 h using 20-mL syringe connected to Millex® W Syringe Drive Filter unit PVDF 0.1 μm, and 2-L vacuum Erlenmeyer with a MicroScience – MS3 – 240 mm filter paper under vacuum. Precipitated solids were dried at 40 °C for 24 h.

The mass of solid was measured in an electronic analytical mass balance with four digits' precision for each experiment (Figure 4.12).

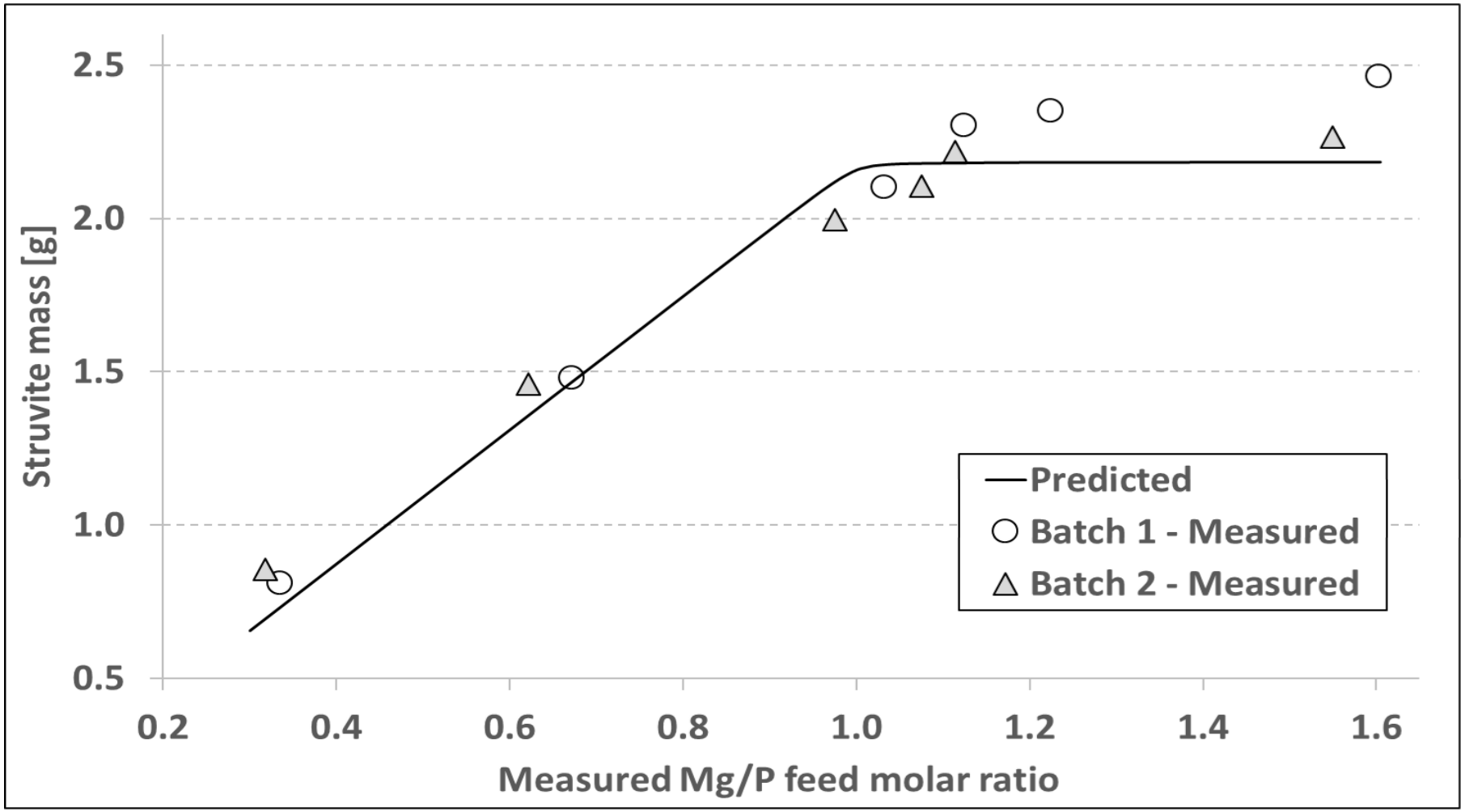

Figure 4.12 – Experimental validation using solid as struvite mass .The P concentrations in the filtered $CSUU$ and Mg in $MgSO_4.7H_2O$ mixture were measured to estimate the actual Mg/P feed molar ratio in each experiment.

Figure 4.12 validates the struvite mass prediction at different Mg/P feed molar ratio. The system shows a maximum solid precipitation at Mg/P feed molar ratio of one, which plateaus owing to the fact that the P becomes the limiting reagent. At Mg/P ratios less than 1, we see a steady rise in the amount of precipitant that results, which is as expected.

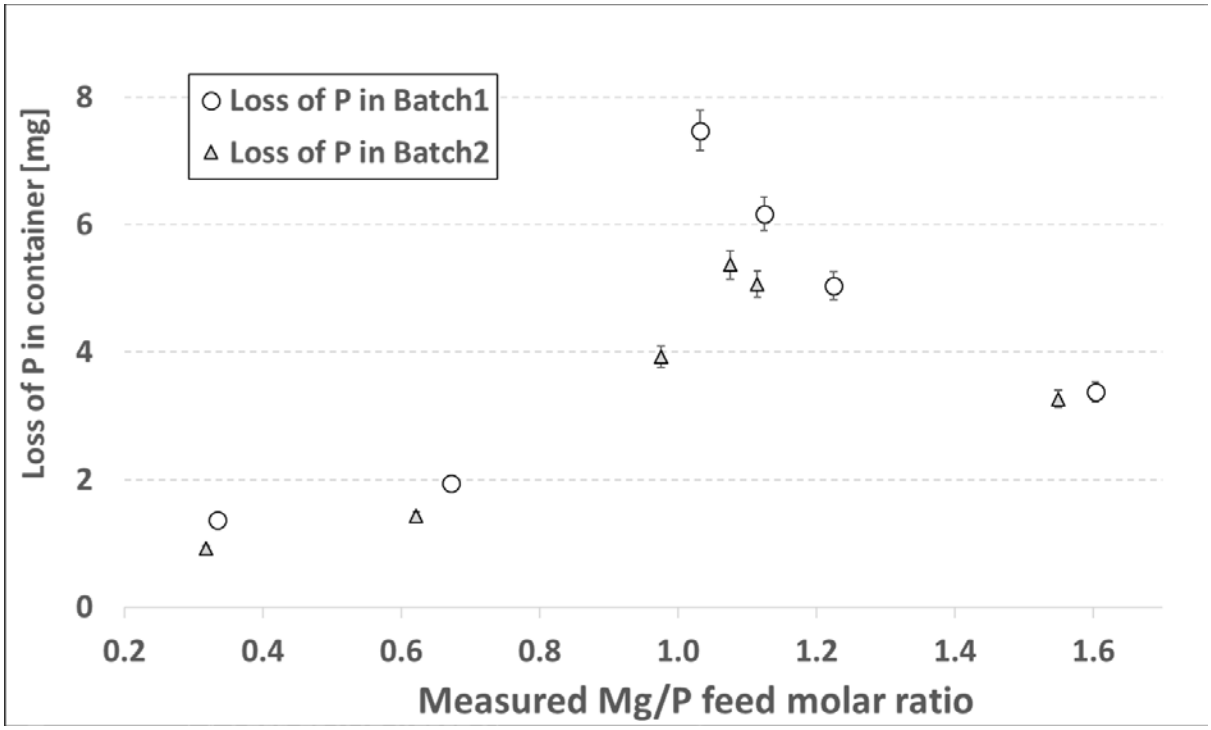

Figure 4.13 – P loss in glass bottles. Error bars are 2σ. Adhered crystals (that would otherwise be lost) on the bottle walls were analysed for elemental P by adding 100mL of deionised water and 1 mL 10.2 $M\ HCl$.

Figure 4.13. shows small quantities of P loss in each of the batch experiments. Struvite mass can be calculated by multiplying P molar quantity by molecular weight of struvite/molecular weight of P. Results showed losses between 0.78 % and 2.82 % can be expected, which is well within experimental error.

Figure 4.14.A and B show strong agreement between predicted and measured P and Mg concentration in the equilibrium solutions. These results provided confidence in the thermodynamic model's capacity and in the confidence of the analysis methodologies, a pleasing result.

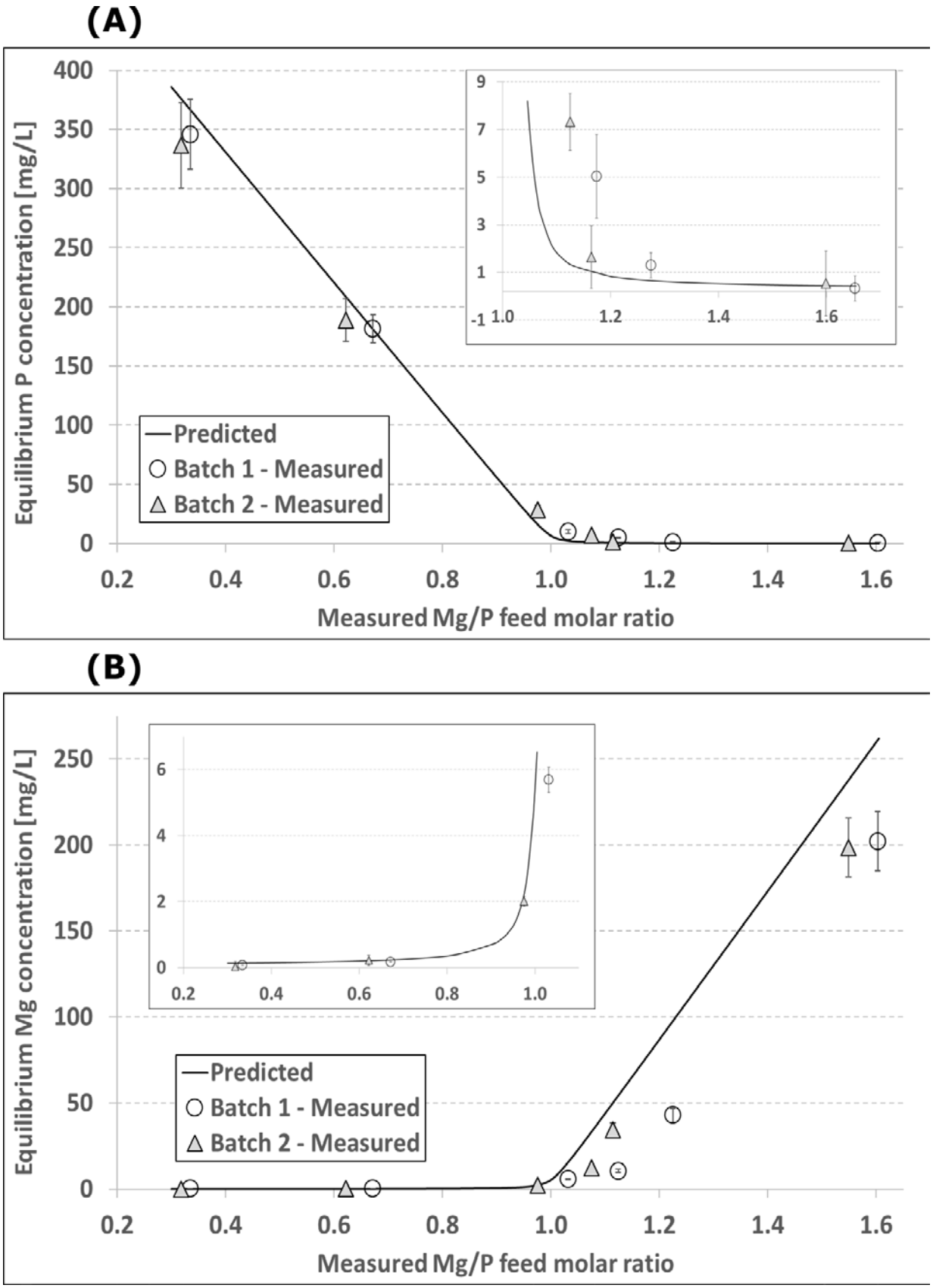

Figure 4.14 – Experimental validation using elemental P (A) and Mg (B) concentration in equilibrium. Error bars are 2σ.

Figure 4.14.a shows that Mg/P feed molar ratio lower than one are suitable for P analysis, because Mg/P ratios higher than 1 would lead to P losses that would give concentrations under limit of detection. Moreover, analysis of Mg in the equilibrium solution become less informative at Mg/P feed molar ratio < 1, because it will be essentially completely removed.

In Figure 4.14.B, disagreement between model and measurements suggested that at Mg/P larger than one Mg could be larger in the solid phase, and production of magnesium phosphates could be possible in small quantities. Even though, this quantity could not be significant, it can partially explain deviations in Figure 4.13 at large Mg/P feed molar ratio.

Figure 4.15 shows the percentage of Mg, N and P in the solid samples from batch 1 and batch 2 experiments. The analysis of N was developed with two duplicate analyses per sample.
Figure 4.15 a, b and c did not show a trend based on Mg/P feed molar ratio. In all three cases, the elemental % in the solid almost matches the expected, if the solid was pure struvite. The error bars were in each measurement considered the measurement uncertainty based on calibration slope and sample preparation (dissolution and dilutions).

The average of each of the elemental components showed larger deviation in the Mg element (Figure 4.15d); however, the expected point is included in the error bars. These error bars were estimated as a pooled standard deviation with two group set (Skoog, Holler, & Crouch, 2006). Moreover, a slightly larger content of Mg in the solid could be related to the lower concentration in the equilibrium solution.

Figure 4.16 represented the estimation of Mg/P and N/P molar ratios. As expected, values larger than 1 for Mg and lower than for N. This means that other possible solid phases could be formed in smaller amounts compared to struvite, but for the purpose of this thesis modelling using struvite as the only possible solid phase is more than adequate to describe the system

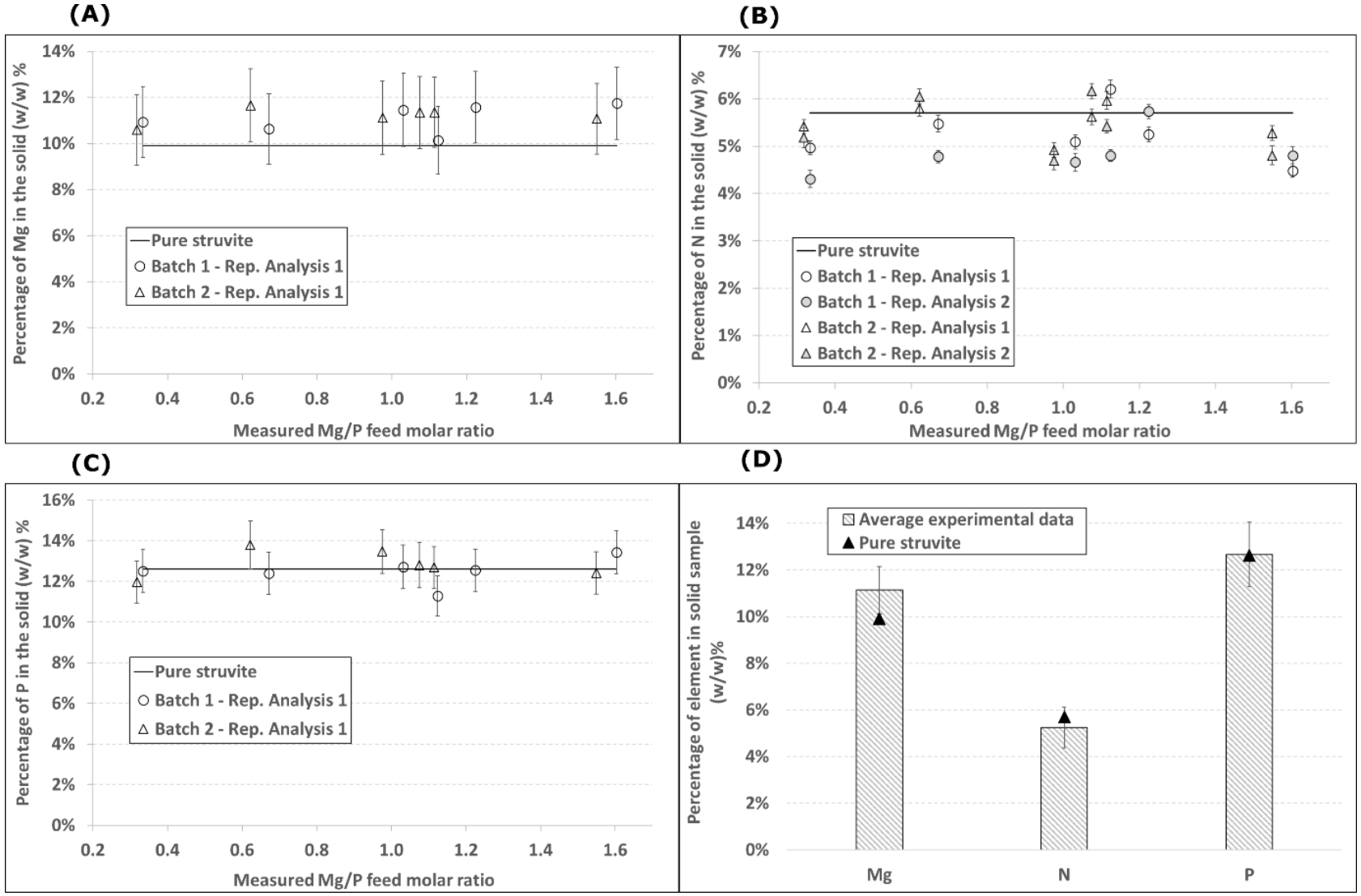

Figure 4.15 – Elemental composition of Mg (A), N (B), P (C), and sample average (D). Error bars as +/- 2σ in A, B and C; and 2x pool σ.

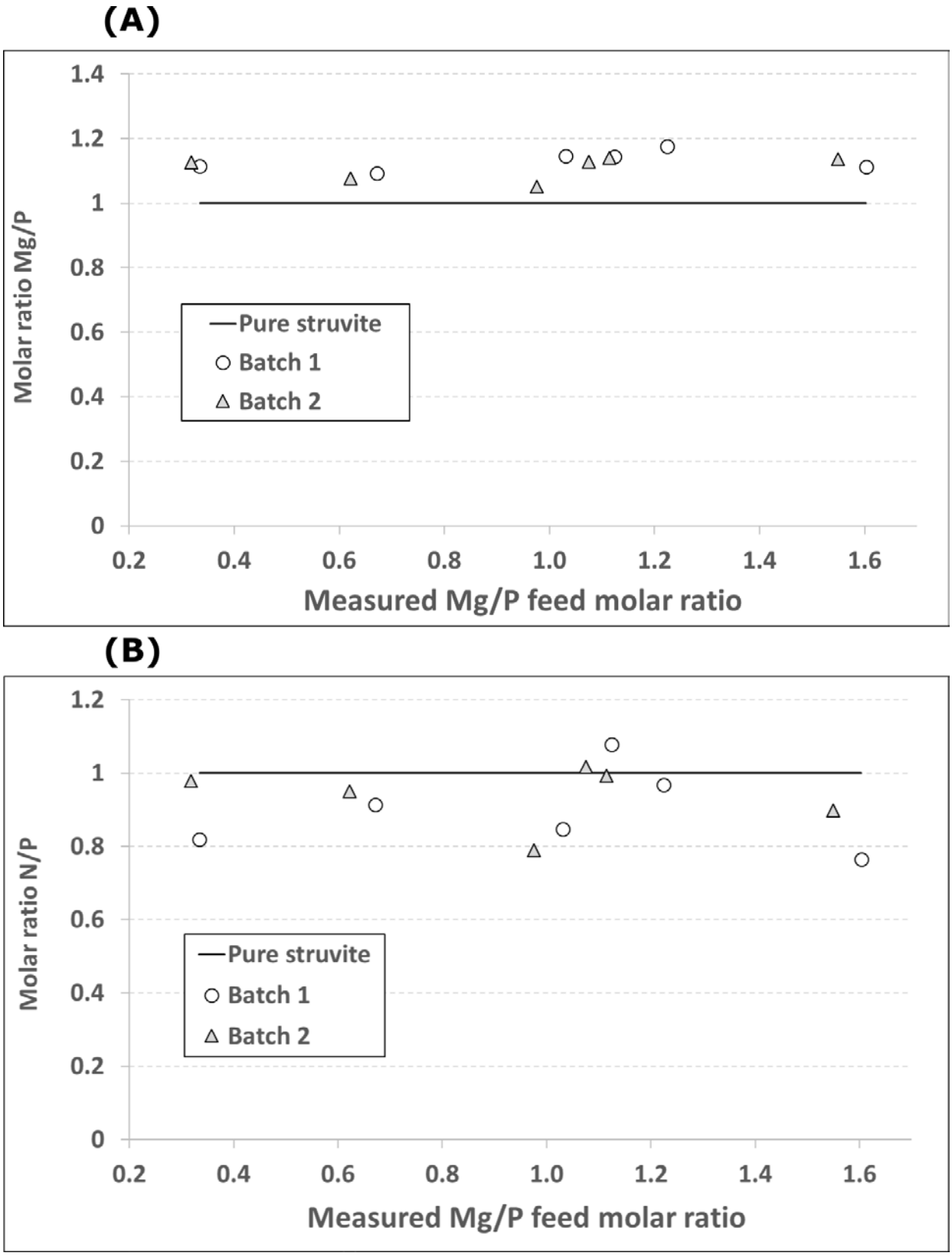

Figure 4.16 – Estimation of Mg/P (A) and N/P (B) molar ratio in solid samples at different Mg/P feed molar ratio. Data comes from two repeat sets of experiments.

4.3.4 Elemental mass balance in batch experiments

The elemental mass balance of P and Mg in each of the batches is presented in Figure 4.17. Every point was determined by analytical measurements. Figure 4.17.A.1 and Figure 4.17.A.2 show that the P from the solid phase represents more of the total P mass at higher Mg/P feed molar ratio, which stands to reason, since more Mg is available to precipitate struvite. The high proximity between the initial mass of P, and addition of P coming from the liquid and solid phase expresses confidence in the experimental procedure. Moreover, based on these experimental data, it is suitable to measure only the initial P concentration in the filtered concentrated synthetic ureolysed urine (initial P), and the concentration of P in the liquid. Therefore, the percentage of P in the solid sample could be easily estimated with large accuracy by difference

Figure 4.17.B.1 and Figure 4.17.B.2 show agreement between the initial Mg mass in the $MgSO_4.7H_2O$ source solution with the overall mass after precipitation. In batch 1 and 2, the final mass of Mg after precipitation (liquid and solid phase) is larger than the initial measured Mg. Similar to case of P mass balance, the composition of the solid phase is almost the total. Since the experimental struvite mass becomes constant at Mg/P larger than one, the analysis of the liquid phase is also important in this range.

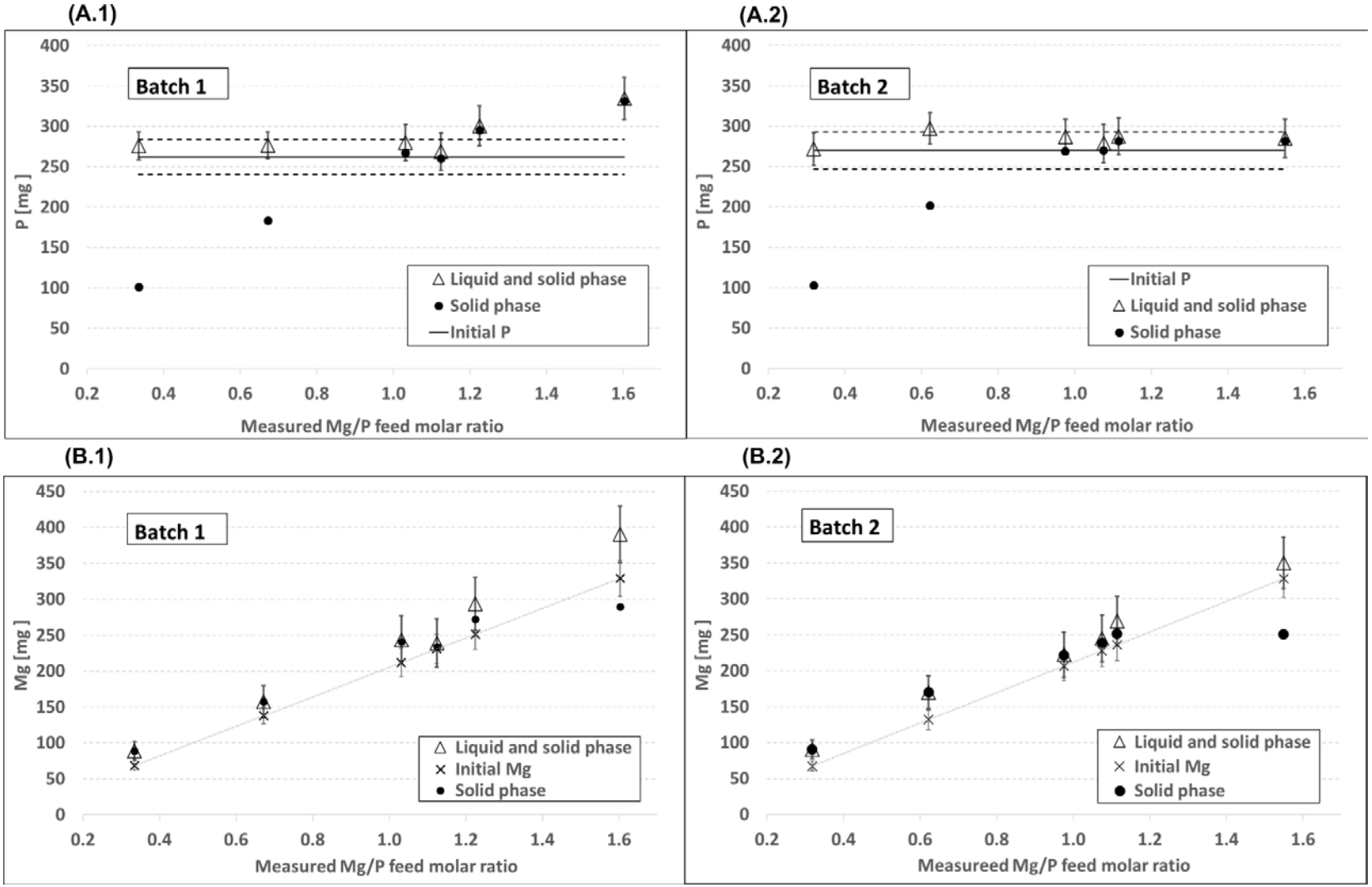

Figure 4.17 – Mass balance of P in Batch 1 (A.1) and Batch 2 (A.2); and Mg in Batch 1 (B.1) and Batch 2 (B.2). Dashed lines in (A.1) and (A.2) represented 2σ.

4.4 Laboratory tests before continuous experiments

This section describes the process configuration for continuous struvite precipitation experiments. It also includes assessment of on-line measurements, such as pH and conductivity. Mixing flow characteristics were also assessed in preliminary experiments using the continuous reactor. Methodology description to prepare initial struvite seeds in a fed-batch reactor is described. Methodologies to quantify and characterise struvite seeds were tested.

4.4.1 Continuous bench-scale reactor

The continuous nutrient recovery reactor was made from an acrylic cylindrical vessel of 12.1-L capacity and 145-mm internal diameter. Two axial propellers of 58.28-mm diameter and separated by 120 mm mixed the solution between 100 RPM to 200 RPM, which created a solid bed height of approximately 350 mm. Four baffles, width of 1/12 of the internal container diameter, were used to prevent a vortex during agitation.

Figure 4.18 shows the experimental set-up. Solutions containing the nutrient and Mg were pumped at the same flow rate from two sources. Unlike the real situation, it was decided to use equal flows of the two feed streams to minimise the uncertainty in Mg molar addition rate. Therefore, the nutrient feed tank was double the concentration of typical ureolysed urine. Two interconnected feeding tanks were used provide flexibility of reagent preparation in long-term operation. For instance, nutrient solution was prepared inside the top tank, while bottom tank fed the reactor. Bottom tanks are intermittently refilled by the top tanks during continuous operation. The outlet flow was discharged to waste or collected when saturated solution was needed for subsequent experiments. The reactor had three sampling taps, which were used during experiment especially at the beginning of the process when liquid concentration is most variable due to approach to steady state operation.

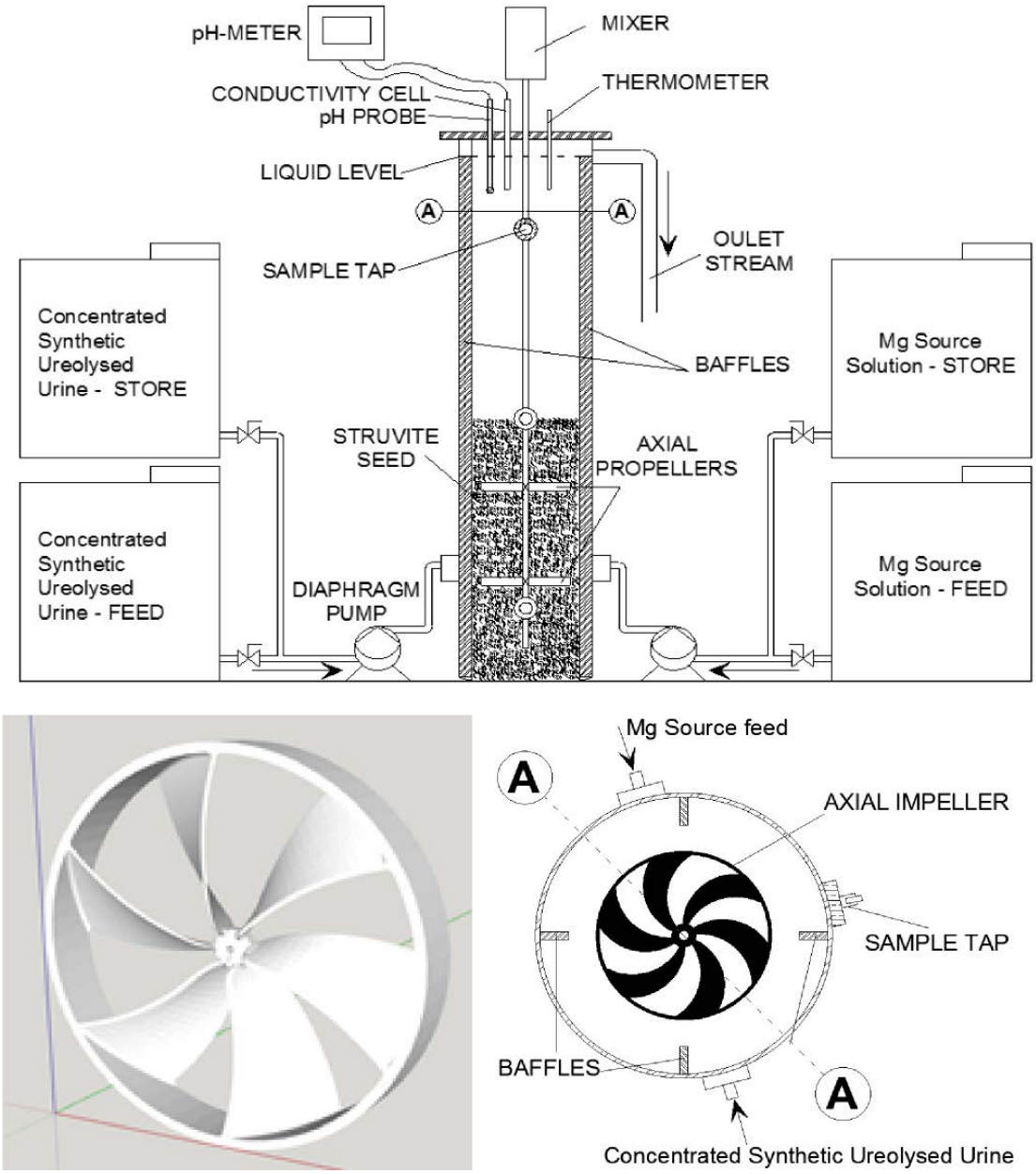

Figure 4.18 – Continuous process scheme of reactor operation.

4.4.2 pH and conductivity measurements

Continuous measurements of pH, conductivity and temperature (Appendix C.1) were made given their importance in continuous precipitation monitoring. The model of the continuous reactor operation does not consider open system and neither variation of pH and ionic strength due to adsorption of CO_2 or desorption of NH_3 over long operating campaigns. However, experimental data could provide a range of variable magnitude to be consider in long continuous and open system

experiments. Figure 4.19 A and B showed variability of pH and conductivity in open and closed systems. The synthetic urine composition used in this experiment was NH_4Cl (95 $mmol/L$), NH_4HCO_3 (266 $mmol/L$), $NaH_2PO_4.2H_2O$ (17 $mmol/L$), $(NH_4)_2SO_4$ (16 $mmol/L$), $NaOH$ (205 $mmol/L$), KOH (87 $mmol/L$) with a predicted 9.38 pH and 0.5 M ionic strength.

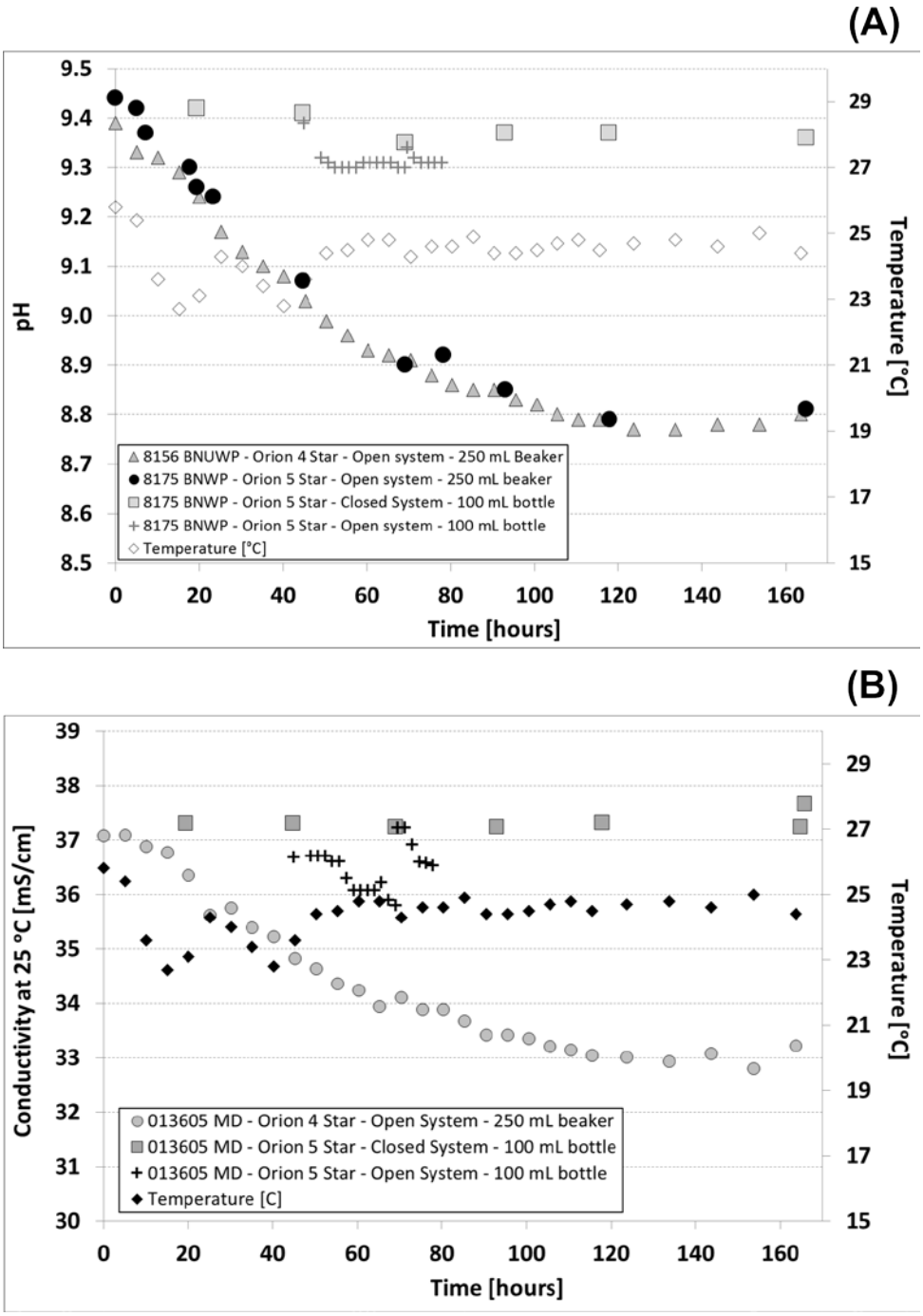

Figure 4.19 – pH (A) and conductivity (B) and temperature profiles in closed and open synthetic urine solution. Synthetic urine was placed within an open 250 mL beaker and within closed 100 mL glass

bottles. The 8156 $BNUWP\ pH$ probe recorded data in the open beaker; while the 8175 $BNWP\ pH$ probe was used in closed containers.

Figure 4.19.A shows a decrease of 0.6 pH units and 4 mS/cm in the conductivity were open containers. These variations also were affected by the container size due to the mass transfer area with environment, where CO_2 gain and NH_3 loss could be attributed to these observations.

An additional test was performed using the concentrated synthetic ureolysed urine (from chapter 3). In this test, equal volume of $CSUU$ and $MgSO_4.7H_2O$ (Mg/P = 0.9). The pH probe connected to a $LabVIEW$ interface recorded pH, temperature and conductivity of the $CSUU$ before, in the moment and after addition of the Mg solution to the $CSUU$ in an open beaker.

Figure 4.20 shows the evolution of pH during precipitation (A.1), and after precipitation (A.2). Conductivity measurements (B.1), and (B.2) were also monitored. Figure 4.20 (A.1) shows that Mg solution addition decreased the solution pH by around 0.10 units, while the conductivity change was more obvious because after mixing equal volumes of $CSUU$ and Mg solution, synthetic ureolysed urine solution was obtained plus Mg. Moreover, the small decreased in the solution pH corroborated the buffer capacity of urine due to its large ammonium-ammonia N concentration, which would tend to keep solution at $pH = \sim 9.1$.

Figure 4.20 (A.2) and (B.2) show that temperature does affect pH and conductivity data over several hours. Conductivity and temperature had a directly proportional relationship. A decrease of 0.2 pH in the 25 minutes after precipitation Figure 4.20 (A.2) could also be influenced by the system thermodynamics as explained in Figure 4.19. The 0.2 pH units change means that pH is not a suitable as a monitoring variable, since thermodynamic changes in the solution could be hidden by the open system effects. However, the abrupt decrease of pH during a minor interval, with conductivity variations larger than 2 mS/cm (+/-3°C) could show precipitation or changes following continuous experiments.

.

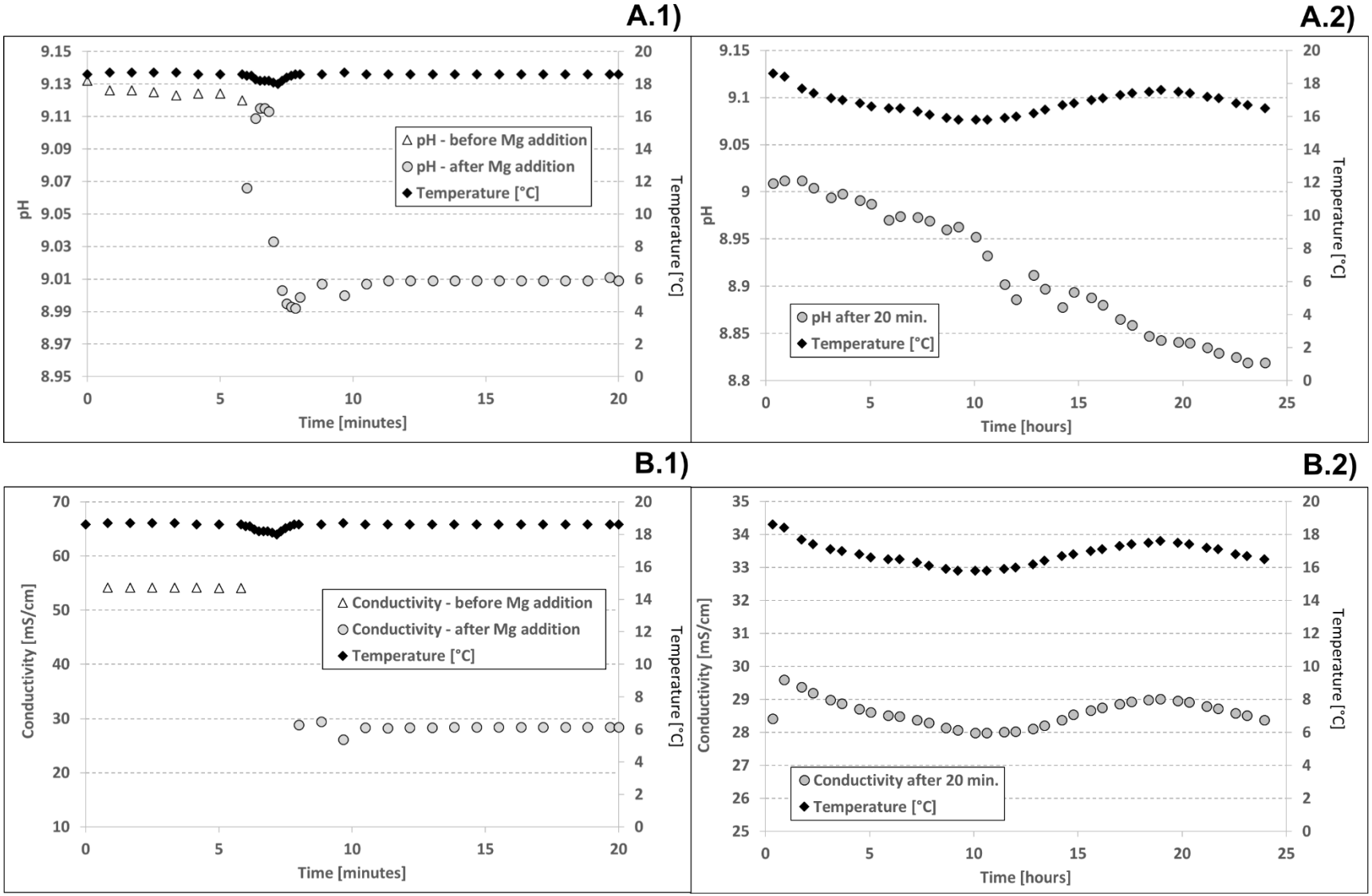

Figure 4.20 – pH, conductivity, and temperature during batch struvite precipitation from concentrated synthetic ureolysed urine.

4.4.3 Mixing characteristics of the continuous reactor

The mixing characteristics of a continuous reactor (Figure 4.18) were studied through tracer studies to determine the presence of intermixing flow rates between the top and the bottom zones (with seeds). Two studies were designed to determine the mixing behaviour of the reactor with, and without, suspended crystal.

The 12.1-L reactor was operated at 150 RPM (Figure 4.18), by injecting a coloured tracer at the level of the inlet feed. The tracer concentration was measured by spectrophotometry at 510 nm and 630 nm wavelength for red and blue, respectively. The first study consisted of feeding deionised water at 0.3 L/h to the reactor, without struvite (Figure 4.21.A); and the second consisted on feeding saturated solution to the reactor, containing 180 g struvite solid crystals (Figure 4.21.B). The second test had to use saturated solution in order to avoid dissolving the suspended struvite crystals. Periodically, samples were taken from the bottom and overflow of the reactor to compare tracer dispersion in the continuous reactor.

In both cases, dye concentration depletion was modelled by a first order expression in EES. In the singled-phase experiment (Figure 4.21.A), the estimated hydraulic residence time (HRT) must be 20 h (Volume of reactor/feeding flow rate = 12 L /0.6 L/h). This estimation that the effective volume (11.77 L) was similar as the container (12.1 L). Comparison of samples from the bottom and outlet sample points show that 10 minutes are necessary to achieve a homogeneous dispersion in single-phase (*i.e.* liquid only) reactor operation. This suggests that samples taken at any reactor height could be more representative of the overall system after the first 10 minutes, considering this reactor shape, mixing, and feeding flow rate. Sampling before this interval of 10 minutes should be developed at different sampling points to obtain meaningful data.

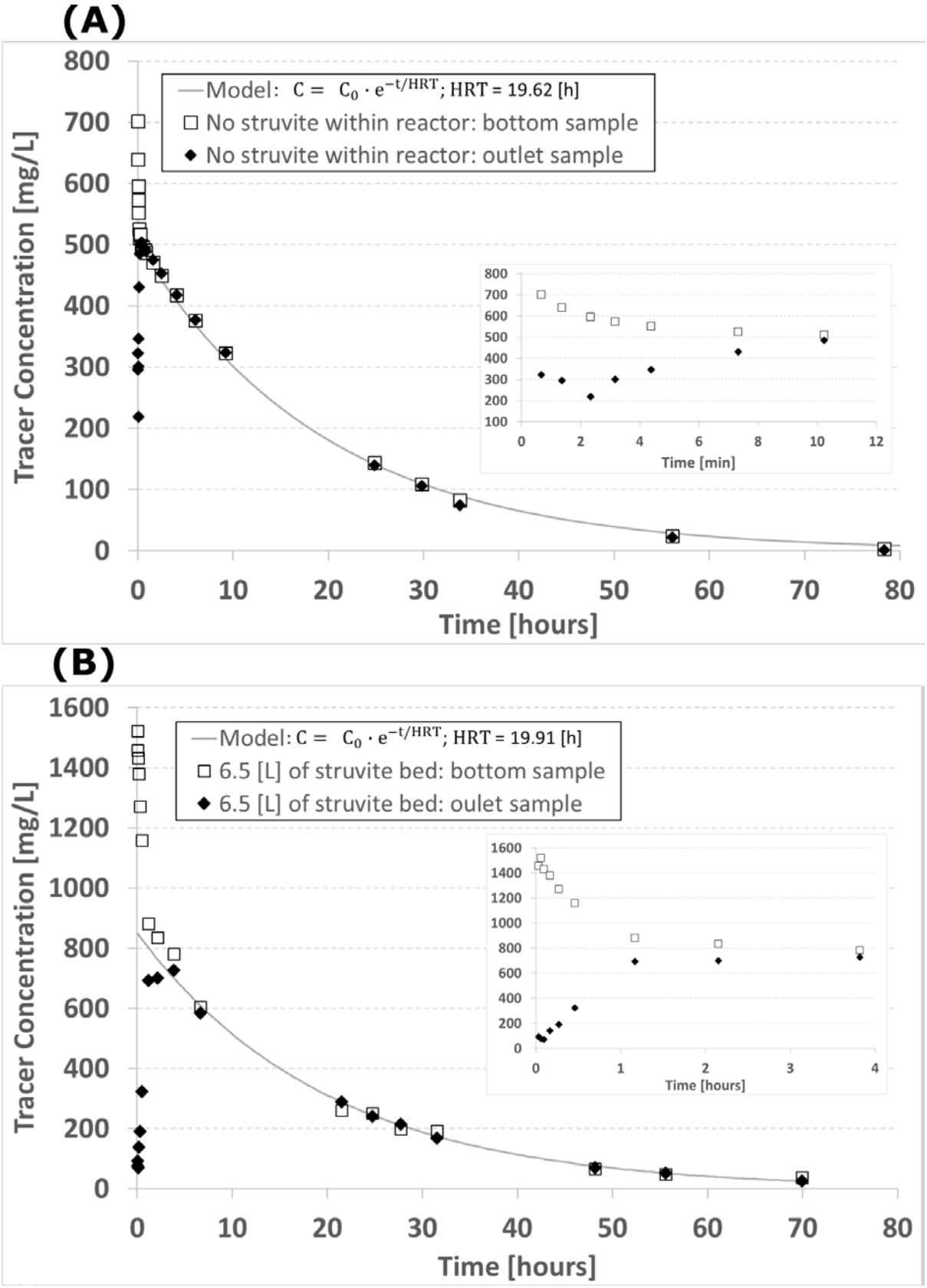

Figure 4.21 – Tracer studies using 150 RPM: without struvite (A) and with 180 g of struvite (B). The sub plots indicate the behaviour of the tracer in the first minutes of the test in each case.

In the two-phase experiment (*i.e.* with liquid and suspended crystals) (Figure 4.21.B), the experimental HRT was similar to first single-phase scenario. The estimation of the effective volume was 11.95 L. In both tracer studies, the estimation of effective volume smaller than reactor indicated the presence of a zone of poor mixing within reactor. Tracer concentrations at bottom and top showed that 4 hours are needed to collect samples that are equivalent across the two reactor points, because of the concentration profiles in the subplot of Figure 4.21.B. Moreover, the estimation of an effective volume similar to the actual reactor, and differences between tracer concentrations collected at the top and bottom showed that the system does not behave as a well-mixed tank reactor.

4.4.4 A two-zone reactor mixing model

Figure 4.21.B shows that the system does not behave entirely as a $CSTR$ followed by a sedimentation zone, which was assumed to be represented as a plug flow reactor (PFR). Further, since the top concentration did not show a peak concentration similar to the bottom, as expected for PFR systems (Fogler, 1999). Therefore, the entire system was modelled as two well-mixed zones, with intermixing liquid flow between them.

Figure 4.22 describes the new model configuration, where intermixing flow rates ($F_{intermix}$) was included in the dynamic balance in each of the one (bottom) and two (top) zones. In this figure, C_{j1}^{in} represents the concentration of the "j" element entering the zone 1; C_{j1}^{out} represent the elemental concentration of the "j" element leaving the zone 1; C_{j2}^{out} is the concentration of the "j" element leaving the zone 2. This figure also considered an overall flow rate (F) entering and leaving each volume, with separate and arbitrary values for the intermixing flow rates ($F_{intermix}$), which is related to agitation characteristics. The intermixing flow represents an additional degree of freedom that can be adjusted to fit the experimental data.

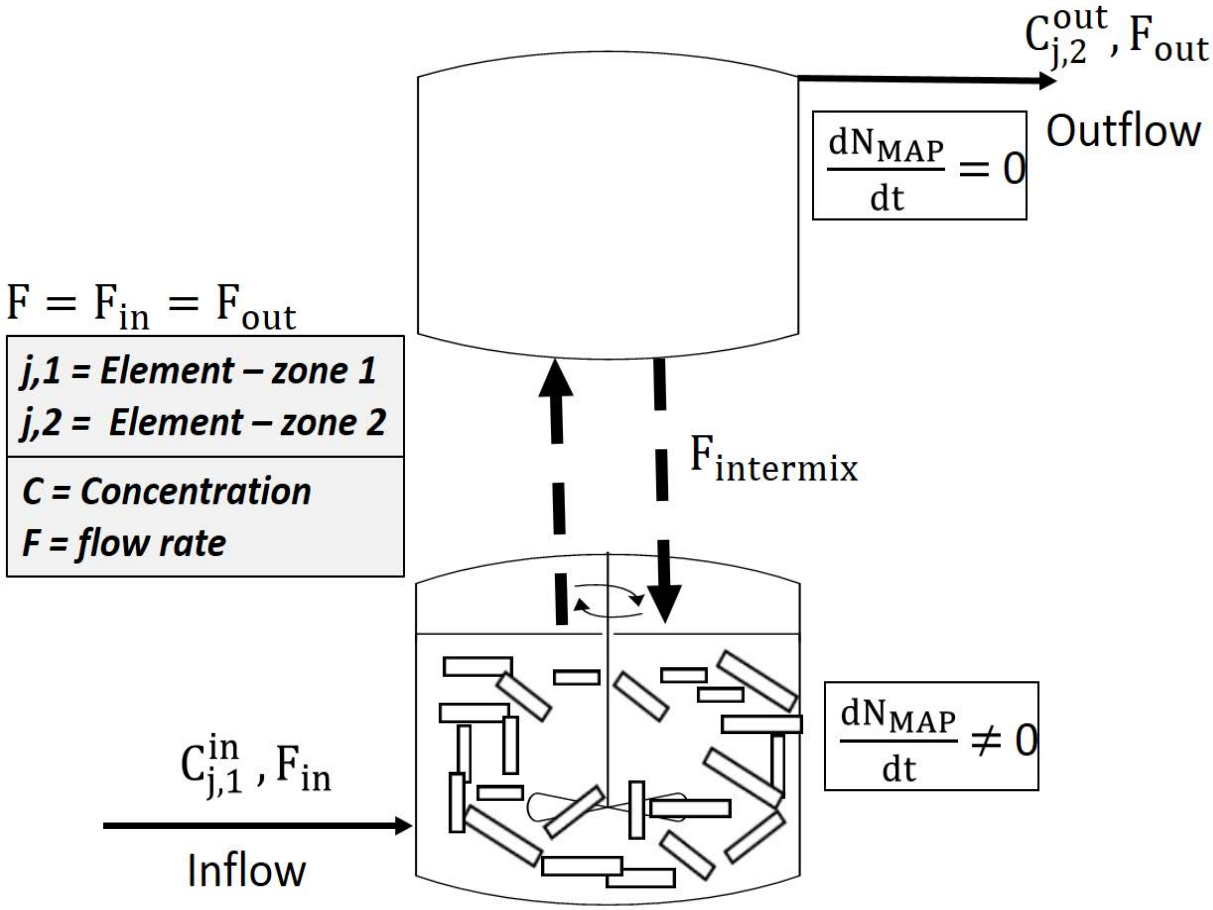

Figure 4.22 – Modelling configuration considering intermixing flow rate.

Infinite $F_{intermix}$ represents the ideal continuous stirred tank behaviour while close-to-zero mean no back-mixing from zone 2 to zone 1. Tracer concentration at the top and bottom zones were predicted with a dynamic mass balance model in EES to regress the experimental $F_{intermix}$, which is shown in Figure 4.21.B.

The tracer concentrations at the bottom (C_1) and top (C_2) zones of the reactor were estimated with EES using Equation 4.6 and Equation 4.7. Figure 4.22 describes the input and output streams in each of the reactor zones as predicted by the two-zone mixing model. The struvite seed bed volume in the seeded tracer experiment (section 4.4.3), which was assumed 6.25 L, was used as the bottom reactor zone (V_1), while the difference with the total volume container (12.1 L) was the top zone volume (V_2). The process flow rate (F) was 0.6 L/h, the intermixing flow rate ($F_{intermix}$) was set to a value that matched the experimental data with that from the simulation (Figure 4.21.B). The initial concentration

condition in the bottom zone considered an addition of 10 mL of tracer, which was distributed in V_1 very rapidly. The initial concentration condition in the top zone was set to zero to match reality. And, of course, the concentration in the feed streams ($C_{1,feed}$) was set to zero, because was added in just one pulse.

$$V_1 \cdot \frac{dC_1}{dt} = F \cdot C_{1,feed} - (F + F_{intermix}) \cdot C_1 + F_{intermix} \cdot C_2 \quad 4.6$$

$$V_2 \cdot \frac{dC_2}{dt} = (F + F_{intermix}) \cdot C_1 - (F + F_{intermix}) \cdot C_2 \quad 4.7$$

Figure 4.23 (A) and (B) show the comparison between experimental and predicted tracer concentration in EES with different intermix flow rates values. Several simulations were performed by varying the intermixing flow rate to determine the best match with the experimental data. An intermixing flow rate of ~$4L/h$ allows the simulation to overlap the experimental data, thus suggests that there is reasonably rapid intermixing between the zones – but certainly not infinite intermixing. These estimations confirmed that reactor modelling should include intermixing zones, instead of modelling two non-interacting zones, as had been done previously.

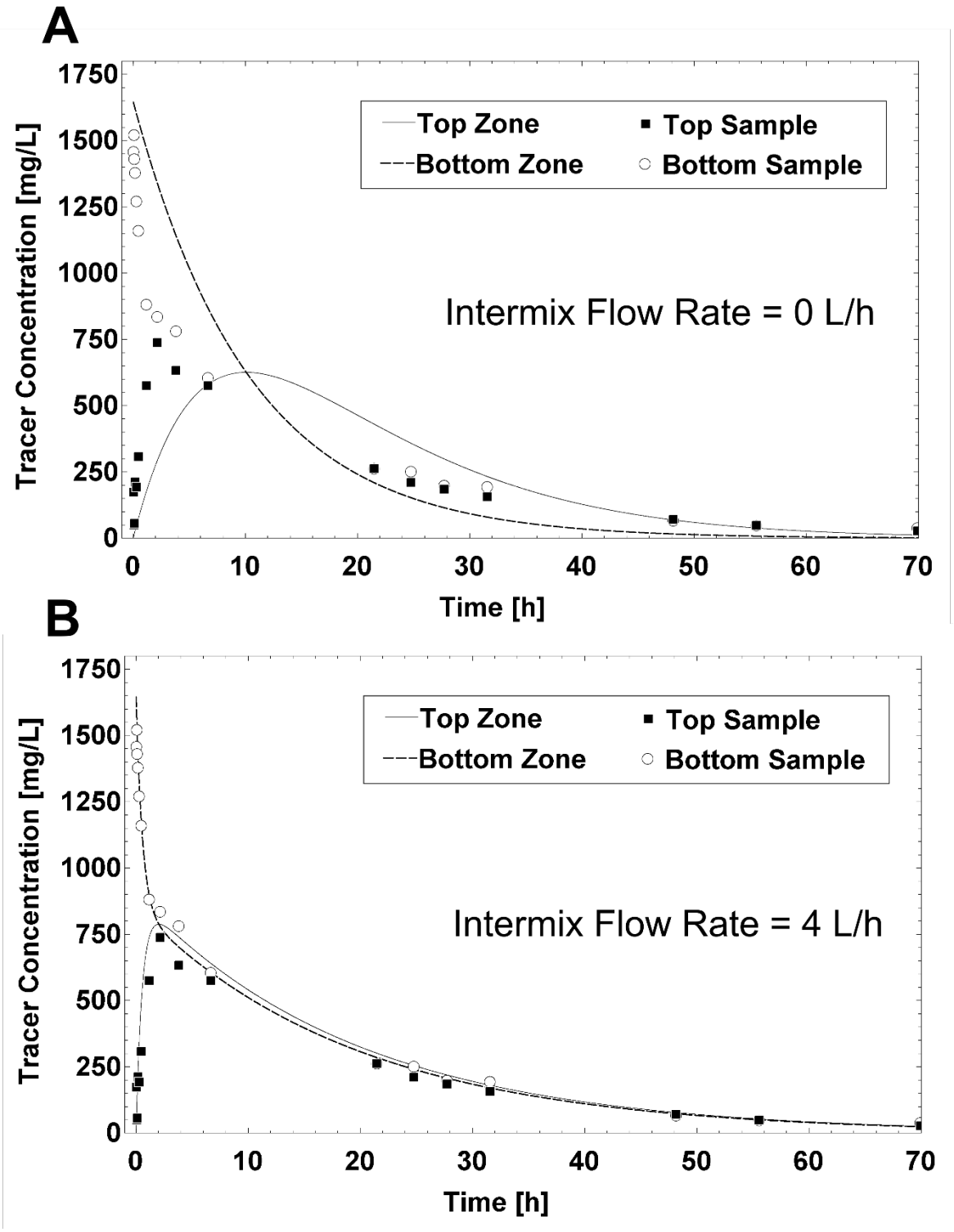

Figure 4.23 – Tracer concentration prediction in two zones without (A) and with intermixing flows (B).

4.4.5 Struvite seed preparation

Continuous nutrient recovery can be developed in unseeded and seeded reactors. The first case was not assessed in this thesis, because nucleation was not included in model development. In the second

case, the seed quantity and mean particle size impact the Saturation Index and the struvite production rate. In a first stage of this thesis, seed particles were prepared at controlled conditions in a laboratory fed-batch reactor. This experiment was simulated in section 3.3.3.

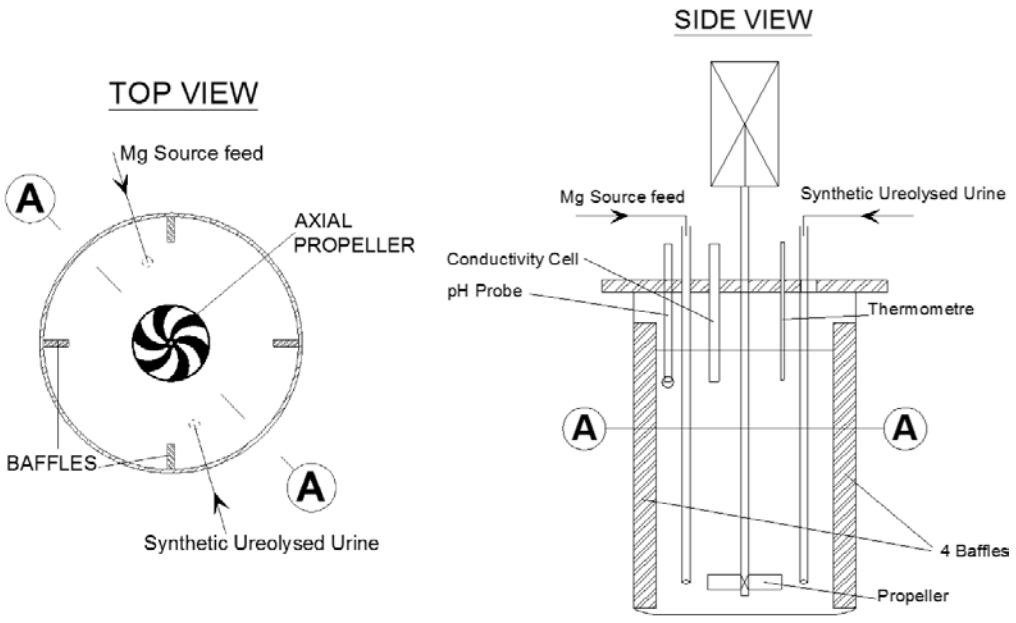

Figure 4.24 – Fed-batch reactor configuration.

The laboratory reactor was built in a 6-L borosilicate beaker with an internal diameter of 175 mm, and effective height of 230 mm (Figure 4.24). The beaker was modified by placing four acrylic baffles of 12.1 mm width to break mixing vortex. An IKA (R) RW 20 digital mixer was attached to a six-blade impeller to agitate the liquid at 200 RPM in clockwise direction. The impeller diameter and the baffle width were 1/3 and 1/12 of the internal beaker diameter, respectively (Lane & Koh, 1997; McCabe, Smith, & Harriot, 1993). An additional outlet stream was attached at the reactor top to prevent draining when liquid surface surpassed volume capacity.

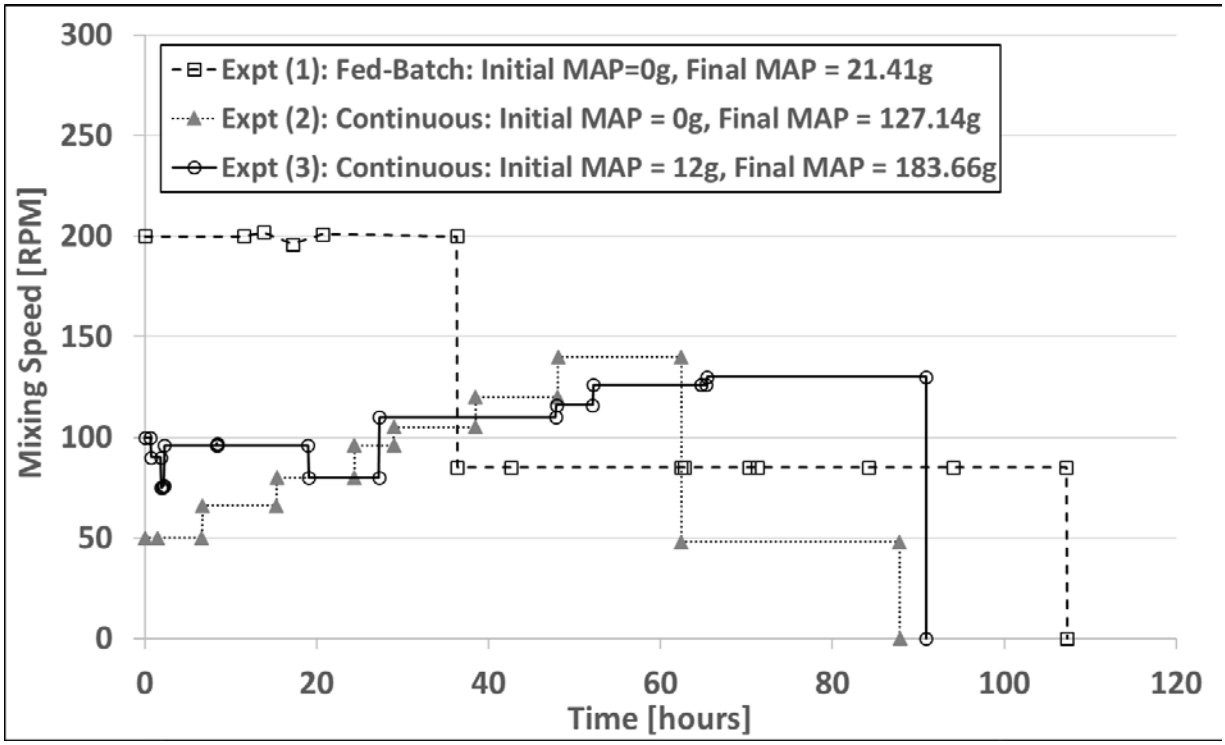

Figure 4.25 – Mixing speed in struvite seed production using a 6-L reactor and 9 h residence time.

The initial struvite seed were prepared by manually adding volumes of nutrient and $NaOH$ solution with volumetric pipettes (15 mL of 2 M $NaOH$, 25 mL of 1 M NH_4Cl and 15 mL of 1 M $MgCl_2.6H_2O$). Subsequent experiments were also performed by continuous addition of synthetic urine in one feed and Mg source in the second one. These solutions were fed at the level of the mixing impeller with two Grundfos DME12 diaphragm pumps.

Figure 4.25 shows that agitation speed has to be adjusted according to struvite quantity to avoid particle losses at the outlet top. The agitation speed to keep particles in suspension had to be decreased over time when more struvite particles had precipitated and grown. For this reason, in first experiment (Expt. 1) the mixing speed was 200 RPM at the beginning, but has to be changed to less than 100 RPM almost at the middle part of the process. Second (Expt.2) and third experiment (Expt. 3) started with lower mixing speed; however, mixing had to be slightly increased due to the increasing mass of seeds within reactor. Continuous mixing variations during the process suggested that a larger

height container with an top sedimentation zone is suitable to avoid particle loss in the outlet stream (§ 4.4.1).

4.4.6 Struvite mass quantification

The quantity of struvite mass measured indirectly with a density method. The purpose of this methodology was to avoid dehydrating the struvite seed crystals before continuous reactor operation. Dehydration of crystal could cause changes in the morphology/structure of the crystals, and possible loss of water mass when drying temperature is not correctly selected and monitored. In this methodology, struvite crystals are suspended in saturated solution. The mass of the crystals within the container is calculated by considering a balance of mass and volume of the saturated solution and the struvite mass in a graduated container. The calculations consider as input data: the volume of the flask with crystals and saturated solution, the density of the saturated solution and the mass of the container and the container with the crystals in saturated solution.

Figure 4.26.A shows that the quantity of crystals within the 2-L conical flask has to be a larger than 250 g to ensure an uncertainty lower the 2 % in the estimation of the struvite mass.

Figure 4.26.B shows the measured density of the saturated solution using the relative density method and hydrometer. The relative density method consisted in comparing the mass of the water with the saturated solution using the same volumetric flask (250 mL). Results show a systematic deviation between two types of measurements for four tests.

Figure 4.26.C shows the estimation of struvite crystals by considering the same overall mass measurement, but considering different densities of saturated solution.

In overall results show that this methodology is highly sensitive to the density of the saturated solution and the quantity of solid placed in the container.

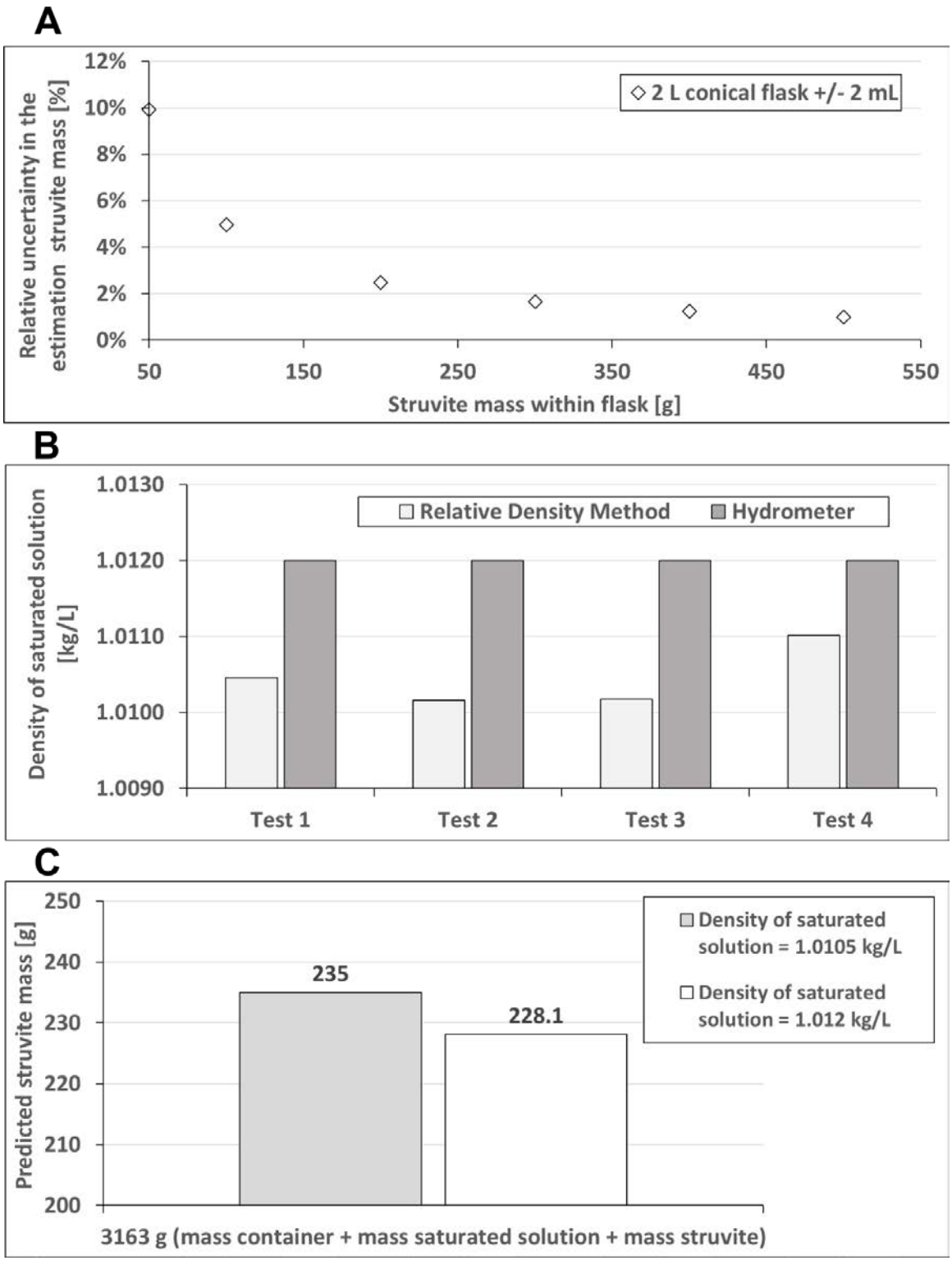

Figure 4.26 – Density Methodology test to determine quantity of struvite crystals. Plot A: uncertainty in predicted struvite mass according to different quantity of struvite in the flask, Plot B: the density of the saturated solution, Plot C: predicted struvite mass considering different densities of saturated solution.

4.5 Summary

- Concentrated synthetic ureolysed urine and $MgSO_4.7H_2O$ were chosen as feed solutions
- Monitoring of pH and conductivity are of interest, but not highly informative due to the effect of temperature and possible transport of $NH_3(g)$ and $CO_2(g)$ from solution to environment in open systems and pH buffering
- Struvite bed height level depended on mixing speed, reactor shape, and struvite quantity during struvite seed production in a 6-L fed-batch reactor
- Comparison of background standards (equilibrium solution as complex solution) with $MgSO_4.7H_2O$ standard showed that negligible interference can be found
- Preparation of concentrated synthetic ureolysed urine triggered the spontaneous solid precipitation due to impurities in chemical reagent. Therefore, the analysis of the liquid phase before further experiments was compulsory. Deionised water is suitable for all experiments based on solid precipitation quantity, and analysis of P and Mg in liquid and solid samples. The precipitated solid from $CSUU$ preparation was likely to be struvite
- The precipitated solid was likely to be struvite, but with probably very small quantities of other solid phases based on analysis in liquid phase. Elemental mass balance was used to determine the reliability of the experimental procedure.

5 Application of the Continuous Struvite Precipitation Model to a real reactor – experimental design and performance prediction

---

Highlights:

- *Simulations of continuous struvite precipitation considering two-zones reactor model*
- *Sensitivity analysis of different process variables in saturation and struvite precipitation rate*
- *Application of the model to select process conditions in continuous struvite precipitation*
- *Discussion of the kinetic parameters and the selection of diverse kinetic models*

5.1 Continuous reactor simulations

Process modelling of continuous struvite precipitation is scarce in literature review. Previous research has only focused on modelling batch struvite precipitation reactors. The dynamic model developed in § 2.2.2 was updated by including two zones according to tracer studies (§ 4.4.4). The application of a two-zones reactor represented a purposefully simple approach to describe the hydrodynamics in continuous struvite precipitation reactors. The dynamic model was solved in EES.This dynamic model was also applied to predict elemental concentrations at equilibrium (Appendix B.3). The base case scenario was illustrated considering typical reactor operating conditions. This base case scenario was simulated as starting point for later assessment within this Chapter.

5.1.1 Equilibrium calculations

The dynamic model simulated the system at positive struvite saturation index (SI_{MAP}) at non-equilibrium. In addition, the calculation of the equilibrium concentration at any time provides the advantage of knowing the maximum quantity of struvite to be recovered as well its expected elemental concentration profile. The addition of an "Equilibrium Module" within the dynamic model makes possible the estimation of the non-equilibrium and equilibrium elemental concentration at any processing time. In this work, this "module" calculated the equilibrium concentrations of elemental P and Mg by setting the SI_{MAP} to zero (*i.e*. equilibrium). This feature allows any potential struvite to form, which returned the equations to zero degrees of freedom.

Comparisons of non-equilibrium and equilibrium conditions using the dynamic model are a quick indicator of how far the reactor is operation from equilibrium conditions at any given time. This approach comprises the equilibrium batch model (§ 3.2.2) inside the dynamic one. The "Module Equilibrium" feature.

5.1.2 Definition of Mg/P feed molar ratio

Simulations considered the use of filtered concentrated synthetic ureolysed urine ($FCSUU$) and the magnesium solution fed to the reactor from two different streams. The $FCSUU$ is the concentrated synthetic ureolysed urine composition after precipitation (§ 4.3.2). The addition of Mg in the simulations was parameterised through the elemental Mg/P feed molar ratio (equation 5.1).

$$\left(\frac{Mg}{P}\right)_{feed\ molar\ ratio} = \frac{\mathrm{C_{MgSO4.7H2O}} \cdot \mathrm{V_{MgSO4.7H2O}}}{\mathrm{C_{P_{CSUU}}} \cdot \mathrm{V_{CSUU}}} = \frac{\mathrm{C_{MgSO4.7H2O}} \cdot \mathrm{F_{MgSO4.7H2O}}}{\mathrm{C_{P_{CSUU}}} \cdot \mathrm{F_{CSUU}}} \qquad 5.1$$

The second and the third term of the equation 1 represent either the batch and continuous reactor operation, respectively, where $C_{MgSO4.7H2O}$ is the molar concentration of $MgSO_4.7H_2O$ in the feed, $C_{P_{CSUU}}$ is the elemental concentration of after precipitation in the concentrated synthetic ureolysed

urine, $V_{MgSO_4.7H_2O}$ and V_{CSUU} are the volume of the magnesium solution and the concentrated synthetic ureolysed urine in Litres. $F_{MgSO4.7H_2O}$ and F_{CSUU} are the flow rates in each of the feeding tanks in L/h during continuous reactor operation.

5.1.3 Operating conditions of base case scenario

Input data for dynamic simulation considered specifications of the bench-scale reactor (12.1-L volume) and an intermixing flow rate of 4 L/h (§ 4.4.4). The initial conditions in each simulation were based on the assumption that the liquid phase composition was saturated (*i.e.* $SI_{MAP} = 0$). This initial saturated solution was prepared by mixing equal volumes of $FCSUU$ and Mg source and leaving to reach equilibrium (SI_{MAP} = 0). The composition at equilibrium was predicted by the batch model implemented in EES (Appendix B.2). The $FCSUU$ suffered a 6 % loss of P from the expected concentration based on batch experiments in § 4.3.2. Table 5.1 summarises the base case and lower and upper values considered for simulation assessment.

Table 5.1 — Condition for continuous simulations, showing base, lower and upper parameter ranges

Assessment of design variables	**Base**	**Lower**	**Upper**
Mg/P molar feed ratio	0.6	0.3	1.2
Flow rates of nutrient and Mg source $[L/h]$	0.3	0.1	1
Initial mass of seeds $[g]$	225	50	500
Initial mean particle size $[\mu m]$	100	10	200
Operational variables	**Base**	**Lower**	**Upper**
Effective volume $[L]$	6	3	8
Initial mean particle size of the seeds$[\mu m]$	100	10	200
Intermixing flow rate $[L/h]$	4	3	5
Kinetics: Power – law parameters			
k $[m/h]$, n	1e-6, 1	-	-
Simulation parameters			
Simulation time	110 h	-	-
Feeding time range	0 – 100 h	-	-
Stopping time range	100h to 110h	-	-

5.1.4 Solving technique

Solving in EES showed strong numerical instabilities at the start of the process in trial simulations. This situation caused strong transients in saturation index profiles owing to sudden changes in feed flows. For instance, simulation for 100 h reactor operation showed atypical data at the beginning. This atypical data was characterised by abrupt changes in the calculated struvite saturation index to very large and negative values. To overcome this issue, the integration step size in the software was reduced, however, solving by the software required much more computing time. Therefore, a "Macros was implement in EES to integrate by time segments (Appendix B.4).

Integration by time segments commanded the numerical solution to divide in smaller steps initial and final time segments. The $Macros$ integrated across three segments in time: from 0 - 1 h, 1 - 100 h and finally from 100 - 110 h. The $Macros$ assigned the values of the end of the time segment to the initial value to following one. For instance, the calculated variables at 1 h in the first segment were assigned as the initial condition in the second time segment. This simulation methodology allowed numerical stability in predictions and shorter computing time.

5.1.5 Base case simulations

This section discusses the simulation of the base case scenario cited in Table 5.1. Simulations considered top and bottom zones of the reactor. The chosen key output variable were the struvite saturation index (SI_{MAP}), the struvite mass production (m) and the specific productivity rate of struvite (SPR). The SI_{MAP} was selected as an indicator of saturation.

The m_{MAP} in kg was calculated at any time to determine evolution of the struvite quantity within the reactor. The SPR was already defined in § 3.4.6 as the molar production rate divided by the liquid volume (in this chapter consider as effective volume: V_{eff} and $V_{eff} < V_{reactor}$) and the quantity of struvite mol.

The saturation index profile was estimated for the top and bottom zone considering different intermixing flowrates between zones (Figure 5.1).

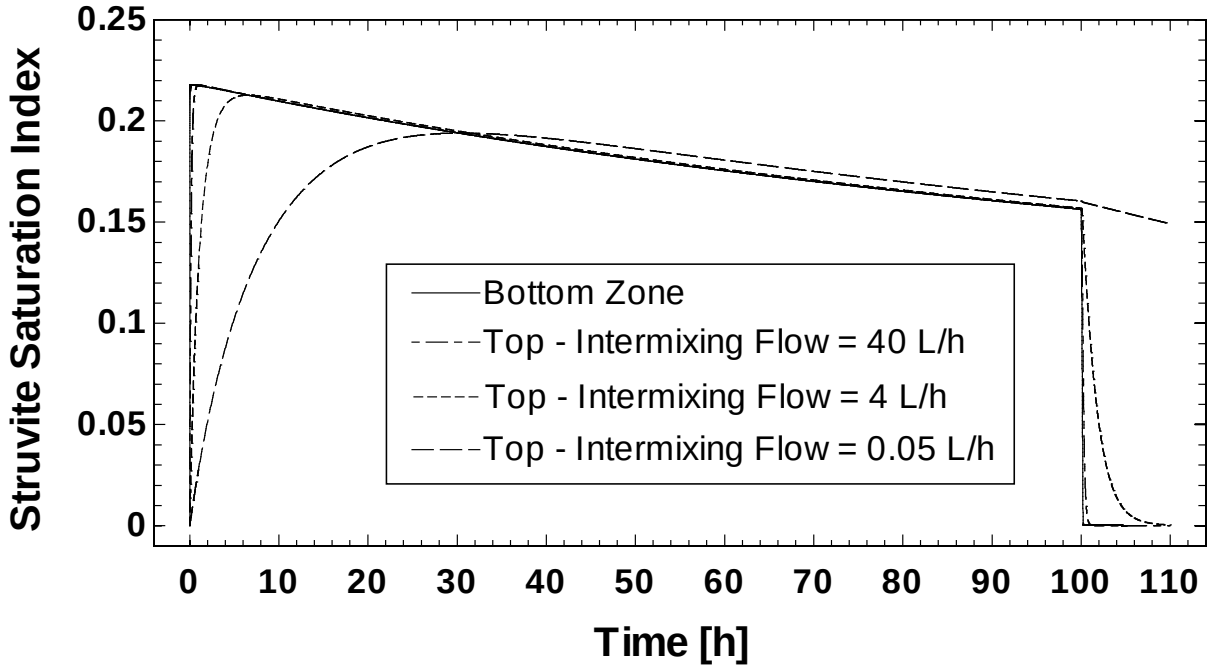

Figure 5.1 — Struvite saturation index at in two zones, considering different intermixing flows.

Figure 5.1 shows that in the bottom – zone (where the crystals are suspended) the SI_{MAP} rapidly increases to a maximum and then declines over time. The profile of the top – zone SI_{MAP} dynamically lags the bottom – zone because the components fed into the bottom – zone. The addition of the nutrient solution at the bottom – zone distribute and decline slower at the start and end of the process, which can be attributed to the intermixing flow rate between zones.as profiles at 0.05 L/h to 40 L/h are indicating in this plot. This plot also indicates that a selection of an intermixing flow rate of 4 L/h constrains simulation to the assessment of the bottom zone assessment.

Figure 5.2 shows the linear increase of struvite within the reactor. This tendency is linear because of the presence of initial quantity of struvite seeds. Stopping the flow rate of the feed stream immediately stopped in the struvite precipitation in the last 10 h. This profile was also observed in previous studies modelling continuous struvite precipitation at $Mg/P = 1$ (Schneider et al., 2013).

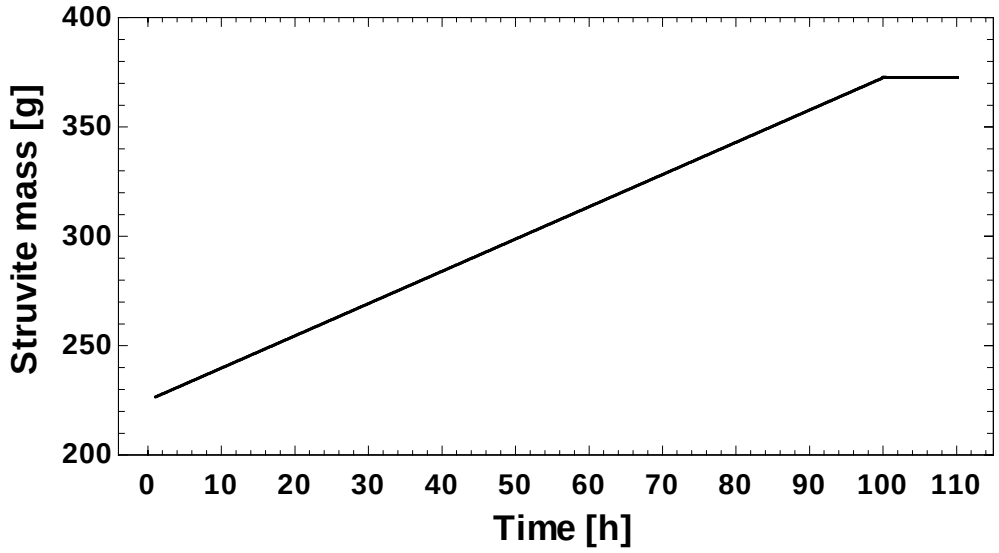

Figure 5.2 — Prediction of the struvite mass in the base case scenarios.

Figure 5.3 describes a decreasing tendency of the specific productivity rate due to the increase in the struvite mass and the decrease of the struvite production rate. This struvite specific productivity rate closely follows the SI_{MAP} behaviour in Figure 5.1. This similarity is explained by recalling that the struvite production rate (dn_{MAP}/dt) was is a function of the linear growth rate and therefore the SI_{MAP}. It is clear that the SPR after 100 h becomes zero, since the struvite production rate also becomes zero.

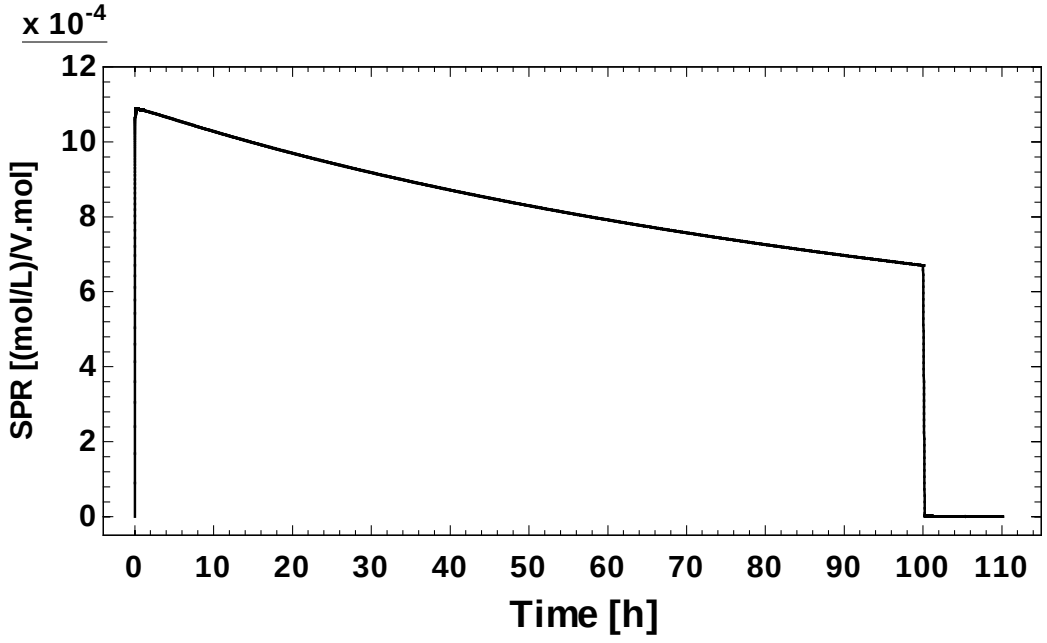

Figure 5.3 — Prediction of the Production rate per volume of reactor in base case scenario.

5.2 Assessment of process variables

The top and lower values of the process variables cited in Table 5.1 are assessed through simulations in this section. The main goal of this section is to determine those variables having greatest impact in key output process variables such as SI_{MAP}, SPR and struvite mass. Simulations were focused on the bottom – zone because of the small difference between SI_{MAP} cited in Figure 5.1.

5.2.1 Mg/P molar ratio in the feed

An increase in the Mg/P feed molar ratio increases the operational SI_{MAP} (Figure 5.4.A), SPR (Figure 5.4.B) and struvite mass (Figure 5.4.C). A maximum value for struvite production rate was observed at Mg/P = 1. This maximum recovery can be explained by the limiting effect of the total P. Once the P is reduced due to precipitation, there is more PO_4^{3-} available to keep the same precipitation rate.

Figure 5.5 shows the average activities of struvite constituent ions, which were determined across the 100-h simulation time, shown in Figure 5.4. Activities were averaged since their values do not change significantly (%C.V. = Standard deviation/Average < 6%) in each Mg/P considered. However, comparison of activities at four different Mg/P shows that PO_4^{3-} becomes limiting in the system and its contribution to the precipitated mass of struvite becomes negligible.

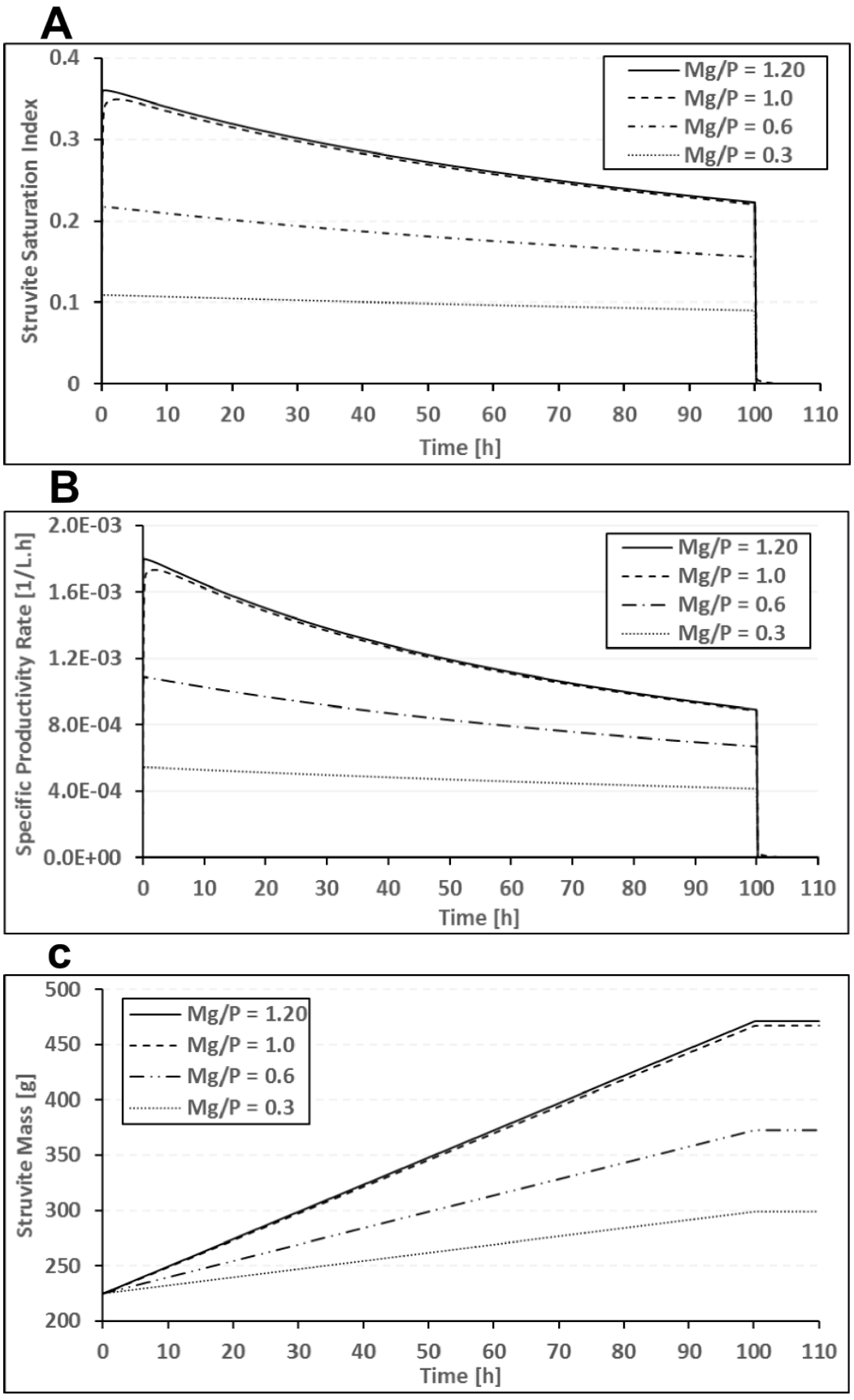

Figure 5.4 — Prediction of struvite saturation index (A), SPR (B) and struvite mass (C) at different Mg/P feed molar ratio.

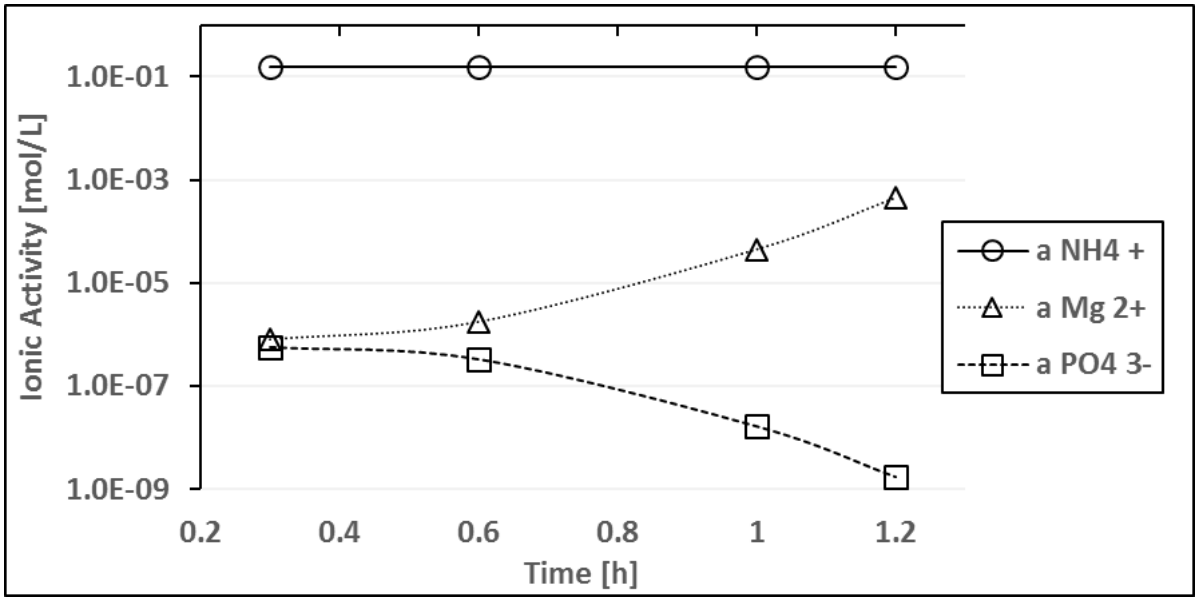

Figure 5.5 — Average ionic activities for struvite precipitation, calculated in the first 100 h

The sensitivity is defined as the partial derivative of a dependent variable respect to an independent variable. This approach provides the % of contribution of ion activity in the estimation of the SI_{MAP}. Equation 5.2 shows that the sensitivity of the SI_{MAP} is inversely proportional to the constituent ion activities (Mg^{2+}, NH_4^+ and PO_4^{3-}). Given its very high concentration, the effect of NH_4^+ in struvite precipitation is negligible. A sensitivity analysis described that changes in SI_{MAP} are almost completely dependent on variations in PO_4^{3-} ions at large Mg/P feed molar ratio.

$$\frac{\partial SI}{\partial a_{ion}} = \frac{1}{\ln(10) \cdot a_{ion}} \qquad 5.2$$

Figure 5.6shows the ionic activity of the struvite components. Simulations at Mg/P larger than 0.95 showed that formation of $MgCO_{3_{(s)}}$ could be possible since its saturation index is positive. Therefore, elemental analysis of Mg and P is suggested to corroborate the presence of this additional solid phase. The formation of another competing solid phase would decrease the expected Mg in the liquid phase, reducing the rate of recovery of struvite.

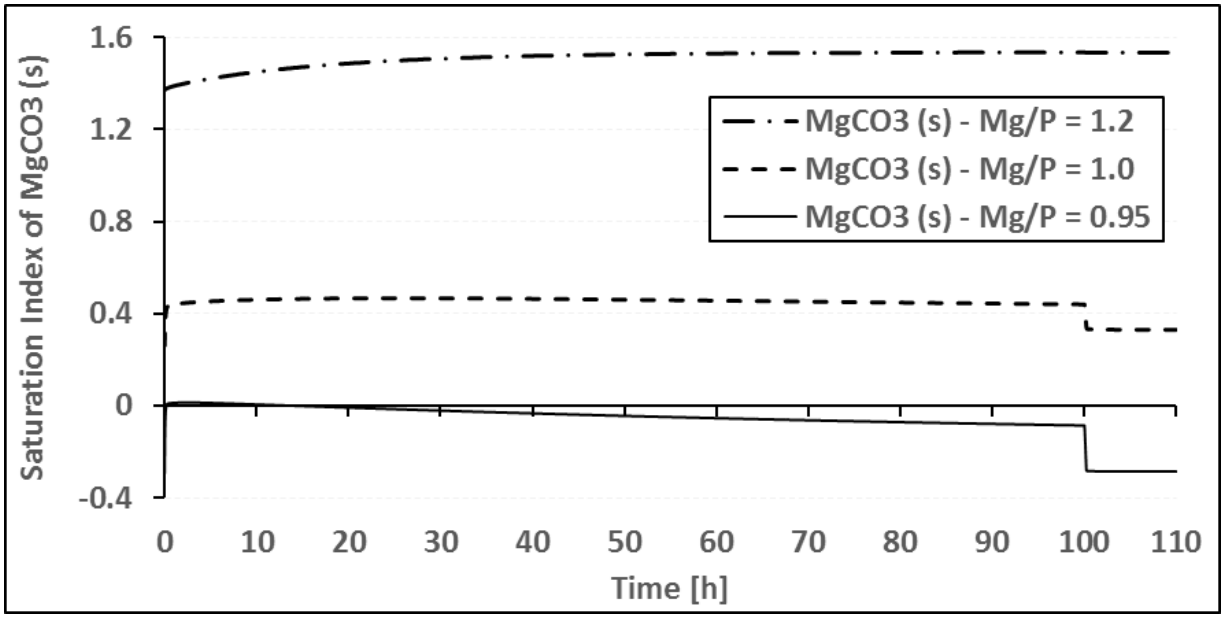

Figure 5.6 — Prediction of magnesium carbonate saturation Index, considering different Mg/P feed molar ratio.

5.2.2 Hydraulic residence time effect

Figure 5.7 shows an increase in all key variables when HRT was decreased (flow rates were increased). This suggests that increasing the nutrient feed to the reactor would increase the overall struvite precipitation rate. However, SI_{MAP} increases to higher values, compared to Figure 5.4.A where the maximum SI_{MAP} (around 0.4), which means that excessive nucleation would likely occur. Moreover, the SI_{MAP} and SPR shows less dependency at reduced HRTs, which suggests more abrupt variability in the elemental composition of the liquid phase.

Even though large SI_{MAP} is predicted by the model, it is likely not possible in the real system because high SI_{MAP} will lead to more nucleation, which will rapidly drop it back towards equilibrium. As such, the SI_{MAP} prediction can assist to decide a suitable HRT for the process operation. For instance, a process focused on recovering the largest quantity of nutrient as soon as possible, without considering the size of the particles, can use larger flow rates. On the other hand, a process focused on recovering the largest crystals as possible and avoiding nucleation will be operated at larger Mg/P feed molar ratio (up to one) and larger HRT (low feed flow rates).

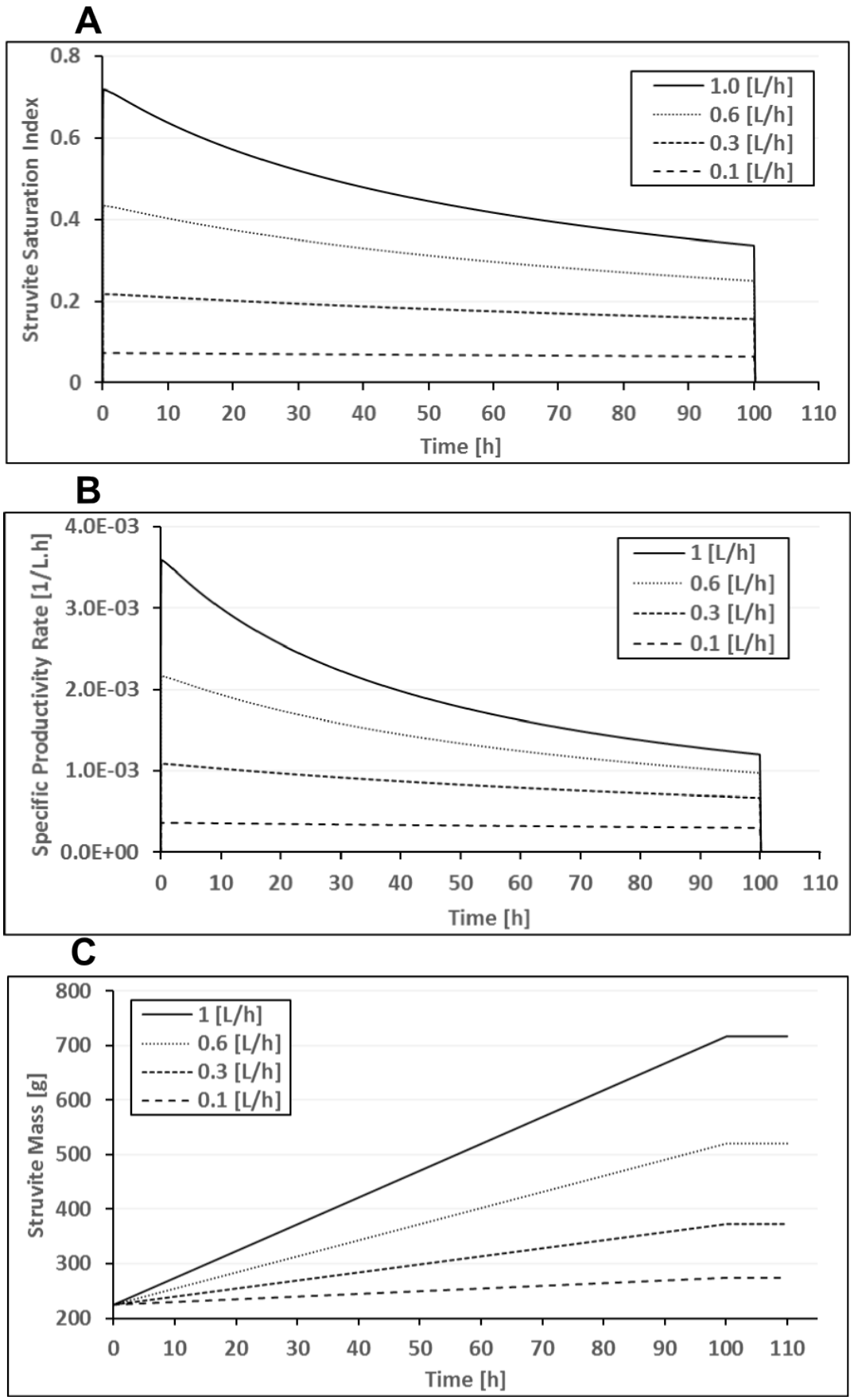

Figure 5.7 — Prediction of SI (A), SPR (B) and struvite mass (C) at different HRT molar ratio.

5.2.3 Initial quantity of seed

Surface area is defined by both initial seed mass and initial mean particle size, by particle geometry. Simulations with lower seed mass triggered an abrupt increase in SI_{MAP} (Figure 5.9.A), while large quantity of seed, which implies larger available surface area for mass transfer, and, therefore, an increase in the overall struvite production rate. Figure 5.8 also suggests that application of struvite mass of seeds larger than 100 g is suitable to contain the peak SI_{MAP}. The mass of seed and crystals is only an indirect indication of surface area; however, it can be accessed experimentally. The mass of seed and crystals impacts the mass balance, and therefore is a suitable choice as a process variable.

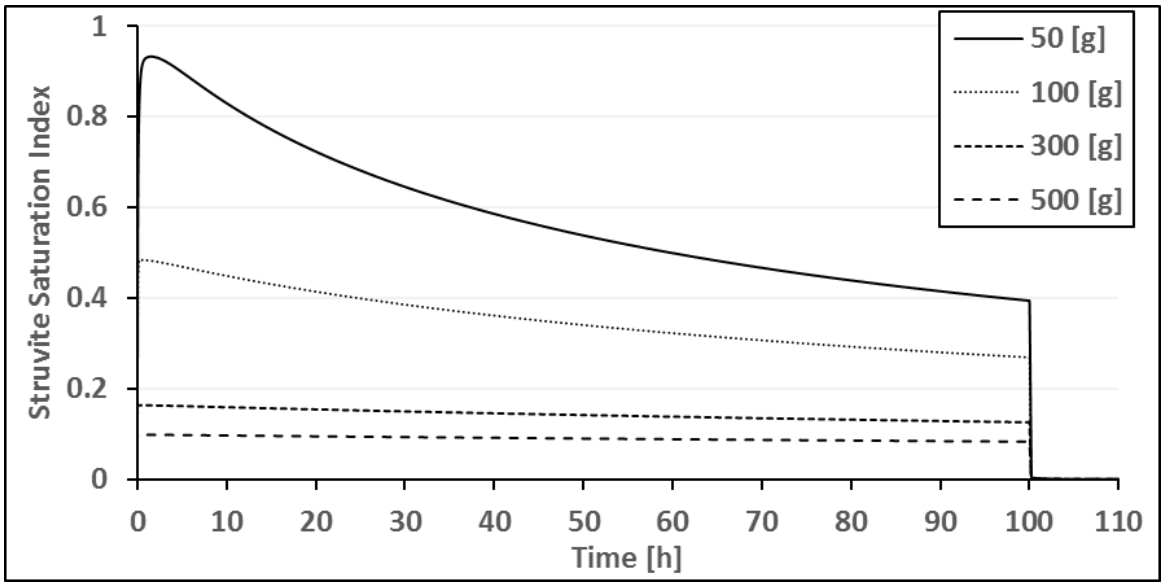

Figure 5.8 — Prediction of struvite saturation index with varying struvite seed mass, showing effect on peak struvite saturation index in each condition.

SI, SPR and struvite mass prediction were assessed at seed quantities lower than 50 g and profiles are shown in Figure 5.9. Figure 5.9.A describes an incremental behaviour of the SI_{MAP} at very small quantity of seeds. it's unlikely that the SI_{MAP} would actually remain at such high levels. At such high level of SI_{MAP}, nucleation takes place. Presence of new particles within the reactor increases the

specific surface area. Larger available surface increases the struvite production rate, bringing the SI_{MAP} down.

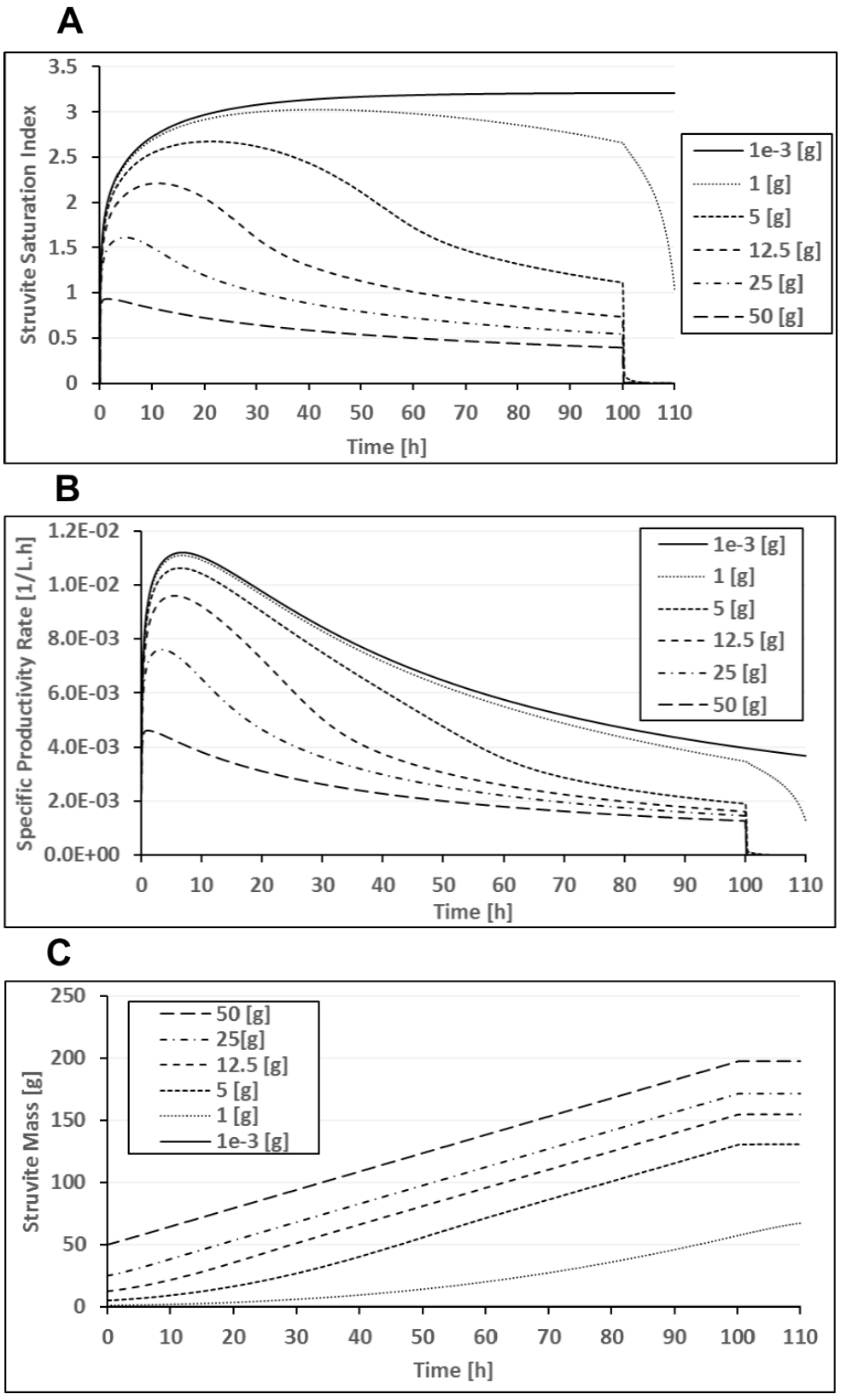

Figure 5.9 — Prediction of SI_{MAP} (A), SPR (B) and struvite mass (C) at different struvite seed mass.

Figure 5.9.B shows that the specific productivity rate has similar shape as the SI_{MAP}. Small quantities of initial struvite seed produces large SPR at the start of the process. On the other hand, Figure 5.9.C shows that small quantity of seed produced a decline in the struvite mass production Comparison between Figure 5.9.B and Figure 5.9.C suggested the application of SPR as target variable could not be suitable in cases where the surface area is the variable to be assess.

Figure 5.9.C also shows a non-linear behaviour of the struvite mass in the first 24 h at struvite seed quantity lower than 12.5 g. The minimum quantity of seed to ensure a constant slope of struvite production is 12.5 g within the reactor. Lower quantity of seeds will cause a delay in the struvite production rate since nuclei have to be formed to increase the available surface area.

5.2.1 Effective volume of the reactor

The bed height of the crystals depends on mixing speed impeller, which impacts on the solution that interacts with the growing crystals. Figure 5.10 shows the limitations in the application of SPR as a process key target variable. The struvite production rate is the same in any case. However, the SPR decreases with smaller effective volume, because of the equation where the volume is in the denominator.

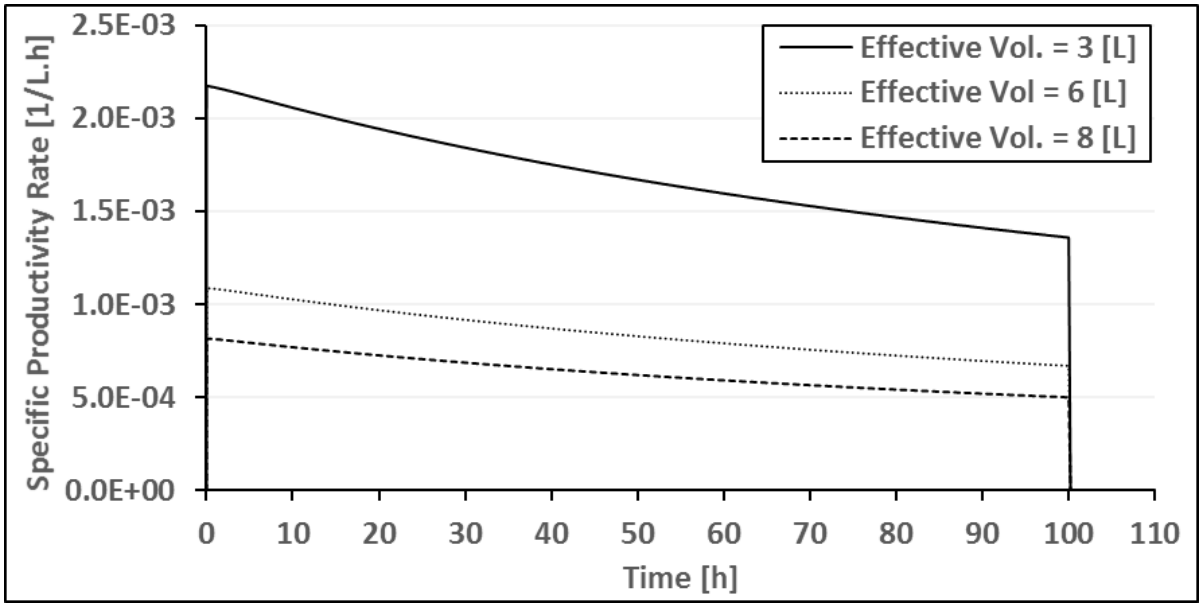

Figure 5.10 — Specific productivity rate at different effective volume in the bottom reactor.

Small differences in the SI_{MAP} in the top – zone were observed according to Figure 5.11. Larger effective volume (bottom – zone) represented faster distribution of chemical species in the top – zone of the reactor. Differences of SI_{MAP} at different effective volume, however are negligible. Consequently, effective volume has a negligible effect in the reactor operation.

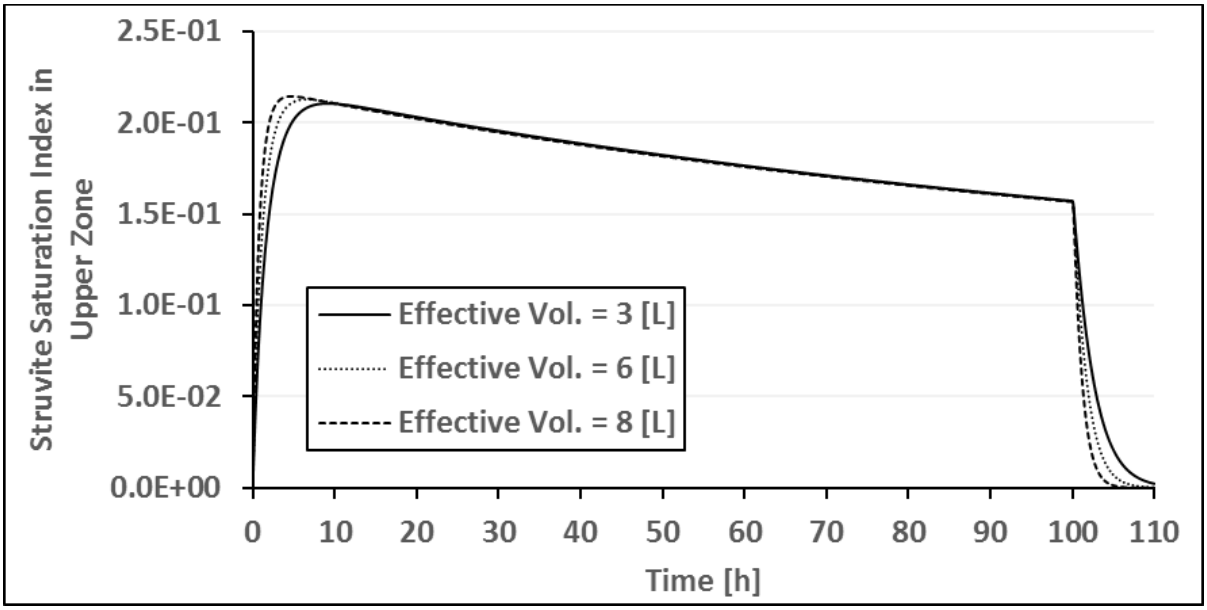

Figure 5.11 —Struvite saturation index in the top – zone of the reactor considering different effective volumes.

5.2.2 Intermixing flow rate

Figure 5.12 shows that the effect of the intermixing flow rate in the overall process is negligible considering a deviation of +/- 1 L/h from the base case scenario. Difference of P and Mg concentration profile in the top – zone were observed. However, these differences are less than 1 mg/L in the case of P (Figure 5.12. A1 and Figure 5.12.A2), and less than 0.5 mg/L for Mg profiles. These difference can only be observed in the transient operation intervals at the start of the process and when the flow rates were stopped at the end of the campaign. The effect of the intermixing in the model prediction suggests that 4 L/h, as determined by the tracer studies, produces small, but significant differences between the top and the bottom – zone of the reactor.

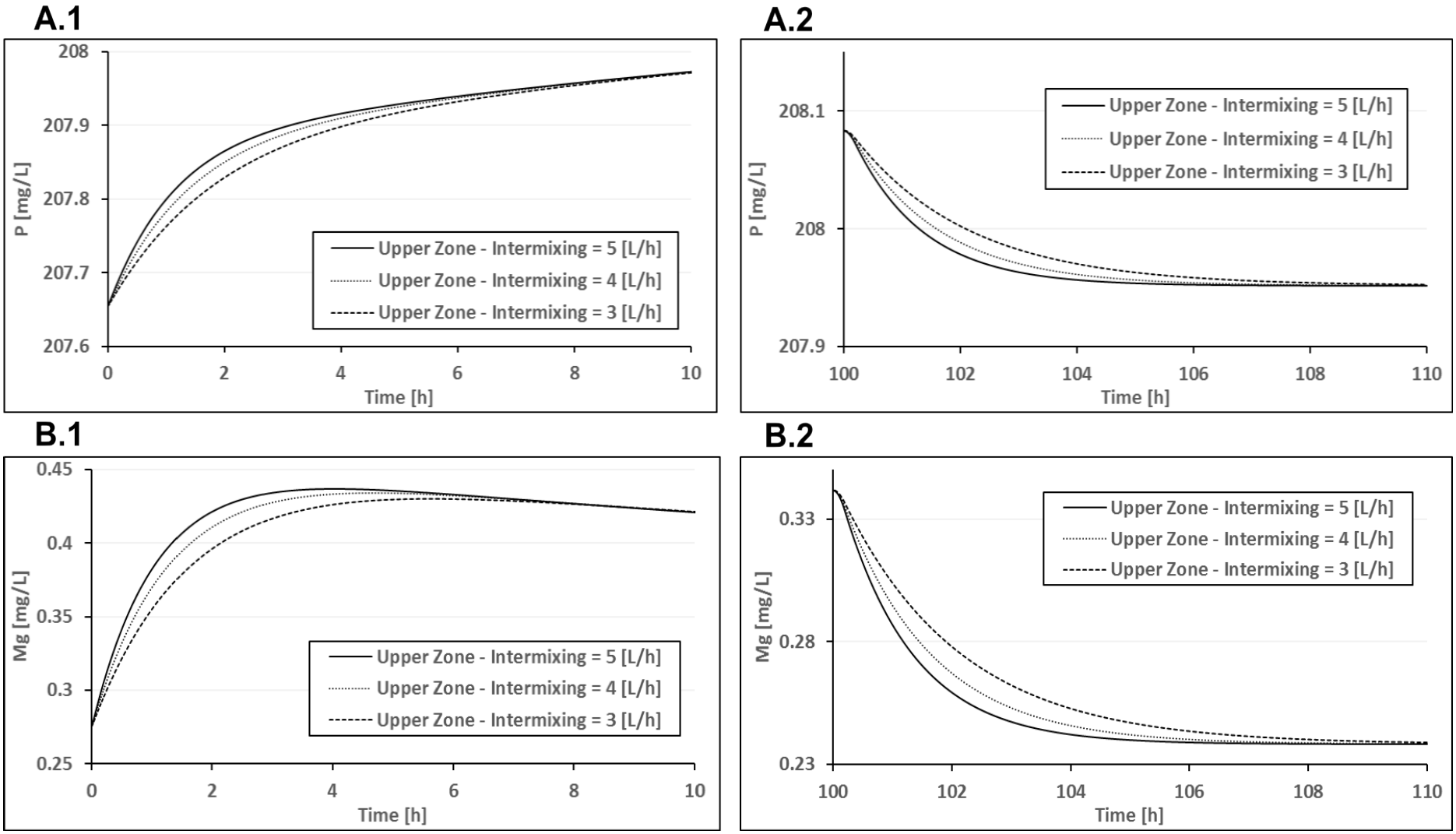

Figure 5.12 — Prediction of P concentration (A) and Mg (B) concentration in the top – zone at intermixing flow rates of 3 L/h, 4 L/h and 5 L/h. Differences in each of the cases are shown in the first 10 h and last 10 h of operation.

5.2.3 Initial seed size

The initial particle size changes the specific surface area of the crystals, which alters the total amount of surface available for mass transfer. This model considered a mean weight particle size, which is a limitation because it does not consider the particle size distribution.

Figure 5.13 shows a proportional increase of the SI_{MAP} profiles with respect to the initial particle size. considering the same mass. By considering the same quantity of struvite mass, the prediction of SI_{MAP} is largest at small particle size. This means that considering the larger initial particle size for an unknown seed triggers largest predictions of SI_{MAP}. This idea can be used in the process design by assuming the largest particle size and therefore estimating the maximum possible saturation index at a given condition.

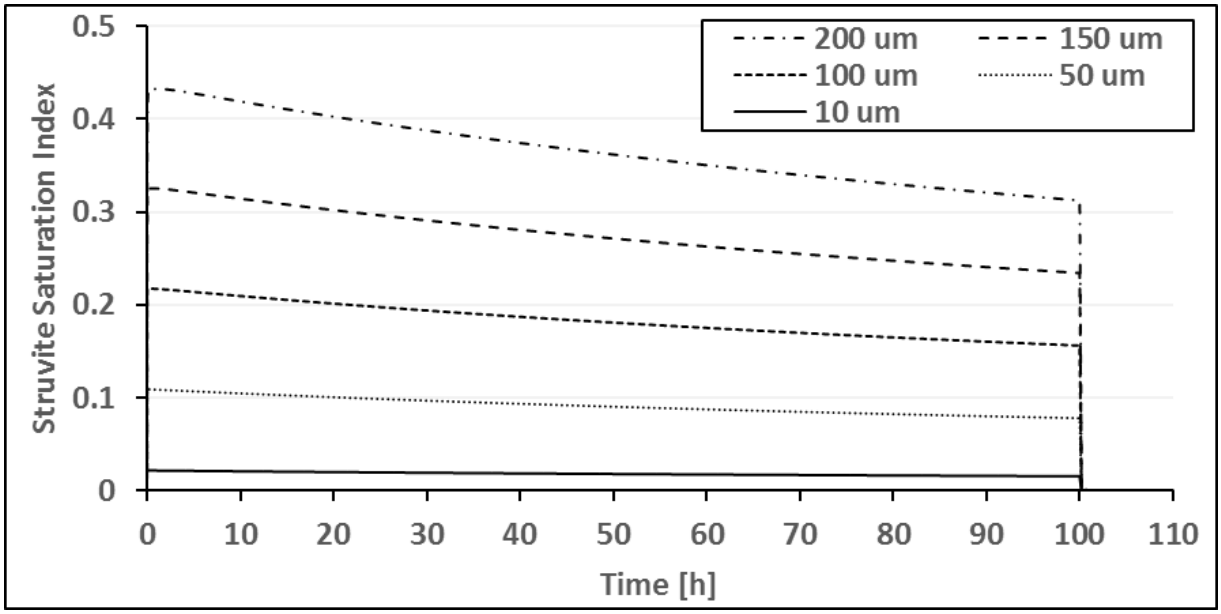

Figure 5.13 —Struvite saturation index at different initial seed size.

5.3 Application of the model

This section shows the applicability of the model in the design of experimental conditions. This section also intends to demonstrate that the same key output variable can be obtained at different

operational conditions. Simulations in this section applied “Procedures” in the language of EES code to solve the continuous reactor. This provide the advantage of applying changes in the operation, such as taking out struvite crystals from the container or even stopping flow rates to the continuous reactor.

5.3.1 Available surface area vs saturation index

Figure 5.14 applied the dynamic model to three different reactors starting struvite precipitation at different times. The base case scenario simulated the SI_{MAP} profile considering 225 g at 100 μm and it is shown in Figure 5.14.A and Figure 5.14.B. Two reactors started at 17 h and 50 h using the expected quantity of struvite seed predicted from the first reactor at those times.

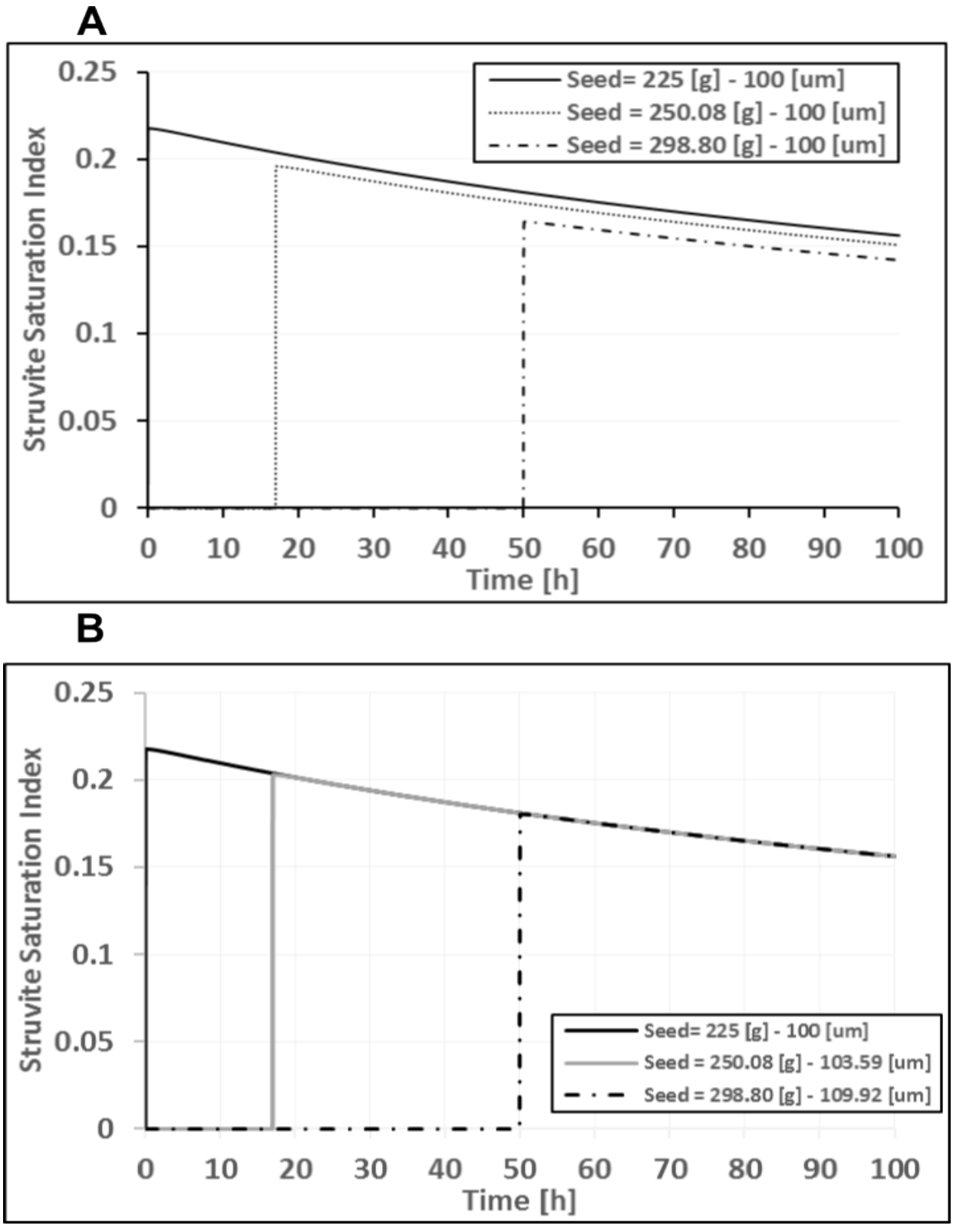

Figure 5.14 — Saturation index, predicting similar profiles under different quantity of struvite

Figure 5.14.A predicted the struvite SI_{MAP} in the second and third reactor, considering the same initial mean particle size as used in the first reactor. The SI_{MAP} profiles for the last two reactors did not

overlap the first one because the mean particle size would have grown over that time. Therefore, using smaller crystals as seeds in the second and third condition decreases the SI profile.

Figure 5.14.B presented the case where struvite mass and mean particle size are introduced in the second and third condition. Figure 5.14. B demonstrated the overlapping SI_{MAP} when the same surface area is considered at different time. This simulation recommend that it is possible to design continuous reactor operation by setting the struvite mass and initial mean particle size. The SI_{MAP} profiles clearly is related to surface area available within the reactor. As such, the peak SI_{MAP} value can likely be predicted before the reactor operates at those conditions, which gives flexibility to the design engineer.

5.3.2 Harvesting product crystal during operation

A procedure for harvesting struvite crystal from the reactor was developed in the model, and assessed in a long reactor campaign of 400 h, to consider how this operation might be designed in an actual nutrient recovery reactor. In this assessment, the struvite harvested decreased the quantity of crystals to the initial quantity of seeds (in this case 225 g).

This procedure provides the advantage of longer reactor campaigns without losing within the vessel for suspended crystals. Moreover, a decrease in the struvite crystals leads to larger SI_{MAP}, and therefore production of more available surface to allow mass transfer. Harvesting can keep the reactor operating for longer.

It is almost running at some kind of steady state (at least over some period of time it can be averaged).

Three harvests episodes were developed, and the addition of the final mass of crystals with harvested quantity of crystals goes to the expected quantity, as if the reactor were not harvested. This mean that the same struvite precipitation mass can be obtained by two different types of reactor operation.

.

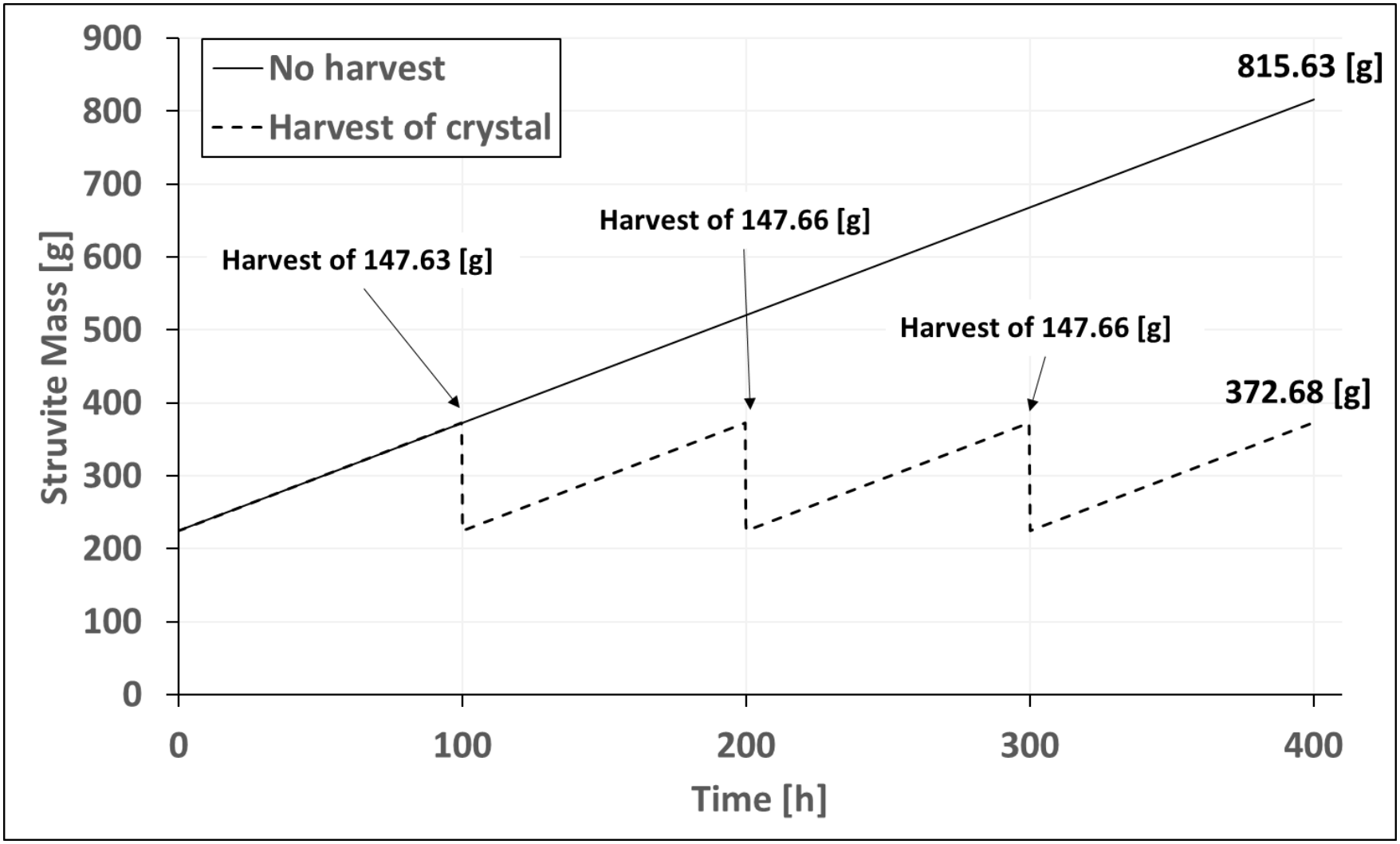

Figure 5.15 — Comparison of struvite mass profile without and with harvesting of struvite crystals. Harvesting was programmed every 100 hours to leave in the reactor similar quantity of struvite seed at the start of the experiment.

5.4 Kinetic parameters effect

The kinetic model was assessed by using different kinetic parameters in the power-law expression (n, and k). This section range of the rate coefficient ("k") in simulations of continuous reactor to corroborate the selection in the base case scenario (k = 1e-6 m/h). In the following sub-section, the kinetic order of power-law equation was tested through simulations to determine the effect of including this parameter as a value different than one (base case scenario considered n = 1). The last sub section tested two other kinetic models.

5.4.1 Assessment of the rate of coefficient

The rate of coefficient k was assessed between 1e-9 m/h to 1e-6 m/h to estimate SI_{MAP}, SPR and the struvite mass at base case condition. Figure 5.16.A shows that values of "k" smaller than 1e - 6 m/h are related to larger SI_{MAP} predictions. Considering k at values smaller than 1e-6 m/h also correlates a SPR with the same profile as the SI_{MAP}, and with much smaller struvite production over time. Figure 5.16.C also indicates that a constrained behaviour when k become closer 1e-6 m/h because the ionic speciation is also constraining the struvite precipitation due the to the available PO_4^{3-} in solution. An inference from these plots demonstrated that the application of a k = 1e-6 m/h can be considered valid because it does not constrains struvite mass production.

Figure 5.17 shows the predictions of P and Mg concentration for different values of the rate of coefficient (k). These plots indicated that k values smaller than the threshold ($k = 1e-6\ m/h$) predicted large concentrations of P and Mg in the liquid phase, which corroborates the small production of struvite in Figure 5.16.C. Figure 5.17.A.2 and B.2 also considered a range larger than k= 1e-6 m/h where a minimum concentration of P and Mg can be predicted. This "limiting" trend in both P and Mg indicates that rapid struvite precipitation depletes the P in the liquid solution, and therefore achieves to equilibrium.

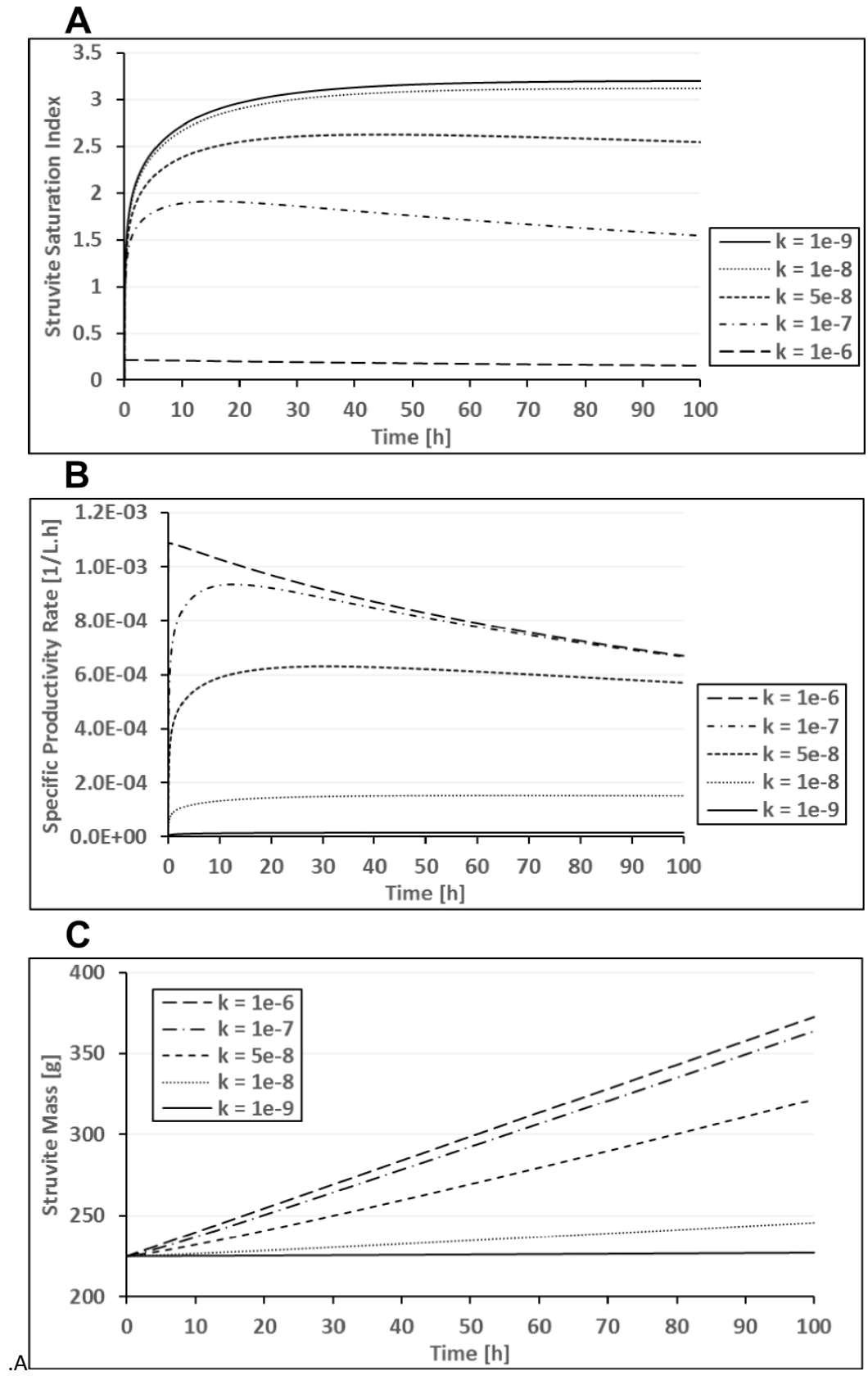

.A

Figure 5.16 — Prediction of target output variables considering different values of "k". Profiles of saturation index (A), productivity rate (B) and struvite mass (C).

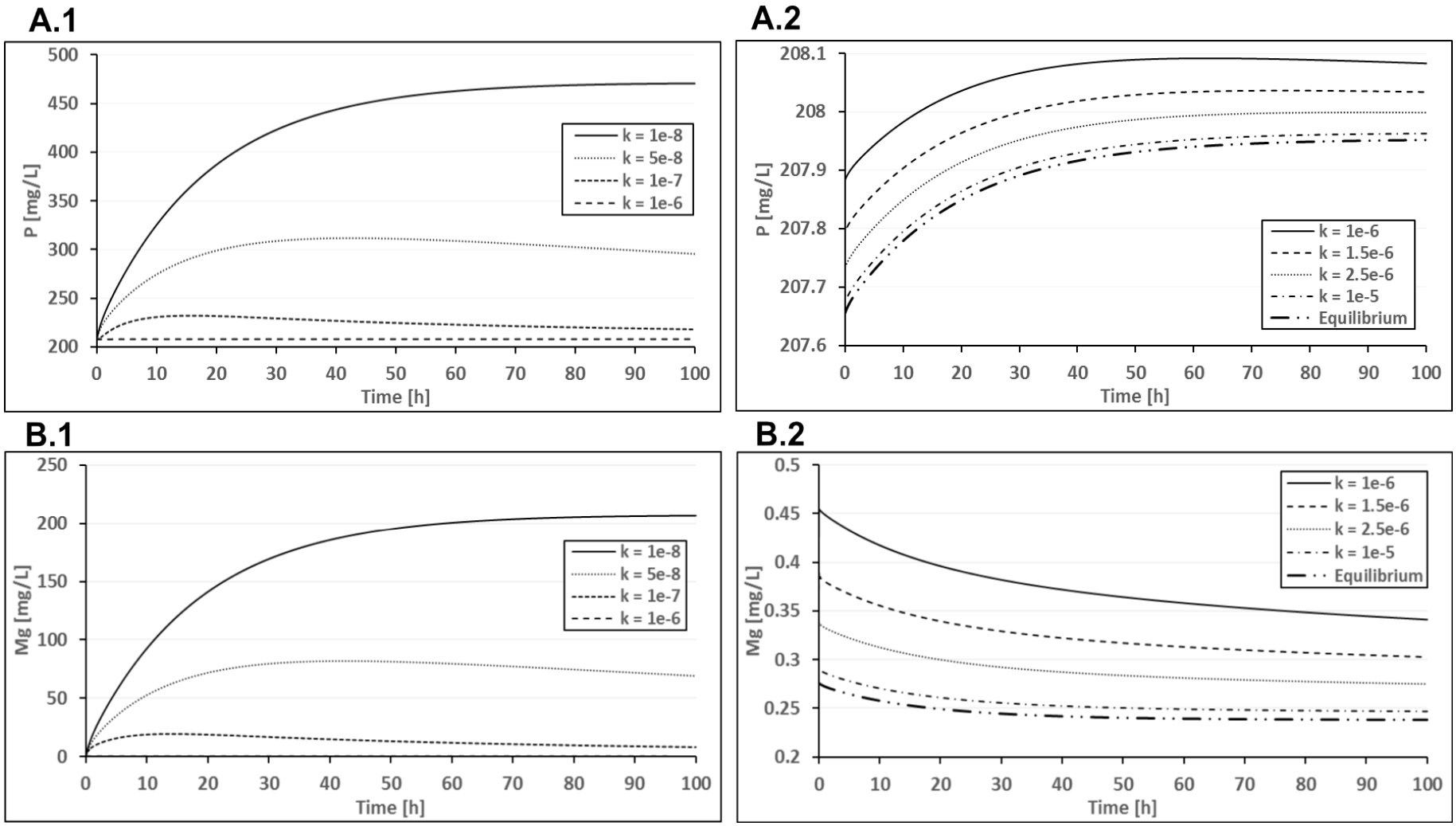

Figure 5.17 — Profiles of P (A) and Mg (B) using diverse kinetic parameters . Larger P concentration are estimated with smaller k (A.1), while P approaches to equilibrium at k larger than 1e-6 m/h (A.2). Similar estimations are given for Mg (A.1) and (B.2)

5.4.2 Application of other kinetic expressions

The model developed in this thesis was limited by the consideration of the linear growth rate as a function of the SI_{MAP}. Based on previous simulation, the SI_{MAP} in most of the cases when there is sufficient quantity of seeds within the reactor has value close to zero in almost all the operational time (pseudo-steady state). SI_{MAP} as a constant and close to zero value constrains the prediction of the linear growth rate (G_L) and therefore the struvite production rate (dn_{MAP}/dt) by making the struvite mass prediction insensitive to the kinetic parameters (k, n). This sub-section tested different kinetic models to understand behaviour of the system, and the possibility of making the process more sensitive to the change in the kinetic parameter in each equation.

To develop this assessment two kinetics equations were formulated. The kinetic expression in equation 5.3 (second model) was arbitrarily formulated by considering the SI_{MAP} as an exponent. In this equation, k_1 is expressed as m/h.

$$\mathrm{G_L} = k_1 \cdot (10^{SI_{MAP}} - 1) \qquad 5.3$$

Equation 5.4 (third model) was formulated based on the expression given by Harrison (Harrison et al., 2011), with the only difference of considering the Mg concentration instead of P. In this equation k_2 is expressed in m/h. One interesting feature of this expression is that the driving force does not depend on the SI_{MAP}, but instead on the difference between the elemental concentration of the limiting reagent (Mg) and its predicted concentration at equilibrium.

$$\mathrm{G_L} = k_2 \cdot (C_{Mg} - C_{Mg}equilibrium) \qquad 5.4$$

Figure 5.18 predicts the elemental concentration of P and Mg considering the three different kinetic models. Both plots inform that the same production can be achieved by any of them only by changing the values of their respective kinetic parameters. This scenario indicates that assessing any kinetic model, including parameter estimation could be irrelevant at close to equilibrium conditions.

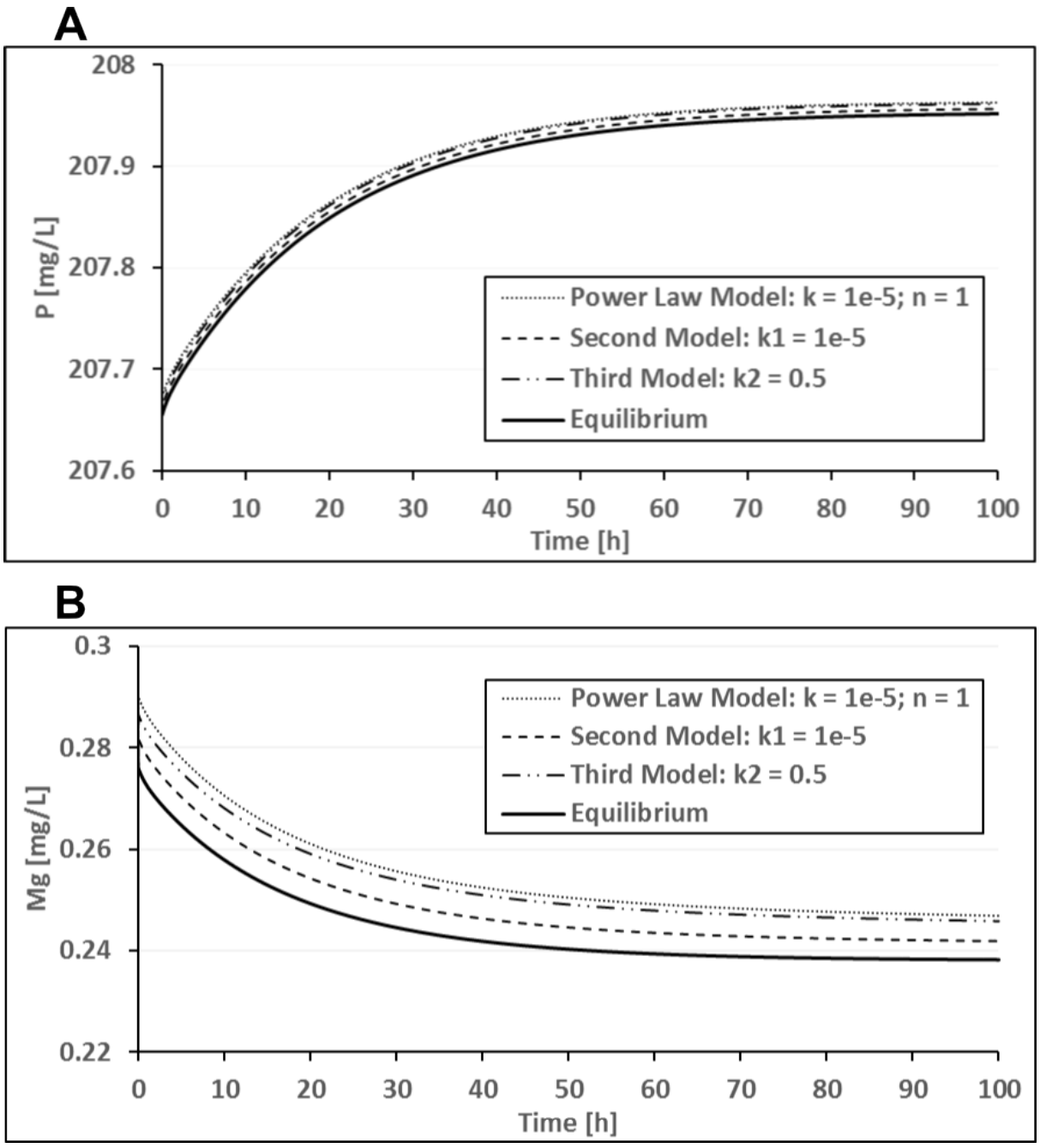

Figure 5.18 — Estimation of total phosphorus and magnesium concentration over time, using the power-law kinetic model, additional kinetic expressions in equations 2.2 and 2.3.

5.5 Summary

- The dynamic model was studied by developing simulation using diverse variable range
- The Mg/P feed molar ratio has a direct effect in the struvite production rate and SI_{MAP}

- Longer HRT are suitable to run the reactor at low saturation index, however, this condition decreases the struvite mass produced
- The presence of an initial mass of seed facilitates reactor operation by decreasing the SI_{MAP} and by providing enough surface area
- The dynamic model can be applied to understand the relationship between available surface area and saturation index at different reactor conditions
- The procedure of crystal harvesting was simulated in the dynamic model showing the capacity of the approach in planning experimental reactor campaigns
- The expression of kinetics could not consider the addition of the thermodynamics as the driving force if the system operates close to equilibrium conditions.

6 Operation of a Continuous Struvite Precipitation Reactor – System Performance and Model Assessment

---

Highlights:

- *Assessment of monitoring variables in continuous nutrient recovery*
- *Comparison of simulation and experimentation in continuous nutrient recovery*
- *Insight of limitations of modelling and experimentations in this work*
- *Assessment of the electric sensing to characterise men particle size*

6.1 Literature review

Similar reactor configurations and monitoring of struvite precipitation are presented with a focus on continuous reactors. Struvite morphology, identification and particle size range were also explored. Experimental approaches to determine struvite solubility product were reviewed.

6.1.1 Continuous reactor configuration and operation

Continuous struvite precipitation has been studied using different types of nutrient solutions. Nutrient composition, magnesium solution sources and use (or otherwise) of $NaOH$ were used to drive precipitation. Struvite precipitated by keeping the solution pH in the range of 8 to 9. Some studies applied alkali (Münch & Barr, 2001) or stripping of the CO_2 with air (Battistoni, Paci, Fatone, & Pavan, 2006). However, urine did not require base addition (Zamora et al., 2017), owing to ammonia-ammonium pH buffering.

Studies in continuous struvite precipitation applied fluidised bed reactors (FBR) and also stirred reactors. Full-scale examples of FBR are the *Unitika Phosnix* and *Ostara PEARL* processes, while the *Phospaq* and *NuReSys* process were stirred reactors with aeration (Crutchik, Morales, Vázquez-Padín, & Garrido, 2017). Within reactor configurations, FBR were designed with a large-diameter upper zone to mitigate loss of struvite fines from the outlet flow. These reactors were designed with two (Battistoni et al., 2006; Shimamura et al., 2006; Zamora et al., 2017) or even more (Md Saifur Rahaman, Mavinic, Meikleham, & Ellis, 2014) vertical zones. The bottom zone was claimed as the "reacting zone" since it is where most of the particle are suspended. This part is where the feed point is, and therefore the reaction. The upper zone was identified as the "settling zone" with the main characteristics of larger tank cross sectional diameter than the bottom zone. Another advantage of this configuration is that the bottom zone can be used as harvesting zone during long campaigns. Other configuration also included additional reactors where pH was adjusted (Ohlinger, Young, & Schroeder, 2000), or a sub-tank to trap the fines from the reactor outlet (Shimamura et al., 2006).

A frequent feature of continuous struvite precipitation has been "seeding" the reactor with a population of crystals. The application of seed material promotes secondary nucleation in struvite precipitation (Crutchik et al., 2017; Mehta & Batstone, 2013). Seeds from the same material were found to be suitable compared to other materials (Md. I. Ali & Schneider, 2006). Application of seeds was claimed to ensure crystal growth in high-energy mixing systems (Ohlinger et al., 2000). In continuous process, seeds were prepared from collecting the fines overflowing from the reactor outlet (Shimamura et al., 2006). These small crystals were then introduced again in the bottom zone of the main reactor to avoid production of overly larger particle populations. Another reason for using seeds was to increase the available surface are to facilitate mass transfer (M. Burns et al., 2016). Other works applied seed but they did not explain the reason for this choice, probably because of its known advantage (von Munch & Barr, 2001).

6.1.2 Monitoring variables in continuous reactors

On-line monitoring using pH is common in most research focused on struvite precipitation. These measurements are key when nutrient solution has a low pH, such as supernatant (Battistoni et al., 2006; Ohlinger et al., 2000). Urine as nutrient solution (Wilsenach et al., 2007; Zamora et al., 2017) however already have a pH suitably high and highly buffered for struvite precipitation. In this context, pH monitoring becomes less relevant, but still a potentially useful variable to be monitored (Crutchik et al., 2017; Laridi, Auclair, & Benmoussa, 2005).

Conductivity was applied in continuous struvite precipitation. Some studies tried to link conductivity measurements with urine ionic strength at different dilution (Ronteltap et al., 2010). This study reported linearity between conductivity and ionic strength. Other studies used on-line conductivity measurements as methodology to monitor constant conditions during reactor operation (Crutchik et al., 2017; Pastor, Mangin, Barat, & Seco, 2008; Tarragó et al., 2016; Zamora et al., 2017). However, none of the previous tried to compare on-line measurements with predicted ionic strength during continuous operation.

6.1.3 Struvite solid characteristics

Struvite particles (crystals and aggregates of crystals) were identified by X-ray diffraction (XRD) and microscopy. Continuous struvite precipitation using urine as nutrient identified the presence of only struvite (Wilsenach et al., 2007). Continuous nutrient recovery from dewater anaerobically digested sludge also reported > 90 % of struvite based on XRD (Münch & Barr, 2001).

Scanning Electron Microscopy (SEM) identified the presence of needle—like orthorhombic crystals, which, after aggregation, led to X-branched shape crystals (Zamora et al., 2017). Crystals particle length according to microscopy showed crystals in the range of 100 μm in approximate 135 min (Wilsenach et al., 2007). Moreover, larger intervals of experiments could lead to struvite crystals from

0.3 mm to 6 mm when harvesting was developed between intervals of 7 h to 72 h (Zamora et al., 2017).

6.2 Continuous process operation

This section assesses the previous studies in continuous struvite precipitation, where the experimental conditions were selected based on Chapter 5 simulations. Elemental concentration of the liquid phase leaving the reactor validated the dynamic model. Since experiments were performed close to equilibrium, kinetic parameters were not estimated. The experimental approached considered analysis of the liquid phase and characterisation of the struvite solid product.

6.2.1 Experimental description

Two continuous experiments were performed to assess and validate the dynamic process model of struvite precipitation. The first experiment ($Expt.1$) was performed at Mg/P feed molar ratio = 0.34 to keep the saturation index at low levels and enables the P concentration to be above the limiting detection for spectrophotometry analysis. The second experiment ($Expt.2$) was performed at two different Mg/P feed molar ratio. The first part of experiment 2 ($Expt.2.A$) fed the reactor with Mg/P = 0.64 and the second part of this experiment ($Expt.2.B$) used a Mg/P = 1.29. The Mg/P were estimated considering the P concentration after any spontaneous precipitation in the concentrated synthetic ureolysed urine ($CSUU$) that may have occurred. The filtered $CSUU$ was cited in this chapter as $FCSUU$.

$Expt.1$ and $Expt.2.A$ were designed such that magnesium was the limiting reagent. This choice provided the advantage of keeping P concentration in the liquid phase well above the detection limit when spectrophotometric measurements were employed. The $Expt.2.B$ was performed at Mg/P larger than one to corroborate the limiting production of struvite mas at Mg/P larger than one according to § 4.3.3. The change of condition from $Expt.2.A$ to $Expt.2.B$ was performed by feeding

a higher concentration of $MgSO_4.7H_2O$ feed solution. Variables in the experiment, which were also introduced in the model as input data, are presented in Table 6.1.

Table 6.1– *Conditions of experiments 1 and 2*

Variables	**Experiment 1**	**Experiment 2**
Mg/P feed molar ratio	0.34	2.A = 0.64: 2.B = 1.29
Initial struvite mass $[g]$	228.1[(a)]	226.4[(a)]
Initial mean particle size $[\mu m]$	17.58[(b)]	19.15[(c)]
Flow rate of $FCSUU$ $[L/h]$	0.3	0.3
Flow rate of $MgSO_4.7H_2O$ $[L/h]$	0.3	0.3
Equilibrium solution at time zero	Equilibrium solution after mixing 7 L of FCSUU with 7 L of $MgSO_4.7H_2O$	Equilibrium solution from the end of the Expt. 1.
Effective Volume $[L]$	Approx. 6	Approx. 6
Mixing speed $[RPM\}$	Approx. 150 RPM	Approx. 150 RPM
Operational time $[h]$	87.17	99.50
Final desaturation time $[h]$	10.21	7.82

*Note: (a) The initial struvite mass was determined by density methodology in § 4.4.6*using a 2L conical flask. *(b) Initial mean particle size was the measured mean weight particle size (§ 4.4.6). It was estimated from microscopy photos using 96 crystals (see Appendix C.7). (c) The initial size was estimated from the final size estimated in Expt. 1. Struvite seed in Expt.2 was a subset of the the product crystal from Expt.1.*

Individual flow rates were assessed at the start of the operation by separately feeding the reactor with $FCSUU$, and then with the Mg-source solution. At the end of each experiment, the feeding was stopped, while mixing continued to reach the equilibrium. During the process liquid and solid samples were taken to perform elemental analysis and struvite particle characterisation. Figure 6.1 and Figure 6.2 described the flow rates in $Expt.1$ and $Expt.2$. Additionally, every solid sample was weighed and digitally removed from the model, using an EES procedure to account for its removal from the system.

Figure 6.3 shows the experimental set-up in $Expt.1$ and $Expt.2$. Probes of pH and conductivity were placed at the top of the reactor to collect data from the liquid surface. Measurements were recorded using $LabVIEW$ software every 5 minutes. The outlet hose of the reactor was fixed to a retort stand and clamp in the same position to ensure consistency in flow rates measurements using a 50-mL cylinder.

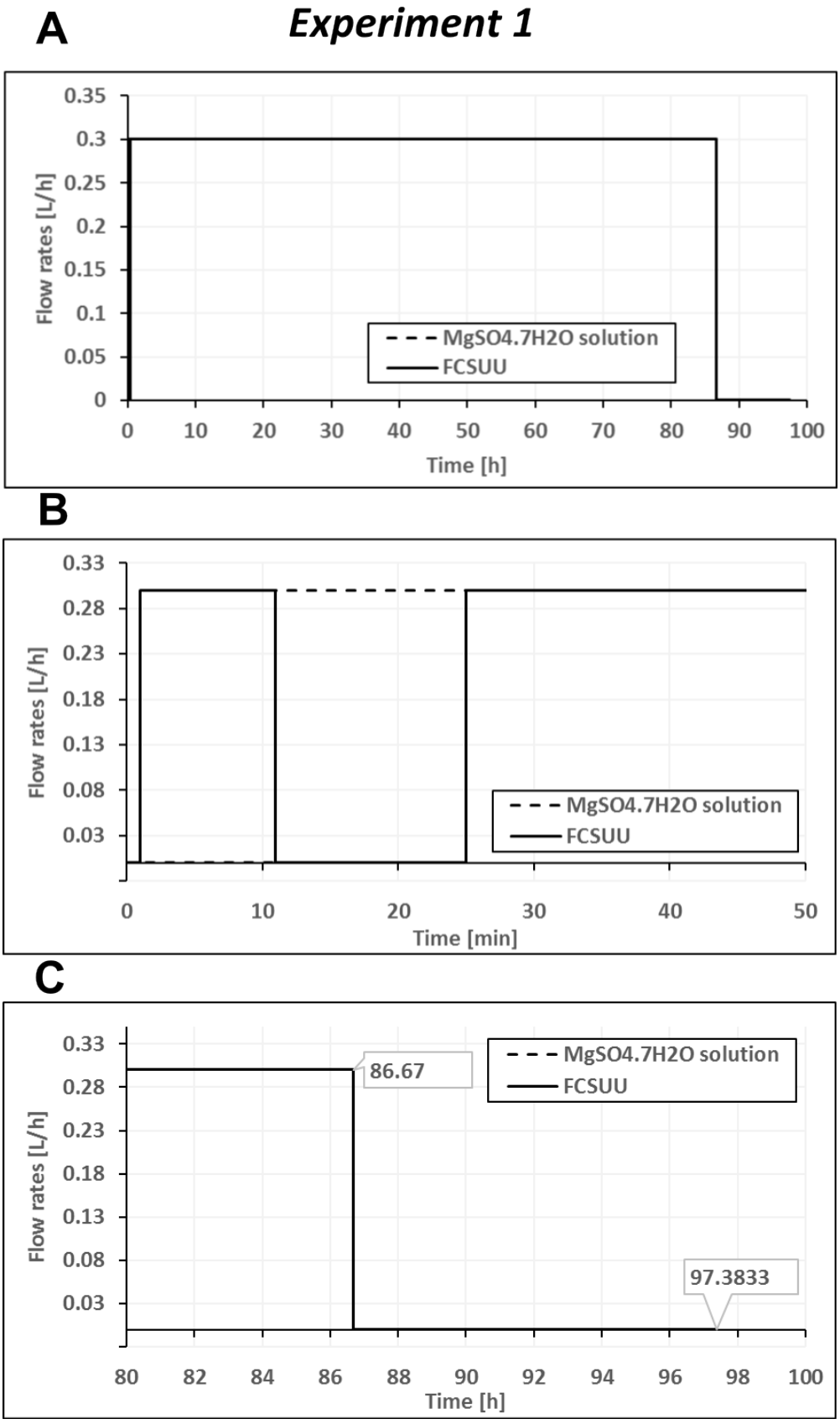

Figure 6.1 – Feeding flow rates in $Expt.1$. The reactor was fed continuously (A). At the start of the process flow rates were measured individually (B). At the end, the feeding was stopped (C).

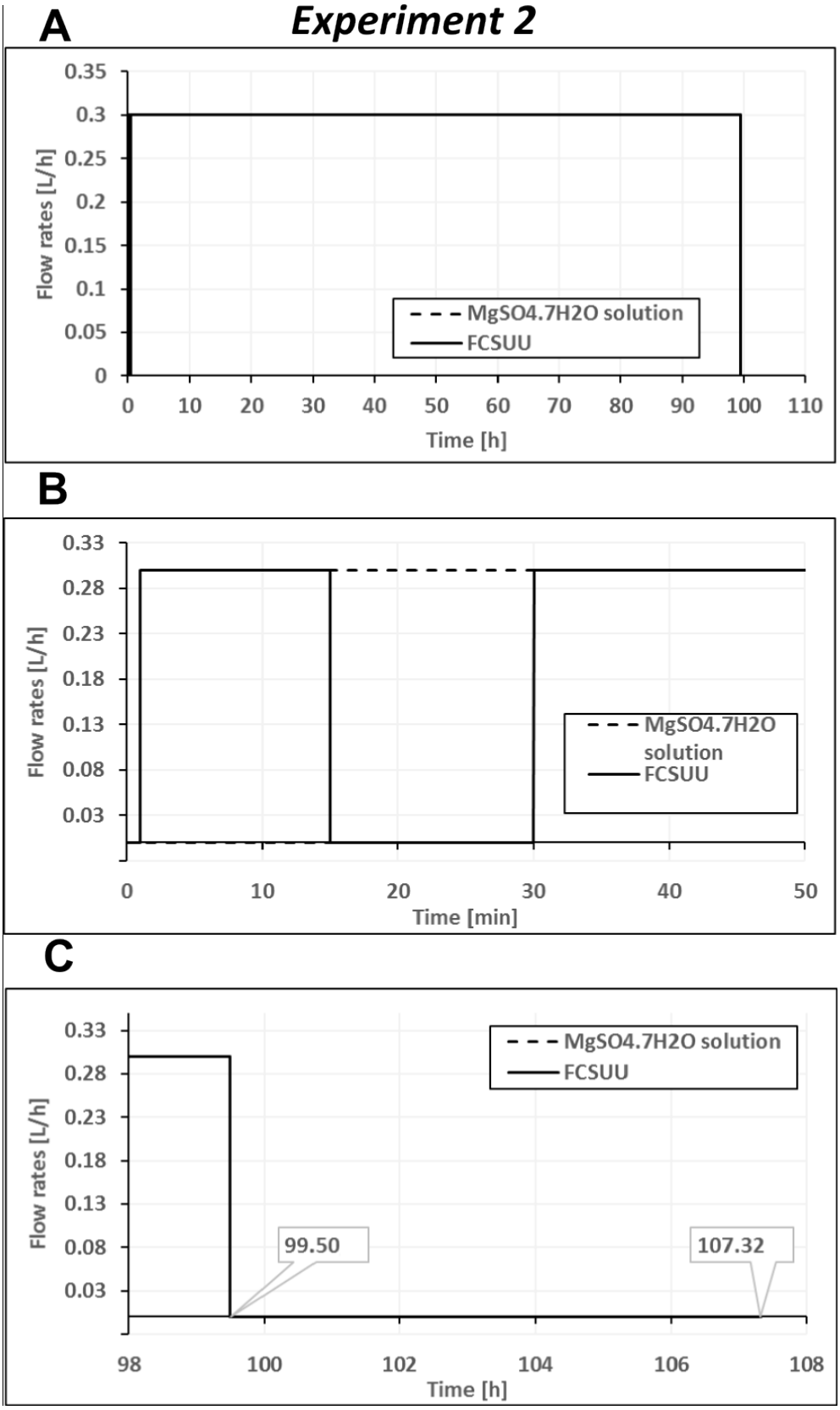

Figure 6.2 – Feeding flow rates in $Expt.2$. The reactor was fed continuously (A). At the start of the process flow rates were measured individually (B). At the end, the feeding was stopped (C).

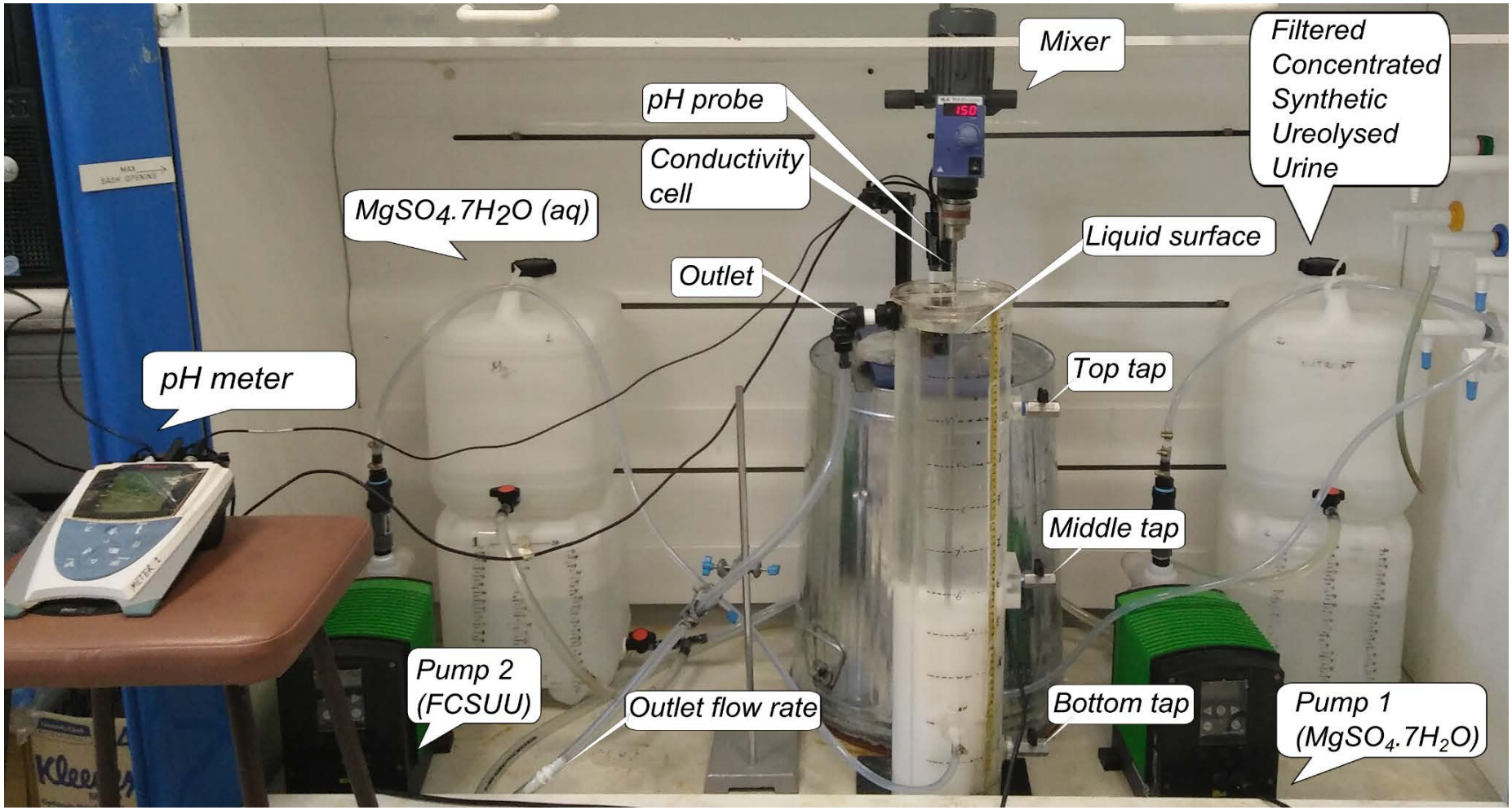

Figure 6.3 – Experimental set-up for continuous struvite production. Solutions of $MgSO_4.7H_2O$ (left) and filtered concentrated synthetic ureolysed urine (right) were fed to the reactor. Mixing kept struvite particles in suspension. Measurement of pH and conductivity were recorded during the experiment. Outlet flow rate was measured in the outlet bottom hose leaving the reactor.

6.2.2 Monitoring of flow rates

Measurements of the outlet flow ensured constant hydraulic residence time and Mg/P feed molar ratio in reactor operation. The presence of atypical flow rates was a call to adjust nominal flow rates in the pumps. Two types of flow rates were measured during reactor operation: instantaneous flow rates, and average flow rate obtained from the change in the liquid level in the feed tank over time.

Instantaneous outlet flow rates were measured by collecting the exiting liquid from the reactor in a cylinder of 50 mL +/- 1 mL over four minutes. Figure 6.4 shows that the outlet flow rate was kept close to 0.6 L/h during each experiment. The outlet flow rate however cannot distinguish the individual feed flow rates from each of the pumps. Therefore, each pump was individually assessed at the start of the experiment.

Flow rates were measured by recording the liquid level in the feeding tanks over time. Observation of the same liquid level drop in both tanks indicated that nutrient and magnesium source were fed at the same rate to the reactor, which was the intended aim for this system. Figure 6.5 shows that the liquid dropped the same level for all experiments, meaning that the process performed according to design values.

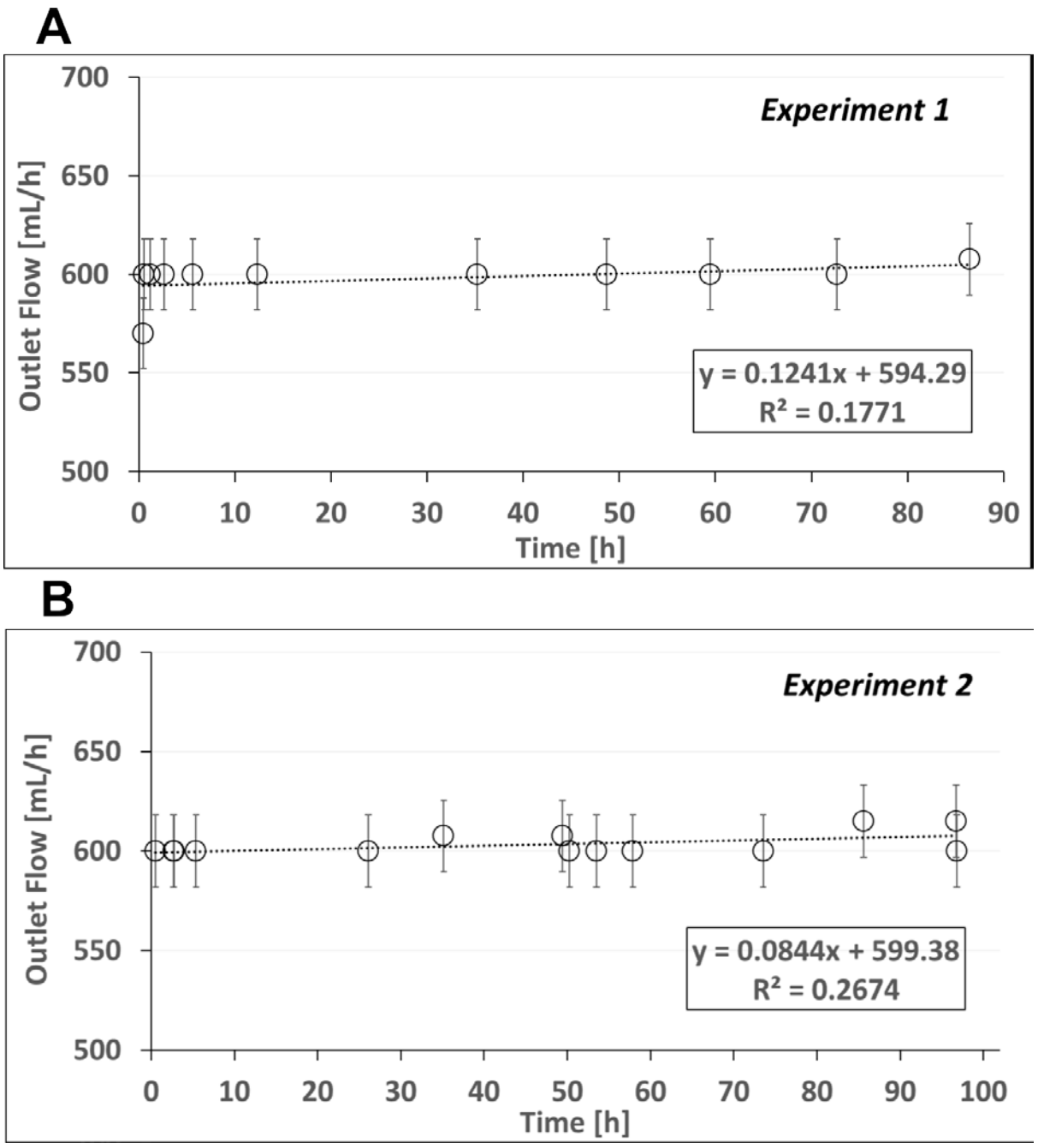

Figure 6.4 – Outlet flow rates in $Expt.1$ and $Exp.2$. Error bars are +/- 2σ. Error bars were calculated considering 1-mL as the minimum reading in the cylinder, and 2 seconds as time uncertainty.

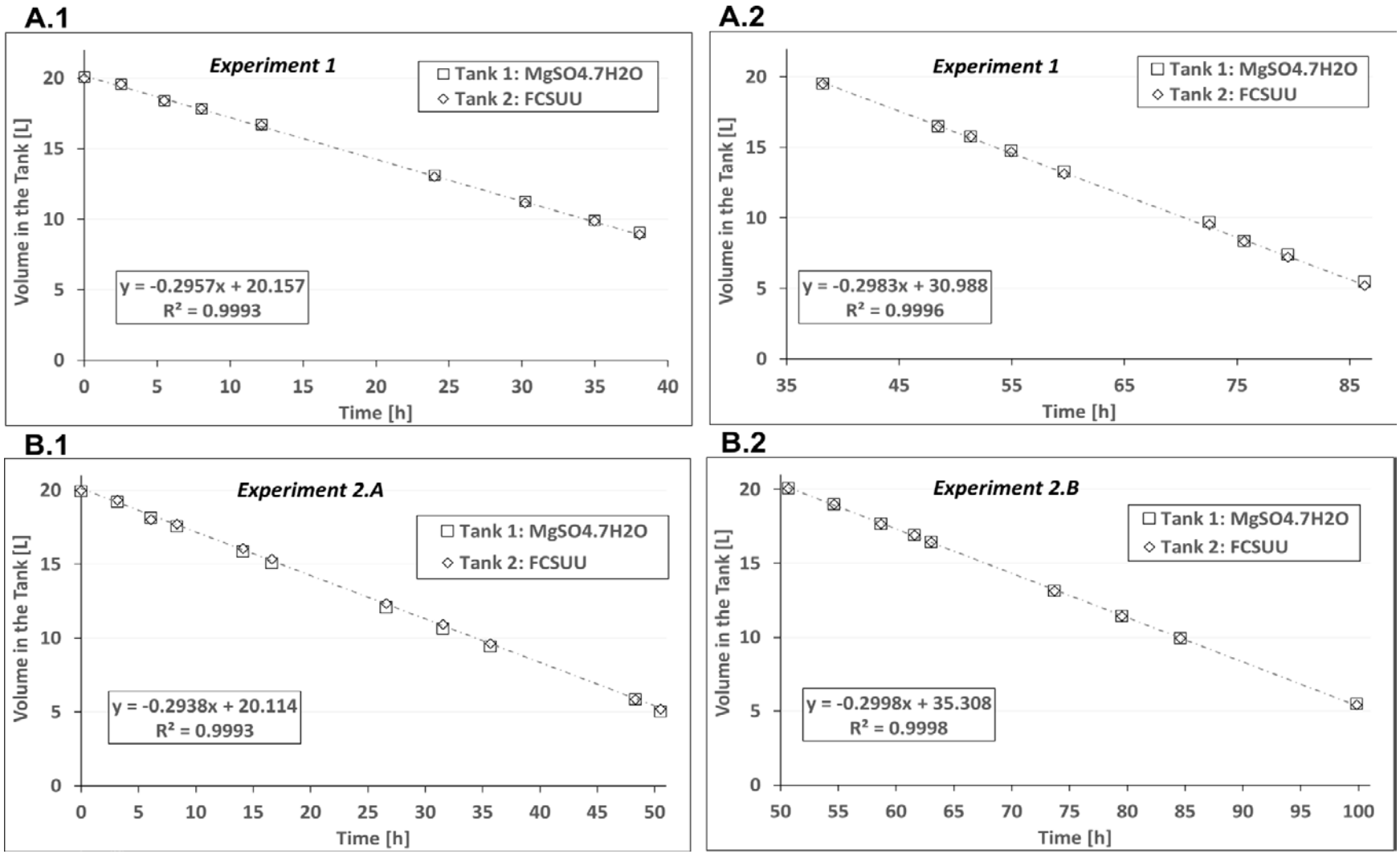

Figure 6.5 – Liquid level in feeding tanks during the first 38.23 h (A.1), and after refilling of solution up to 20-L (A.2) in $Expt.1$. Liquid level in in feeding tanks in the first 50 h ($Expt.2.A$) and in the last interval of the experiment ($Expt.2.B$).

6.2.3 On-line pH monitoring

Owing to very strong buffering of the NH_4^+/NH_3, measurements of pH are not highly relevant, but they can report unexpected variations, such as sudden stop of feeding. Measurements of pH (Fig. Figure 6.6.A and Figure 6.7A) were temperature compensated to 25 °C (Figure 6.6.B. and Figure 6.7.B) with equation 1.1.

$$pH_{25°C} = pH_T + \left(\frac{dpH}{dT}\right) \cdot (25°C - T) \qquad 6.1$$

Equation 6.1 expressed the pH at 25 °C ($pH_{25°C}$) as a function of the pH at any temperature (pH_T), the rate of change of pH per every 1 °C (dpH/dT) and the temperature (T) difference respect to 25 °C. The slope was estimated from $Expt.1$ data by correlating the temperature and the pH to determine an average slope and intercept of - 0.025 °C^{-1} and 9.416, respectively. This approach predicted pH of 8.783 at 25 °C. Temperature compensation for $Expt.2$ was corrected with the slope from $Expt.1$. Previous correction assumption was considered because according to Figure 6.7.C, the pH was expected to change due to chemical equilibrium.

The pH at 25°C in $Expt.1$ and $Expt.2$ showed a variations of around 0.04 units. This deviation of 0.04 units was expected in $Expt.1$ (Figure 6.6.C), but this deviation was lower than expected in $Expt.2$. Moreover, pH @ 25°C described an opposite trajectory to that of the simulated pH, which can indicate that the thermodynamics in the liquid interface is being affected by CO_2 adsorption, which was not modelled in this work.

Figure 6.6.B and Figure 6.7.B showed that the pH rapidly declines after feeding was stopped, which, strangely, is not predicted by the model. This change accounted for a 0.03 units in the first experiment, and 0.02 units in the second experiment. Even though this difference is small, dropping rate is high compared to overall process. This deviation can suggest transition of the liquid composition to

equilibrium. This pH drop rate could be applied to detect unexpected issues in the reactor feeding especially when the pH is not expected to change.

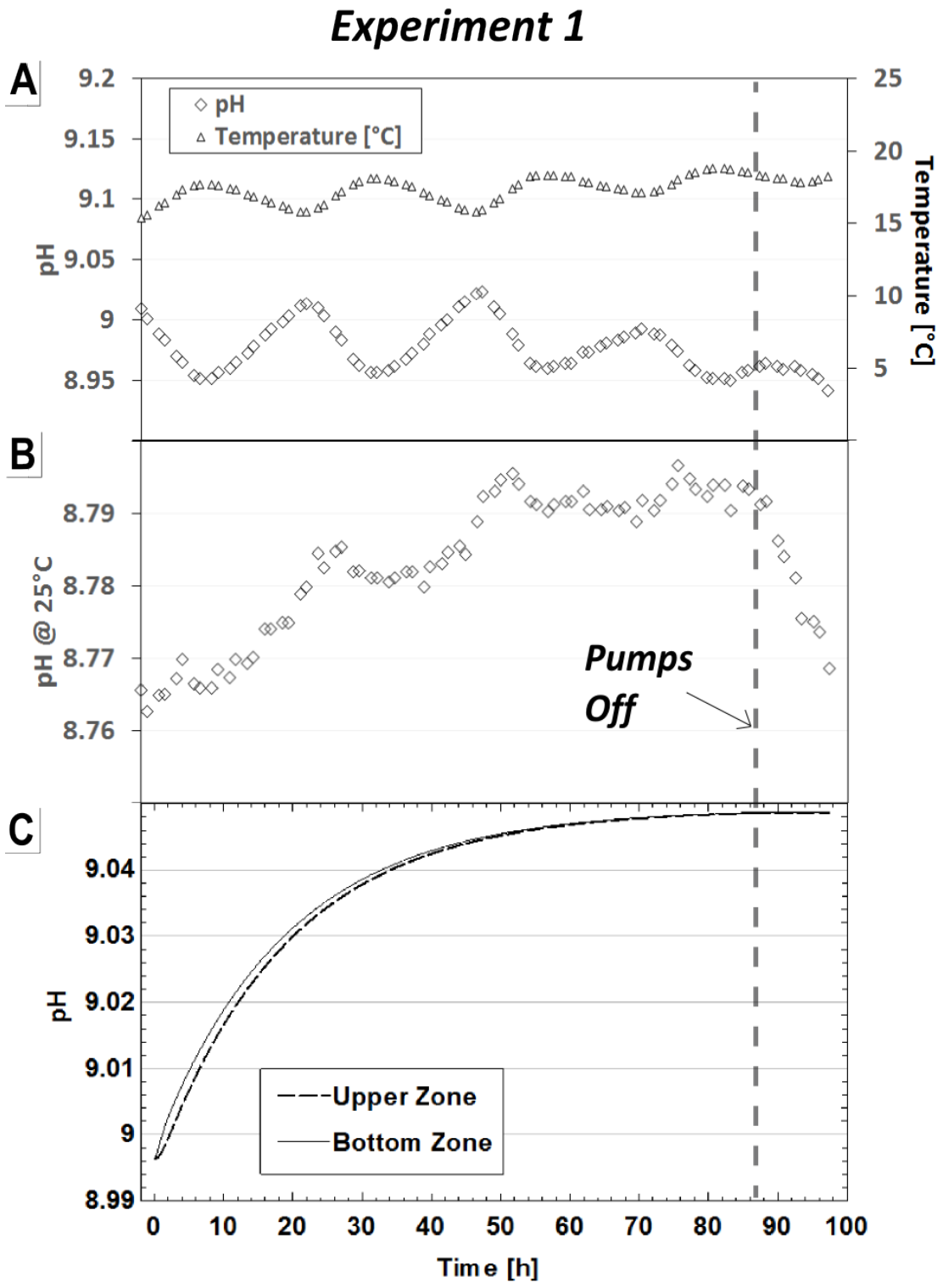

Figure 6.6 – Measured and predicted pH in $Expt.1$. Measurements without (A) and with (B) temperature compensation. pH was also predicted by the model (C).

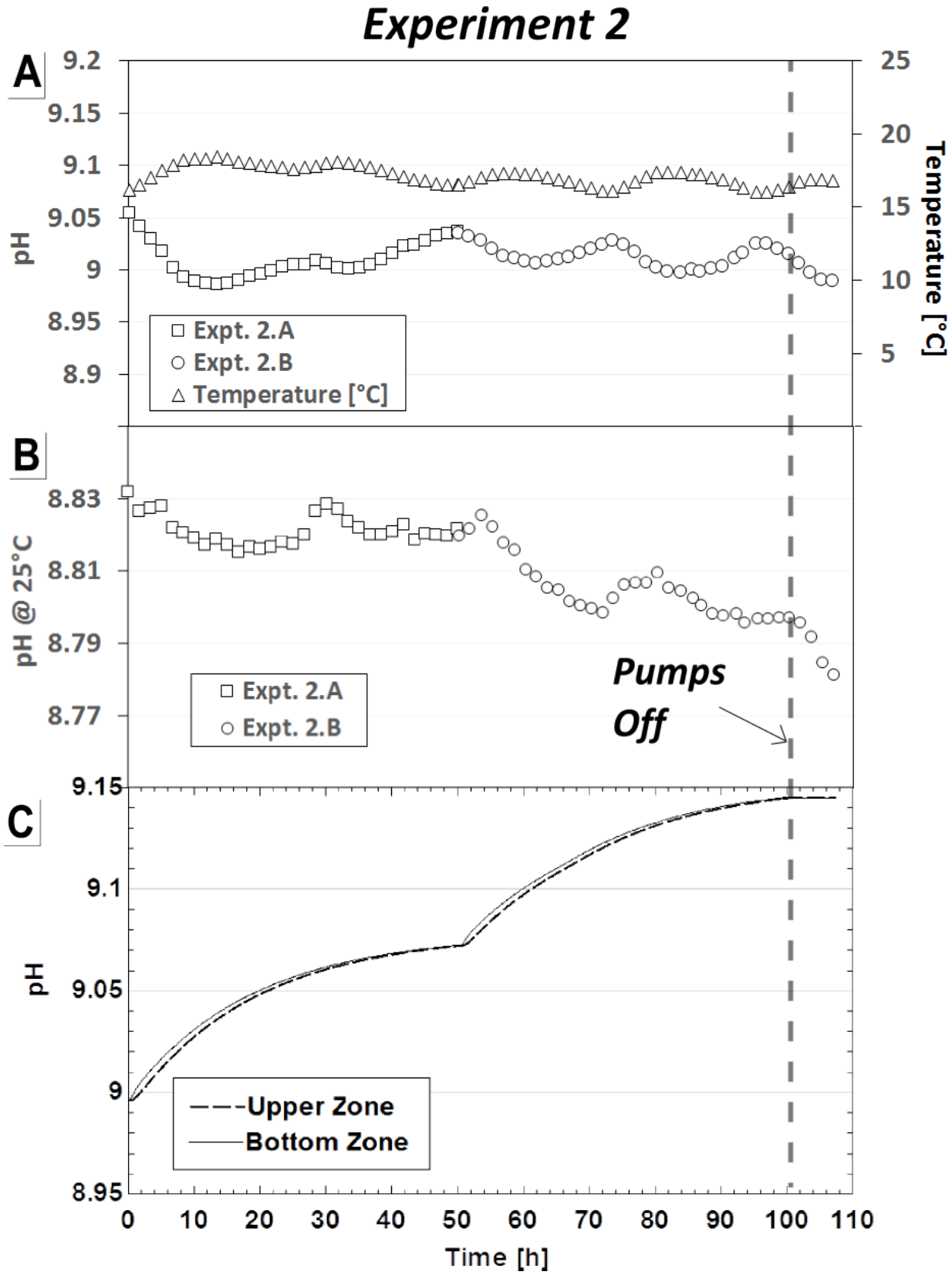

Figure 6.7 – Comparison of measured and predicted pH in $Expt.2$. Measurements without (A) and with (B) temperature compensation. pH was also predicted by the model (C).

6.2.4 On-line conductivity monitoring

The conductivity of the process was adjusted to 25 °C with the equation 6.2 given by McCleskey, et al. (McCleskey, Nordstrom, Ryan, & Ball, 2012).

$$K_{25°C} = \frac{K_T}{1 + \alpha(T - 25°C)} \quad 6.2$$

Equation 6.2 estimates the conductivity at 25 °C (K_{25}) at any given temperature (K_T) as a function of the recorded Temperature (T) in °C. In this equation, α is the temperature compensation factor which ranges from 0.019 to 0.023 $°C^{-1}$.

The estimation of α for this system was developed by measuring the conductivity of synthetic ureolysed urine (SUU) at varying temperatures. The SUU was prepared by adding the same quantity of water to the $FCSUU$. The temperature compensation factor was determined to be 0.018773 $°C^{-1}$ and 0.01848 $°C^{-1}$ for $Expt.1$ and $Expt.2$, respectively.

Figure 6.8.A and Figure 6.9.A showed that temperature correction is key to visualise conductivity trend during reactor operation (Figure 6.8.B and Figure 6.9B). The conductivity and the ionic strength in $Expt.1$ are almost constant during the overall reactor operation. The stop of feed streams does not affect the conductivity, nor the simulated ionic strength.

Figure 6.9.B and Figure 6.9.C indicates that the trend of the conductivity and ionic strength are similar in Expt. 2.B, but not in Expt. 2.A. However, it is possible to observe through conductivity change the moment when the Mg/P feed molar ratio was increased. The opposite behaviour of the ionic strength and the conductivity could be explained by the compositional distribution within the reactor in upper and bottom zone. This model only considers two zones and a constant intermixing flow rate estimated in a reactor operation with smaller quantity of seed, which deviates from $Expt.1$ and $Expt.2$.

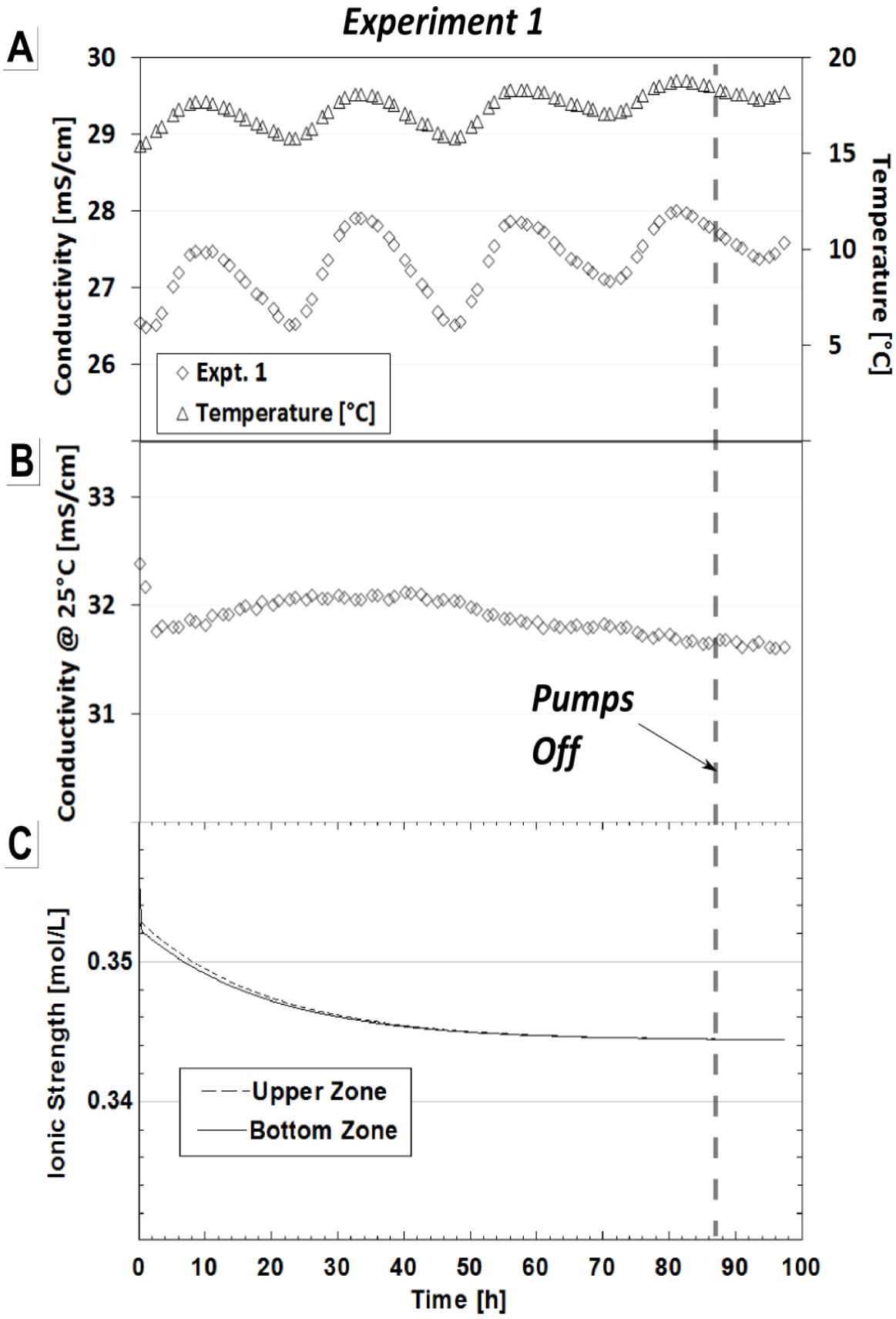

Figure 6.8 – Conductivity in $Expt.1$ without (A) and with (B) temperature compensation. Ionic strength was predicted by EES (C).

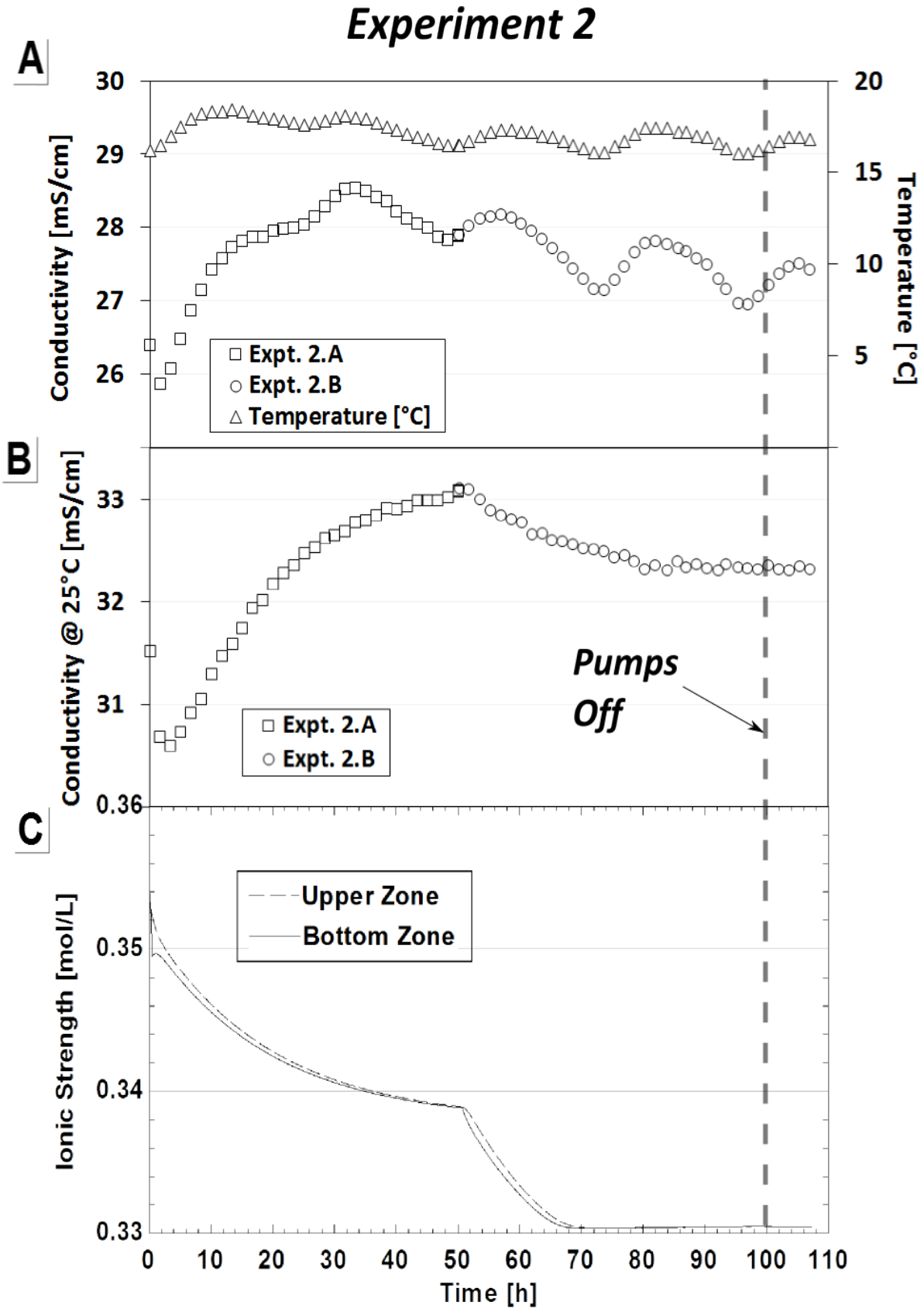

Figure 6.9 –Conductivity in $Expt.2$ without (A) and with (B) temperature compensation to 25 °C. Ionic strength was predicted by EES (C).

SUU was also diluted to determine the dilution factor effect in the conductivity. Figure 6.10 showed a linear correlation between these two variables. This has the same linear trend as previous work (Ronteltap et al., 2010); however, the ionic strength and conductivity were lower this work.

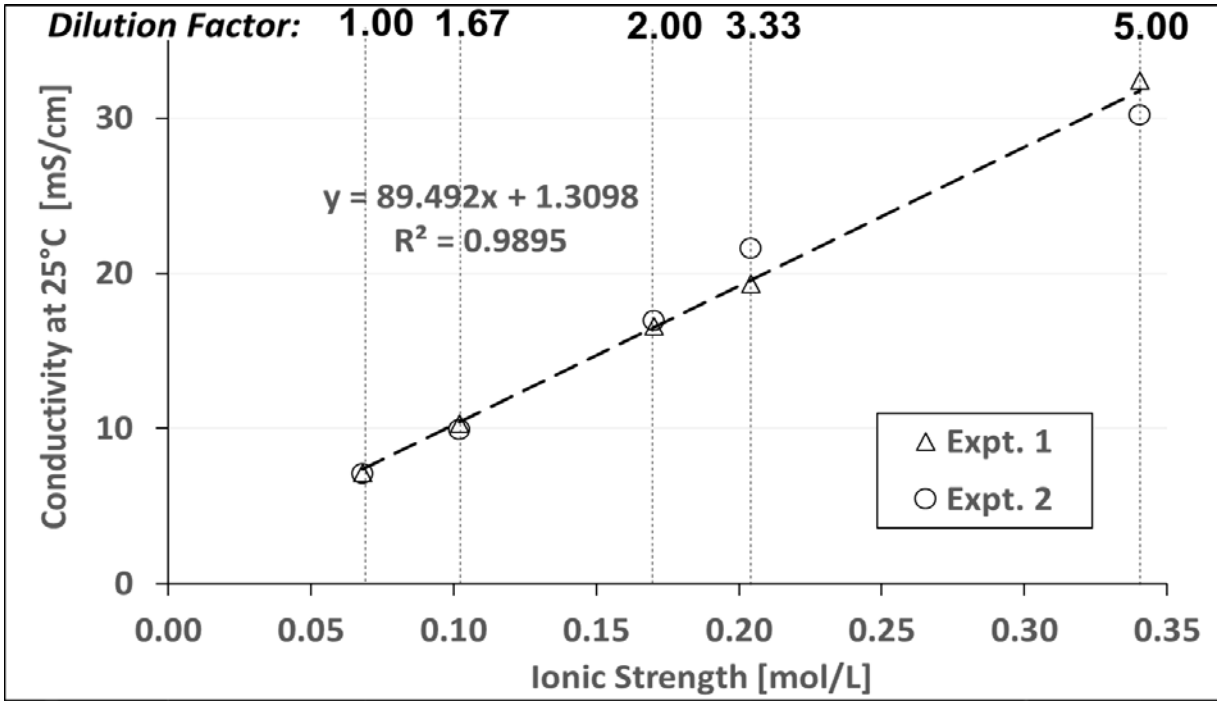

Figure 6.10 – Effect of dilution factor in the conductivity of synthetic ureolysed urine (SUU) at 25°C.

6.2.5 Mixing speed and bed height

Mixing speed within the reactor was adjusted to maintain a constant bed height over time within the reactor, despite the increase in struvite crystal mass. Figure 6.11.A showed that 150 RPM was sufficient to keep the struvite bed height around the same level in $Expt.1$. Figure 6.11.B showed that an increase of Mg/P feed molar ratio in $Expt.2A$ and $Expt.2.B$ increased the struvite crystals within the reactor and the bed height decreased rapidly. This data suggests that mixing speed has to be gradually increased when reactor operates at $Mg/P > 0.6$ if the struvite bed height is aimed to keep constant. This plot also showed a change in the bed height level of around 5 cm over 20 h (50 h – 70 h in $Exp.2.B$) indicates that mixing speed has to be increased in order to keep the bed height reasonably constant.

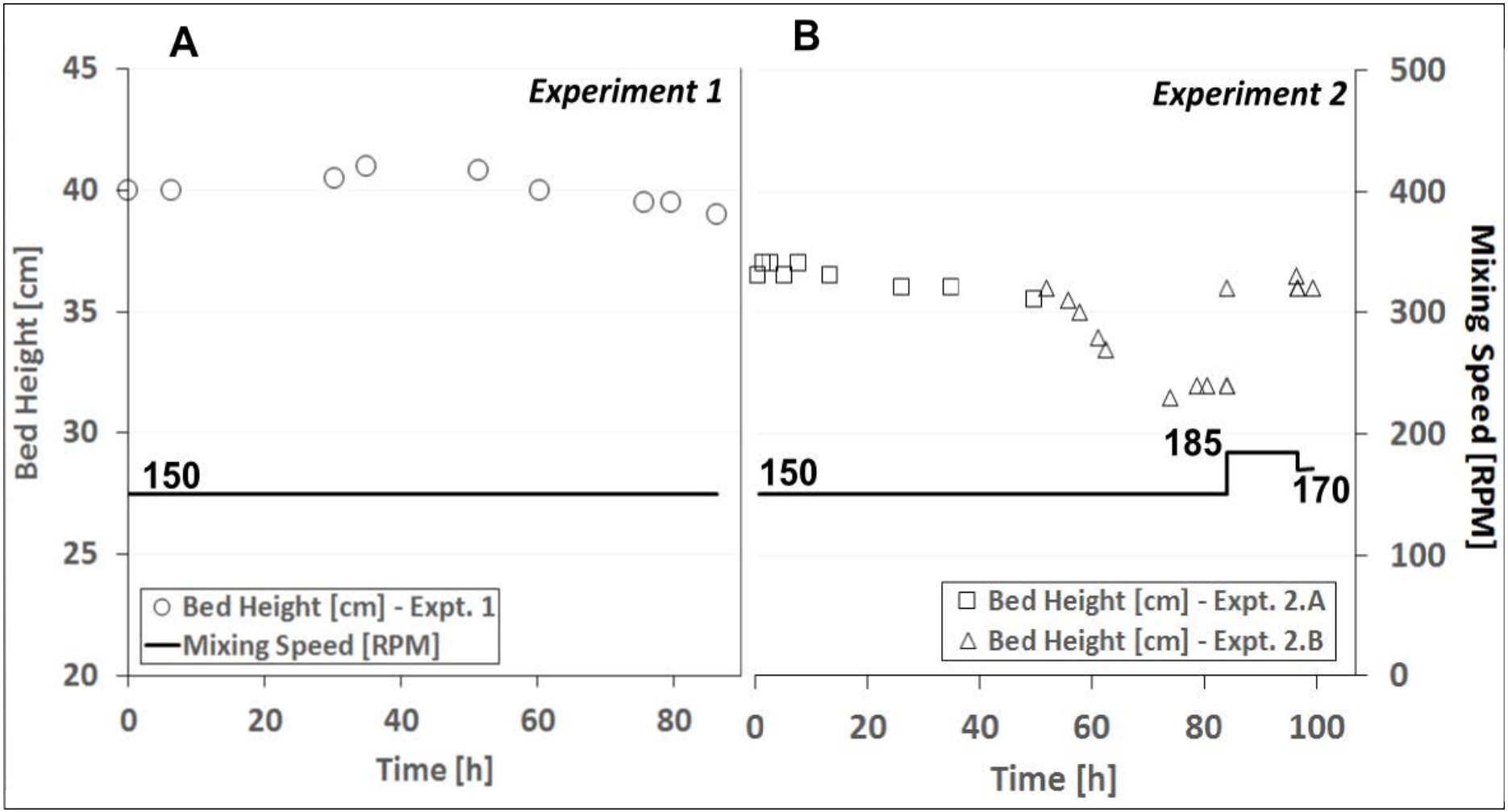

Figure 6.11 – Bed height of struvite crystals within the reactor. Adjustment of mixing speed of the impeller to keep the bed height almost the same level.

Measurement of bed height was taken visually during reactor operation.

6.2.6 Microscopy of struvite crystals

Figure 6.12 showed struvite crystal which were produced in a 5-L fed-batch reactor according to § 4.4.5 showed orthorhombic shape and individual sizes larger than 100 μm in scanning electron microscopy (SEM). Aggregates larger than 500 μm can also be observed (Figure 6.12.B). These crystals were uniform in shape but not in size. Additionally, SEM also showed that small particles adhered to the surface of larger crystals. The morphology and approximate size of these crystals compared well with the struvite crystals from $Expt.1$ and $Expt.2$.

Figure 6.13, Figure 6.14 and Figure 6.15 showed the simultaneous presence of nucleation, growth and aggregation in the struvite crystals. This means that localised high saturation index zones occurred in all experiments, very likely at the feeding band of the bottom zone of the reactor. In these photos, the aggregates can be larger than 100 μm, but individual crystals did not surpass 50 μm in length. Larger quantities of small crystals the in continuous experiments adhered to each other, compared to the aggregates in the fed-batch process. These observations described that nucleation was not stopped in $Expt.1$ and $Expt.2$, and the application of the power-law kinetic model (§ 2.2.6) is, at best, an approximation.

The orthorhombic shape of struvite crystals in fed-batch and continuous experiments was predominant. However, microscopy in continuous experiment showed a rounded shape, compared to the rectangular shape in crystals from fed-batch experiment. This main difference can be explained by the reactor configuration and the methodology nutrient addition. For instance, the nutrient in the fed-batch experiment was added in a short interval (few seconds), and then the crystal was allowed to grow through transfer of the ions from the liquid solution to the crystal surface. In the continuous process, the nutrient was added continuously, which means that nucleation was likely favourable more than growth.

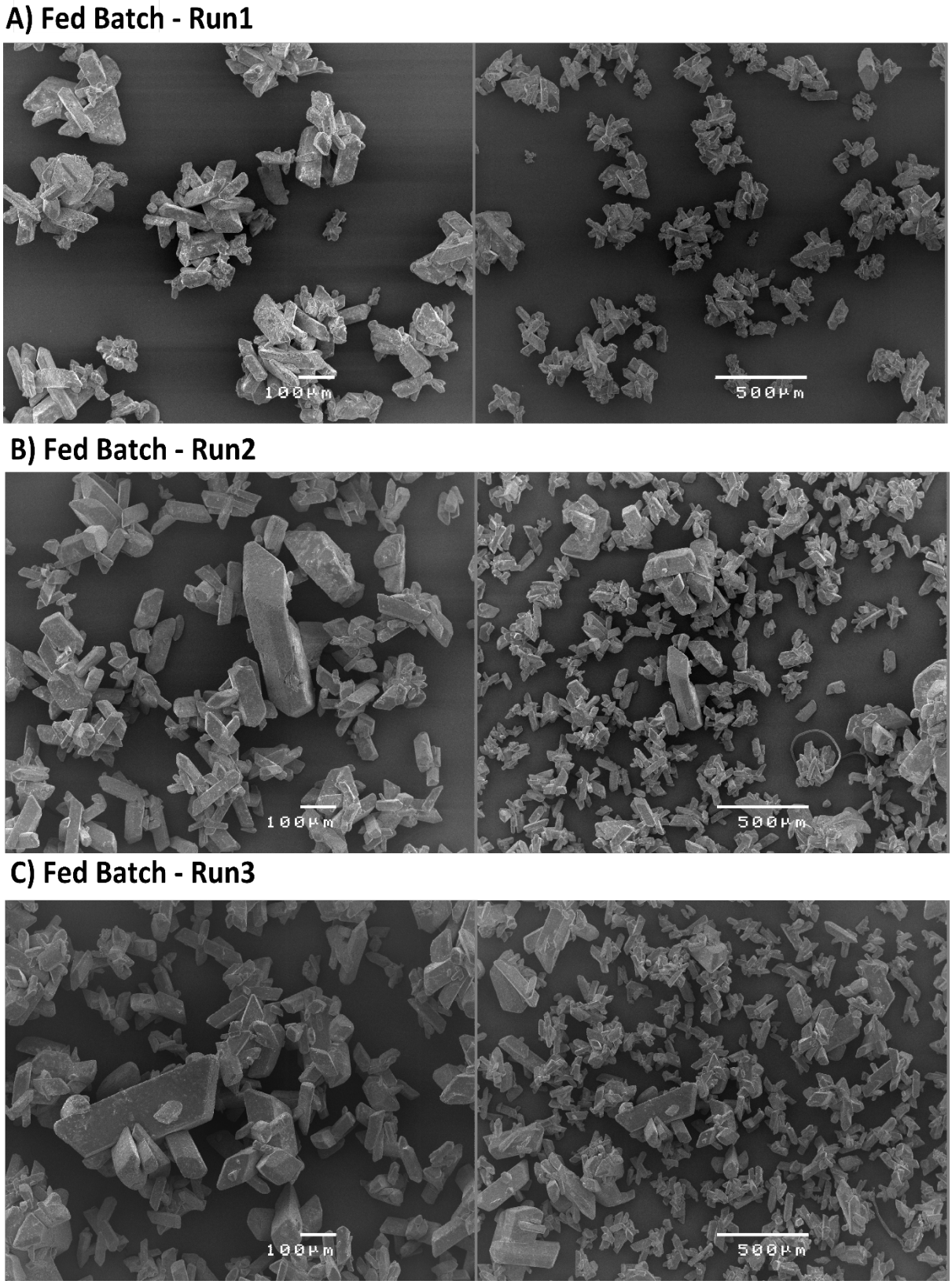

Figure 6.12 – Scanning Electron Microscopy of struvite seeds produced in a 5-L Fed-batch reactor. Preparation of crystals was according to § 3.3

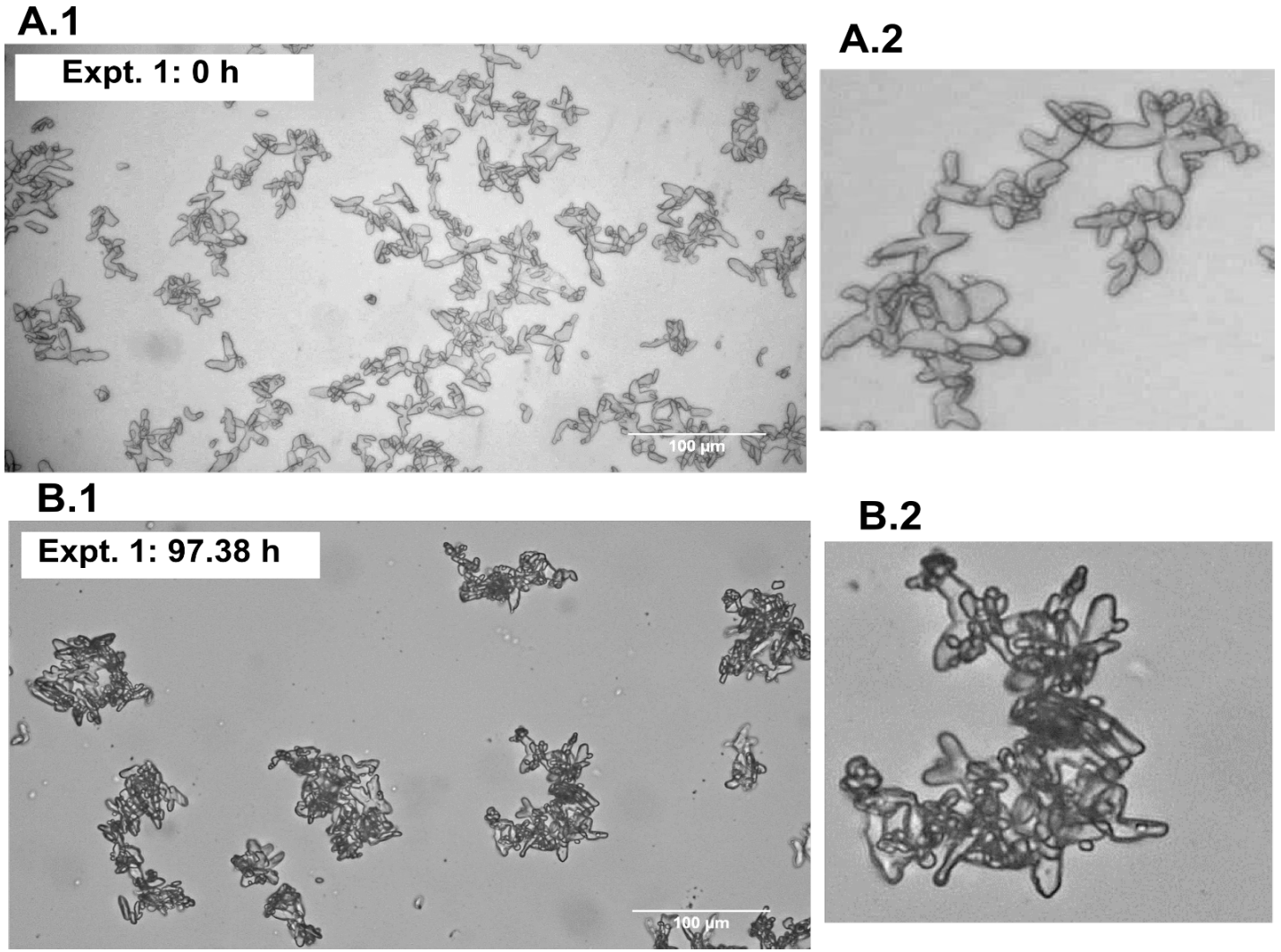

Figure 6.13 – Microscopy photos of struvite crystals taken in sample from the bottom tap of the reactor in $Expt.\,1$ at the start and end of the process.

Photos were taken with a Nikon E200 LED Laboratory Microscope at $20\ X$ amplification. Photos were zoomed using $ImageJ$ software.

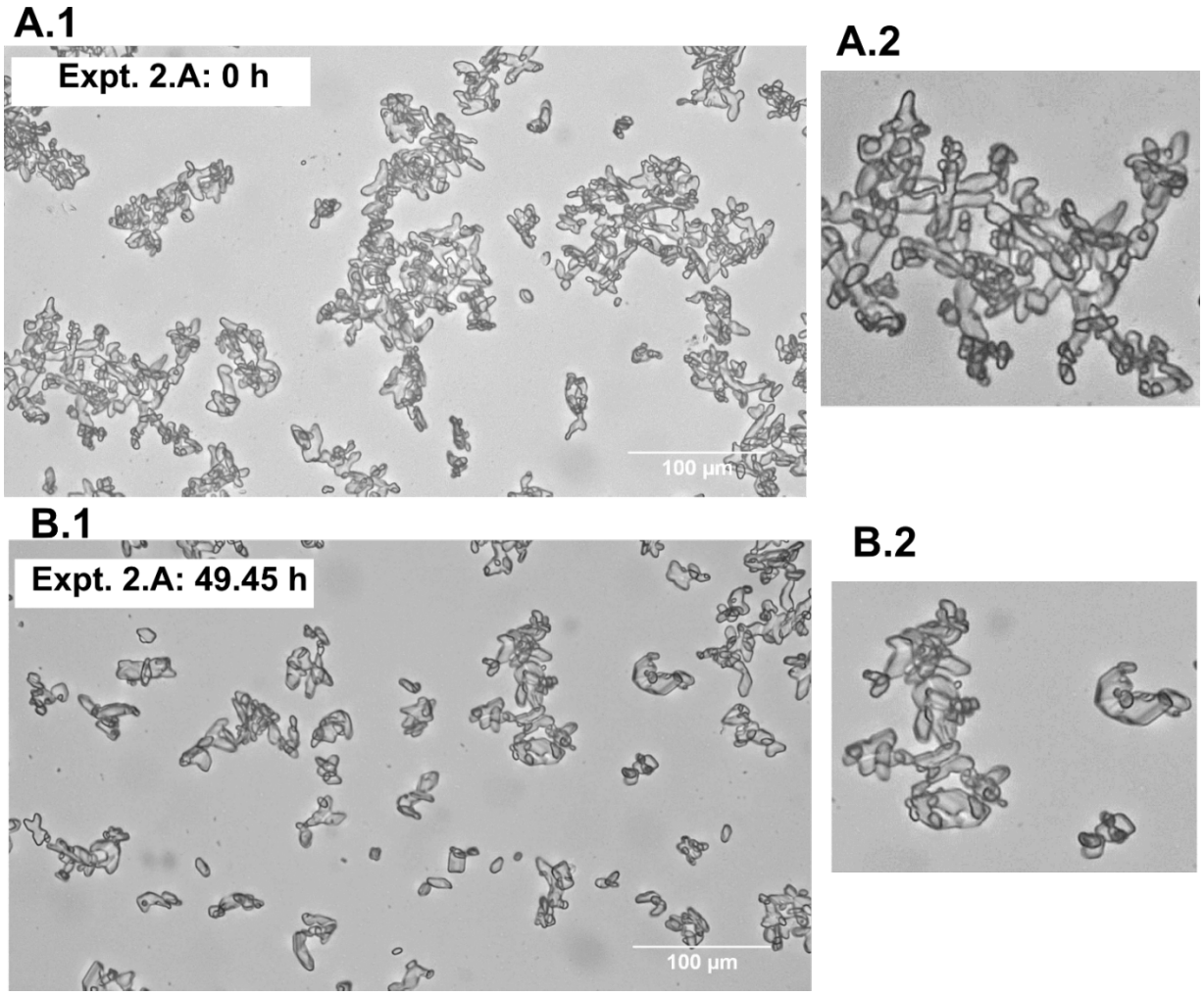

Figure 6.14 – Microscopy photos of struvite crystals taken in sample from the bottom tap of the reactor in $Expt.\,2.A$ at the start and end of the process. Photos were taken with a Nikon E200 LED Laboratory Microscope at $20\ X$ amplification. Photos were zoomed using $ImageJ$ software.

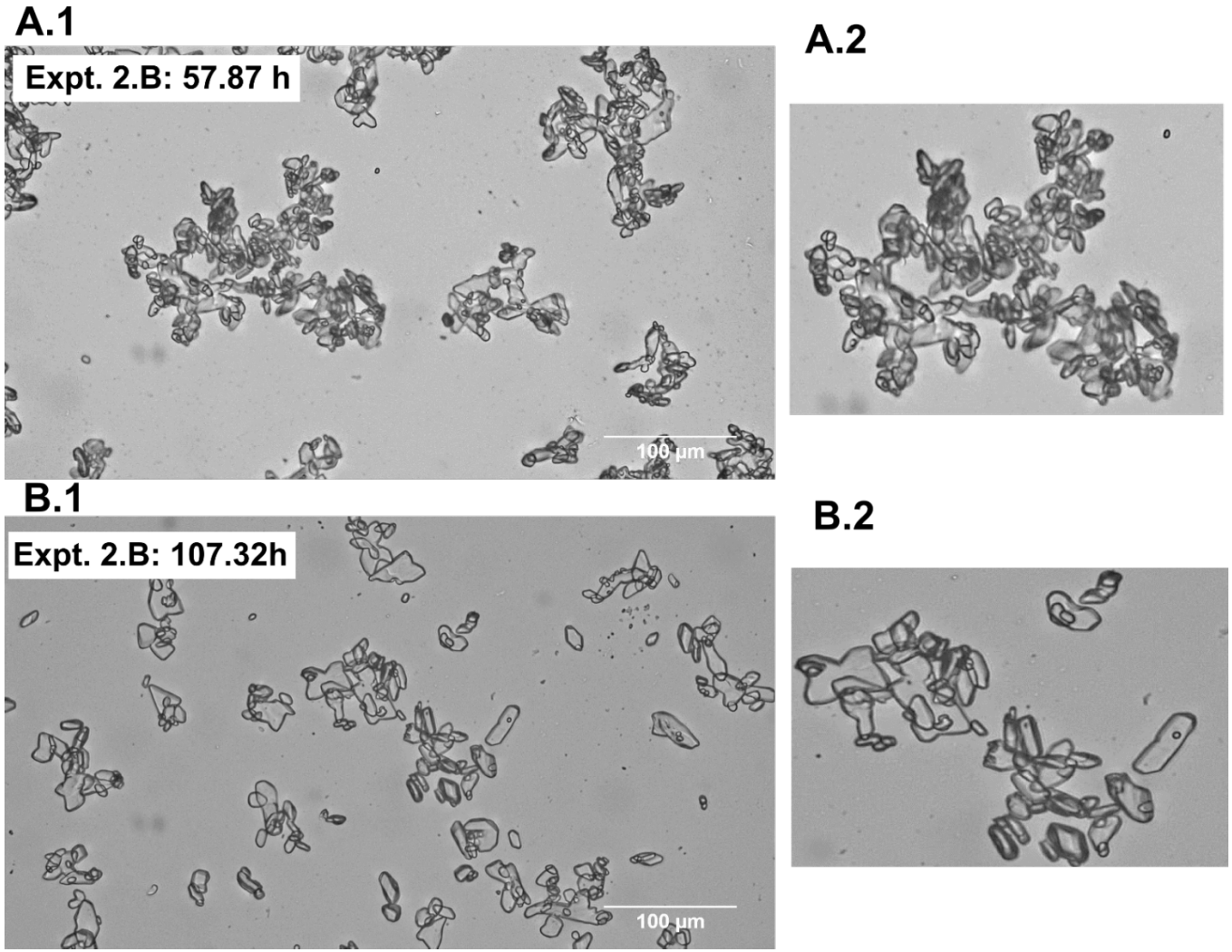

Figure 6.15 – Microscopy photos of struvite crystals taken in sample from the bottom tap of the reactor in $Expt.2.B$ at the start and end of the process. Photos were taken with a Nikon E200 LED Laboratory Microscope at $20\ X$ amplification. Photos were zoomed using $ImageJ$ software.

6.2.7 Elemental composition of Mg and P in solid

Percentage of P and Mg in solid samples taken at the start and at the end of $Expt.1$ and $Expt.2$ showed that the solid is most likely struvite (Figure 6.16). The analysis of the solid sample was performed according to § 4.3.3. Analysis by spectrophotometry and atomic absorption spectroscopy were used in the dissolved solid sample for P and Mg, respectively. An atypical % of P in the solid was observed in the solid for seeds in $Expt.2$; however, Mg analysis of this sample suggested that it is struvite.

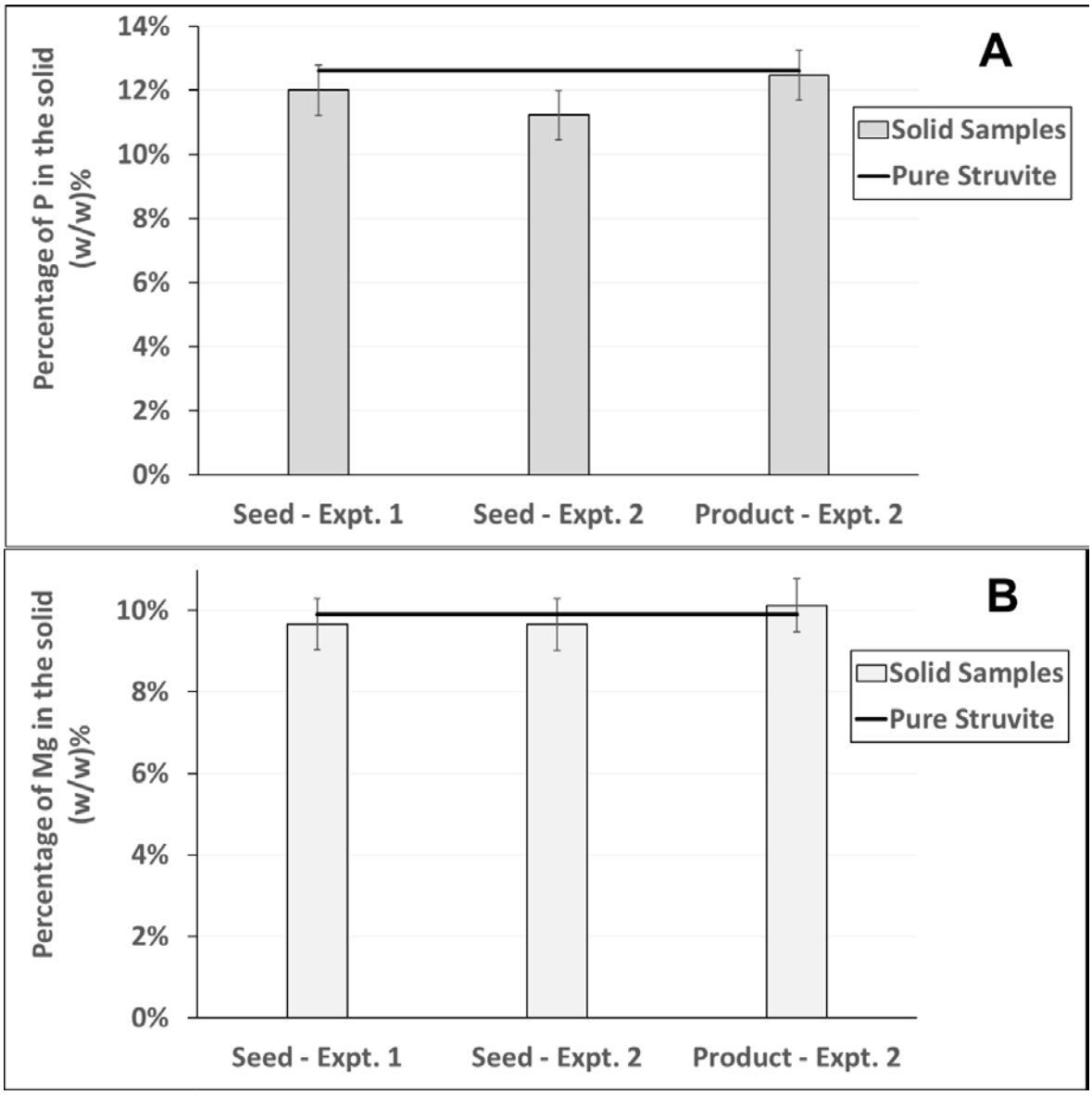

Figure 6.16 – Percentage of P and Mg in the solid. Struvite seed in the $Expt.2$ was the product from $Expt.1$. Error bars as +/- 2σ.

6.2.8 Solid identification X-ray diffraction measurements

X-ray diffraction (XRD) pattern assessed in the same samples from Fig. 6.16 corroborated the only presence of struvite. The samples were dried at 40 °C for 4 h. The patterns of each sample were compared to struvite database from Bruker software. The XRD patterns of every solid also showed similar relative intensity.

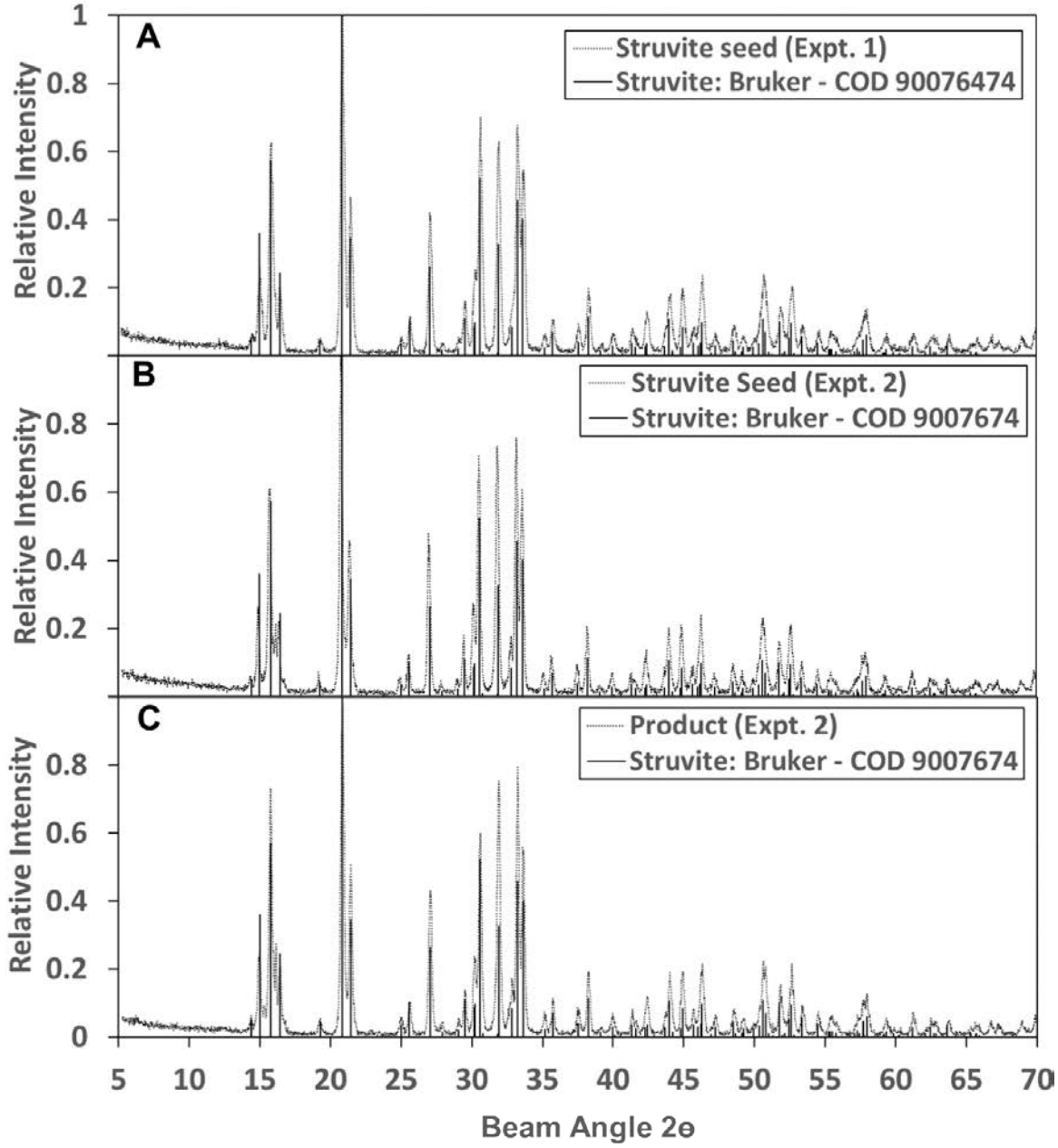

Figure 6.17 – Relative Intensity patterns from X-ray diffraction in the initial struvite seed for $Expt.1$, struvite seed for $Expt.2$, and final product from $Expt.2$.

Previous XRD analysis was developed to assess the possible presence of magnesite. Simulations of $Expt.2$ predicted a positive saturation index of this solid phase after 70 h operation (Figure 6.18A), owing to the increase Mg being fed to the reactor. The possible presence of magnesite was also compared with its X-ray diffraction pattern. Figure 6.18.B showed that the main peaks lies very close to the peaks of struvite, which could make more challenging the assessment of this solid phase. For instance, some peaks in the beam angle 2ɵ for struvite and magnesite are close: (32.84, .32.53), (35.72,35.74), (42.29,42.89), (53.36, 53.72). Previous comments suggested that magnesite could be present, but § 6.2.6 suggested that its impact in the solid composition can be considered negligible.

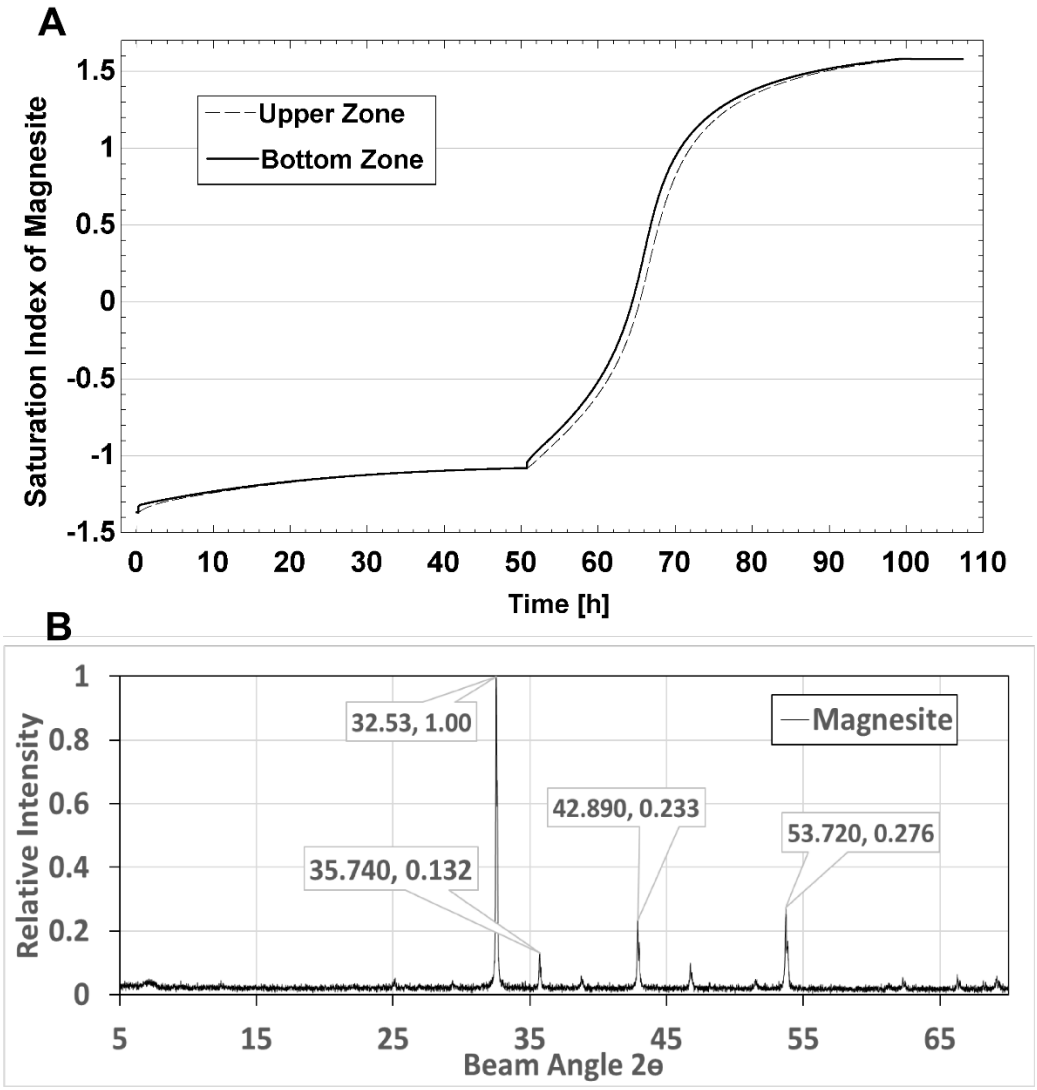

Figure 6.18 – Prediction of magnesite saturation index (A) in $Expt.2$ and X-ray diffraction pattern (B) from rruff.info/R050676. Source of Arizona Mineral Museum.

6.2.9 Solid loss in the reactor

The quantity of struvite loss in the walls of the reactor after collecting the struvite product at the end of the experiment was less than 1% the initial struvite seed mass (Figure 6.19). This assessment was developed by dissolving the remaining particles with 2.5 L of deionised water and 50 mL of 10.1 M HCl . This dissolution was analysed for P by spectrophotometry. The mass of P was determined by considering the volume of 2.55 L., and the estimation of struvite mass was estimated with molecular weight of struvite and P.

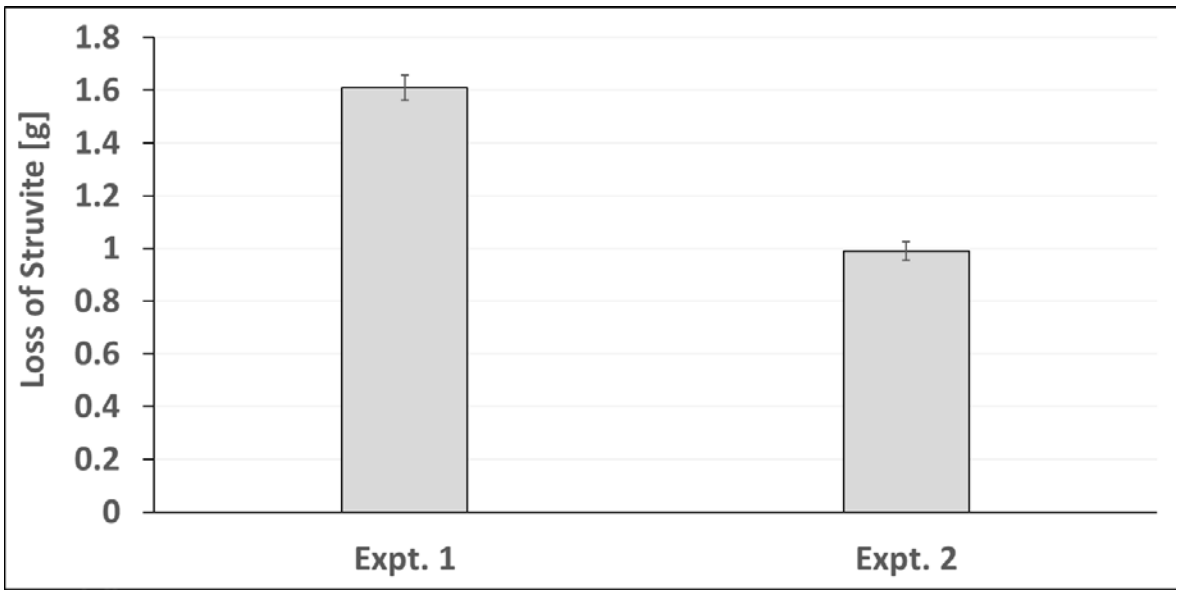

Figure 6.19 – Measurement of struvite loss in the reactor walls at the end of the each experiment. Error bars as +/- 2σ.

6.3 Modelling and experimental data

This section compares the modelling and experimental data of $Expt.1$ and $Expt.2$. Elemental concentration of P and Mg, struvite mass, and mean weight diameter were assessed. Simulations in this section considered kinetic parameters of k = 1e-6 and n = 1 according to § 5.1.5.

6.3.1 Concentration of P an Mg in the liquid phase

The dynamic model was able to predict experimental P and Mg concentration in the liquid phase. Samples were taken from the outlet hose, liquid surface and bottom tap of the reactor (see Figure 6.3). Every sample was collected in a 25-mL plastic container and immediately filtered with a 25-mL syringe connected to 0.2 μm filter. The filtered sample was stored for analysis of P and Mg. Simulation of the upper and bottom zone showed negligible differences in the $Expt.1$ (Figure 6.20.A and B), with very small variability in $Expt.2$ (Fig. Figure 6.21.A and B).

$Expt.1$ showed that simulations agree with the elemental concentration of P (Figure 6.20.A). Prediction of elemental Mg concentration in the liquid phases over estimated the measured concentration. Simulation trials showed that varying the kinetic parameters (n, k) did not help in matching the model to the measurements, because the system was running very close to equilibrium. Despite deviation of the model and the experimental Mg concentration, 0.1 mg/L difference in Mg cannot provoke a significant effect in the overall struvite mass production.

Expt. 2 showed agreement in the P concentration in the overall experiment (Figure 6.21.A). However, some deviations can be observed in the predicted Mg during $Expt.2.B$ at larger Mg/P feed molar ratio (Figure 6.21.B). Deviations between the model and measurements still lie within experimental uncertainty.

This experiment also highlighted the utility of the model to determine which element should be monitored during experimentation (see § 4.3.3). Selection of P or Mg as elements for validation depends of their concentration range. For instance, P is a more suitable variable to be assessed when Mg/P is lower than one and this element is above detection limit ($Expt.1$ and $Expt.2.A$). Concentration of Mg was suitable when P lies below limiting detection ($Expt.2.B$).

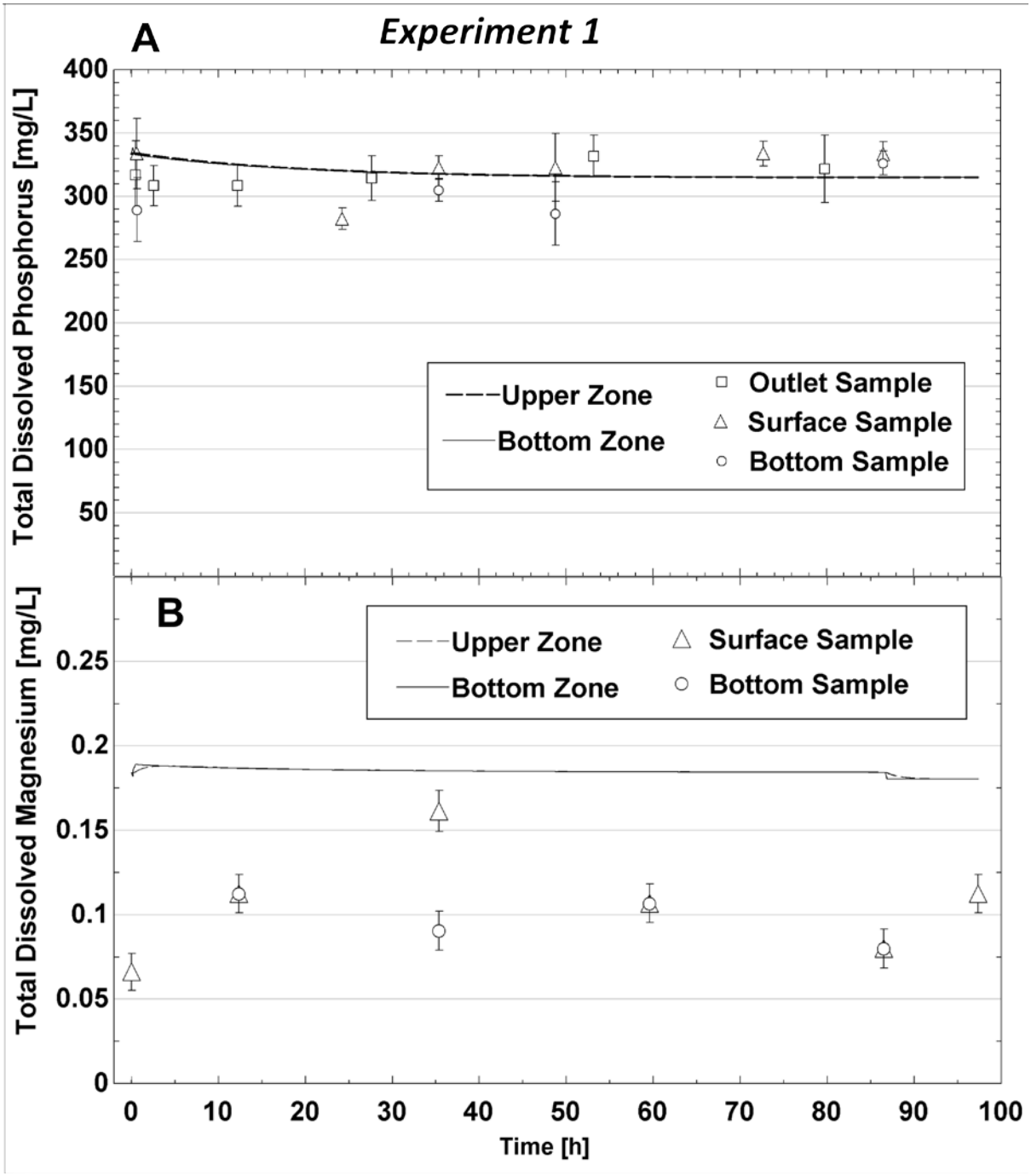

Figure 6.20 – Experimental and modelled data of P and Mg in the liquid phase in the $Expt.1$. Error bars as +/- 2σ.

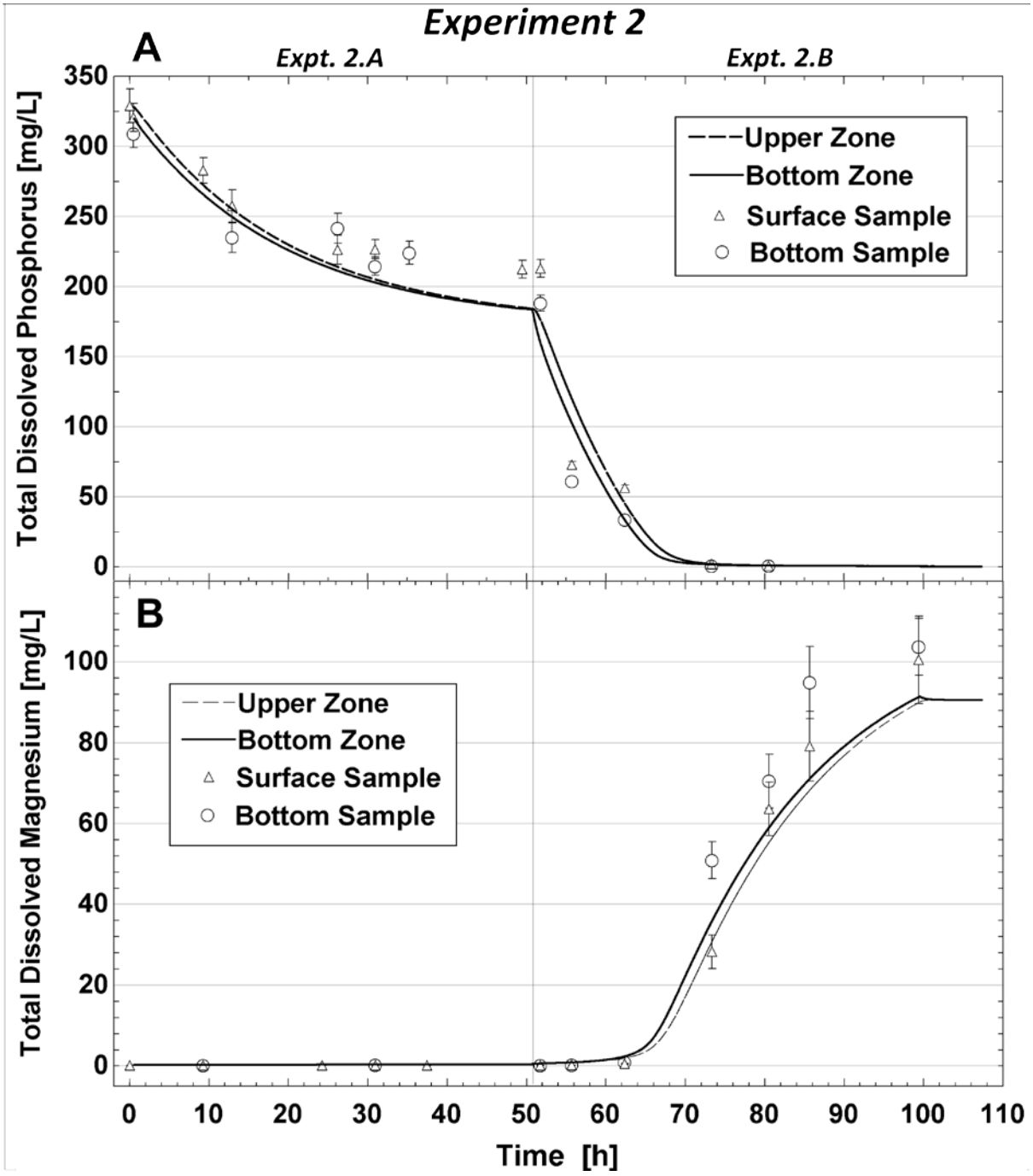

Figure 6.21 – Experimental and modelled data of P and Mg in the liquid phase of $Expt.2$. Error bars as +/- 2σ.

6.3.2 Struvite mass production

The model-predicted struvite mass production approached the experimental data. The quantification of struvite mass is constrained by the uncertainty in the methodology (§ 4.4.6). Because of the systematic uncertainty in the estimation of the quantity of seeds, two simulations were performed using different initial struvite seed quantity based on the range of possible densities of saturated solution. Figure 6.22.A and B showed that deviation between the predicted and measured struvite mass was less than 5 %. This error range could be used as a reference for future works relying on a similar methodology to quantify struvite crystals.

6.3.3 Particle size measurement

Mean weight particle size (MWS) (see § 4.4.6) cannot be predicted by the model because of aggregated particles. In Chapter 3, the model assumed a monodisperse particle population, however, in reality a polydisperse distribution was found. To compare experimental data with model predictions, this work converted the coulter data (counts and mean diameter) into MWS per each sample.

Samples were taken from the bottom tap (see Figure 6.3) of the reactor and immediately filtered and stored before analysis. Every solid sample taken from the reactor weighed and separated in two sub-samples. The smaller sample was destined for microscopy and the larger for counting and sizing by electric zone sensing ($i.e.$ Coulter Counter).

The MWS was processed using Coulter data. Unfortunately, the lower size ranges of the population are below the noise threshold ($i.e.$ 30 μm) and therefore, part of the sample cannot be detected. The undetected population below the noise in Coulter also can affect the estimation of the MWS or any information from size distribution. Figure 6.22 reported an under prediction of mean particle size compared to MWS measurements.

Another cause of deviation is that the model assumed uniform size distribution, however in reality larger particles occupy lower regions in the reactor and smaller crystal will be suspended close to the

bed height interface. This means that larger particles are to be found in the lowest part of the reactor while smaller one higher in the bottom zone.

Figure 6.23 showed that the overall growth in particle size is less than 2 μm in the first experiment while the increased on Mg/P in experiment 2 was predicted to be less than 5 μm. This small increase of the mean particle size multiplied by the quantity of crystal within the reactor represented the quantity of struvite mass produced in each experiment. Measurement of larger particle sizes than expected also corroborated the aggregation of individual particles detected by microscopy (§ 6.2.6).

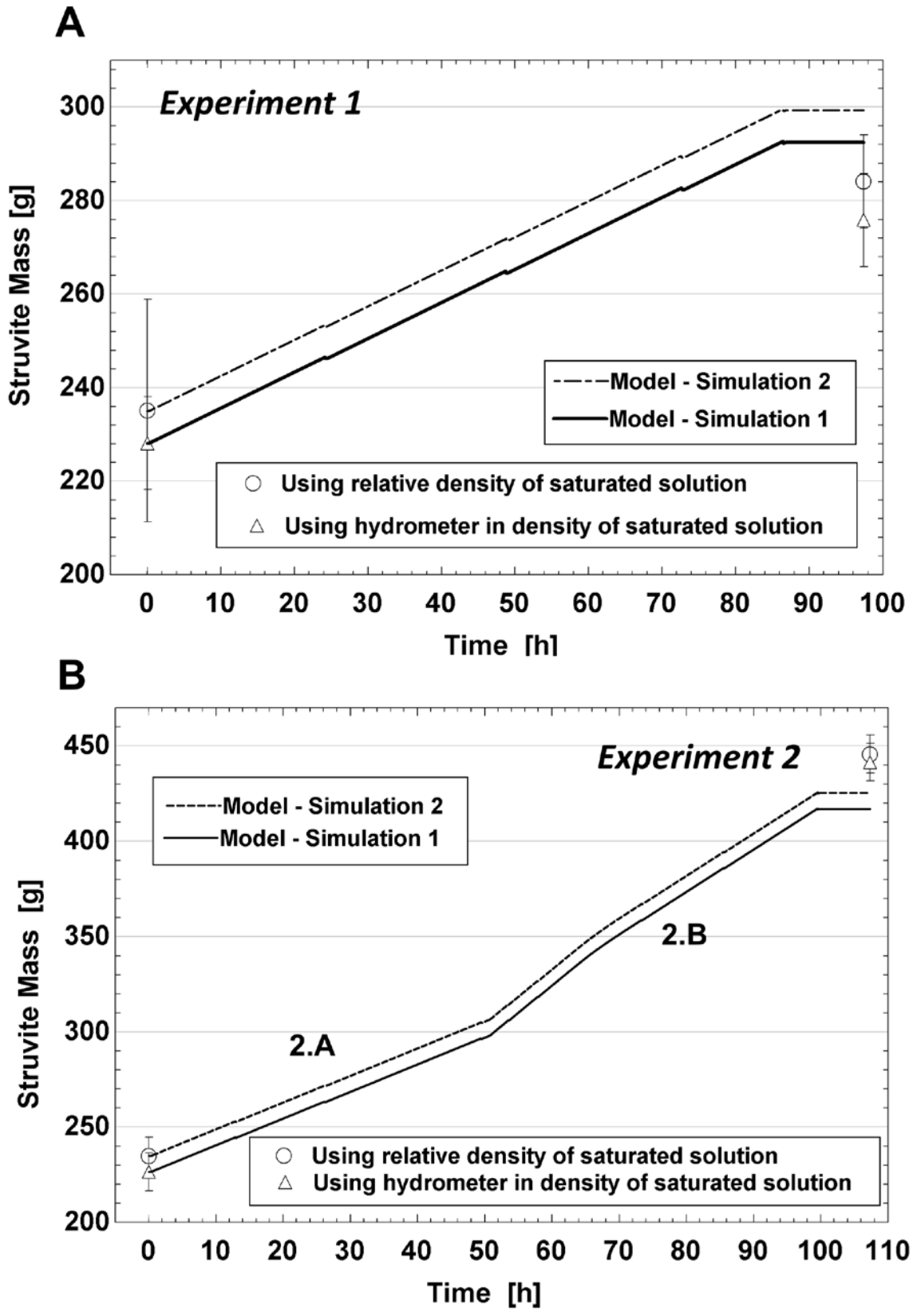

Figure 6.22 – Struvite mass prediction using the indirect density methodology to quantify struvite crystals. Struvite mass in $Expt.1$ and $Expt.2$.

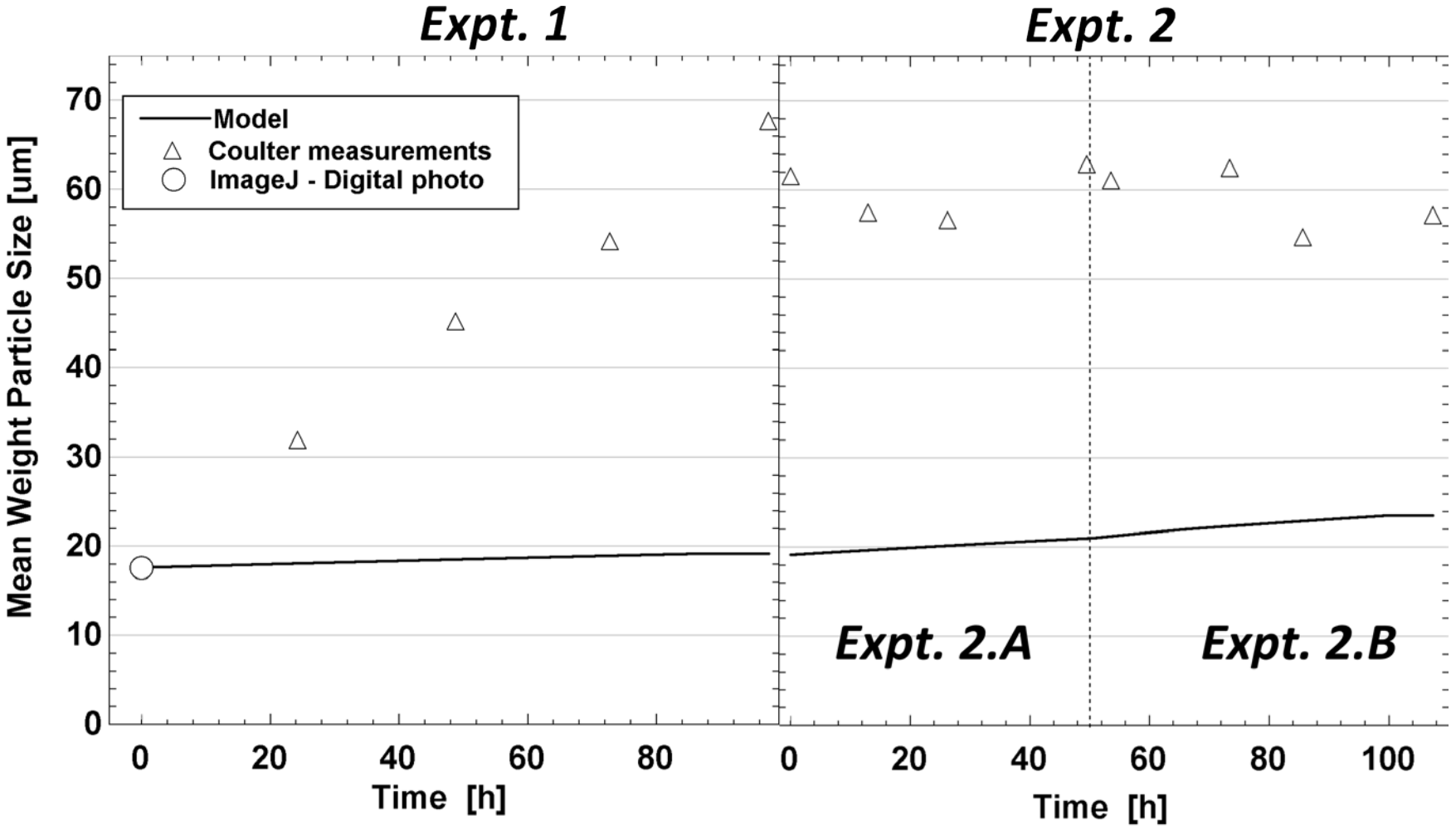

Figure 6.23 – Comparison of predicted and measured mean weight particle in $Expt.1$ and $Expt.2$. Data was collected with Coulter Beckman Multisizer 4, and initial mean particle size estimated with $ImageJ$ software.

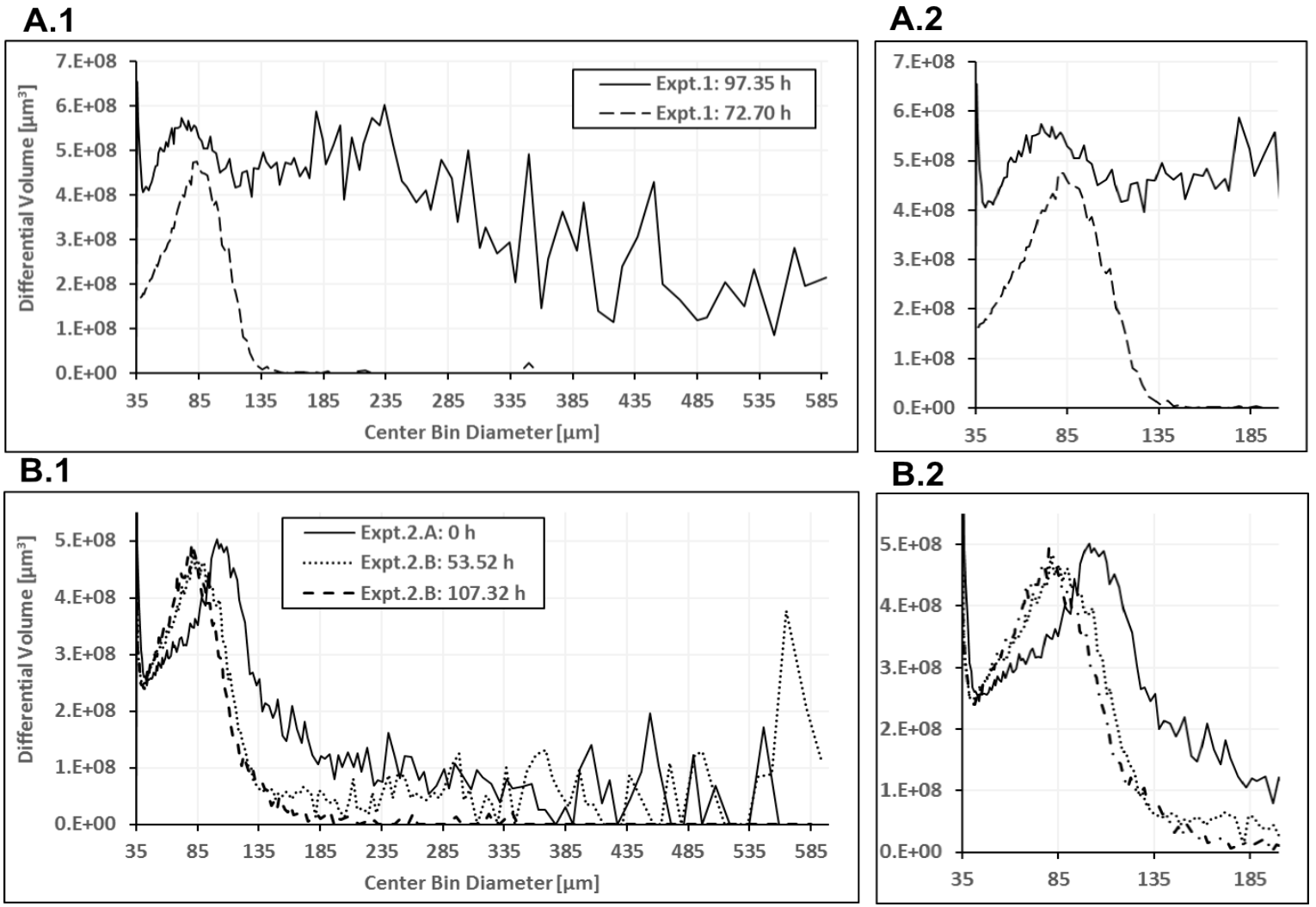

Figure 6.24 – Differential volume measurement of samples in $Expt.1$ (A), and $Expt.2$ (B). Data was measured in Coulter Multisizer 4. Fig. A.2 and Fig. B.2 are the amplified image of Fig. A.1, and Fig B.2 respectively.

Inadequate suspension of particles during Coulter measurements can lead to atypical data as shown in Figure 6.24.A. Aggregated particles may be present during coulter measurements. This can be explained by comparing the differential volume of the last sample of $Expt.1$ (97.35 h) with the first sample of $Expt.2$ (0 h), which should be the same. It is clear that the distribution of the 97.35 h sample from $Expt.1$ is not representative of the system due to the counts at sizes larger 200 μm, which were not observed by microscopy in § 6.2.6. This finding suggests that samples should perhaps be sonicated (M. Burns et al., 2016) and analysed more than one time to ensure analytical reliability.

Figure 6.24.A.2 showed that the distribution lower than 35 μm is unknown due to the constraints of the aperture tube size of the Coulter (2% - 60% of 1000 μm) and the detected noise. This undetected part of the plot could be large (large counting of particles) or small (low counting) of the differential volume. Application of Coulter sizer in $Expt.1$ was less reliable than data collected for $Expt.2$, because the quantity of smaller particles.

Figure 6.24.B showed that nuclei production becomes more predominant over time (especially in $Expt.2.B$), because the peaks of the distribution are moving from the right to the left. The displacement of these three distributions can be explained by the increase of saturation index when Mg/P feed molar ratio increases.

6.3.4 Struvite saturation index in the upper reactor zone

Changes in the saturation index when Mg/P feed molar ratio was increased in the transition from $Expt.2.A$ to $Expt.2.B$ was detected by microscopy. Simulation of SI_{MAP} in the upper and bottom zone of the reactor suggested a high increase of this variable when the reactor operation changes from $Expt.2.A$ to $Expt.2.B$ (Figure 6.25). This prediction suggested that nucleation will likely occur in the upper zone reactor of the reactor, so nuclei would be expected to appear in this zone.

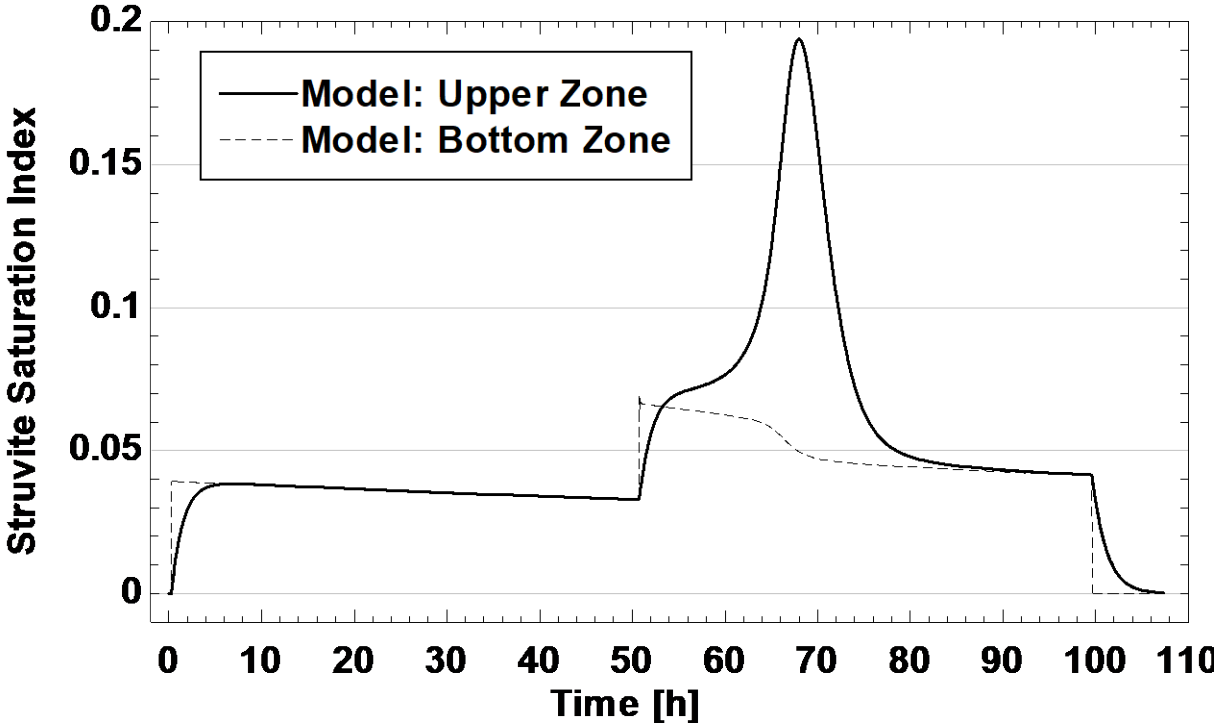

Figure 6.25 – Struvite saturation Index in the upper and bottom zone of the reactor in $Expt.2$.

Figure 6.26 showed the presence of small nuclei in samples taken in the upper zone of the reactor. Fig. 6.26.A showed that nucleation occurred at the beginning of $Expt.2.B$, and Figure 6.26.B showed that these particles increased inside the upper zone of the reactor over time. Moreover, microscopy revealed that the length particle size did not surpass 100 μm, which is consistent with the particle size evolution in samples taken from the bottom tap of the reactor (see § 6.2.5).

Photos of the upper zone of the reactor made visible the presence of nucleation (Figure 6.27). The first photo on the left was taken before the change to $Expt.2.B$. This photo showed transparency in the upper zone liquid with negligible presence of crystals. The second photo was taken after $Expt.2.B$ was set, and it clearly shows turbidity in the upper liquid of the reactor. The last photo on the right demonstrated that crystals were still present in this zone until the end of $Expt.2.B$. Figure 6.27 agrees with Figure 6.26, and therefore, it is also possible to detect nucleation by transparency in the upper liquid of the reactor. This also suggests that following works could apply non-invasive methodologies such as light scattering in similar reactor configuration.

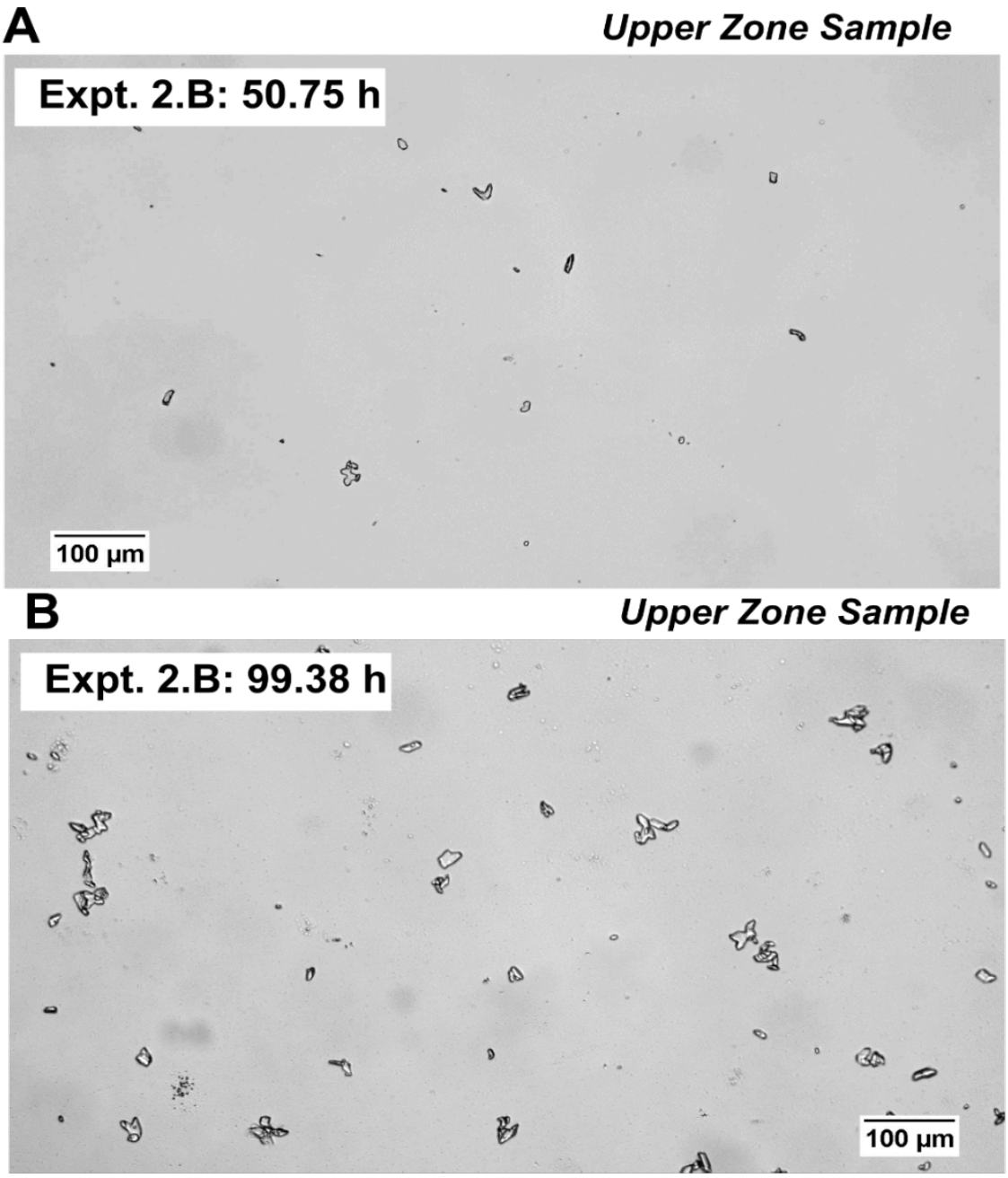

Figure 6.26 – Microscopy of samples from top tap of the reactor in $Expt.\,2.B$.

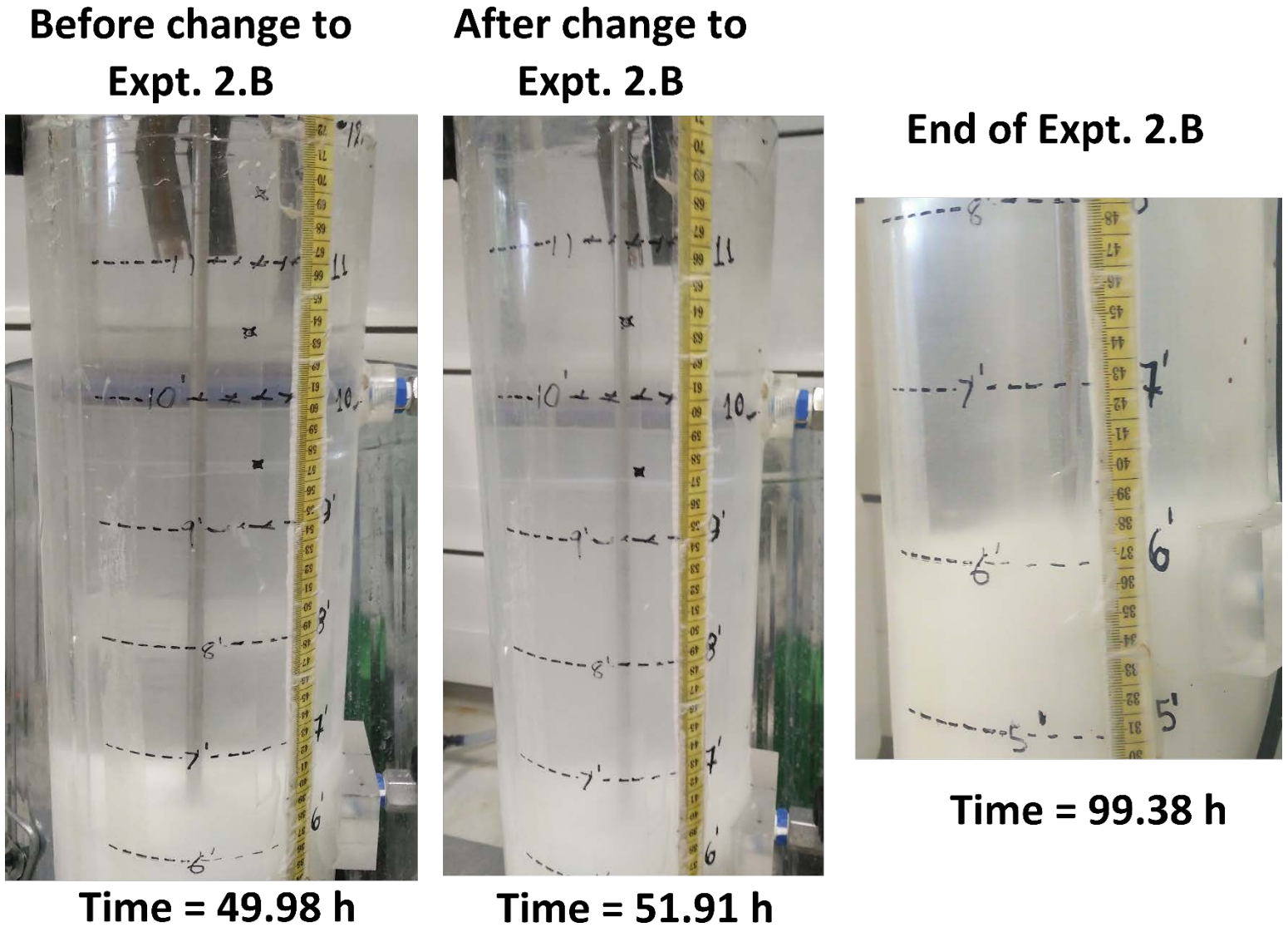

Figure 6.27 – Photos of the upper zone of the reactor before and after increasing the Mg/P feed molar ratio during $Expt.\,2$.

6.3.5 Estimation of solubility product constant

Variation in the solubility product constant from $pKsp$ = 13.26 to 13.60 improved the agreement between predicted and measured elemental Mg concentration.

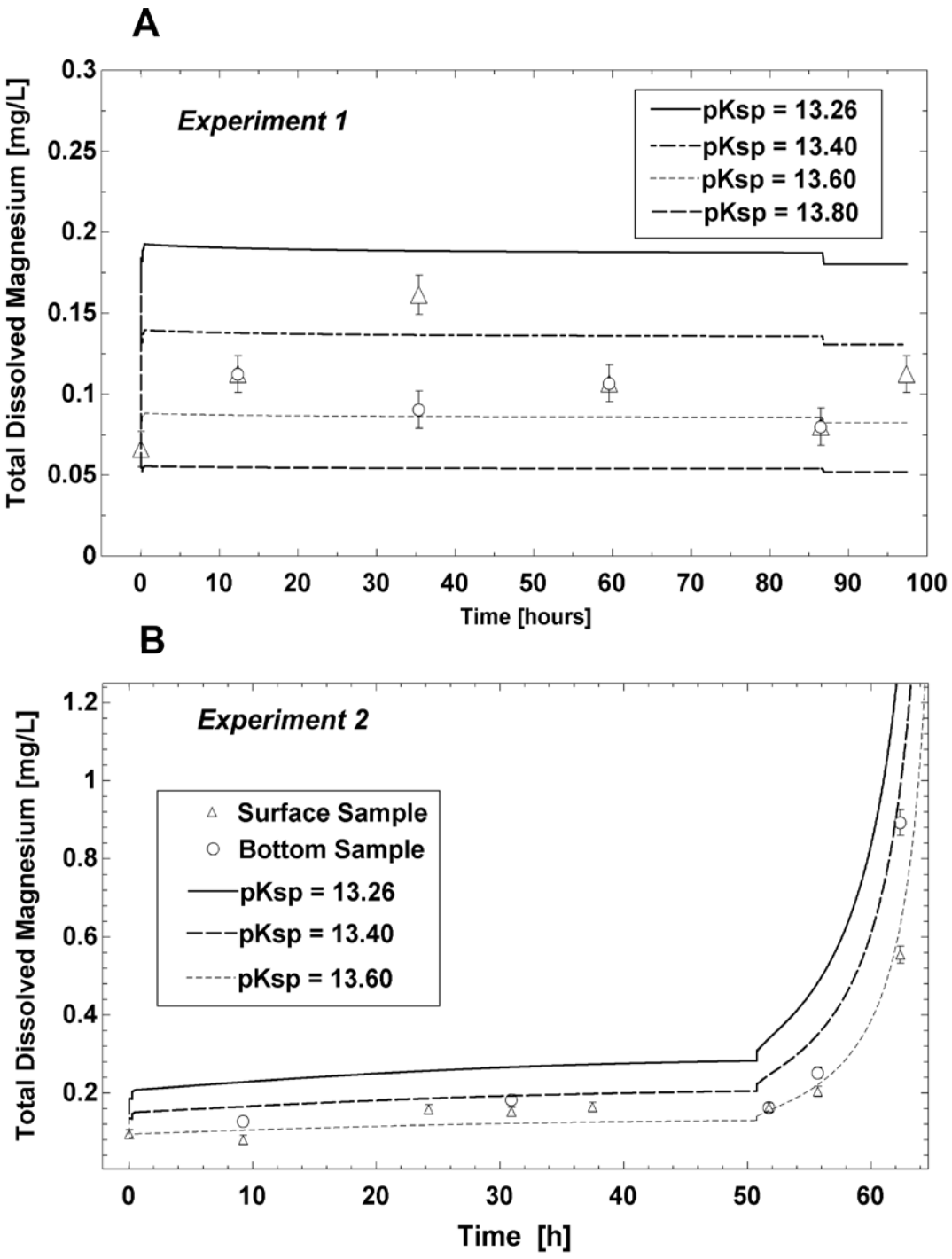

Figure 6.28 – Adjustment of constant solubility product of struvite ($pKsp$) to improve validation at low Mg concentration in $Expt.1$ and $Expt.2$.

Figure 6.28 showed that over-prediction in the elemental concentration of Mg can be corrected by decreasing the pK_{sp} value. Even though, it is small the impact in the overall mass balance of the reactor, this approach could improve the selection of the struvite solubility constant in high ionic strength solutions such as this case.

The pK_{sp} of 13.26 was considered from Ohlinger et al. (Ohlinger et al., 1998), however this process was performed at also considered low ionic strength solution in the range of 0.1 mol/L. This work used nutrient solutions at ionic strength larger than 0.30 mol/L.

6.3.6 Counting of particles and mass balance with coulter

Particle counting with Coulter suggested similar value from samples in $Expt.2$, while larger variability of samples from $Expt.1$ (Figure 6.29.A). Section 6.3.3 explained that larger particles were likely to provide a more reliable data. Smaller size particles could not be detected since they lied within the reading noise range occupy the size range that is subject to noise effects. In each measurement different minimum bin size with data was recorded, which also makes more difficult the comparison between samples in $Expt.1$ and $Expt.2$.

The mean weight size and the overall counting of particles was used to estimate the mass of sample entering to the Coulter (Figure 6.29.B). This assessment was developed by suspending a known quantity of solid sample in the 200-mL Coulter beaker. This sample was measured several times, with continuous additions of saturated solution until the liquid becomes visually transparent. Figure 6.29.B showed that that the estimated mass approaches to the expected mass of struvite in $Expt.2$; however, underprediction of more than 50 % of the sample mass suggested that this assessment was not successfully developed due to the presence of particles smaller than the noise threshold.

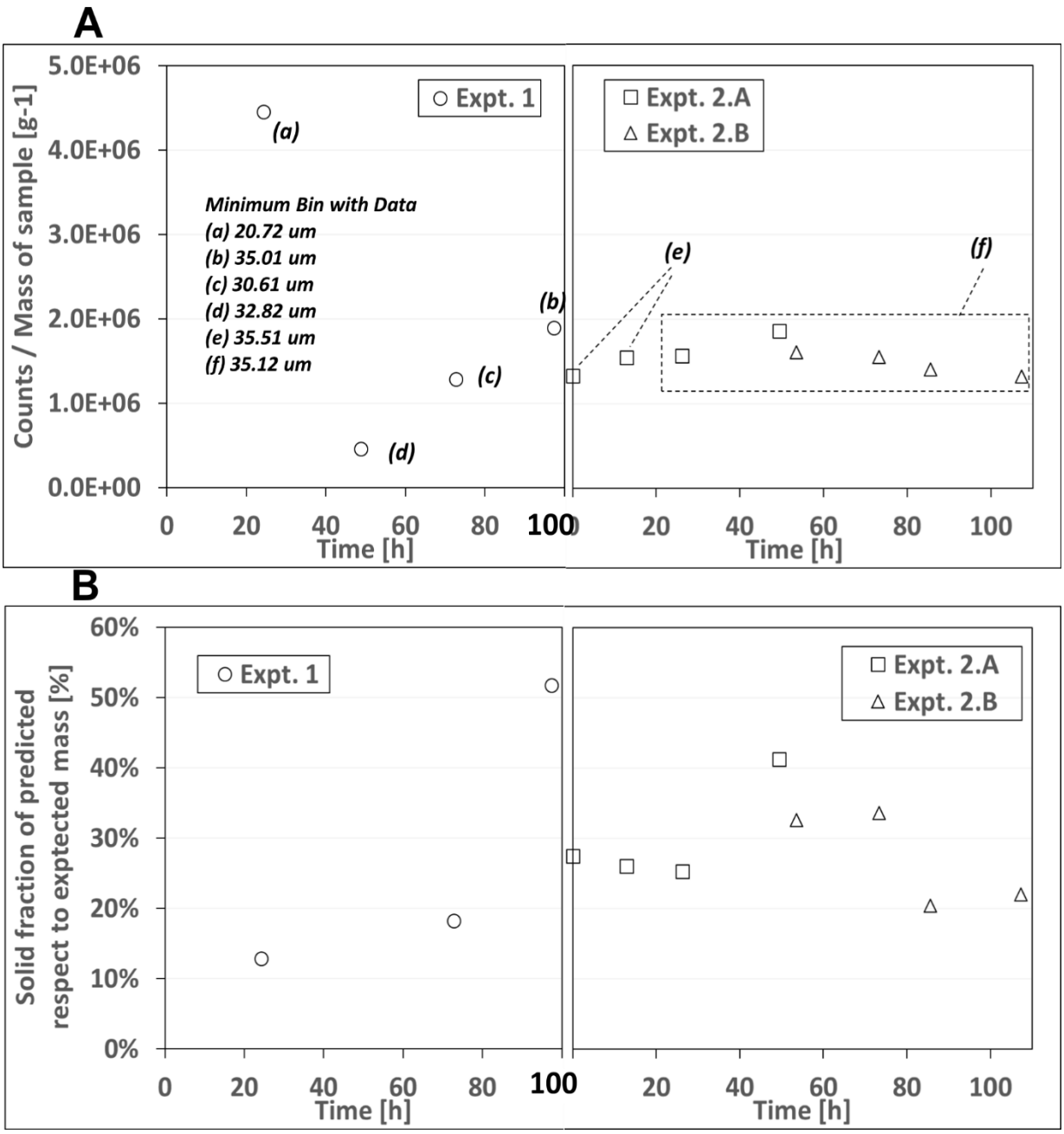

Figure 6.29 – Quantity of particle counts per mass of solid sample used in electric sensing zone measurement (A), and processed solid fraction estimated as the percentage of solid mass predicted with Coulter data and initial mass of struvite dissolved in the beaker sample (B).

6.4 Summary

- Two continuous experiments were performed at the same hydraulic residence time (0.3 L/h in the filtered concentrated synthetic ureolysed urine and 0.3 L/h in the Mg source solution. The fist

experiment was performed at Mg/P = 0.34, while the second was performed in the first part using Mg/P = 0.64 and in the last part a Mg/P = 1.29

- Processing variables, such as flow rates, pH, conductivity, mixing and struvite bed height were recorded and visually monitored
- Liquid and solid samples were taken from different points of the reactor to determine validity of the dynamic model discussed in previous chapters
- Solid sample characterisation focused on morphology (microscopy), elemental composition (Mg and P), mean weight size and X-ray diffraction patterns
- Dynamic model simulations predicted the elemental concentration of Mg and P concentration in the liquid phase, struvite mass, but they could not predict the mean particle size
- The two-zones model was able to predict the behaviour in the struvite saturation index in the upper zone of the reactor when Mg/P was increased
- Application of electric zone was limited by the presence of particles smaller than the noise and the presence of aggregates.

7 Conclusions and Recommendations

Highlights:

- *Overall comments linked to the objectives of the thesis are presented.*
- *Conclusions of this work are presented classified by chapters*
- *Recommendation are suggested for future work*

7.1 Thesis objectives

Overall objectives of the thesis were introduced in § 1.4 of this thesis.

i. Develop a dynamic model to predict nutrient recovery rate at arbitrary operating conditions.

ii. Sensitivity analysis of variables in a continuous process to select suitable operating conditions.

iii. Evaluation of kinetic parameters from experimental data.

iv. Validation of model against an independent process data.

7.2 Conclusions

Conclusions were discussed based on every objective formulated in § 7.1

7.2.1 Conclusions for Objective 1: "Develop a dynamic model to predict nutrient recovery rate at arbitrary operating conditions"

This objective was studied in Chapters 2, 3 and 4.

a) **Chapter 2.** This chapter provided the model formulation step by step.

- A dynamic model comprising mass balance, thermodynamics and kinetics described struvite precipitation in batch, fed-batch and continuous operating modes.

- The thermodynamics was modelled through a set of equilibrium equations to estimate struvite saturation index.
- The kinetics was modelled as a power-law rate equation. This equation is a function of the saturation index.
- Struvite mass transfer depended on the available surface area and the length rate of change.
- A model containing thermodynamics and mass balance can predict saturation index at non-equilibrium conditions and struvite mass formation at equilibrium conditions.

b) **Chapter 3.** This chapter applied the model from Chapter 2 through simulations.

- Model predictions of struvite precipitation in batch reactors from previous studies.
- A sensitivity analysis in the prediction of struvite saturation index demonstrated that the system could represented by 11 equilibria, instead of 27 (Appendix. A1)
- Simulations in $PHREEQC$ and $gPROMS$ software mathematically verified the model in EES.
- The dynamic model can design fed-batch and continuous experiments.
- Design of fed-batch systems through simulations can ensure the presence of only struvite.
- Dynamic simulations suggested the application of larger quantity of seeds with small particle size to minimise saturation index, and therefore nucleation.
- Simulations showed that maximum struvite precipitation rate can be achieved at Mg/P feed molar ratio equal to one. Application of larger Mg/P feed molar ratios larger than one do not offer advantage in the overall struvite production.

7.2.2 Conclusion for Objective 2: "Sensitivity analysis of variables in a continuous process to select suitable operating conditions"

This objective was studied in Chapters 4 and 5.

a) **Chapter 4.** Experimental data was collected in this chapter through batch experiments.

- Batch experiments showed that pH is not a relevant variable to be monitored in nutrient recovery from source separated urine, since pH buffering in urine is very strong, so pH does not change with changes in struvite solubility state.
- Mass balance of P and Mg confirmed that spectrophotometric and atomic absorption spectroscopy were suitable methodologies to assess struvite precipitation.
- Analytical methodologies should be assessed before experimentation to avoid interferences in complex solutions like urine.
- Experimental validation in batch precipitation experiments at different Mg/P feed molar ratios demonstrated the capacity of the model and the precision of experimental analysis.
- Preparation of standards using complex solutions showed that no interference could be detected in P analysis by spectrophotometry. A wavelength of 420 nm was chosen for the purpose based on linearity up to 30 $mg\ P/L$.
- Determination of NH_3 as N by Salicylate method was applied to determine struvite purity in the solid. Reaction time and solution pH had effect in the absorbance. On the other hand, the presence of P and application of different UV treatment did not have an effect in the absorbance.
- Analysis of $NH_3 - N$ in solid samples to determine purity of struvite has to be developed cautiously. Propagation of uncertainty was used as a tool to determine possible error sources.

b) **Chapter 5.** This chapter assessed diverse process variables through simulations.

- Struvite production rate in continuous nutrient recovery from urine source is highly sensitive to Mg/P feed molar ratio
- Struvite saturation index is sensitive to the available surface area (struvite seed mass) and the chosen Mg/P feed molar ratio.
- Dynamic simulations showed that higher struvite precipitation can be achieved by decreasing the hydraulic residence time (HRT). However, that scenario does not preclude the possibility of excessive nucleation.

- Continuous struvite precipitation can be achieved at larger HRT and large struvite seed quantities.
- Deviations of +/- 1 L/h in the intermixing flow rate of 4 L/h (estimated in Chapter 4) produced small differences in the P and Mg concentration in the upper zone of the reactor.
- The specific surface area available within the reactor was affected by the initial particle size of the struvite seeds.
- Dynamic model can determine the same struvite saturation index profile by considering different quantity of seeds within the reactor.
- The dynamic model can design harvesting procedures of product crystal during long processing campaigns.

7.2.3 Conclusions for Objective 3: "Evaluation of kinetic parameters from experimental data"

This objective was studied in Chapter 5.

- This chapter demonstrated that continuous nutrient recovery from urine source using large quantity of seeds is insensitive to kinetic parameters. The continuous struvite precipitation is controlled by thermodynamics when available surface area within the reactor is large. Therefore, kinetic parameters were not estimated in continuous struvite precipitation.
- After assessing suitable operating conditions in continuous experiments, such as Mg/P feed molar ratio, hydraulic residence time and struvite mass, the kinetic parameters for the power-law kinetic model were k = 1e-6 m/h and n = 1.

7.2.4 Objective 4: "Validation of model against an independent process data"

This objective was studied in Chapter 4 and 6.

a) Chapter 4. This chapter collected data for model validation using batch experiments.

- Prediction of P, Mg and struvite mass at equilibrium were validated against different batch experiment at Mg/P feed molar ratio from 0.3 to 1.6.

- Tracer studies in the continuous reactor showed that a two-zone reactor model was able to represent the system's mixing behaviour. A 12-L reactor with mixers at 150 RPM and 0.6 L/h total feed flow rate requires an intermixing flow rate of 4 L/h to describe liquid concentration in the upper and bottom reactor zones.

b) Chapter 6. Continuous experiments were performed to validate the dynamic model.

- Continuous struvite precipitation using urine source and large struvite seed mass was operated at close-to-equilibrium conditions. In this case, model predictions are insensitive to the kinetic parameters.
- Struvite mass was predicted, but agreement between model and experimental data was constrained by the methodology to quantify struvite suspended in solution.
- The model cannot be validated through prediction of mean struvite size. The dynamic model predicts the struvite precipitation in the continuous reactor, but it is not suitable to predict the mean weight size of particles. The mean weight size was used as an approach to assess a polydisperse as a monodisperse particle distribution.
- Solid characterisation of samples with X-ray diffraction and elemental composition (P and Mg) showed the presence of only struvite. The presence of magnesite was suggested, due to positive saturation index, but it could not be detected in the analysis.
- Temperature compensation is key in pH and conductivity measurement over long experimental campaigns to track the changes in the liquid phase. Measurement of pH and conductivity at 25°C in $Expt.1$ (Mg/P = 0.34) follow a similar behaviour suggested by the model. On the other hand, pH and conductivity measurements at 25 °C in $Expt.2$ (Mg/P = 0.64 and Mg/P = 1.29) did not show the same behaviour as the model predicted. This means that predicting pH and conductivity with the dynamic model still needs to be reviewed in future work.
- Increase of the Mg source concentration can be observed in conductivity data in the same reactor operation campaign

- Mixer agitation speed has to be increased when struvite production rate increases due to larger concentration of Mg in the feed. Experimental data for this reactor configuration showed at least an increase of 20 RPM is necessary when continuous precipitation is run at Mg/P = 1.29 with approximately 400 g of struvite within the reactor.
- Nucleation and aggregation was observed in $Expt.1$ and $Expt.2$. Some aggregates in continuous experiments can surpass the 100 μm, while individual particle size did not surpass this size according to microscopy.
- The two-well-mixed-zone model was suitable to predict changes in the struvite saturation index due to changes in the Mg/P feed molar ratio. Predictions validated the presence of struvite particles in the upper liquid with microscopy and photos.
- A constant solubility product for struvite of 13.60 was suggested instead of pK_{sp} of 13.26 based on modelling predictions of limiting Mg concentration in the liquid phase.

7.3 Recommendations for further work

This section identifies challenges in the development of our understanding of continuous struvite precipitation. Recommendations involve both modelling and experimental approaches.

7.3.1 Recommendations in modelling work

- This work only applied a two-zone reactor model. However, following research could consider the modelling of more than two zones in the reactor.
- Computational fluid dynamics was out of scope of this thesis, but its inclusion could improve the understanding of mixing, intermixing and it could suggest a better reactor design to avoid high saturation index zones.
- This work employed the approximation of crystal size as the equivalent of sphere diameter. Following studies could consider a different particle modelling of struvite crystals.

- Modelling of real urine solutions could include a more complex thermodynamics, considering Ca and other elements.
- Modelling of carbonate chemistry in open systems could be studied to improve model predictions.
- Future works could consider the inclusion of more competing ions in the formulation of synthetic ureolysed urine to study its effect in the model development and solid phase composition.

7.3.2 Recommendations in analytical development

- Development of a methodology to measure pH in solutions at high ionic strength, such as urine.
- Implementation of mass balance in the sample using Coulter. Application of a sample with larger size or measurements with smaller aperture tube is suggested.
- Implementation of the indirect mass methodology through density is necessary for following studies.
- Automatic microscopy photos with *Macros* in $ImageJ$ software could provide larger quantity of data in regards to the particle size distribution.
- Comparison of laser diffraction, electric sensing zone and microscopy could be considered for further studies in nutrient recovery.

7.3.3 Recommendation in experimental validation

- Tracer studies should be developed with different quantity of struvite seeds within the reactor to determine experimental intermixing flow rates.
- The inclusion of population balance modelling in the kinetics could provide a better estimation of the mean particle size in continuous experiments.
- The reactor could be automatically monitored by connecting the conductivity to feeding flow rates in the pumps.

- Kinetic parameters could be evaluated in reactor with negligible or small quantity of seeds.
- Light scattering should be considered as a non-invasive methodology to determine quantity of particles within the reactor at different heights in the suspension.

7.3.4 Future approaches in reactor design

- The dynamic model employed in this mixed batch-continuous mode reactor could also be adjusted and applied for other type of reactor configurations such as fluidised bed or air agitated reactors.
- This continuous reactor could include an additional, previous continuous process reactor where struvite seeds are prepared, then fed to the recovery reactor.
- Implementation of other types of mixing are suggested in scaled-up reactors.
- Locations of the feeding points of the nutrient and Mg source should be investigated.

8 Bibliography

Abbona, F., & Boistelle, R. (1985). Nucleation of Struvite (MgNH4PO4.6H2O) Single Crystals and Aggregates. *Crystal Research and Technology*, *20*(2), 133–140.

Agilent. (2017). Flame Atomic Absorption Spectrometry: Analytical Methods, 124.

Ali, M I, & Schneider, P. A. P. A. (2008). An approach of estimating struvite growth kinetic incorporating thermodynamic and solution chemistry, kinetic and process description. *Chemical Engineering Science*, *63*(13), 3514–3525.

Ali, Md. I., & Schneider, P. A. P. A. (2006). A fed-batch design approach of struvite system in controlled supersaturation. *Chemical Engineering Science*, *61*(12), 3951–3961. https://doi.org/10.1016/j.ces.2006.01.028

Antonin, V. S., Santos, M. C., Garcia-Segura, S., & Brillas, E. (2015). Electrochemical incineration of the antibiotic ciprofloxacin in sulfate medium and synthetic urine matrix. *Water Research*, *83*, 31–41. https://doi.org/10.1016/j.watres.2015.05.066

APHA. (1999). *Standard Methods for the Examination of Water and Wastewater-Part 1000 Standard Methods for the Examination of Water and Wastewater*. (American Public Health Association, Ed.).

Ariyanto, E., Sen, T. K., & Ang, H. M. (2014). The influence of various physico-chemical process parameters on kinetics and growth mechanism of struvite crystallisation. *Advanced Powder Technology*, *25*(2), 682–694.

Ashley, K., Cordell, D., & Mavinic, D. (2011). A brief history of phosphorus: from the philosopher's stone to nutrient recovery and reuse. *Chemosphere*, *84*(6), 737–746.

Babić-Ivancić, V., Kontrec, J., Brecević, L., & Kralj, D. (2006). Kinetics of struvite to newberyite transformation in the precipitation system MgCl2-NH4H2PO4NaOH-H2O. *Water Research*, *40*(18),

3447–3455.

Barbosa, S. G., Peixoto, L., Meulman, B., Alves, M. M., & Pereira, M. A. (2016). A design of experiments to assess phosphorous removal and crystal properties in struvite precipitation of source separated urine using different Mg sources. *Chemical Engineering Journal*, *298*, 146–153. https://doi.org/10.1016/j.cej.2016.03.148

Battistoni, P., Paci, B., Fatone, F., & Pavan, P. (2005). Phosphorus Removal from Supernatants at Low Concentration Using Packed and Fluidized-Bed Reactors. *Industrial & Engineering Chemistry Research*, *44*, 6701–6707.

Battistoni, Paci, B., Fatone, F., & Pavan, P. (2006). Phosphorus Removal from Anaerobic Supernatants: Start-Up and Steady-State Conditions of a Fluidized Bed Reactor Full-Scale Plant. *Industrial & Engineering Chemistry Research*, *45*(2), 663–669.

Bolleter, W. T., Bushman, C. J., & Tidwell, P. W. (1961). Spectrophotometric Determination of Ammonia as Indophenol. *Analytical Chemistry*, *33*(4), 592–594. https://doi.org/10.1021/ac60172a034

Bramley, A. S., Hounslow, M. J., & Ryall, R. L. (1997). Aggregation during precipitation from solution. Kinetics for calcium oxalate monohydrate. *Chemical Engineering Science*, *52*(5), 747–757. https://doi.org/10.1016/S0009-2509(96)00447-2

Bromley, L. A. (1974). Thermodynamic Properties of Strong Electrolytes in Aqueous Solutions. *AIChE Journal*, *19*(2), 313–320.

Burns, M., Natividad Marin, L., & Schneider, P. A. (2016). Investigations of a continuous Poiseuille flow struvite seed crystallizer - Mixer performance and aggregate disruption by sonication. *Chemical Engineering Journal*, *295*. https://doi.org/10.1016/j.cej.2016.03.061

Burns, M. W. (2017). Kinetic Investigations of Struvite Crystallisation in Poiseuille Flow Using Discretised Population Balance Methods, (July). Retrieved from https://researchonline.jcu.edu.au/52364/

Cordell, D., Drangert, J., & White, S. (2009). The story of phosphorus : Global food security and food for thought. *Global Environmental Change Journal*, *19*, 292–305.

Crutchik, D., Morales, N., Vázquez-Padín, J. R., & Garrido, J. M. (2017). Enhancement of struvite pellets crystallization in a full-scale plant using an industrial grade magnesium product. *Water Science and Technology*, *75*(3), 609–618. https://doi.org/10.2166/wst.2016.527

Dai, J., Tang, W. T., Zheng, Y. S., Mackey, H. R., Chui, H. K., van Loosdrecht, M. C. M., & Chen, G. H. (2014). An exploratory study on seawater-catalysed urine phosphorus recovery (SUPR). *Water Research*, *66*, 75–84. https://doi.org/10.1016/j.watres.2014.08.008

Doyle, J. D., & Parsons, S. A. (2002). Struvite formation, control and recovery. *Water Research*, *36*(16), 3925–3940.

Fevotte, G., Gherras, N., & Moutte, J. (2013). Batch cooling solution crystallization of ammonium oxalate in the presence of impurities: Study of solubility, supersaturation, and steady-state inhibition. *Crystal Growth and Design*, *13*(7), 2737–2748. https://doi.org/10.1021/cg301737s

Fogler, S. (1999). *Elements of Chemical Reaction Engineering* (Third Edit). Prentice-Hall.

Gadekar, S., & Pullammanappallil, P. (2009). Validation and Applications of a Chemical Equilibrium Model for Struvite Precipitation. *Environmental Modeling & Assessment*, *15*(3), 201–209.

Galbraith, S. C. (2011). *A study of struvite nucleation, crystal growth and aggregation*.

Galbraith, S. C., & Schneider, P. A. (2014). Modelling and simulation of inorganic precipitation with nucleation, crystal growth and aggregation: A new approach to an old method. *Chemical Engineering Journal*, *240*, 124–132. https://doi.org/10.1016/j.cej.2013.11.070

Galbraith, S. C., Schneider, P. A., & Flood, A. E. (2014). Model-driven experimental evaluation of struvite nucleation, growth and aggregation kinetics. *Water Research*, *56C*, 122–132. https://doi.org/10.1016/j.watres.2014.03.002

Golubev, S. V, Pokrovsky, O. S., & Savenko, V. S. (2001). Homogeneous precipitation of magnesium phosphates from seawater solutions. *Journal of Crystal Growth*, *223*, 550–556.

Grau, M. G. P., Rhoton, S. L., Brouckaert, C. J., & Buckley1, C. a. (2012). Evaluation of an automated struvite reactor to recover phosphorus from source-separated urine collected at urine diversion toilets in eThekwini. *Water SA*, *41*(3), 383–389.

Griffith, D. P., Musher, D. M., & Itin, C. (1976). The Primary Cause of Infection-Induced Urinary Systems. *Investigative Urology*, *13*(5).

Harada, H., Shimizu, Y., Miyagoshi, Y., Matsui, S., Matsuda, T., & Nagasaka, T. (2006). Predicting struvite formation for phosphorus recovery from human urine using an equilibrium model. *Water Science and Technology*, *54*(8), 247–255. https://doi.org/10.2166/wst.2006.720

Harrison, M. L., Johns, M. R., White, E. T., & Mehta, C. M. (2011). Growth Rate Kinetics for Struvite Crystallisation. *Chemical Engineering Transactions*, *25*, 309–314.

Ipe, D. S., & Ulett, G. C. (2016). Evaluation of the in vitro growth of urinary tract infection-causing gram-negative and gram-positive bacteria in a proposed synthetic human urine (SHU) medium. *Journal of Microbiological Methods*, *127*, 164–171. https://doi.org/10.1016/j.mimet.2016.06.013

Jones, A. G. (2002). *Crystallization Process Systems* (First). London: Heinemann, Butterworth.

Jönsson, H., Stenström, T. A., Svensson, J., & Sundin, A. (1997). Source separated urine-nutrient and heavy metal content, water saving and faecal contamination. *Water Science and Technology*, *35*(9), 145–152. https://doi.org/10.1016/S0273-1223(97)00192-3

Kabore, S., Ito, R., & Funamizu, N. (2016). Reaction kinetics for the production of methylene urea from synthetic human urine. *Journal of Environmental Chemical Engineering*, *4*(2), 2510–2517. https://doi.org/10.1016/j.jece.2016.04.028

Kazadi Mbamba, C., Batstone, D. J., Flores-Alsina, X., & Tait, S. (2015). A generalised chemical precipitation

modelling approach in wastewater treatment applied to calcite. *Water Research*, *68*, 342–353. https://doi.org/10.1016/j.watres.2014.10.011

Kazadi Mbamba, C., Tait, S., Flores-Alsina, X., & Batstone, D. J. (2015). A systematic study of multiple minerals precipitation modelling in wastewater treatment. *Water Research*, *85*, 359–370. https://doi.org/10.1016/j.watres.2015.08.041

Kirchmann, H., & Petterson, S. (1995). Human urine - Chemical composition and fertilizer use efficiency. *Fertilizer Research*, *40*, 149–154.

Klein, S., & Alvarado, F. (2002). Engineering equation solver. *F-Chart Software, Box*.

Koralewska, J., Piotrowski, K., Wierzbowska, B., & Matynia, A. (2009). Kinetics of Reaction-Crystallization of Struvite in the Continuous Draft Tube Magma Type Crystallizers-Influence of Different Internal Hydrodynamics. *Chinese Journal of Chemical Engineering*, *17*(2), 330–339. https://doi.org/10.1016/S1004-9541(08)60212-8

Lane, G. L., & Koh, P. T. . (1997). CFD Simulation of a Rushton Turbine in a Baffled Tank. *International Conference on CFD in Mineral and Metal Processing and Power Generation*.

Laridi, R., Auclair, J. C., & Benmoussa, H. (2005). Laboratory and pilot-scale phosphate and ammonium removal by controlled struvite precipitation following coagulation and flocculation of swine wastewater. *Environmental Technology*, *26*(5), 525–536. https://doi.org/10.1080/09593332608618533

Le Corre, K. S., Valsami-Jones, E., Hobbs, P., & Parsons, S. A. (2007). Kinetics of Struvite Precipitation: Effect of the Magnesium Dose on Induction Times and Precipitation Rates. *Environmental Technology*, *28*(12), 1317–1324.

Lee, S. I., Weon, S. Y., Lee, C. W., & Koopman, B. (2003). Removal of nitrogen and phosphate from wastewater by addition of bittern. *Chemosphere*, *51*(4), 265–271. https://doi.org/10.1016/S0045-6535(02)00807-X

Liu, B., Giannis, A., Zhang, J., Chang, V. W.-C., & Wang, J.-Y. (2013). Characterization of induced struvite formation from source-separated urine using seawater and brine as magnesium sources. *Chemosphere*, *93*(11), 2738–2747.

Liu, Z., Zhao, Q., Wang, K., Lee, D., Qiu, W., & Wang, J. (2008). Urea hydrolysis and recovery of nitrogen and phosphorous as MAP from stale human urine. *Journal of Environmental Sciences*, *20*(8), 1018–1024. https://doi.org/10.1016/S1001-0742(08)62202-0

McCabe, W. L., Smith, J. C., & Harriot, P. (1993). *Unit Operations of Chemical Engineering* (Fifth Edit). New York: McGraw Hill Book Company, INC.

McCleskey, R. B., Nordstrom, D. K., Ryan, J. N., & Ball, J. W. (2012). A new method of calculating electrical conductivity with applications to natural waters. *Geochimica et Cosmochimica Acta*, *77*(January), 369–382. https://doi.org/10.1016/j.gca.2011.10.031

Mehta, C. M., & Batstone, D. J. (2013). Nucleation and growth kinetics of struvite crystallization. *Water Research*, *47*(8), 2890–2900. https://doi.org/10.1016/j.watres.2013.03.007

Moffett, J. H. (1995). Determination of magnesium , calcium and potassium in brines by flame AAS using the SIPS-10 accessory for automated calibration and on-line sample dilution. Agilent Technologies.

Mullin, J. W. (2001). Crystallization. https://doi.org/10.1002/0471238961.0318251918152119.a01.pub3

Münch, E. V, & Barr, K. (2001). Controlled struvite crystallisation for removing phosphorus from anaerobic digester sidestreams. *Water Research*, *35*(1), 151–159.

Musvoto, E. V., Wentzel, M. C., & Ekama, G. A. (2000). Integrated chemical-physical processes modelling - II. Simulating aeration treatment of anaerobic digester supernatants. *Water Research*, *34*(6), 1868–1880. https://doi.org/10.1016/S0043-1354(99)00335-8

Nelson, N. O., Mikkelsen, R. L., & Hesterberg, D. L. (2003). Struvite precipitation in anaerobic swine lagoon liquid: effect of pH and Mg:P ratio and determination of rate constant. *Bioresource Technology*,

89(3), 229–236.

Nordstrom, D. K., Plummer, L. N., Langmuir, D., Busenberg, E., May, H. M., Jones, B. F., & Parkhurst, D. L. (1990). Revised Chemical Equilibrium Data for Major Water-Mineral Reactions and Their Limitations. In D. C. Melchior & R. L. Bassett (Eds.), *Chemical modeling of aqueous systems II: American Chemical Society Symposium series 416* (pp. 399–413). Washington, DC, USA: American Chemical Society.

Ohlinger, K. N., Young, T. M., & Schroeder, E. D. (2000). Postdigestion struvite precipitation using a fluidized bed reactor. *Journal of Environmental Engineering*, *126*(4), 361–368.

Ohlinger, Young, & Schroeder. (1998). Predicting struvite formation in digestion. *Water Research*, *32*(12), 3607–3614.

Pastor, L., Mangin, D., Barat, R., & Seco, A. (2008). A pilot-scale study of struvite precipitation in a stirred tank reactor : Conditions influencing the process. *Bioresource Technology*, *99*, 6285–6291.

Rahaman, M S, Ellis, N., & Mavinic, D. S. (2008). Effects of Various Process Parameters on Struvite Precipitation. *Water Science and Technology*, *57*(5), 647–654. https://doi.org/10.2166/wst.2008.022

Rahaman, Md Saifur, Mavinic, D. S., Meikleham, A., & Ellis, N. (2014). Modeling phosphorus removal and recovery from anaerobic digester supernatant through struvite crystallization in a fluidized bed reactor. *Water Research*, *51*, 1–10. https://doi.org/10.1016/j.watres.2013.11.048

Roncal-Herrero, T., & Oelkers, E. H. (2011). Experimental determination of struvite dissolution and precipitation rates as a function of pH. *Applied Geochemistry*, *26*(5), 921–928. https://doi.org/10.1016/j.apgeochem.2011.03.002

Ronteltap, M., Maurer, M., & Gujer, W. (2007). Struvite precipitation thermodynamics in source-separated urine. *Water Research*, *41*(5), 977–984.

Ronteltap, M., Maurer, M., Hausherr, R., & Gujer, W. (2010). Struvite precipitation from urine - Influencing

factors on particle size. *Water Research*, *44*(6), 2038–2046.

Sakthivel, S. R., Tilley, E., & Udert, K. M. (2012). Wood ash as a magnesium source for phosphorus recovery from source-separated urine. *The Science of the Total Environment*, *419*, 68–75.

Samson, E., Lemaire, G., Marchand, J., & Beaudoin, J. J. (1999). Modeling chemical activity effects in strong ionic solutions. *Computing Materials Science*, *15*, 285–294.

Schneider, Wallace, & Tickle. (2013). Modelling and dynamic simulation of struvite precipitation from source-separated urine. *Water Science and Technology*, *67*(12), 2724–2732.

Shimamura, K., Hirasawa, I., Ishikawa, H., & Tanaka, T. (2006). Phosphorus Recovery in a Fluidized Bed Crystallization Reactor. *Journal of Chemical Engineering of Japan*, *39*(10), 1119–1127.

Shu, L., Schneider, P., Jegatheesan, V., & Johnson, J. (2006). An economic evaluation of phosphorus recovery as struvite from digester supernatant. *Bioresource Technology*, *97*, 2211–2216.

Skoog, D. A., Holler, J. F., & Crouch, S. (2006). *Principles of Instrumental Analysis* (6th Editio). Cengage Learning.

Snoeyink, V. L., & Jenkins, D. (1980). *Water Chemistry*. (J. W. and Sons, Ed.) (First Edit). New York: Wiley, John & Sons.

Sohnel, O., & Garside, J. (1992). *Precipitation: Basic principles and industrial applications*. *Science And Technology*. Butterworth Heinemann.

Suzuki, K., Tanaka, Y., Kuroda, K., Hanajima, D., Fukumoto, Y., Yasuda, T., & Waki, M. (2007). Removal and recovery of phosphorous from swine wastewater by demonstration crystallization reactor and struvite accumulation device. *Bioresource Technology*, *98*(8), 1573–1578. https://doi.org/10.1016/j.biortech.2006.06.008

Tarragó, E., Puig, S., Ruscalleda, M., Balaguer, M. D., & Colprim, J. (2016). Controlling struvite particles' size using the up-flow velocity. *Chemical Engineering Journal*, *302*, 819–827.

https://doi.org/10.1016/j.cej.2016.06.036

Taylor, B. N., & Kuyatt, C. E. (1994). Guidelines for evaluating and expressing the uncertainty of NIST measurement results, Gaithersburg, MD, U.S. Departmente of Commerce, Technology Administration, National Institute of Standards and Technology.

Tilley, E., Atwater, J., & Mavinic, D. (2008a). Effects of Storage on Phosphorus Recovery From Urine. *Environmental Technology*, *29*(7), 807–816. https://doi.org/10.1080/09593330801987145

Tilley, E., Atwater, J., & Mavinic, D. (2008b). Recovery of struvite from stored human urine. *Environmental Technology*, *29*(7), 797–806. https://doi.org/10.1080/09593330801987129

Triger, A., Pic, J.-S., & Cabassud, C. (2012). Determination of struvite crystallization mechanisms in urine using turbidity measurement. *Water Research*, *46*(18), 6084–6094.

Türker, M., & Celen, I. (2007). Removal of ammonia as struvite from anaerobic digester effluents and recycling of magnesium and phosphate. *Bioresource Technology*, *98*(8), 1529–1534.

Udert, K. M., Larsen, T. A., & Gujer, W. (2006). Fate of major compounds in source-separated urine. *Water Science and Technology*, *54*(11–12), 413–420. https://doi.org/10.2166/wst.2006.921

Udert, K M, & Wächter, M. (2012). Complete nutrient recovery from source-separated urine by nitrification and distillation. *Water Research*, *46*(2), 453–464. https://doi.org/10.1016/j.watres.2011.11.020

Udert, Kai M, Larsen, T. a, & Gujer, W. (2003). Estimating the precipitation potential in urine-collecting systems. *Water Research*, *37*(11), 2667–2677.

United States EPA. (1998). *MINTEQA2/PRODEFA2, A Geochemical Assessment Model for Environmental Systems: User Manual Supplement for Version 4.0*. U.S. Enviromental Protection Agency.

Verdouw, H., Van Echteld, C. J. A., & Dekkers, E. M. J. (1978). Ammonia determination based on indophenol formation with sodium salicylate. *Water Research*, *12*(6), 399–402.

https://doi.org/10.1016/0043-1354(78)90107-0

von Munch, E., & Barr, K. (2001). Controlled struvite crystallization for removing phosphorus from anaerobic digester side stream. *Water Research*, *35*(1), 151–159.

Wilsenach, J. a, Schuurbiers, C. a H., & van Loosdrecht, M. C. M. (2007). Phosphate and potassium recovery from source separated urine through struvite precipitation. *Water Research*, *41*(2), 458–466.

Xu, K., Li, J., Zheng, M., Zhang, C., Xie, T., & Wang, C. (2015). The precipitation of magnesium potassium phosphate hexahydrate for P and K recovery from synthetic urine. *Water Research*, *80*, 71–79. https://doi.org/10.1016/j.watres.2015.05.026

Zamora, P., Georgieva, T., Salcedo, I., Elzinga, N., Kuntke, P., & Buisman, C. J. N. (2017). Long-term operation of a pilot-scale reactor for phosphorus recovery as struvite from source-separated urine. *Journal of Chemical Technology and Biotechnology*, *92*(5), 1035–1045. https://doi.org/10.1002/jctb.5079

Zhang, T., Li, Q., Ding, L., Ren, H., Xu, K., Wu, Y., & Sheng, D. (2011). Modeling assessment for ammonium nitrogen recovery from wastewater by chemical precipitation. *Journal of Environmental Sciences*, *23*(6), 881–890. https://doi.org/10.1016/S1001-0742(10)60485-8

Appendix A Thermodynamic Database

A.1. Liquid Phase Thermodynamics

Table 0.1 — Thermodynamic equilibria and their equations

Equations (T = 25°C, μ = 0)	pK	References
$H_2O = H^+ + OH^-$	14	(Kai M Udert et al., 2003)
$NH_4^+ = NH_3 + H^+$	9.24	(Kai M Udert et al., 2003)
$MgOH^+ = OH^- + Mg^{2+}$	2.560	(Ohlinger et al., 1998)
$NaOH + H^+ = Na^+ + H2O$	-14.18	(Nordstrom et al., 1990)
$KOH + H^+ = K^+ + H2O$	-14.46	(Nordstrom et al., 1990)
$HPO_4^{2-} = PO_4^{3-} + H^+$	12.35	(Kai M Udert et al., 2003)
$H_2PO_4^- = HPO_4^{2-} + H^+$	7.21	(Kai M Udert et al., 2003)
$H_3PO_4 = H_2PO_4^- + H^+$	2.15	(Ohlinger et al., 1998)
$NaH_2PO_4 = Na^+ + H_2PO_4^-$	0.25	(Kai M Udert et al., 2003)
$Na_2HPO_4 + H^+ = 2Na^+ + H_2PO_4^-$	-6.11	(Kai M Udert et al., 2003)
$NaHPO_4 + H^+ = Na^+ + H_2PO_4^-$	-6.01	(Kai M Udert et al., 2003)
$MgHPO_4 + H^+ = Mg^{2+} + H_2PO_4^-$	-4.3	(Kai M Udert et al., 2003)
$MgPO_4 + 2H^+ = Mg^{2+} + H_2PO_4^-$	-12.96	(Kai M Udert et al., 2003)
$MgH_2PO_4 = Mg^{2+} + H_2PO_4^-$	1.51	(Kai M Udert et al., 2003)
$NH_4H_2PO_4 = NH_4^+ + H_2PO_4^-$	0.10	(Kai M Udert et al., 2003)
$NH_4HPO_4 = NH_4 + HPO_4^{2-}$	1.30	(Kai M Udert et al., 2003)
$KH_2PO4 = K^+ + H_2PO_4^-$	0.23	(Kai M Udert et al., 2003)
$KHPO4^- + H^+ = K^+ + H_2PO_4^-$	-6.12	(Kai M Udert et al., 2003)
$H_2CO_3 = H^+ + HCO_3^-$	6.35	(Kai M Udert et al., 2003)
$HCO_3^- = CO_3^{2-} + H^+$	10.329	(Kai M Udert et al., 2003)
$NaHCO_3 = Na^+ + HCO_3^-$	- 0.25	(Kai M Udert et al., 2003)
$NaCO_3^- = Na^+ + CO_3^{2-}$	1.27	(Kai M Udert et al., 2003)
$MgHCO_3^+ = Mg^{2+} + HCO_3^-$	1.07	(Kai M Udert et al., 2003)
$MgCO_3 = Mg^{2+} + CO_3^{2-}$	2.98	(Nordstrom et al., 1990)
$NaSO_4^- = Na^+ + SO_4^{2-}$	0.70	(Nordstrom et al., 1990)
$MgSO_4 = Mg^{2+} + SO_4^{2-}$	2.37	(Nordstrom et al., 1990)
$NH_4SO_4^- = NH_4^+ + SO_4^{2-}$	1.03	(Kai M Udert et al., 2003)
$KSO_4^- = K^+ + SO_4^{2-}$	0.85	(Nordstrom et al., 1990)

Note: μ represents the ionic strength

A.2. Solid Phase Thermodynamics

Table 0.2 — Solubility constants of solid phases

Equations (T = 25 °C)	pKsp	References
Struvite: $MgNH_4PO_4.6H_2O\ (s) = Mg^{2+} + NH_4^+ + PO_4^{3-} + 6H_2O$	13.26	(Ohlinger et al., 1998)
Newberyite: $MgHPO_4.3H_2O\ (s) = Mg^{2+} + HPO4^{2-} + 3H_2O$	5.51	(Babić-Ivancić, Kontrec, Brecević, & Kralj, 2006)
Bobierite: $Mg_3(PO_4)_2.8H_2O\ (s) = 3Mg^{2+} + 2PO_4^{3-} + 8H_2O$	23.98	(Gadekar & Pullammanappallil, 2009)
Cattite: $Mg_3(PO_4)_2.22H_2O\ (s) = 3Mg^{2+} + 2PO_4^{3-} + 22H_2O$	22.89	
Dimagnesium phosphate: $MgHPO_4\ (s) = MgHPO_4$	0.15	
Brucite: $Mg(OH)_2.6H_2O = Mg^{2+} + 2OH^- + 6H_2O$	10.7	
Magnesium sodium phosphate hexahydrate (Na-struvite): $MgNaPO_4.6H_2O\ (s) = Mg^{2+} + Na^+ + PO_4^{3-} + 6H_2O$	11.60	(Xu et al., 2015)
Magnesium Potassium Phosphate Hexahydrate (K-struvite): $MgKPO_4.6H_2O\ (s) = Mg^{2+} + K^+ + PO_4^{3-} + 6H_2O$	12.20	
Magnesite: $MgCO_3(s) = Mg^{2+} + CO_3^{2-}$	7.37 (*)	(Musvoto, Wentzel, & Ekama, 2000)
Nesquehonite: $MgCO_3.3H_2O\ (s) = Mg^{2+} + CO_3^{2-} + 3H_2O$	4.93 (*)	
Artinite: $Mg_2CO_3(OH)_2.3H_2O\ (s) = 2Mg^{2+} + CO_3^{2-} + 2OH^- + 3H_2O$	9.60	(United States EPA, 1998)
Hydromagnesite: $Mg_5(CO_3)_4(OH)_2.4H_2O(s) = 5Mg^{2+} + 4CO_3^{2-} + 2OH^- + 4H_2O$	-8.766	
Thermonatrite: $Na_2CO_3.H_2O\ (s) = 2Na^+ + CO_3^{2-} + H_2O$	0.637	
Natron: $Na_2CO_3.10H_2O\ (s) = 2Na^+ + CO_3^{2-} + 10H_2O$	-1.311	
Magnesium Phosphate: $Mg_3(PO_4)_2\ (s) = 3Mg^{2+} + 2\ PO_4^{3-}$	-23.28	

Note: (*) Average data cited by the author

Appendix B Simulation Modelling

B.1. Fed-batch simulation procedure

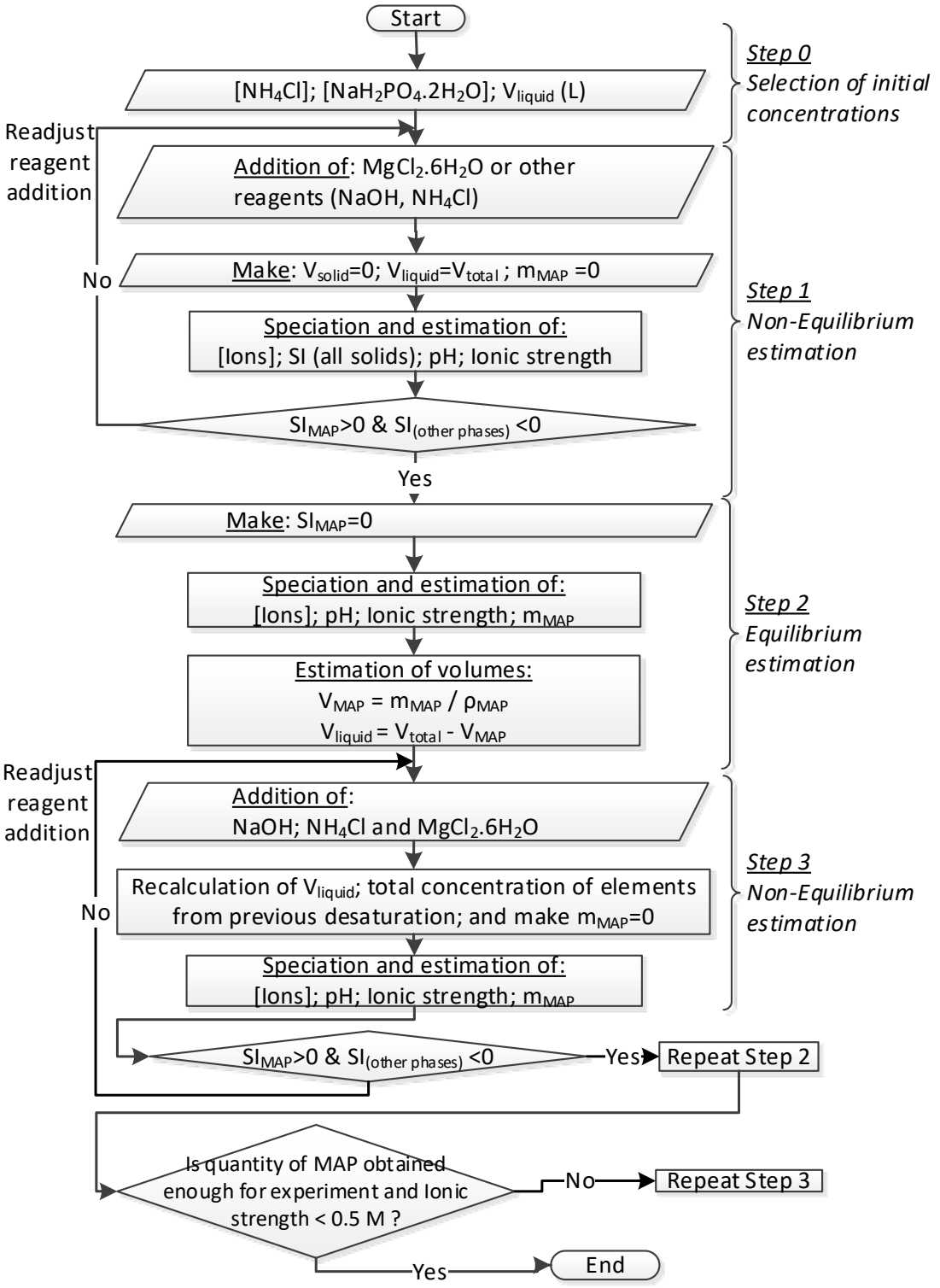

Figure 0.1 – Model solution procedure to design struvite seed in fed-batch reactor

B.2. EES code – batch model

```
"! ---------------------------------- a) CONSTANTS----------------------------------------------------------------------------"
“! (a.1) Equilibrium pK and equations"
        pK_w = 14
        pK_NH4 = 9.24
        pK_MgOH = 2.560
        pK_NaOH = -14.180
        pK_KOH = -14.46
        pK_HPO4 = 12.35
        pK_H2PO4 = 7.21
        pK_H3PO4 = 2.15
        pK_NaH2PO4 = 0.25
        pK_Na2HPO4 = - 6.11
        pK_NaHPO4 = - 6.01
        pK_MgHPO4 = - 4.3
        pK_MgPO4 = - 12.96
        pK_MgH2PO4 = 1.51
        pK_NH4H2PO4 = 0.10
        pK_NH4HPO4 = 1.30
        pK_KH2PO4 = 0.23
        pK_KHPO4 = - 6.12
        pK_H2CO3 = 6.35
        pK_HCO3 = 10.329
        pK_NaHCO3 = - 0.25
        pK_NaCO3 = 1.27
        pK_MgHCO3 = 1.07
        pK_MgCO3 = 2.98
        pK_NaSO4 = 0.70
        pK_MgSO4 = 2.37
        pK_NH4SO4 = 1.03
        pK_KSO4 = 0.85

“! (a.2) Average solubility product"
        pKsp_MAP = 13.26 "Struvite: MgNH4PO4.6H2O - MAP"
        pKsp_MgHP_3w = 5.51 "Newberite: MgHPO4.3H2O"
        pKsp_Mg3P2_8w = 23.98 "Bobierite: Mg3(PO4)2.8H2O"
        pKsp_Mg3P2_22w = 22.89 "Cattite Mg3(PO4)2.22H2O"
        pKsp_MgHPO4 = 0.15 "Dimagnesium phosphate MgHPO4"
        pKsp_MgOH2_6w = 10.7 "Brucite: Mg(OH)2.6H2O"
        pKsp_MgNaP = 11.60 "Na-struvite: MgNaPO4.6H2O "
        pKsp_MgKP = 12.20 "K-struvite: MgKPO4.6H2O"
        pKsp_MgC = 7.37 "Magnesite: MgCO3"
        pKsp_MC3w = 4.93 "Nesquehonite: MgCO3.3H2O"
        pKsp_Artinite = 9.60 "Artinite: MgCO3.Mg(OH)2.3H2O"
        pKsp_Hydromagnesite = -8.766 "Hydromagnesite: Mg5(CO3)4(OH)2.4H2O"
        pKsp_NaCw = 0.637 "Thermonatrite: Na2CO3.H2O"
        pKsp_NaC10w = -1.311 "Natron: Na2CO3.10H2O"
        pKsp_Mg3P2 = -23.28 "Mg3(PO4)2"

“! (a.3) Ion Characteristics - Debye-Hückel modified by Davies at 25ºC"
```

```
        A=0.5092; charge_1 = 1; charge_2 = 2; charge_3 = 3; a_D=1.0; b_D=-0.3

"! (a.4) Valencies of Species - Z_i"
"+"     Z_H = 1
        Z_Na = 1
        Z_K = 1
        Z_NH4 = 1
        Z_MgOH = 1
        Z_Mg = 2
        Z_MgH2PO4 = 1
        Z_MgHCO3 = 1

"-"Z_OH = -1
        Z_Cl = -1
        Z_HPO4 = -2
        Z_PO4 = -3
        Z_H2PO4 = -1
        Z_NaHPO4 = -1
        Z_NH4HPO4 = -1
        Z_MgPO4 = -1
        Z_HCO3 = -1
        Z_CO3 = -2
        Z_NaCO3 = -1
        Z_KHPO4 = -1
        Z_SO4 = -2
        Z_KSO4 = -1
        Z_NaSO4 = -1
        Z_NH4SO4 = -1

"! (a.5) Constants: Molecular weight [g/mol], density"
        Mw_NH4HCO3 = 79.056; Mw_NH4Cl = 53.491; Mw_NaOH = 39.997;
        Mw_KOH = 56.1056; Mw_NH42SO4 = 132.14; Mw_NH4H2PO4 = 115.03;
        Mw_Ca = 40; Mw_K=39.1; Mw_P = 30.974; Mw_Na = 22.99; Mw_N=14.007;
        Mw_Cl = 35.453; Mw_Mg = 24.305; Mw_C = 12.011; Mw_S = 32.065;
        Mw_CO3 = 60.01; Mw_SO4 = 96.06; Mw_NH4 = 18.039; Mw_MgSO47H2O = 246.47;
        Mw_MAP=245.41e-3 [kg/mol] "Struvite (MAP)"; rho_MAP_kgL=1.7[kg/L]

"! ---------------------------------------------- b) BALANCE-------------------------------------------------------------"
"! (b.1). Elemental mass balance and chemical speciation"
   "C_E_dissolved [mol/L] is the concentration of E element in the liquid,
   n_E_total [mol] is the moles of E inside the reactor,
   n_MAP_net [mol] is the overall struvite moles, including moles at the start (seed) and produced/consumed,
   n_MAP_seed [mol] is the moles of struvite seeds at the beginning of the process,
   C_M_nutrient [mol/L] is the M concentration in the nutrient solution (concentrated synthetic ureolysed urine),
   C_N_MgSource [mol/L] is the N concentration in the MgSO4.7H2O solution,
   V_liq is the liquid volume, V_nutrient is the volume of nutrient added to reactor in L."
n_P_total = C_P_nutrient*V_nutrient + n_MAP_seed
n_P_total=C_P_dissolved*V_liq + (n_MAP_net)
```

```
C_P_dissolved=C_PO4+ C_HPO4 + C_H2PO4 + C_H3PO4+&
        C_NaH2PO4+&
        C_Na2HPO4+&
        C_NaHPO4+&
        C_MgHPO4+&
        C_MgPO4+&
        C_MgH2PO4+&
        C_NH4H2PO4+&
        C_NH4HPO4+&
        C_KH2PO4+&
        C_KHPO4

n_N_total = C_N_nutrient*V_nutrient + n_MAP_seed
n_N_total=C_N_dissolved*V_liq + (n_MAP_net)

C_N_dissolved=C_NH3+&
        C_NH4+&
        C_NH4H2PO4+&
        C_NH4HPO4+&
        C_NH4SO4

n_Mg_total = C_Mg_MgSO47H2O*V_MgSource + C_Mg_nutrient*V_nutrient + n_MAP_seed
n_Mg_total=C_Mg_dissolved*V_liq + (n_MAP_net)

C_Mg_dissolved=C_Mg+&
        C_MgOH+&
        C_MgHPO4+&
        C_MgPO4+&
        C_MgH2PO4+&
        C_MgHCO3+&
        C_MgCO3+&
        C_MgSO4

n_Na_total = C_Na_nutrient*V_nutrient + C_NaOH_base*V_NaOH
n_Na_total=C_Na_dissolved*V_liq

C_Na_dissolved=C_Na+&
        C_NaOH+&
        C_NaH2PO4+&
        C_Na2HPO4+&
        C_NaHPO4+&
        C_NaHCO3+&
        C_NaCO3+&
        C_NaSO4

n_Cl_total = C_Cl_nutrient*V_nutrient + C_HCl_acid*V_HCl
n_Cl_total=C_Cl_dissolved*V_liq
C_Cl_dissolved=C_Cl

n_C_total = C_C_nutrient*V_nutrient
n_C_total=C_C_dissolved*V_liq
```

```
C_C_dissolved=C_H2CO3+&
        C_HCO3+&
        C_CO3+&
        C_NaHCO3+&
        C_NaCO3+&
        C_MgHCO3+&
        C_MgCO3

n_K_total = C_K_nutrient*V_nutrient
n_K_total=C_K_dissolved*V_liq
C_K_dissolved=C_K+&
        C_KOH+&
        C_KH2PO4+&
        C_KHPO4+&
        C_KSO4

n_S_total = C_S_nutrient*V_nutrient + C_S_MgSO47H2O*V_MgSource
n_S_total=C_S_dissolved*V_liq
C_S_dissolved=C_SO4+&
        C_NaSO4+&
        C_NH4SO4+&
        C_MgSO4+&
        C_KSO4

“! (b.2) Solid Phase Balance"
    "n_MAP_precip is the quantity of struvite moles produced after precipitation"
    "MW_MAP [Kg/mol] is the struvite molecular weight"
    "m_MAP_net, m_MAP_seed and m_MAP are struvite mass from moles"
        n_MAP_net =  n_MAP_seed + n_MAP_precip "moles"
        n_MAP_net = m_MAP_net/MW_MAP
        n_MAP_seed = m_MAP_seed/MW_MAP
        n_MAP_precip = m_MAP/Mw_MAP "Kg - struvite mass"

“! (b.3) Volume balance"
    "V_liq is the volume of liquid, V_total is the total volume,
    V_nutrient is the volume of concentrated synthetic ureolysed urine,
    V_MgSource is the volume of MgSO4.7H2O solution,
        V_liq = V_total - V_MAP "L"
        V_liq = V_nutrient + V_MgSource "L"
        V_MAP = (m_MAP + m_MAP_seed)/rho_MAP_kgL "L"

“! ------------------------------- c) THERMODYNAMICS-------------------------------------------------------------------"
“! (c.1) Estimation of Saturation Index (SI):"
        "IAP is the Ion Activity Product; log_a_E = log10(a_E)"
 "*"SI_MAP = log_IAP_MAP - log_Ksp_MAP                    "Struvite: MgNH4PO4.6H2O-(MAP)"
        log_IAP_MAP= log_a_Mg+ log_a_NH4+log_a_PO4
        log_Ksp_MAP = - pKsp_MAP

"*"SI_MgHP_3w = log_IAP_MgHP_3w - log_Ksp_MgHP_3w       "Newberite: MgHPO4.3H2O"
        log_IAP_MgHP_3w=log_a_Mg+log_a_HPO4
        log_Ksp_MgHP_3w = - pKsp_MgHP_3w
```

```
"*"SI_Mg3P2_8w = log_IAP_Mg3P2_8w - log_Ksp_Mg3P2_8w    "Bobierite: Mg3(PO4)2.8H2O"
        log_IAP_Mg3P2_8w=3*log_a_Mg+2*log_a_PO4
        log_Ksp_Mg3P2_8w = - pKsp_Mg3P2_8w

"*"SI_Mg3P2_22w = log_IAP_Mg3P2_22w - log_Ksp_Mg3P2_22w         "Cattite Mg3(PO4)2.22H2O"
        log_IAP_Mg3P2_22w=3*log_a_Mg+2*log_a_PO4
        log_Ksp_Mg3P2_22w = - pKsp_Mg3P2_22w

"*"SI_Mg3P2 = log_IAP_Mg3P2 - log_Ksp_Mg3P2          "Magnesium Phosphate: Mg3(PO4)2"
        log_IAP_Mg3P2=3*log_a_Mg+2*log_a_PO4
        log_Ksp_Mg3P2 = - pKsp_Mg3P2

"*"SI_MgHPO4 = log_IAP_MgHPO4 - log_Ksp_MgHPO4          "Dimagnesium phosphate MgHPO4"
        log_IAP_MgHPO4=log_a_MgHPO4
        log_Ksp_MgHPO4 = - pKsp_MgHPO4

"*"SI_MgNaP = log_IAP_MgNaP - log_Ksp_MgNaP             "Na-struvite: MgNaPO4.6H2O"
        log_IAP_MgNaP = log_a_Mg+ log_a_Na+log_a_PO4
        log_Ksp_MgNaP = - pKsp_MgNaP

"*"SI_MgKP = log_IAP_MgKP - log_Ksp_MgKP                "K-struvite: MgKPO4.6H2O"
        log_IAP_MgKP = log_a_Mg+ log_a_K+log_a_PO4
        log_Ksp_MgKP = - pKsp_MgKP

"*"SI_MgC = log_IAP_MgC - log_Ksp_MgC                       "Magnesite: MgCO3"
        log_IAP_MgC = log_a_Mg+log_a_CO3
        log_Ksp_MgC = - pKsp_MgC

"*"SI_MgC3w = log_IAP_MC3w - log_Ksp_MC3w                "Nesquehonite: MgCO3.3H2O"
        log_IAP_MC3w = log_a_Mg+log_a_CO3
        log_Ksp_MC3w = - pKsp_MC3w

"*"SI_Artinite = log_IAP_Artinite - log_Ksp_Artinite     "Artinite: MgCO3.Mg(OH)2.3H2O"
        log_IAP_Artinite=2*log_a_Mg+log_a_CO3+log_a_OH
        log_Ksp_Artinite = - pKsp_Artinite

"*"SI_Hydromagnesite = log_IAP_Hydromagnesite - log_Ksp_Hydromagnesite
        log_IAP_Hydromagnesite = 5*log_a_Mg+4*log_a_CO3+2*log_a_OH
        log_Ksp_Hydromagnesite = - pKsp_Hydromagnesite          "Hydromagnesite:
Mg5(CO3)4(OH)2.4H2O"

"*"SI_NaCw = log_IAP_NaCw - log_Ksp_NaCw                 "Thermonatrite: Na2CO3.H2O"
        log_IAP_NaCw = 2*log_a_Na+log_a_CO3
        log_Ksp_NaCw = - pKsp_NaCw

"*"SI_NaC10w = log_IAP_NaC10w - log_Ksp_NaC10w           "Natron: Na2CO3.10H2O"
        log_IAP_NaC10w = 2*log_a_Na+log_a_CO3
        log_Ksp_NaC10w = - pKsp_NaC10w

"*"SI_MgOH2_6w = log_IAP_MgOH2_6w - log_Ksp_MgOH2_6w
```

```
        log_IAP_MgOH2_6w = log_a_Mg+2*log_a_OH
        log_Ksp_MgOH2_6w = - pKsp_MgOH2_6w                "Brucite: Mg(OH)2.6H2O"

"IAP conversion:"
        IAP_MAP = 10^log_IAP_MAP
        IAP_MgHP_3w = 10^log_IAP_MgHP_3w
        IAP_Mg3P2_8w = 10^log_IAP_Mg3P2_8w
        IAP_Mg3P2_22w = 10^log_IAP_Mg3P2_22w
        IAP_Mg3P2 = 10^log_IAP_Mg3P2
        IAP_MgHPO4 = 10^log_IAP_MgHPO4
        IAP_MgNaP = 10^log_IAP_MgNaP
        IAP_MgKP = 10^log_IAP_MgKP
        IAP_MgC = 10^log_IAP_MgC
        IAP_MC3w = 10^log_IAP_MC3w
        IAP_Artinite = 10^log_IAP_Artinite
        IAP_Hydromagnesite = 10^log_IAP_Hydromagnesite
        IAP_NaCw = 10^log_IAP_NaCw
        IAP_NaC10w = 10^log_IAP_NaC10w
        IAP_MgOH2_6w = 10^log_IAP_MgOH2_6w

"! (c.2) Estimation of ionic activities"
      "Equations are related to reactions in (a.1)"
      "Log_a_i = log10(a_i); estimations in log_a_i for faster solving"
        -pK_w = log_a_H + log_a_OH
        -pK_NH4 = log_a_H + log_a_NH3 - log_a_NH4
        -pK_MgOH = log_a_Mg + log_a_OH - log_a_MgOH
        -pK_NaOH = log_a_Na - log_a_NaOH - log_a_H
        -pK_KOH = log_a_K - log_a_KOH - log_a_H
        -pK_HPO4 = log_a_PO4 + log_a_H - log_a_HPO4
        -pK_H2PO4 = log_a_HPO4 + log_a_H - log_a_H2PO4
        -pK_H3PO4 = log_a_H2PO4 + log_a_H - log_a_H3PO4
        -pK_NaH2PO4 = log_a_Na + log_a_H2PO4 - log_a_NaH2PO4
        -pK_Na2HPO4 = 2*log_a_Na + log_a_H2PO4 - log_a_Na2HPO4 - log_a_H
        -pK_NaHPO4 = log_a_Na + log_a_H2PO4 - log_a_NaHPO4 - log_a_H
        -pK_MgHPO4 = log_a_Mg + log_a_H2PO4 - log_a_MgHPO4 - log_a_H
        -pK_MgPO4 = log_a_Mg + log_a_H2PO4 - log_a_MgPO4 - 2*log_a_H
        -pK_MgH2PO4 = log_a_Mg + log_a_H2PO4 - log_a_MgH2PO4
        -pK_NH4H2PO4 = log_a_NH4 + log_a_H2PO4 - log_a_NH4H2PO4
        -pK_NH4HPO4 = log_a_NH4 + log_a_HPO4 - log_a_NH4HPO4
        -pK_KH2PO4 = log_a_K + log_a_H2PO4 - log_a_KH2PO4
        -pK_KHPO4 = log_a_K + log_a_H2PO4 - log_a_KHPO4 - log_a_H
        -pK_H2CO3 = log_a_HCO3 + log_a_H - log_a_H2CO3
        -pK_HCO3 = log_a_CO3 + log_a_H - log_a_HCO3
        -pK_NaHCO3 = log_a_Na + log_a_HCO3 - log_a_NaHCO3
        -pK_NaCO3 = log_a_Na + log_a_CO3 - log_a_NaCO3
        -pK_MgHCO3 = log_a_Mg + log_a_HCO3 - log_a_MgHCO3
        -pK_MgCO3 = log_a_Mg + log_a_CO3 - log_a_MgCO3
        -pK_NaSO4 = log_a_Na + log_a_SO4 - log_a_NaSO4
        -pK_MgSO4 = log_a_Mg + log_a_SO4 - log_a_MgSO4
        -pK_NH4SO4 = log_a_NH4 + log_a_SO4 - log_a_NH4SO4
        -pK_KSO4 = log_a_K + log_a_SO4 - log_a_KSO4
```

```
“! (c.3) Estimation of Ionic concentrations (C_i) from Ionic activities (a_i)"
        "a_i = gamma_j*C_i; log_a_i = log10(a_i)"
        "gamma_1, gamm_2, and gamma_3 are the activity coefficients"
"+"     log_a_H = log_gamma_1+ log_C_H
        log_a_Na = log_gamma_1+ log_C_Na
        log_a_K = log_gamma_1+ log_C_K
        log_a_NH4 = log_gamma_1+ log_C_NH4
        log_a_MgOH = log_gamma_1 + log_C_MgOH
        log_a_Mg = log_gamma_2 + log_C_Mg
        log_a_MgH2PO4 = log_gamma_1 + log_C_MgH2PO4
        log_a_MgHCO3 = log_gamma_1 + log_C_MgHCO3

"-"     log_a_OH = log_gamma_1+ log_C_OH
        log_a_HPO4 = log_gamma_2 + log_C_HPO4
        log_a_PO4 = log_gamma_3 + log_C_PO4
        log_a_H2PO4 = log_gamma_1 + log_C_H2PO4
        log_a_NaHPO4 = log_gamma_1 + log_C_NaHPO4
        log_a_NH4HPO4 = log_gamma_1 + log_C_NH4HPO4
        log_a_MgPO4 = log_gamma_1 + log_C_MgPO4
        log_a_KHPO4 = log_gamma_1 + log_C_KHPO4
        log_a_HCO3 = log_gamma_1 + log_C_HCO3
        log_a_CO3 = log_gamma_2 + log_C_CO3
        log_a_NaCO3 = log_gamma_1 + log_C_NaCO3
        log_a_SO4 = log_gamma_2 + log_C_SO4
        log_a_KSO4 = log_gamma_1 + log_C_KSO4
        log_a_NaSO4 = log_gamma_1 + log_C_NaSO4
        log_a_NH4SO4 = log_gamma_1 + log_C_NH4SO4

"0"log_a_NaOH = log_C_NaOH
        log_a_KOH = log_C_KOH
        log_a_NH3 = log_C_NH3
        log_a_H3PO4 = log_C_H3PO4
        log_a_NaH2PO4 = log_C_NaH2PO4
        log_a_Na2HPO4 = log_C_Na2HPO4
        log_a_NH4H2PO4 = log_C_NH4H2PO4
        log_a_MgHPO4 = log_C_MgHPO4
        log_a_KH2PO4 = log_C_KH2PO4
        log_a_H2CO3 = log_C_H2CO3
        log_a_NaHCO3 = log_C_NaHCO3
        log_a_MgCO3 = log_C_MgCO3
        log_a_MgSO4 = log_C_MgSO4

“! (c.4) Activity coefficients of Debye Hückel modified by Davies Equation"

        gamma_1=10^log_gamma_1; gamma_2=10^log_gamma_2; gamma_3=10^log_gamma_3
        -log_gamma_1 = (A*(charge_1^2) * (((I^0.5)/(1+a_D*(I^0.5))) + b_D*I))
        -log_gamma_2 = (A*(charge_2^2) * (((I^0.5)/(1+a_D*(I^0.5))) + b_D*I))
        -log_gamma_3 = (A*(charge_3^2) * (((I^0.5)/(1+a_D*(I^0.5))) + b_D*I))

“! (c.5) Electroneutrality and pH definition"
```

```
        CB=0;

"*"     pH=-log_a_H

        CB=&
        C_H*Z_H+&
        C_Na*Z_Na+&
        C_K*Z_K+&
        C_NH4*Z_NH4+&
        C_MgOH*Z_MgOH+&
        C_Mg*Z_Mg+&
        C_OH*Z_OH+&
        C_MgH2PO4*Z_MgH2PO4+&
        C_HPO4*Z_HPO4+&
        C_PO4*Z_PO4+&
        C_H2PO4*Z_H2PO4+&
        C_NaHPO4*Z_NaHPO4+&
        C_NH4HPO4*Z_NH4HPO4+&
        C_MgPO4*Z_MgPO4+&
        C_KHPO4*Z_KHPO4+&
        C_MgHCO3*Z_MgHCO3+&
        C_Cl*Z_Cl+&
        C_HCO3*Z_HCO3+&
        C_CO3*Z_CO3+&
        C_NaCO3*Z_NaCO3+&
        C_SO4*Z_SO4+&
        C_KSO4*Z_KSO4+&
        C_NaSO4*Z_NaSO4+&
        C_NH4SO4*Z_NH4SO4

"! (c.6) Variable conversion from logarithm form"
    "The estimation of ionic concentrations (C_x) are necessary in elemental balance in (b.7)"
    "The estimation of ionic activities (a_x) are necessary to estimate Ion activity product"
"+"     C_H = 10^log_C_H
        C_Na = 10^log_C_Na
        C_K = 10^log_C_K
        C_NH4 = 10^log_C_NH4
        C_MgOH = 10^log_C_MgOH
        C_Mg = 10^log_C_Mg
        C_MgH2PO4 = 10^log_C_MgH2PO4
        C_MgHCO3 = 10^log_C_MgHCO3

"-"     C_OH = 10^log_C_OH
        C_HPO4 = 10^log_C_HPO4
        C_PO4 = 10^log_C_PO4
        C_H2PO4 = 10^log_C_H2PO4
        C_NaHPO4 = 10^log_C_NaHPO4
        C_NH4HPO4 = 10^log_C_NH4HPO4
        C_MgPO4 = 10^log_C_MgPO4
        C_KHPO4 = 10^log_C_KHPO4
        C_HCO3 = 10^log_C_HCO3
```

```
        C_CO3 = 10^log_C_CO3
        C_NaCO3 = 10^log_C_NaCO3
        C_SO4 = 10^log_C_SO4
        C_KSO4 = 10^log_C_KSO4
        C_NaSO4 = 10^log_C_NaSO4
        C_NH4SO4 = 10^log_C_NH4SO4

"0"     C_NaOH = 10^log_C_NaOH
        C_KOH = 10^log_C_KOH
        C_NH3 = 10^log_C_NH3
        C_H3PO4 = 10^log_C_H3PO4
        C_NaH2PO4 =10^log_C_NaH2PO4
        C_Na2HPO4 = 10^log_C_Na2HPO4
        C_NH4H2PO4 = 10^log_C_NH4H2PO4
        C_MgHPO4 = 10^log_C_MgHPO4
        C_H2CO3 = 10^log_C_H2CO3
        C_NaHCO3 = 10^log_C_NaHCO3
        C_MgCO3 = 10^log_C_MgCO3
        C_KH2PO4 =10^log_C_KH2PO4
        C_MgSO4 = 10^log_C_MgSO4

"+"     a_H = 10^log_a_H
        a_Na = 10^log_a_Na
        a_K = 10^log_a_K
        a_NH4 = 10^log_a_NH4
        a_MgOH = 10^log_a_MgOH
        a_Mg = 10^log_a_Mg
        a_MgH2PO4 =10^log_a_MgH2PO4
        a_MgHCO3 =10^log_a_MgHCO3

"-"a_OH = 10^log_a_OH
        a_HPO4 = 10^log_a_HPO4
        a_PO4 =10^log_a_PO4
        a_H2PO4 =10^log_a_H2PO4
        a_NaHPO4 = 10^log_a_NaHPO4
        a_NH4HPO4 = 10^log_a_NH4HPO4
        a_MgPO4 = 10^log_a_MgPO4
        a_KHPO4 =10^log_a_KHPO4
        a_HCO3 = 10^log_a_HCO3
        a_CO3 = 10^log_a_CO3
        a_NaCO3 = 10^log_a_NaCO3
        a_SO4 = 10^log_a_SO4
        a_KSO4 = 10^log_a_KSO4
        a_NaSO4 = 10^log_a_NaSO4
        a_NH4SO4 = 10^log_a_NH4SO4

"0"a_NaOH = 10^log_a_NaOH
        a_KOH = 10^log_a_KOH
        a_NH3 = 10^log_a_NH3
        a_H3PO4 = 10^log_a_H3PO4
        a_NaH2PO4 =10^log_a_NaH2PO4
```

```
a_Na2HPO4 = 10^log_a_Na2HPO4
a_NH4H2PO4 = 10^log_a_NH4H2PO4
a_MgHPO4 = 10^log_a_MgHPO4
a_H2CO3 = 10^log_a_H2CO3
a_NaHCO3 = 10^log_a_NaHCO3
a_MgCO3 = 10^log_a_MgCO3
a_KH2PO4 = 10^log_a_KH2PO4
a_MgSO4 = 10^log_a_MgSO4

"! (c.7) Estimation of the Ionic strength: I=0,5*Sum(Ci*Zi^2)"
    "The ionic strength range defines if Activity Model Equation is valid"
   "Maximum ionic strength suitable for Debye Hückel-Davies 0.5M"
   "Concentrations are in mol/L"
      I=0.5*(&
      C_H*Z_H^2+&
      C_Na*Z_Na^2+&
      C_K*Z_K^2+&
      C_NH4*Z_NH4^2+&
      C_MgOH*Z_MgOH^2+&
      C_Mg*Z_Mg^2+&
      C_OH*Z_OH^2+&
      C_MgH2PO4*Z_MgH2PO4^2+&
      C_HPO4*Z_HPO4^2+&
      C_PO4*Z_PO4^2+&
      C_H2PO4*Z_H2PO4^2+&
      C_NaHPO4*Z_NaHPO4^2+&
      C_NH4HPO4*Z_NH4HPO4^2+&
      C_MgPO4*Z_MgPO4^2+&
      C_KHPO4*Z_KHPO4^2+&
      C_MgHCO3*Z_MgHCO3^2+&
      C_Cl*Z_Cl^2+&
      C_HCO3*Z_HCO3^2+&
      C_CO3*Z_CO3^2+&
      C_NaCO3*Z_NaCO3^2+&
      C_SO4*Z_SO4^2+&
      C_KSO4*Z_KSO4^2+&
      C_NaSO4*Z_NaSO4^2+&
      C_NH4SO4*Z_NH4SO4^2)

“! ----------d) SOLUTIONS MIXING----------"
“! (d.1) Estimation of Mg/P molar ratio immediately after mixing"
      MgP_FeedMolarRatio = (C_Mg_MgSO47H2O*V_MgSource)/(C_P_nutrient*V_nutrient)

“! (d.2) Nutrient solution composition"
"----Elemental distribution of mixing of reagents: -Regent concentration in mol/L:"

      C_N_nutrient = C_NH4HCO3_nutrient + C_NH4Cl_nutrient + 2*C_NH42SO4_nutrient +
C_NH4H2PO4_nutrient "
      C_C_nutrient = C_NH4HCO3_nutrient
      C_Cl_nutrient = C_NH4Cl_nutrient
      C_Na_nutrient = C_NaOH_nutrient
```

```
C_K_nutrient = C_KOH_nutrient
C_S_nutrient = C_NH42SO4_nutrient
C_P_nutrient = C_NH4H2PO4_nutrient
C_Mg_nutrient = 1e-12

"----Composition of concentrated synthetic ureolysed urine-[mol/L]"
C_NH4HCO3_nutrient = 0.181593
C_KOH_nutrient = 0.100917
C_NaOH_nutrient = 0.145200
C_NH42SO4_nutrient = 0.014799
C_NH4Cl_nutrient = 0.403058
C_NH4H2PO4_nutrient =0.035608

“! (d.3) Composition of MgSO4.7H2O solution – [mol/L]"
C_Mg_MgSO47H2O = C_MgSO47H2O "mol/L"
C_S_MgSO47H2O = C_MgSO47H2O "mol/L"
m_MgSO47H2O_source = C_Mg_MgSO47H2O*Mw_MgSO47H2O*V_MgSource

“! ----------e) INPUT DATA----------"

m_MAP_seed_g = ..... "g - Initial struvite mass within the reactor"
V_nutrient = ..... "L – volume of nutrient mixed with MgSO4.7H2O solution"
V_MgSource = ....."L - volume of Mg source solution mixed with nutrient solution"

“! ----------f) ADJUSTABLE VARIABLES----------"
“This section describes the equilibrium and non-equilibrium estimations”
“If the quantity of struvite at equilibrium is estimated, the saturation index is set to zero”
“If the estimation of the saturation index has to be estimated at non-equilibrium, the moles of precipitated struvite has to be set to zero.

"! (f.1) Non-Equilibrium"
n_MAP_precip = 0 “Moles of precipitated struvite after mixing of nutrient with Mg source”

"! (f.2) Equilibrium"
SI_MAP=0 “Saturation Index”
```

B.3. EES code – continuous Model

```
"! ----------------------------------1. PROCEDURES-----------------------------------------------------------------------"
"! (1.1) Input Source Mg-----------------------------------------------------------------------------------------------"
  Procedure cmgsource(t,t_sim:C_MgSO47H2O_feed)
    {C_P_filteredCSUU = 0.03347152} "Considering a %P loss of 6%"
    If (t < 50) Then C_MgSO47H2O_feed = ......
    If (t >= 50) Then C_MgSO47H2O_feed = ......
  End

"! (1.2) Input Source Mg-----------------------------------------------------------------------------------------------"
 Procedure csuu_feed (t,t_sim:C_P_NutrientSource, C_Na_NutrientSource, C_Cl_NutrientSource,
C_C_NutrientSource, C_S_NutrientSource, C_K_NutrientSource, C_N_NutrientSource)
"Following concentrations in mol/L"
      C_P_NutrientSource = ......
      C_N_NutrientSource = ......
      C_K_NutrientSource = ......
      C_S_NutrientSource = ......
      C_C_NutrientSource = ......
      C_Na_NutrientSource = ......
      C_Cl_NutrientSource = ......
End

"! (1.3) Input Flows--------------------------------------------------------------------------------------------------"
 "F_MgSource is the flow rate in L/h of the MgSO4.7H2O solution added to the reactor (pump 1)"
"F_NutrientSource is the flow rate in L/h of the concentrated synthetic ureolysed urine (pump 2)"
"F_intermix is the intermixing flow rate between the bottom and upper zones"
"F_out is the outlet flow rate leaving the reactor"
 Procedure flow (t, t_sim: F_MgSource, F_NutrientSource, F_intermix,F_out)
     "The flow rates between time = 0 and 1minute (1/60 h) are set to zero"
      F_MgSource: = 1e-9 [L/h]; F_NutrientSource: = 1e-9 [L/h]; F_intermix: =4[L/h]

    If t >= 1/60 Then "After 1minute - checking flow rate of pump 2"
   F_MgSource: = 1e-9[L/h]; F_NutrientSource: = 0.3 [L/h]; F_intermix: = 4[L/h]
     Endif

    If t >= 6/60 Then "checking flow rate of pump 1, Mg source addition"
   F_MgSource: = 0.3[L/h]; F_NutrientSource: = 1e-9 [L/h]; F_intermix: = 4[L/h]
    Endif

    If t >= 11/60 Then "nominal flow, after calibration"
   F_MgSource: = 0.3[L/h]; F_NutrientSource: = 0.3 [L/h]; F_intermix: = 4[L/h]
     Endif

    If t >= 100 Then "shut off all flow to system"
    F_MgSource: = 1e-9[L/h]; F_NutrientSource: = 1e-9 [L/h]; F_intermix: = 4[L/h]
    Endif
    F_out: = F_MgSource + F_NutrientSource
 End

"! (1.4) Struvite sample----------------------------------------------------------------------------------------------"
```

"This procedure estimate the quantity of MAP taken during continuous reactor operation"
"n_MAP_sample is the moles of struvite within sample"

Procedure **sample** (t:m_MAP_sample) "moles of struvite in sample"
samples = 8 "number of samples"
m_total_sample [1] = 0 "kg- Sample "
m_total_sample [2] = 0 "kg - Sample "
m_total_sample [3] = 0 "kg - Sample "
m_total_sample [4] = 0"kg Sample "
m_total_sample [5] = 0"kg - Sample "
m_total_sample [6] = 0"kg - Sample "
m_total_sample [7] = 0"kg - Sample "
m_total_sample [8] = 0 "kg - Sample "

"m_sample[i] is the mass of sample in Kg taken from the reactor at any time"
"wt_i is the solid fraction of struvite within the sample comprised by liquid and solid phase"
m_sample[1] = 0; m_sample[2] = 0; m_sample[3] = 0
m_sample[4] = 0; m_sample[5] = 0; m_sample[6] = 0; m_sample[7] = 0
m_sample[8] = 0

wt_1 = 1; wt_2 = 1; wt_3 = 1; wt_4 = 1; wt_5 = 1; wt_6 = 1; wt_7 = 1; wt_8=1
"solid fraction was one since weight
comes from filtered solid sample (negligible quantity of water in sample)"
If (t>= 12.90) ***Then*** m_sample[1] = wt_1*m_total_sample[1] "kg"
If (t>=26.17) ***Then*** m_sample[2] = wt_2*m_total_sample[2] "kg"
If (t>=49.45) Then m_sample[3] = wt_3*m_total_sample[3] "kg"
If (t>=53.52) Then m_sample[4] = wt_4*m_total_sample[4] "kg"
If (t>=57.87) Then m_sample[5] = wt_4*m_total_sample[5] "kg"
If (t>=73.32) Then m_sample[6] = wt_5*m_total_sample[6] "kg"
If (t>=85.55) Then m_sample[7] = wt_6*m_total_sample[7] "kg"
If (t>=99.499) Then m_sample[8] = wt_7*m_total_sample[8] "kg"
"m_sample is the overall sum of different samples during reactor operation"
m_MAP_sample=**sum**(m_sample[1..samples]) "total mass of struvite in samples"
End

"! ----------2. MODULE: EQUILIBRIUM----------"
"This module perform an equilibrium mass balance during the continuous process by adding the concentration
at equilibrium, and by considering an initial saturated solution close to zero values"

Module **equil** (C_P_dissolved, C_N_dissolved, C_Mg_dissolved,C_K_dissolved,C_S_dissolved,C_C_dissolved,C_Na_dissolved,C_Cl_dissolved:C_P_dissolved_equil,C_Mg_dissolved_equil,C_N_dissolved_equil)

Similar to Appendix B.2 with the following variation in the mass balance in section b:

"Input data to determine equilibrium in the system"
SI_MAP = 1e-4

"Chemical speciation- Liquid phase"

```
C_P_dissolved_equil = C_P_dissolved - n_MAP
C_P_dissolved = n_MAP + C_PO4+&
    C_HPO4+&
    C_H2PO4+&
    C_H3PO4+&
    C_NaH2PO4+&
    C_Na2HPO4+&
    C_NaHPO4+&
    C_MgHPO4+&
    C_MgPO4+&
    C_MgH2PO4+&
    C_NH4H2PO4+&
    C_NH4HPO4+&
    C_KH2PO4+&
    C_KHPO4

C_N_dissolved_equil = C_N_dissolved - n_MAP

C_N_dissolved = n_MAP + C_NH3+&
    C_NH4+&
    C_NH4H2PO4+&
    C_NH4HPO4+&
    C_NH4SO4

C_Mg_dissolved_equil = C_Mg_dissolved - n_MAP
C_Mg_dissolved = n_MAP + C_Mg+&
    C_MgOH+&
    C_MgHPO4+&
    C_MgPO4+&
    C_MgH2PO4+&
    C_MgHCO3+&
    C_MgCO3+&
    C_MgSO4

C_Na_dissolved = C_Na+&
    C_NaOH+&
    C_NaH2PO4+&
    C_Na2HPO4+&
    C_NaHPO4+&
    C_NaHCO3+&
    C_NaCO3+&
    C_NaSO4

C_Cl_dissolved = C_Cl

C_C_dissolved = C_H2CO3+&
    C_HCO3+&
    C_CO3+&
    C_NaHCO3+&
    C_NaCO3+&
    C_MgHCO3+&
```

C_MgCO3

C_S_dissolved=C_SO4+&
C_MgSO4+&
C_NaSO4+&
C_NH4SO4+&
C_KSO4

C_K_dissolved = C_K+&
C_KOH+&
C_KH2PO4+&
C_KHPO4+&
C_KSO4

END "module EQUIL"

"! ----------3. MODULE: THERMODYNAMIC COMPONENT----------"
Module **thermo** (C_P_dissolved, C_N_dissolved, C_Mg_dissolved, C_K_dissolved, C_S_dissolved, C_C_dissolved, C_Na_dissolved, C_Cl_dissolved: pH, SI_MAP, C_PO4, C_Mg, C_NH4, I, a_Mg, a_PO4, a_NH4)

Similar to Appendix B.2, but without mass balance in section b

END "module THERMO"

"! ---------- CALLING PROCEDURES----------"
Call cmgsource (t, t_sim:C_MgSO47H2O_feed)
Call csuu_feed (t, t_sim:C_P_NutrientSource, C_Na_NutrientSource, C_Cl_NutrientSource, C_C_NutrientSource, C_S_NutrientSource, C_K_NutrientSource, C_N_NutrientSource)
Call flow (t, t_sim:F_MgSource,F_NutrientSource,F_intermix,F_out)
Call sample (t:m_MAP_sample)

"! ---------- CALLING MODULES----------"
"Equilibrium balance"
Call equil(C_P_dissolved, C_N_dissolved, C_Mg_dissolved,C_K_dissolved,C_S_dissolved,C_C_dissolved,C_Na_dissolved,C_Cl_dissolved:C_P_dissolved_equil,C_Mg_dissolved_equil,C_N_dissolved_equil)

"Bottom reactor"
Call thermo (C_P_dissolved, C_N_dissolved, C_Mg_dissolved, C_K_dissolved, C_S_dissolved, C_C_dissolved, C_Na_dissolved, C_Cl_dissolved: pH, SI_MAP, C_PO4, C_Mg_ion, C_NH4, I, a_Mg, a_PO4, a_NH4)

"Upper reactor"
Call **thermo** (C_P_dissolved_z2, C_N_dissolved_z2, C_Mg_dissolved_z2,C_K_dissolved_z2,C_S_dissolved_z2,C_C_dissolved_z2,C_Na_dissolved_z2,C_Cl_dissolved_z2:pH_z2,SI_MAP_z2,C_PO4_z2,C_Mg_ion_z2,C_NH4_z2,I_z2, a_Mg_z2, a_PO4_z2,a_NH4_z2)

"! ----------4. DYNAMIC BALANCE----------"
"The reactor is modelled considering two reactors in series: the main reactor where the the most of precipitation takes place is the zone 1 - bottom, while the second reactor operating as a sedimentation place is the zone 2 - upper "

```
“! (4.1) ----------Intermixing specification----------"
 "F_intermix is the flow rate of the liquid between bottom and upper zone"
"V_liquid_z2 is the volume of the upper zone"
"V_liquid is the volume of the bottom zone"
"V_MAP is the volume of struvite within reactor"
"d_V_liquid_dt_z2 is the volume change of the upper zone"
      V_liquid_z2 = 12.1 - V_liquid - V_MAP
     dV_liquid_dt_z2 = 0

“! (4.2) ----------Balance per each element----------"
 "C_E_dissolved is the concentration of the Element (E) in the liquid phase"
"dCEdt is the change of elemental concentration over time"
"dn_MAPdt is the struvite production rate (mol/h)"
"C_E_0 is the initial concentration of the element in the liquid phase at time zero"
"t_sim is the simulation time"

"-------------------------------------------------------------------------------"
"-------P - Zone 1 - bottom:"
     C_P_dissolved*dV_liquid_dt + V_liquid*dCPdt = &
     C_P_NutrientSource*F_NutrientSource - &
     C_P_dissolved*(F_out + F_intermix) + &
     C_P_dissolved_z2*F_intermix - &
     dn_MAP_dt
   C_P_dissolved = C_P_0 + integral(dCPdt,t,t_init,t_sim) "mol/L"

"P - Zone 2 - upper:"
     C_P_dissolved_z2*dV_liquid_dt_z2 + V_liquid_z2*dCPdt_z2 = &
     C_P_dissolved*(F_out + F_intermix) - &
     C_P_dissolved_z2*F_out - &
     C_P_dissolved_z2*F_intermix
   C_P_dissolved_z2 = C_P_0_z2 + integral (dCPdt_z2, t,t_init,t_sim) "mol/L"
"-------------------------------------------------------------------------------"
 "-------N - Zone 1 - bottom:"
     C_N_dissolved*dV_liquid_dt + V_liquid*dCNdt = &
     C_N_NutrientSource*F_NutrientSource - &
     C_N_dissolved*(F_out + F_intermix) + &
     C_N_dissolved_z2*F_intermix - &
     dn_MAP_dt
     C_N_dissolved = C_N_0 + integral(dCNdt,t,t_init,t_sim)"mol/L"

 "N - Zone 2 - upper:"
     C_N_dissolved_z2*dV_liquid_dt_z2 + V_liquid_z2*dCNdt_z2 = &
     C_N_dissolved*(F_out + F_intermix) - &
     C_N_dissolved_z2*F_out - &
     C_N_dissolved_z2*F_intermix
   C_N_dissolved_z2 = C_N_0_z2 + integral (dCNdt_z2, t,t_init,t_sim) "mol/L"
 "-------------------------------------------------------------------------------"
 "-------Mg - Zone 1 - bottom:"
     C_Mg_dissolved*dV_liquid_dt + V_liquid*dCMgdt=&
     C_Mg_MgSource*F_MgSource - &
```

```
    C_Mg_dissolved*(F_out + F_intermix) + &
    C_Mg_dissolved_z2*F_intermix - &
    dn_MAP_dt
    C_Mg_dissolved = C_Mg_0+integral(dCMgdt,t,t_init,t_sim)"mol/L"

"Mg - Zone 2 - upper"
    C_Mg_dissolved_z2*dV_liquid_dt_z2 + V_liquid_z2*dCMgdt_z2 = &
    C_Mg_dissolved*(F_out + F_intermix) - &
    C_Mg_dissolved_z2*F_out - &
    C_Mg_dissolved_z2*F_intermix
  C_Mg_dissolved_z2 = C_Mg_0_z2 + integral(dCMgdt_z2,t,t_init,t_sim) "mol/L"
"-------------------------------------------------------------------------------"
 "-------Na - Zone 1-upper"
    C_Na_dissolved*dV_liquid_dt+V_liquid*dCNadt = &
    C_Na_NutrientSource*F_NutrientSource - &
    C_Na_dissolved*(F_out + F_intermix) + &
    C_Na_dissolved_z2*F_intermix
    C_Na_dissolved = C_Na_0 + integral(dCNadt,t,t_init,t_sim)"mol/L"

 "Na - Zone 2 - upper"
    C_Na_dissolved_z2*dV_liquid_dt_z2 + V_liquid_z2*dCNadt_z2 = &
    C_Na_dissolved*(F_out + F_intermix) - &
    C_Na_dissolved_z2*F_out - &
    C_Na_dissolved_z2*F_intermix
    C_Na_dissolved_z2 = C_Na_0_z2 + integral (dCNadt_z2, t,t_init,t_sim)"mol/L"
"-------------------------------------------------------------------------------"
"-------Cl - Zone 1-upper"
    C_Cl_dissolved*dV_liquid_dt + V_liquid*dCCldt = &
    C_Cl_NutrientSource*F_NutrientSource - &
    C_Cl_dissolved*(F_out + F_intermix) + &
    C_Cl_dissolved_z2*F_intermix
    C_Cl_dissolved = C_Cl_0 + integral(dCCldt,t,t_init,t_sim)"mol/L"

 "Cl - Zone 2 - upper"
    C_Cl_dissolved_z2*dV_liquid_dt_z2 + V_liquid_z2*dCCldt_z2 = &
    C_Cl_dissolved*(F_out + F_intermix) - &
    C_Cl_dissolved_z2*F_out - &
    C_Cl_dissolved_z2*F_intermix
    C_Cl_dissolved_z2 = C_Cl_0_z2 + integral(dCCldt_z2,t,t_init,t_sim)"mol/L"
"-------------------------------------------------------------------------------"
"-------C - Zone 1-upper"
    C_C_dissolved*dV_liquid_dt + V_liquid*dCCdt = &
    C_C_NutrientSource*F_NutrientSource - &
    C_C_dissolved*(F_out + F_intermix) + &
    C_C_dissolved_z2*(F_intermix)
    C_C_dissolved = C_C_0 + integral(dCCdt,t,t_init,t_sim)"mol/L"

"C - Zone 2 - upper"
    C_C_dissolved_z2*dV_liquid_dt_z2 + V_liquid_z2*dCCdt_z2 = &
    C_C_dissolved*(F_out + F_intermix) - &
    C_C_dissolved_z2*F_out - &
```

```
    C_C_dissolved_z2*F_intermix
    C_C_dissolved_z2 = C_C_0_z2 + integral(dCCdt_z2,t,t_init,t_sim)"mol/L"
"-------------------------------------------------------------------------------------"
 "-------K - Zone 1-upper"
    C_K_dissolved*dV_liquid_dt + V_liquid*dCKdt = &
    C_K_NutrientSource*F_NutrientSource - &
    C_K_dissolved*(F_out + F_intermix) + &
    C_K_dissolved_z2*F_intermix
    C_K_dissolved = C_K_0 + integral(dCKdt,t,t_init,t_sim)"mol/L"

 "K - Zone 2 - upper"
    C_K_dissolved_z2*dV_liquid_dt_z2 + V_liquid_z2*dCKdt_z2 = &
    C_K_dissolved*(F_out + F_intermix) - &
    C_K_dissolved_z2*F_out - &
    C_K_dissolved_z2*F_intermix
    C_K_dissolved_z2 = C_K_0_z2 + integral(dCKdt_z2,t,t_init,t_sim)"mol/L"
"-------------------------------------------------------------------------------------"
 "-------S - Zone 1-upper"
    C_S_dissolved*dV_liquid_dt + V_liquid*dCSdt = &
    C_S_NutrientSource*F_NutrientSource - &
    C_S_dissolved*(F_out + F_intermix) + &
    C_S_dissolved_z2*F_intermix
    C_S_dissolved = C_S_0 + integral(dCSdt,t,t_init,t_sim)"mol/L"

 "S - Zone 2 - upper"
    C_S_dissolved_z2*dV_liquid_dt_z2 + V_liquid_z2*dCSdt_z2 = &
    C_S_dissolved*(F_out + F_intermix) - &
    C_S_dissolved_z2*F_out - &
    C_S_dissolved_z2*F_intermix
    C_S_dissolved_z2 = C_S_0_z2 + integral (dCSdt_z2, t,t_init,t_sim)"mol/L"

“! (4.3) ----------Solid Phase Balance ---------------------------------------------------------------------------"
 "n_MAP is the struvite moles within reactor"
"n_MAP_sample is the struvite moles taken in samples during reactor operation"
"Mw_MAP is the molecular weight of struvite in Kg/mol"
"m_MAP is the struvite mass within reactor [Kg]"

m_MAP = m_MAP_0*(L/L_0) ^3 - m_MAP_sample
n_MAP = m_MAP/MW_MAP

"Following equation depends on the initial mass, initial linear size and linear growth rate"
 dm_MAP_dt = m_MAP_0*3*(L/L_0) ^2/L_0*G_L
dn_MAP_dt = dm_MAP_dt/MW_MAP

“! (4.4) ----------Volume Balance ---------------------------------------------------------------------------------"
 "V_liquid is the liquid volume within the reactor"
"V_liquid_0 is the initial liquid volume"
"dV_liquid_dt is the liquid phase variation over time numerically equivalent to the struvite
volume increment dV_MAP_dt"
"rho_MAP_kgL is the struvite density"
"V_MAP is the struvite volume within reactor"
```

```
"dn_MAP_dt is the struvite mol production"

    V_liquid = V_liquid_0 + integral(dV_liquid_dt,t,t_init,t_sim)"[L]"
    dV_liquid_dt = - dV_MAP_dt "[L/h]"
    dV_MAP_dt = dn_MAP_dt*Mw_MAP*(1/rho_MAP_kgL) "[L/h]"
    V_MAP = m_MAP/ rho_MAP_kgL

“! --------------------------------5. KINETIC COMPONENT-----------------------------------------------"
    G_L= sign(SI_MAP) *k*(abs(SI_MAP) ^n)
    L = L_0 + integral(G_L,t,t_init,t_sim)

“! -------------------------Elemental composition of MgSO4.7H2O-------------------------------------"
 "---Reagent concentration in mol/L:"
        C_Mg_MgSource = C_MgSO47H2O_feed
        C_S_MgSource = C_MgSO47H2O_feed

 “! ------------------------------0. INPUT DATA-----------------------------------------"
 “! (0.1) Initial conditions - Comment if Macros is used"
    V_liquid_0 = 6 "[L] Initial volume"
    L_0 = 100e-6 "initial particle size in m"
    m_MAP_0 = 225e-3 "kg - Initial seeds quantity"

“The following is the initial elemental concentration in the upper zone, which at time zero is the same as the bottom zone”
    C_P_0_z2 = C_P_0
    C_N_0_z2 = C_N_0
    C_Mg_0_z2 = C_Mg_0
    C_K_0_z2 = C_K_0
    C_S_0_z2 = C_S_0
    C_C_0_z2 = C_C_0
    C_Na_0_z2 = C_Na_0
    C_Cl_0_z2 = C_Cl_0

$Import ‘INITIAL_TIME_0_MGP0.3.csv' C_P_0, C_N_0, C_Mg_0, C_K_0, C_S_0, C_C_0, C_Na_0, C_Cl_0

“! (0.2) Kinetic parameters"
    k = 1e-6 [m/h]
    n = 1"Kinetics"

“! (0.3) Simulation data"

    t_sim = 100 "h operational time"
    t_init = 0 h
```

B.4. EES Model –Macros Implementation

```
//Macro aims to run simulation over a range times from t_i to t_f.  This can repeat with updated state and limit variables
// This imports the initial conditions (composition)
Import File$ C_P_0, C_N_0, C_Mg_0, C_K_0, C_S_0, C_C_0, C_Na_0, C_Cl_0
        C_MgSO47H2O_feed = .....
// Initial conditions
         V_liquid_0 = 6 //L -initial volume of the liquid
         L_0 = 100e-6 //Initial mean particle size (m)
         m_MAP_0 = 225e-3 //Kg initial quanity of seeds
//Kinetic parameters:
        k =1e-6
        n = 1
//The composition of the upper zone is the sames as the bottom zone at the start
        C_P_0_z2 = C_P_0
        C_N_0_z2 = C_N_0
        C_Mg_0_z2 = C_Mg_0
        C_K_0_z2 = C_K_0
        C_S_0_z2 = C_S_0
        C_C_0_z2 = C_C_0
        C_Na_0_z2 = C_Na_0
        C_Cl_0_z2 = C_Cl_0
//set to zero the first time
        t_init= 0
        t_sim = 0
//Do a solve for zero to zero time - this allows us to create a single row of the integral table, which is need to create the log file
//SOLVE
//Save a dummy set of data, just to create the log file - no /A switch, so will not append
//Save Integral 'Main' F$ /A
//set the time limits on the segments
        t_end[0] = 0
        t_end[1] = 11/60 + 2/60                 //2 min after start of all feed streams
        t_end[2] = 100                  //
//counter is used to track the number of segments - starts at zero, but will be immediately increased
        counter=0
        H1$ = 'tester1.lkt'
        H2$ = 'tester2.lkt'
Repeat
        counter=counter+1
        t_sim = t_end[counter] //First simulation segment before adding Mg
        SOLVE
        if (counter = 1) then SaveIntegral 'Main' H1$
        if (counter = 1) then OpenLookup H1$
        if (counter = 2) then SaveIntegral 'Main' H2$
        if (counter = 2) then OpenLookup H2$
        //reset initial conditions to current state values:
        L_0 = L
        m_MAP_0 = m_MAP + m_MAP_sample
        V_liquid_0 = V_liquid
```

```
C_P_0 = C_P_dissolved
C_N_0 = C_N_dissolved
C_Mg_0 = C_Mg_dissolved
C_K_0 = C_K_dissolved
C_S_0 = C_S_dissolved
C_C_0 = C_C_dissolved
C_Na_0 = C_Na_dissolved
C_Cl_0 = C_Cl_dissolved

C_P_0_z2 = C_P_dissolved_z2
C_N_0_z2 = C_N_dissolved_z2
C_Mg_0_z2 = C_Mg_dissolved_z2
C_K_0_z2 = C_K_dissolved_z2
C_S_0_z2 = C_S_dissolved_z2
C_C_0_z2 = C_C_dissolved_z2
C_Na_0_z2 = C_Na_dissolved_z2
C_Cl_0_z2 = C_Cl_dissolved_z2

t_init = t      //reset start time to current time
//loop back up to the REPEAT above
Until (t > 99.9)
```

B.5. gPROMS C

Model: Thermodynamics_simplified

```
PARAMETER
#Addition - thermodynamics:
   pK_w                AS REAL
   pK_NH4              AS REAL
   pK_HPO4             AS REAL
   pK_H2PO4            AS REAL
   pK_NaHPO4           AS REAL
   pK_MgHPO4           AS REAL
   pK_MgPO4            AS REAL
   pK_NH4HPO4          AS REAL
   pK_KHPO4            AS REAL
   pK_HCO3             AS REAL
   pK_MgHCO3           AS REAL
   pK_MgSO4            AS REAL
   pK_KSO4             AS REAL

#"Product solubility of solid species"
   pKsp_MAP    AS REAL    #"Struvite: MgNH4PO4.6H2O - MAP"

#Debye Huckle modified by Davies - constant A}
   A              AS REAL
   B              AS REAL

#Ionic charges for calculating ionic strength
   Z1          AS REAL
   Z2          AS REAL
   Z3          AS REAL

#Charge balance
   CB          AS REAL

#"Valencies of Species - Z"
#"Positive valencies:"
   Z_H            AS REAL
   Z_Na           AS REAL
   Z_K            AS REAL
   Z_NH4          AS REAL
   Z_Mg           AS REAL
   Z_CaHCO3       AS REAL
   Z_Ca           AS REAL
   Z_CaH2PO4      AS REAL
   Z_MgHCO3       AS REAL
   Z_CaOH         AS REAL

 #"Negative valencies:"
   Z_OH           AS REAL
   Z_Cl           AS REAL
```

```
    Z_HPO4          AS REAL
    Z_PO4           AS REAL
    Z_H2PO4         AS REAL
    Z_NaHPO4        AS REAL
    Z_NH4HPO4       AS REAL
    Z_MgPO4         AS REAL
    Z_HCO3          AS REAL
    Z_CO3           AS REAL
    Z_CaPO4         AS REAL
    Z_SO4           AS REAL
    Z_KHPO4         AS REAL
    Z_KSO4          AS REAL

VARIABLE
#Thermodynamics
    C_P_diss        AS Concentration
    C_N_diss        AS Concentration
    C_Mg_diss       As Concentration
    C_Na_diss       AS Concentration
    C_Cl_diss       AS Concentration
    C_C_diss        AS Concentration
    C_S_diss        AS Concentration
    C_K_diss        AS Concentration

#Speciation
    C_Mg            AS Concentration
    C_MgPO4         AS Concentration
    C_MgHPO4        AS Concentration
    C_NH4           AS Concentration
    C_NH4HPO4       AS Concentration
    C_NH3           AS Concentration
    C_PO4           AS Concentration
    C_HPO4          AS Concentration
    C_H2PO4         AS Concentration
    C_H             AS Concentration
    C_OH            AS Concentration
    C_Cl            AS Concentration
    C_Na            AS Concentration
    C_NaHPO4        AS Concentration
    C_MgHCO3        AS Concentration
    C_HCO3          AS Concentration
    C_CO3           AS Concentration
    C_MgSO4         AS Concentration
    C_SO4           AS Concentration
    C_K             AS Concentration
    C_KHPO4         AS Concentration
    C_KSO4          AS Concentration

# Log free ion concentrations}
    log_C_Mg            AS LogConcentration
    log_C_MgPO4         AS LogConcentration
```

log_C_MgHPO4 AS LogConcentration
log_C_NH4 AS LogConcentration
log_C_NH3 AS LogConcentration
log_C_PO4 AS LogConcentration
log_C_HPO4 AS LogConcentration
log_C_H2PO4 AS LogConcentration
log_C_H AS LogConcentration
log_C_OH AS LogConcentration
log_C_Na AS LogConcentration
log_C_NH4HPO4 AS LogConcentration
log_C_NaHPO4 AS LogConcentration
log_C_MgHCO3 AS LogConcentration
log_C_HCO3 AS LogConcentration
log_C_CO3 AS LogConcentration
log_C_SO4 AS LogConcentration
log_C_MgSO4 AS LogConcentration
log_C_K AS LogConcentration
log_C_KHPO4 AS LogConcentration
log_C_KSO4 AS LogConcentration

Ion activities}
a_Mg AS Activity
a_MgPO4 AS Activity
a_MgHPO4 AS Activity
a_NH4 AS Activity
a_NH3 AS Activity
a_PO4 AS Activity
a_HPO4 AS Activity
a_H2PO4 AS Activity
a_H AS Activity
a_OH AS Activity
a_Na As Activity
a_NH4HPO4 AS Activity
a_NaHPO4 AS Activity
a_MgHCO3 AS Activity
a_HCO3 AS Activity
a_CO3 AS Activity
a_SO4 AS Activity
a_MgSO4 AS Activity
a_K AS Activity
a_KHPO4 AS Activity
a_KSO4 AS Activity

#{log ion activities}- Cations
log_a_Mg AS LogActivity
log_a_MgPO4 AS LogActivity
log_a_MgHPO4 AS LogActivity
log_a_NH4 AS LogActivity
log_a_NH3 AS LogActivity
log_a_NH4HPO4 AS LogActivity
log_a_PO4 AS LogActivity

```
   log_a_HPO4          AS LogActivity
   log_a_H2PO4         AS LogActivity
   log_a_H             AS LogActivity
   log_a_OH             AS LogActivity
   log_a_Na            AS LogActivity
   log_a_NaHPO4        AS LogActivity
   log_a_HCO3          AS LogActivity
   log_a_CO3           AS LogActivity
   log_a_MgHCO3        AS LogActivity
   log_a_SO4           AS LogActivity
  log_a_MgSO4          AS LogActivity
   log_a_K             AS LogActivity
   log_a_KHPO4         AS LogActivity
   log_a_KSO4          AS LogActivity

#Ion activity product estimation through log_IAP
   log_IAP_MAP         AS LogIAP

#Ion activity product estimation IAP
   IAP_MAP             AS IAP
# Conditional solubility product through log_Ksp
log_Ksp_MAP            AS Dimensionless

# Activity coefficients
   log_gamma_1         AS LogActivityCoeff
   log_gamma_2         AS LogActivityCoeff
   log_gamma_3         AS LogActivityCoeff
   gamma_1             AS ActivityCoeff
   gamma_2             AS ActivityCoeff
   gamma_3             AS ActivityCoeff
# Ionic Strength
   I                   AS IonicStrength
# Saturation index
   SI_MAP              AS Dimensionless
   pH                  AS pH

SET
#"Equilibrium pK"
   pK_w          := 14;#  "H2O <---> H+ + OH-"
   pK_NH4        := 9.24;#          "NH4+ <---> NH3 + H"
   pK_HPO4       := 12.350;#        "HPO4-2 <--->  PO4-3 + H+"
   pK_H2PO4      := 7.210;#         "H2PO4 <---> HPO4 + H+"
   pK_NaHPO4     := - 6.01;#        "NaHPO4 + H <---> Na + H2PO4"
   pK_MgHPO4     := - 4.3;#         "MgHPO4 +H <---> Mg + H2PO4 "
   pK_MgPO4      := - 12.96;#       "MgPO4 + 2H <---> Mg +H2PO4"
   pK_NH4HPO4          := 1.30;#          "NH4HPO4 <---> NH4 +  HPO4-2"
   pK_KHPO4            := - 6.12;#        "KHPO4 + H <---> K + H2PO4"
   pK_HCO3             := 10.329;#        "HCO3 <---> CO3 + H"
   pK_MgHCO3           := 1.07;#          "MgHCO3 <---> Mg+2 +HCO3-"
   pK_MgSO4            := 2.37;   #"MgSO4 <---> Mg + SO4"
   pK_KSO4             := 0.85;#          "KSO4  <---> K + SO4"
```

```
#Product solubility of solid species"
   pKsp_MAP    := 13.26;#"Struvite: MgNH4PO4.6H2O - MAP"

# Davies equation with DeBye Huckle modification}
   A           :=   0.509;

# Ionic charges for calculating ionic strength}
   Z1          :=  1;
   Z2          :=  2;
   Z3          :=  3;

#"Positive valencies:"
   Z_H :=1;
   Z_Na :=1;
   Z_K :=1;
   Z_NH4:=1;
   Z_Mg:=2;
   Z_CaHCO3:=1;
   Z_Na:=2;
   Z_CaH2PO4:=1;
   Z_MgHCO3:=1;
   Z_CaOH:=1;

 #Negative valencies:"
   Z_OH:=-1;
   Z_Cl:=-1;
   Z_HPO4:=-2;
   Z_PO4:=-3;
   Z_H2PO4:=-1;
   Z_NaHPO4:=-1;
   Z_NH4HPO4:=-1;
   Z_MgPO4:=-1;
   Z_HCO3:=-1;
   Z_CO3:=-2;
   Z_CaPO4:=-1;
   Z_SO4:=-2;
   Z_KHPO4:=-1;
   Z_KSO4:=-1;

{charge balance}
  CB: =  0;

EQUATION
#Thermodynamics
   log_Ksp_MAP = -pKsp_MAP;# "Struvite: MgNH4PO4.6H2O - (MAP)"

#-------Conversion of pK in -logK in equilibrium equations
   -pK_w = log_a_H+log_a_OH;
   -pK_NH4 = log_a_H+log_a_NH3-log_a_NH4;
   -pK_HPO4 = log_a_PO4+log_a_H-log_a_HPO4;
```

```
   -pK_H2PO4 = log_a_HPO4+log_a_H-log_a_H2PO4;
   -pK_NaHPO4 = log_a_Na+log_a_H2PO4-log_a_NaHPO4-log_a_H;
   -pK_MgHPO4 = log_a_Mg+log_a_H2PO4-log_a_MgHPO4-log_a_H;
   -pK_MgPO4 = log_a_Mg+log_a_H2PO4-log_a_MgPO4-2*log_a_H;
   -pK_NH4HPO4 = log_a_NH4+log_a_HPO4-log_a_NH4HPO4;
   -pK_KHPO4 = log_a_K+log_a_H2PO4-log_a_KHPO4-log_a_H;
   -pK_HCO3 = log_a_CO3+log_a_H-log_a_HCO3;
   -pK_MgHCO3 = log_a_Mg+log_a_HCO3-log_a_MgHCO3;
   -pK_MgSO4 = log_a_Mg+log_a_SO4-log_a_MgSO4;
   -pK_KSO4 = log_a_K+log_a_SO4-log_a_KSO4;

#--------"Chemical speciation- Liquid phase"
        C_P_diss = C_PO4 +C_HPO4 + C_H2PO4 + C_MgHPO4 +  C_MgPO4     +     C_NH4HPO4     +
        C_NaHPO4 + C_KHPO4;
        C_N_diss = C_NH3 + C_NH4 +     C_NH4HPO4;
        C_Mg_diss =C_Mg + C_MgHPO4 + C_MgPO4 + C_MgHCO3+       C_MgSO4;
        C_Na_diss = C_Na +       C_NaHPO4;
        C_Cl_diss = C_Cl;
        C_C_diss=C_HCO3+ C_CO3+C_MgHCO3;
        C_S_diss =C_SO4+ C_MgSO4+       C_KSO4;
        C_K_diss =C_K+ C_KHPO4+        C_KSO4;

#---Charge balance - CB=Sum(Ci*Zi)"
   CB= (C_H*Z_H + C_Na*Z_Na + C_NH4*Z_NH4 + C_Mg*Z_Mg+   C_OH*Z_OH+ C_HPO4*Z_HPO4+
C_PO4*Z_PO4+        C_H2PO4*Z_H2PO4+        C_NaHPO4*Z_NaHPO4+ C_NH4HPO4*Z_NH4HPO4+
C_MgPO4*Z_MgPO4+          C_Cl*Z_Cl+C_MgHCO3*Z_MgHCO3+C_HCO3*Z_HCO3+  C_CO3*Z_CO3+
C_SO4*Z_SO4+ C_K*Z_K+C_KHPO4*Z_KHPO4+  C_KSO4*Z_KSO4);

#-----"Positive valencies:"
        log_a_H=log_gamma_1+log_C_H;
        log_a_Na=log_gamma_1+log_C_Na;
        log_a_K=log_gamma_1+log_C_K;
        log_a_NH4=log_gamma_1+log_C_NH4;
        log_a_Mg=log_gamma_2+log_C_Mg;
        log_a_MgHCO3=log_gamma_1+log_C_MgHCO3;

#------   "Negative valencies:"
        log_a_OH=log_gamma_1+log_C_OH;
        log_a_HPO4=log_gamma_2+log_C_HPO4;
        log_a_PO4=log_gamma_3+log_C_PO4;
        log_a_H2PO4=log_gamma_1+log_C_H2PO4;
        log_a_NaHPO4=log_gamma_1+log_C_NaHPO4;
        log_a_NH4HPO4=log_gamma_1+log_C_NH4HPO4;
        log_a_MgPO4=log_gamma_1+log_C_MgPO4;
        log_a_KHPO4 =   log_gamma_1+log_C_KHPO4;
        log_a_HCO3=log_gamma_1+log_C_HCO3;
        log_a_CO3=log_gamma_2+log_C_CO3;
        log_a_SO4=log_gamma_2+log_C_SO4;
        log_a_KSO4=log_gamma_1+log_C_KSO4;

#-----    "Zero valencies:"
```

```
        log_a_NH3=log_C_NH3;
        log_a_MgHPO4=log_C_MgHPO4;
        log_a_MgSO4=log_C_MgSO4;

#{Activity Co-efficients - Davies eqn with DeBye Huckle approximation}
  log_gamma_1 =   -A*(Z1^2)*((I^0.5)/(1+(I^0.5))-0.3*I);
  gamma_1 = 10^log_gamma_1;
  log_gamma_2 =   -A*(Z2^2)*((I^0.5)/(1+(I^0.5))-0.3*I);
  gamma_2 = 10^log_gamma_2;
  log_gamma_3 =   -A*(Z3^2)*((I^0.5)/(1+(I^0.5))-0.3*I);
  gamma_3 = 10^log_gamma_3;

#{Ionic Strength}
  I= 0.5*(C_H*Z_H^2 + C_Na*Z_Na^2 + C_NH4*Z_NH4^2 +  C_Mg*Z_Mg^2+    C_OH*Z_OH^2+
    C_HPO4*Z_HPO4^2+     C_PO4*Z_PO4^2+      C_H2PO4*Z_H2PO4^2+
    C_NaHPO4*Z_NaHPO4^2+      C_NH4HPO4*Z_NH4HPO4^2+      C_MgPO4*Z_MgPO4^2+
    C_Cl*Z_Cl^2+        C_MgHCO3*Z_MgHCO3^2+      C_HCO3*Z_HCO3^2+
        C_CO3*Z_CO3^2+        C_SO4*Z_SO4^2+      C_K*Z_K^2+        C_KHPO4*Z_KHPO4^2+
        C_KSO4*Z_KSO4^2);

#-----{free ion concentrations}
#Positive valences
  C_H           =  10^log_C_H;
  C_Na          =  10^log_C_Na;
  C_K           =  10^log_C_K;
  C_NH4         =  10^log_C_NH4;
  C_Mg          =  10^log_C_Mg;
  C_MgHCO3      =  10^log_C_MgHCO3;
#Negative valences
  C_OH          =  10^log_C_OH;
  C_HPO4        =  10^log_C_HPO4;
  C_PO4         =  10^log_C_PO4;
  C_H2PO4       =  10^log_C_H2PO4;
  C_NaHPO4      =  10^log_C_NaHPO4;
  C_NH4HPO4     =  10^log_C_NH4HPO4;
  C_MgPO4       =  10^log_C_MgPO4;
  C_HCO3        =  10^log_C_HCO3;
  C_CO3         =  10^log_C_CO3;
  C_SO4         =   10^log_C_SO4;
  C_KSO4        =   10^log_C_KSO4;
  C_KHPO4       =   10^log_C_KHPO4;

#Ionic concentration "Zero valencies:"
  C_NH3         =  10^log_C_NH3;
  C_MgHPO4      =  10^log_C_MgHPO4;
  C_MgSO4       =   10^log_C_MgSO4;

#{ion activities}- Positive
  a_H           =  10^log_a_H;
  a_Na          =  10^log_a_Na;
  a_NH4         =  10^log_a_NH4;
```

```
   a_Mg          =  10^log_a_Mg;
   a_MgHCO3   =  10^log_a_MgHCO3;
   a_K             =   10^log_a_K;

#{ion activities}- Negative
   a_OH           =  10^log_a_OH;
   a_HPO4        =  10^log_a_HPO4;
   a_PO4          =  10^log_a_PO4;
   a_H2PO4       =  10^log_a_H2PO4;
   a_NaHPO4     =  10^log_a_NaHPO4;
   a_NH4HPO4   =  10^log_a_NH4HPO4;
   a_MgPO4       =  10^log_a_MgPO4;
   a_HCO3         =  10^log_a_HCO3;
   a_CO3          =  10^log_a_CO3;
   a_SO4          =   10^log_a_SO4;
   a_KSO4         =10^log_a_KSO4;
   a_KHPO4       =10^log_a_KHPO4;

#{ion activities}- Neutral
   a_NH3          =  10^log_a_NH3;
   a_MgHPO4     =  10^log_a_MgHPO4;
   a_MgSO4       =   10^log_a_MgSO4;

   pH = -log_a_H;

#"Ion Activity Product (IAP):"
   log_IAP_MAP= log_a_Mg+ log_a_NH4+log_a_PO4;#    "Struvite: MgNH4PO4.6H2O-(MAP)"
   IAP_MAP=10^log_IAP_MAP;#

#{Solubility Index}
SI_MAP = log_IAP_MAP- log_Ksp_MAP;
```

Model: Reactor

UNIT

Thermo AS Thermodynamics_simplified

PARAMETER

Mw_MAP	AS REAL #kg/mol
rho_MAP_kgL	AS REAL #Kg/L
Mw_N	AS REAL #g/mol
Mw_P	AS REAL #g/mol
Mw_Mg	AS REAL #g/mol

#Composition of nutrient feed tank

C_N_Nut	AS REAL#mol/L
C_C_Nut	AS REAL
C_Cl_Nut	AS REAL
C_Na_Nut	AS REAL
C_K_Nut	AS REAL
C_P_Nut	AS REAL
C_S_Nut	AS REAL
m_MAP_0	AS REAL #Kg - initial struvite seed mass
L_0	AS REAL #m - Initial mean particle size
V_0_effective	AS REAL #L - Initial effective volume of the reactor

VARIABLE

n	AS Dimensionless #Kinetic parameter
k	As Dimensionless #Kinetic parameter
F_out	AS VolumetricFlowrate #Nutrient flow, Outlet flow rate
V_liquid	AS Volume #L
V_MAP	AS StruviteVolume #L
m_MAP	AS StruviteMass #kg
n_MAP	AS Moles
Dilfactor	AS Dimensionless #Fraction: Volume urine / (V urine + V water)
G_L	AS GrowthRate #m/h
L	AS ParticleSize #m
SI_MAP	AS Dimensionless
F_Nut	AS VolumetricFlowrate #L/h
F_MgSource	AS VolumetricFlowrate #L/h
C_Mg_MgSource	AS Concentration #mol/L
C_S_MgSource	AS Concentration #mol/L

#Unit Converters

C_P_diss_ppm	AS ConcentrationInPPM
C_N_diss_ppm	AS ConcentrationInPPM
C_Mg_diss_ppm	AS ConcentrationInPPM
m_MAP_g	AS StruviteMass_g #g

#Varibles to be solved

C_N_diss	AS Concentration #mo/L
C_C_diss	AS Concentration #mo/L
C_Cl_diss	AS Concentration #mo/L

```
    C_Na_diss      AS Concentration #mo/L
    C_K_diss       AS Concentration #mo/L
    C_P_diss       AS Concentration #mo/L
    C_S_diss       AS Concentration #mo/L
    C_Mg_diss      AS Concentration #mo/L
    C_MgSO47H2O    AS Concentration #Composition in feed tank #mo/L

SET
    C_N_Nut        := 0.32492913294697;
    C_C_Nut        := 0.0907963974903865;
    C_Cl_Nut       := 0.20152922921613;
    C_Na_Nut       := 0.0726;
    C_K_Nut        := 0.0504584212627616;
    C_P_Nut        := 0.0178040511170999;
    C_S_Nut        := 0.00739972756167701;

# Unit connection equations
   Mw_MAP        := 0.24541; #[kg/mol]
   rho_MAP_kgL   := 1.7;#kg/L
   Mw_N          := 14.007;#g/mol
   Mw_P          := 30.974;#g/mol
   Mw_Mg         := 24.305;#g/mol

   m_MAP_0       := 0.150; #Kg
   L_0           := 50e-6;#m
   V_0_effective    := 6;#L

EQUATION
#Linking with thermodynamics
   C_P_diss = Thermo.C_P_diss;
   C_N_diss = Thermo.C_N_diss;
   C_Mg_diss = Thermo.C_Mg_diss;
   C_Na_diss = Thermo.C_Na_diss;
   C_Cl_diss = Thermo.C_Cl_diss;
   C_K_diss = Thermo.C_K_diss;
   C_S_diss = Thermo.C_S_diss;
   C_C_diss = Thermo.C_C_diss;
   SI_MAP = Thermo.SI_MAP;

#Elemental distribution of MgSO4.7H2O in Mg and S
   C_Mg_MgSource = C_MgSO47H2O;#mol/L
   C_S_MgSource =  C_MgSO47H2O;#mol/L

# Concentration Balance
   F_out = F_Nut + F_MgSource;
   $V_liquid = F_MgSource + F_Nut - F_out - $V_MAP;
   $V_MAP = $n_MAP*Mw_MAP*(1/rho_MAP_kgL);
   C_P_diss*$V_liquid + V_liquid*$C_P_diss = C_P_Nut*Dilfactor*F_Nut - C_P_diss*F_out - $n_MAP;
   C_N_diss*$V_liquid + V_liquid*$C_N_diss = C_N_Nut*Dilfactor*F_Nut - C_N_diss*F_out –

$n_MAP;
```

```
  C_Mg_diss*$V_liquid + V_liquid*$C_Mg_diss = C_Mg_MgSource*F_MgSource - C_Mg_diss*F_out -
$n_MAP;
  C_Na_diss*$V_liquid + V_liquid*$C_Na_diss = C_Na_Nut*Dilfactor*F_Nut - C_Na_diss*F_out;
  C_Cl_diss*$V_liquid + V_liquid*$C_Cl_diss = C_Cl_Nut*Dilfactor*F_Nut - C_Cl_diss*F_out;
  C_C_diss*$V_liquid + V_liquid*$C_C_diss = C_C_Nut*Dilfactor*F_Nut - C_C_diss*F_out;
  C_K_diss*$V_liquid + V_liquid*$C_K_diss = C_K_Nut*Dilfactor*F_Nut - C_K_diss*F_out;
  C_S_diss*$V_liquid + V_liquid*$C_S_diss = C_S_Nut*Dilfactor*F_Nut + C_S_MgSource*F_MgSource
- C_S_diss*F_out;
  m_MAP = n_MAP*Mw_MAP;#m_MAP in Kg
  m_MAP_g = m_MAP*1000; #g

#Kinetic equation:
   G_L = k*(abs(SI_MAP))^n;#m/h
   $L = G_L;#m/h
   $n_MAP = (3/Mw_MAP)*m_MAP_0*(L^2)/(L_0^3)*(k)*(abs(SI_MAP))^n;#mol/h

#Unit change
   C_P_diss_ppm = C_P_diss*Mw_P*1000;
   C_N_diss_ppm = C_N_diss*Mw_N*1000;
   C_Mg_diss_ppm = C_Mg_diss*Mw_Mg*1000;
   C_Mg_diss_ppb = C_Mg_diss_ppm*1000;
   L_um = L*1e6; #mean particle size in um
```

PROCESS: Reactor_Proc

UNIT

Sim1 AS Reactor

PARAMETER

NoSamples AS INTEGER#Quantity of time data is taken from reactor operation
IntervalSamples AS REAL#Duration in hours between taking each of the samples

VARIABLE

RunTime AS RunTimeProc#in hours

SET

NoSamples := 5;#If duration of intervals between samples is 5 hours = 60 hours
IntervalSamples := 20;#hours

EQUATION

RunTime = NoSamples*IntervalSamples;

ASSIGN

Sim1.n := 1.5; Sim1.k := 1e-6;
Sim1.F_Nut := 0.3; Sim1.F_MgSource := 0.3;#L/h

Sim1.Dilfactor := 1;#Condition for CSUU + Mg source
Sim1.C_MgSO47H2O := 0.00356081022341998; #"mol/L - Mg/P =0.6"

INITIAL

# Equations -This part is for variables inside ODE
Sim1.V_liquid = 6; #L Initial volume of liquid in the reactor
Sim1.V_MAP = 1e-3;#L

#Following composition is the desaturated solution at Mg/P = 0.1
Sim1.Thermo.C_P_diss = 0.01602873;
Sim1.Thermo.C_N_diss = 0.323153812;
Sim1.Thermo.C_Mg_diss = 0.00000467891739
Sim1.Thermo.C_K_diss = 0.0504584213;
Sim1.Thermo.C_S_diss = 0.00917972756;
Sim1.Thermo.C_C_diss = 0.0907963975;
Sim1.Thermo.C_Na_diss = 0.0726054454;
Sim1.Thermo.C_Cl_diss = 0.201529229;

#Initial quantity of struvite:
Sim1.m_MAP_g= 150;# g

#Initial mean particle size:
Sim1.L = 50e-6;#m

SOLUTIONPARAMETERS

REPORTINGINTERVAL := 0.1;
NLSolver := "BDNLSOL" [
"OutputLevel" := 0,

```
   "BlockSolver" := "SPARSE" [
      "ConvergenceTolerance" := 1E-008,
      "EffectiveZero" := 1E-008,
      "FDPerturbation" := 1E-008,
      "MaxFuncs" := 100000000,
      "MaxIterNoImprove" := 50,
      "MaxIterations" := 1000,
      "NStepReductions" := 50,
      "OutputLevel" := 0,
      "SLRFactor" := 50,
      "SingPertFactor" := 0.0001]];

#DASolver := "DASOLV" ["OutputLevel" := 1;
#"AbsoluteTolerance" := 1E-8] ;
DASolver := "DASOLV" [
"LASolver" := "MA48" [
"FullSwitchFactor" := 0.01,
"PivotStabilityFactor" := 0.99
],
"AbsoluteTolerance" := 1.0E-8,#1e-5
"OutputLevel" := 0,
"RelativeTolerance" := 1.0E-8,#1e-5
"VariablesWithLargestCorrectorSteps" := 2
]
 SCHEDULE
# OperationSchedule
   CONTINUE FOR RunTime
```

Appendix C Experimental Procedures

C.1. pH and conductivity measurements

For the purpose of pH measurements, the following was considered:

- A Thermo Orion $8175BNWP$ Ross sureflow pH electrode and Orion $8156BNUWP$ ROSS Ultra combination pH electrodes were used connected to an Orion 5-Star meter
- A 013605 MD conductivity cell compensated pH at different temperatures
- Calibration with Buffer solutions standards (7.00, 4.01, 10.01)
- Immerse the probe in the sample

For the purpose of conductivity measurements, the following was considered:

- Rinse the 013605MD conductivity probe with $MilliQ$ water and connect to meter
- Calibrate with one standard solution: 1413 $\mu S/cm$
- Immerse the conductivity cell in the sample

C.2. Setting and monitoring of flow rates

Grundfos DME Variant AR 16 to 248 gph (60 mL/h - 940 L/h) were calibrated based on equipment guidelines. The following steps were developed:

- Connect the pumps to the whole system, considering containers and feed tanks.
- Place the hose from the outlet of the reactor inside a 250 mL cylinder
- Select the flow rate in the pump's menu display, then in menu "CALIBR" and press "START".
- The pump performs 100 dosing strokes and all the suctioned solution is collected in the probe.
- The number in the display is corrected by the collected liquid in the cylinder.

C.3. Determination of $PO_4 - P$ by spectrophotometry

Phosphorus in the form of dissolved phosphate (PO_4^{-3}) reacts with ammonium molybdate to produce molybdophosphoric acid in presence of ammonium vanadate. This complex solution is yellow colour and its intensity is directly proportional to the concentration of phosphate (APHA, 1999).

Equipment, Materials and Reagents:

- Spectrophotometer Agilent 8453 and cuvettes 15x45x15 mm.
- Heater (to prepare the colorimetric solutions).
- 2 x 1 L beakers (to prepare the colorimetric solutions).
- 1 x 1 L volumetric flask (to prepare the stock solution containing phosphorus).
- 8 x 250 mL volumetric flask (to dilute standards).
- Potassium dihydrogen orthophosphate anhydrous (KH_2PO_4) (to be used as standard).
- Concentrated acid: 10.2 $M\ HCl$.
- Ammonium molybdate reagent ($(NH_4)_6Mo_7O_{24}.4H_2O$).
- Ammonium metavanadate (NH_4VO_3).

Procedure before measurements:

Volumetric flasks were rinsed with 1$N\ HCl$, and $MilliQ$ water. The colorimetric solution was prepared by combining two solutions. The first was prepared by dissolving 25 g ammonium molybdate in 300 mL distilled water; and the second was prepared by dissolving 1.25 g ammonium metavanadate 300 mL distilled water by heating to boiling. Cool and add 330 mL concentrated hydrochloric acid. The first solution was poured into the second one, mix and dilute up to 1 L.

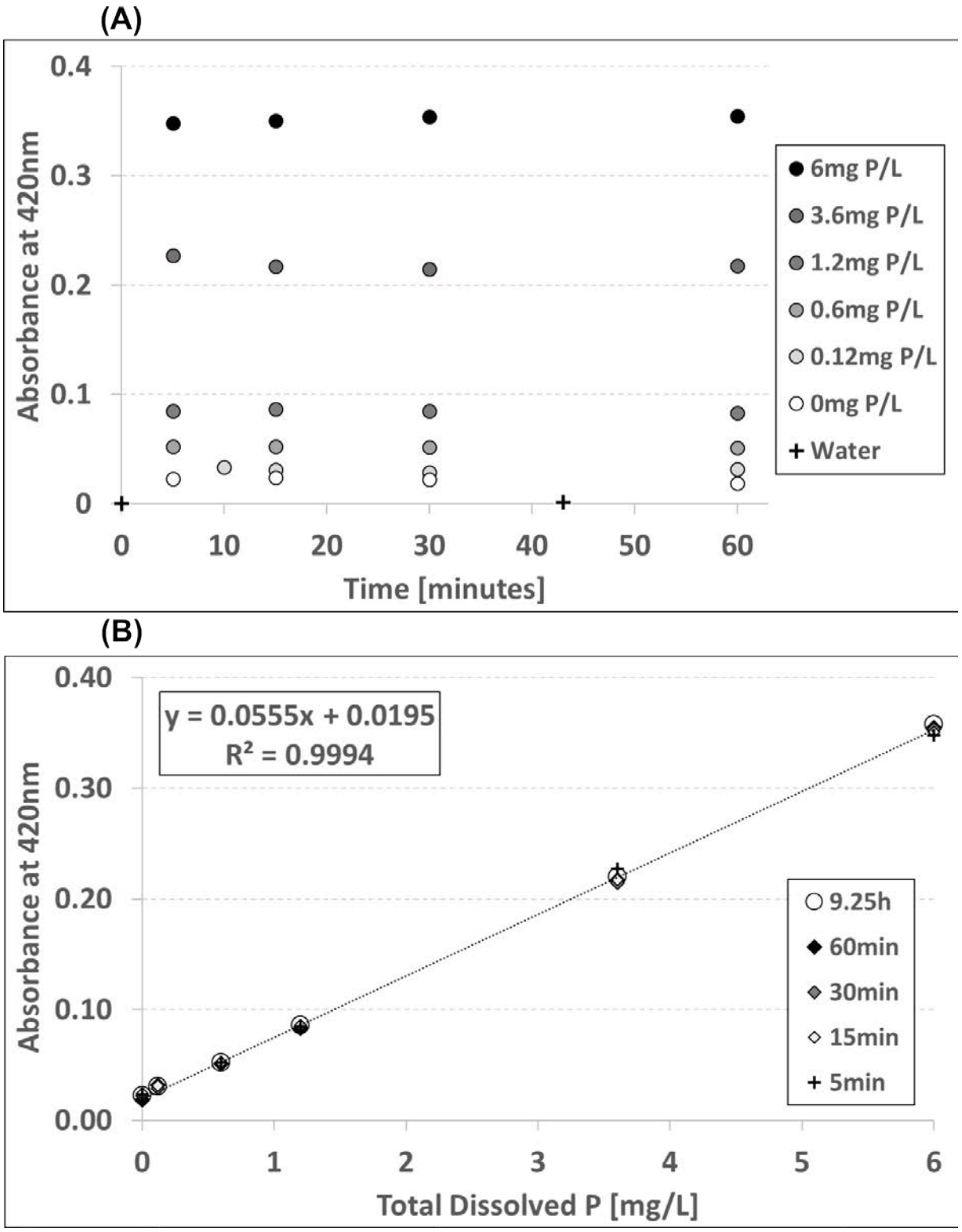

Figure 0.2 – Absorbance of standard samples over time (A), and linearity (B) at 24°C

Standard preparation and calibration curve:

- A stock solution of 50 mg/L potassium dihydrogen orthophosphate in 1 L volumetric flask.
- Standards were prepared from previous stock solutions.

- Pour 15 mL of standard, 5 mL of colour solution and fill up with water up to 25 mL in vol. flask.
- Wait at least 10 minutes before spectrophotometer measurements (Fig. 0.1).
- Tungsten lamp was turned on before measurements, and left on for 30 minutes before use.
- Correlate absorbance with standard concentration at 420 nm to determine slope and intercept.

Quantification of P concentration:

- Follow same procedure as stock solution concentrations to measure in spectrophotometer.
- Add 2 drops of 10.1 $M\ HCl$ when diluting the samples to decrease pH less than 7.
- Estimation of the concentration was developed with slope and intercept from calibration curve.

C.4. NH_3-N by spectrophotometry

The ammonia concentration was measured with a colorimetric methodology through indophenol formation using sodium salicylate (Verdouw et al., 1978). The application of sodium salicylate has the advantage of having less toxicity than phenol methodology (APHA, 1999). An aliquot was mixed with colour solutions A, B, C, and 0.75 mL of 1 M NaOH within a 50 mL volumetric flask to form the blue coloured indophenol. This thesis decreased the concentration of sodium salicylate in Solution A to allow complete dissolution.

Equipment, Materials and Reagents:

- Spectrophotometer Agilent 8453
- Spectrophotometer cuvettes 15x45x15 mm
- Volumetric flask: 50, 100, 250, 500 mL to dilute samples and standards.
- Automatic pipette 0.5 mL – 5 mL, 1 mL – 10 mL
- 1mL plastic transfer pipettes
- Ammonium dihydrogen phosphate ($NH_4H_2PO_4$)
- Sodium salicylate ($C_7H_5NaO_3$)
- Sodium hypochlorite ($NaOCl$)

- Sodium hydroxide (NaOH)
- Sodium Citrate ($\mathrm{Na_3C_6H_5O_7}$)
- Potassium ferrocyanide ($\mathrm{K_4Fe(CN)_6.3H_2O}$)

Table 0.3 — Comparison of original and modification salicylate methodology

Quantity of solutions	**Units**	**Verdouw et al., 1978**	**This work**
Sample quantity	mL	< 38	15
Solution A: sodium salicylate dissolved in water	$\% - mL$	40 % - 5	8 % - 25
Solution B: 1.93 % $NaOCl$ dissolved in 0.1 N $NaOH$	mL	2	2
Solution C: 2 % $K_4Fe(CN)_6.3H_2O$ + 10 % $Na_3Citrate.2H_2O$ dissolved in 0.1 N $NaOH$	mL	5	5
1 M $NaOH$	$mL.$	0	0.75

Standard preparation procedure:

A stock solution of 1mg $NH_3 - N$/L was prepared with $NH_4H_2PO_4$ in 1 L volumetric flask.

1. Stock solution aliquots of 2.5 mL, 5 mL, 7.5 mL, 10 mL, and 15 mL (V_{aliq}) were added to 50 mL flask.
2. 25 mL of solution A (V_A) was added to 50mL volumetric flask in (1).
3. 5 mL of solution C (V_C) was added to liquid in (2).
4. 2 mL of solution B (V_B) was added to liquid in (3).
5. 0.75 mL of 1M $NaOH$ solution (V_{base})was added to in (4).
6. Milli-Q water (V_{water}) was used to fill up the 50mL (V_{flask}).
7. Standard concentrations (C_{std}) were corrected with the aliquot volume in (1) and the final volume of 50mL (V_{flask}), giving concentration range between 0.05 $mg - N/L$ to 0.3 $mg - N/L$.

$$C_{std} \cdot V_{aliq} = C_{meas} \cdot (V_{aliq} + V_A + V_B + V_C + V_{base} + V_{water}) \quad 0.1$$

$$V_{aliq} + V_A + V_B + V_C + V_{base} + V_{water} = V_{flask} \quad 0.2$$

8. The mixed solutions were stored in 70mL plastic containers and left for around 3 h to achieve maximum colour intensity.
9. After 3 h, the absorbance in the sample was measured in the spectrophotometer at 653 nm.
10. A linear correlation of the absorbance as a function of the standard concentration was used to calculate the intercept (b) and slope (m).

Sample preparation procedure:

1. A solid sample of 10mg (m_s) was dissolved with milli-Q water in 1L (V_s).
2. The aliquot was mixed with solution A, B, C, and 0.75 mL of 1 $M\ NaOH$.
3. The absorbance of the unknown sample was measured with a spectrophotometer at 653 nm.
4. The aliquot concentration (C_{meas}) was estimated with the slope and intercept estimated in the standard preparation procedure.

$$Abs_{653} = m \cdot C_{meas} + b \quad 0.3$$

C.5. Mg by Flame Atomic Spectroscopy

The equipment was operated with air- acetylene according to equipment guidelines (Agilent, 2017). 55 AA Flame Atomic Absorption Spectrometer – Agilent Technologies was used (Table 0.2). A stock solution of 100 $mg\ Mg/L$ using $MgSO_4.7H_2O(s)$. A range of standards was prepared by diluting the initial stock solution. During dilution procedure, there was an addition of 1 $mL\ HNO_3$ (1:1) per 100 mL of sample to keep the sample pH < 2 and avoid ionic interferences.

Table 0.4 - Working Conditions from Operational Manual

Wavelength (nm)	Slit Width (nm)	Optimum Working Range (µg/mL)
285.2	0.5	0.003 – 1
202.6	1.0	0.15 – 20

Measurement Procedure:

- Turn on the equipment and set analytical parameters.
- Turn on the air – acetylene flame and optimise position of the burner.
- Measure absorbance of each standard.
- Read absorbance of samples.

C.6. Counting and particle size using *ImageJ*

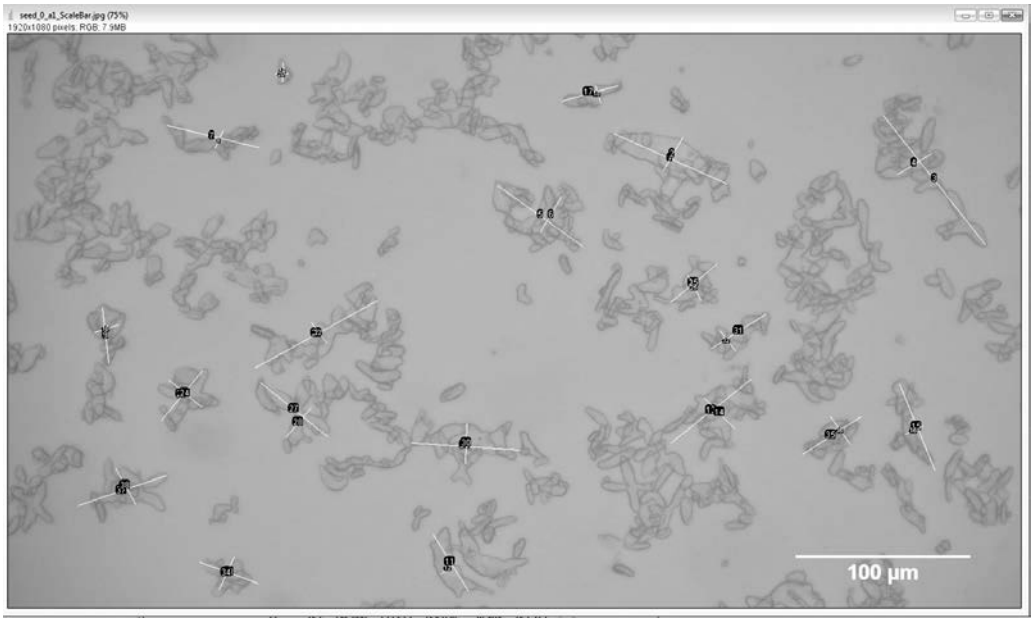

Figure 0.3 — Example of counting and measuring approximate length and width with ImageJ photo processing

The mean particle size equivalent to sphere was estimated through the volume of each of the particles (equation 1). The volume of each particle assumed the same depth and width of the crystal.

$$D_{sphere} = \sqrt[3]{\frac{6 \times V_p}{\pi}} \qquad 0.4$$